

Bogoliubov Excitations of Inhomogeneous Bose-Einstein Condensates

Von der Universität Bayreuth
zur Erlangung des Grades eines
Doktors der Naturwissenschaften (Dr. rer. nat.)
genehmigte Abhandlung

von

CHRISTOPHER GAUL

geboren in Bad Pyrmont

1. Gutachter: Prof. Dr. Cord A. Müller
2. Gutachter: Prof. Dr. Helmut Büttner
3. Gutachter: Prof. Dr. Martin Holthaus

Tag der Einreichung: 22. Februar 2010

Tag des Kolloquiums: 30. März 2010

Zusammenfassung

In dieser Arbeit werden wechselwirkende ultrakalte Bosonen in inhomogenen externen Potentialen behandelt. Im ersten Teil geht es um Bose-Einstein-Kondensate mit repulsiver Wechselwirkung in Speckle-Unordnungspotentialen. Im Bogoliubov-Ansatz wird das Vielteilchenproblem aufgespalten in den Gross-Pitaevskii-Grundzustand (Mean-Field) des Bose-Einstein-Kondensates und die Bogoliubov-Anregungen, die bosonische Quasiteilchen sind. Die Unordnung deformiert den Gross-Pitaevskii-Grundzustand, welcher als Inhomogenität in den Hamiltonian für die Bogoliubov-Anregungen eingeht. Der inhomogene Bogoliubov-Hamiltonian dient als Ausgangspunkt für eine diagrammatische Störungstheorie, die zur Unordnungs-renormierten Dispersionsrelation der Bogoliubov-Quasiteilchen führt. Davon abgeleitet werden insbesondere die mittlere freie Weglänge, sowie Korrekturen der Schallgeschwindigkeit und der Zustandsdichte. Die analytischen Ergebnisse werden mit einer numerischen Studie der Gross-Pitaevskii-Gleichung und einer exakten Diagonalisierung des ungeordneten Bogoliubov-Problems untermauert.

Gegenstand des zweiten Teils sind Bloch-Oszillationen von Bose-Einstein-Kondensaten unter dem Einfluss einer zeitabhängigen Wechselwirkung. Die Wechselwirkung führt im Allgemeinen zu Dekohärenz und zerstört die Bloch-Oszillation. Mit Hilfe von Feshbach-Resonanzen ist es möglich, die Teilchen-Teilchen-Wechselwirkung zu manipulieren. Es wird insbesondere der Fall einer um Null herum modulierten Wechselwirkung betrachtet. Unterschiedliche Modulationen führen entweder zu einer langlebigen periodischen Dynamik des Wellenpaketes oder zu einem schnellen Zerfall. Die Fälle mit periodischer Dynamik werden mit einem Zeitumkehr-Argument erklärt. Der Hauptzerfallsmechanismus in den übrigen Fällen besteht in einer dynamischen Instabilität, d.h. dem exponentiellen Anwachsen kleiner Störungen, die den Bogoliubov-Anregungen aus dem ersten Teil entsprechen.

Abstract

In this thesis, different aspects of interacting ultracold bosons in presence of inhomogeneous external potentials are studied. The first part deals with repulsively interacting Bose-Einstein condensates in speckle disorder potentials. In the Bogoliubov approach, the many-body problem is split into the Gross-Pitaevskii condensate (mean-field) and the Bogoliubov excitations, which are bosonic quasiparticles. The disorder potential causes an imprint in the condensate, which makes the Hamiltonian for the Bogoliubov excitations inhomogeneous. The inhomogeneous Bogoliubov Hamiltonian is the starting point for a diagrammatic perturbation theory that leads to the renormalized Bogoliubov dispersion relation. From this effective dispersion relation, physical quantities are derived, e.g. the mean free path and disorder corrections to the speed of sound and the density of states. The analytical results are supported by a numerical integration of the Gross-Pitaevskii equation and by an exact diagonalization of the disordered Bogoliubov problem.

In the second part, Bloch oscillations of Bose-Einstein condensates in presence of time-dependent interactions are considered. In general, the interaction leads to dephasing and destroys the Bloch oscillation. Feshbach resonances allow the atom-atom interaction to be manipulated as function of time. In particular, modulations around zero are considered. Different modulations lead to very different behavior: either the wave packet evolves periodically with time or it decays rapidly. The former is explained by a periodic time-reversal argument. The decay in the other cases can be described by a dynamical instability with respect to small perturbations, which are similar to the Bogoliubov excitations in the first part.

Contents

1. Interacting Bose Gases	1
1.1. Lattices	2
1.2. Disorder	3
1.3. Interaction	4
1.4. Cold-atoms—Universal model systems	5
1.5. Cold atoms—History and key experiments	6
1.6. Standing of this work	10
I. The Disordered Bogoliubov Problem	15
2. The Inhomogeneous Bogoliubov Hamiltonian	17
2.1. Bose-Einstein condensation of the ideal gas	17
2.1.1. Partition function and Bose statistics	18
2.1.2. Bose-Einstein condensation	19
2.1.3. Order parameter and spontaneous symmetry breaking	21
2.2. Interacting BEC and Gross-Pitaevskii mean-field	22
2.2.1. Basic many-body theory	22
2.2.2. Gross-Pitaevskii energy functional and equation of motion	23
2.2.3. Ground state	25
2.2.4. The smoothed potential	26
2.3. Bogoliubov Excitations	29
2.3.1. The free Bogoliubov problem	30
2.3.2. The inhomogeneous Bogoliubov problem	33
2.3.3. Disorder expansion of the Bogoliubov Hamiltonian	35
2.3.4. Bogoliubov mean-field	38
2.4. Single scattering event	38
2.4.1. Single scattering setting	39
2.4.2. Limiting cases of the elastic scattering amplitude	40
2.4.3. Analytical prediction for arbitrary $k\xi$	41
2.4.4. Numerical verification	44
2.4.5. One-dimensional setting	46

2.5.	Exact diagonalization of the Bogoliubov problem	47
2.5.1.	Analogy to other bosonic systems	48
2.5.2.	Bogoliubov-de-Gennes equations	48
2.5.3.	Zero-frequency mode	50
2.5.4.	Eigenstates of non self-adjoint operators	50
2.5.5.	Bogoliubov eigenstates with non-zero frequency	51
2.5.6.	Non-condensed atom density	54
2.6.	Conclusions on Gross-Pitaevskii and Bogoliubov	56
3.	Disorder	57
3.1.	Optical speckle potential	58
3.1.1.	Speckle amplitude	59
3.1.2.	Generalization to 3D	60
3.1.3.	Intensity and potential correlations	61
3.2.	A suitable basis for the disordered problem	63
3.2.1.	Bogoliubov basis in terms of free particle states	64
3.2.2.	Bogoliubov basis in terms of density and phase	64
3.3.	Effective medium and diagrammatic perturbation theory	66
3.3.1.	Green functions	66
3.3.2.	The self-energy	68
3.3.3.	Computing the self-energy in the Born approximation	71
3.4.	Deriving physical quantities from the self-energy	73
3.4.1.	The physical meaning of the self-energy	73
3.4.2.	Mean free path	74
3.4.3.	Boltzmann transport length	75
3.4.4.	Localization length	75
3.4.5.	Renormalization of the dispersion relation	76
3.4.6.	Density of states	79
4.	Disorder—Results and Limiting Cases	81
4.1.	Hydrodynamic limit I: $\xi = 0$	83
4.1.1.	Direct derivation from hydrodynamic equations of motion	84
4.1.2.	Transport length scales	85
4.1.3.	Speed of sound	87
4.1.4.	Density of states	90
4.2.	Hydrodynamic limit II: towards δ -disorder	92
4.2.1.	Mean free path	92
4.2.2.	Speed of sound	93
4.3.	Numerical study of the speed of sound	96
4.3.1.	The numerical scheme	96

4.3.2.	Disorder average and range of validity of the Born prediction	98
4.3.3.	Non-condensed fraction	100
4.3.4.	Speed of sound as function of the correlation length	101
4.4.	Particle regime	102
4.4.1.	Mean free path	102
4.4.2.	Renormalization of the dispersion relation in the Bogoliubov regime	103
4.4.3.	Transition to really free particles	105
4.4.4.	Closing the gap with a Gross-Pitaevskii integration	106
4.4.5.	Conclusions on the particle limit	108
5.	Conclusions and Outlook (Part I)	109
5.1.	Summary	109
5.2.	Experimental proposals	110
5.3.	Theoretical outlook	111
II.	Bloch Oscillations	113
6.	Bloch Oscillations and Time-Dependent Interactions	115
6.1.	Introduction	115
6.1.1.	Bloch oscillation of a single particle	116
6.1.2.	Experimental realization	117
6.1.3.	Time dependent interaction $g(t)$	118
6.2.	Model	118
6.2.1.	Tight binding approximation	119
6.2.2.	Smooth-envelope approximation	120
6.3.	Periodic solutions	122
6.4.	Numerical examples	123
6.5.	Collective coordinates	124
6.5.1.	Breathing dynamics in the stable cases	127
6.5.2.	Unstable cases—decay mechanisms and other dynamics	127
6.6.	Dynamical instabilities	130
6.6.1.	Linear stability analysis of the infinite wave packet	130
6.6.2.	Bloch periodic perturbations	131
6.6.3.	Unstable sine	132
6.6.4.	Robustness with respect to small perturbations	133
6.7.	Conclusions (Part II)	136
A.	List of Symbols and Abbreviations	137

List of Figures

1.1. Time-of-flight images of Bose-Einstein condensation	7
1.2. Observation of sound propagation	8
2.1. Bunching of bosons in a minimal system	18
2.2. Condensate density profile in presence of an impurity	29
2.3. Bogoliubov dispersion relation	32
2.4. Bogoliubov scattering vertex	35
2.5. 2D single-scattering setup	39
2.6. First-order scattering envelope functions	43
2.7. Fourier analysis of the stationary scattering state	44
2.8. Elastic scattering amplitude	46
2.9. Transmission of Bogoliubov excitations across a narrow im- purity	47
3.1. Schematic representation of the disordered Bogoliubov setting	57
3.2. Principle of the speckle phenomenon	58
3.3. Speckle correlation functions in $d = 1, 2, 3$	62
3.4. Geometry of the scattering process	78
3.5. Bogoliubov density of states	79
4.1. Parameter space of the full Bogoliubov problem	81
4.2. Relative correction of the speed of sound (at $k\xi = 0.05$)	82
4.3. Mean free path and Boltzmann transport length	86
4.4. Disorder-averaged dispersion relation (at $\xi = 0$)	89
4.5. Correction of the density of states (at $\xi = 0$)	91
4.6. Typical virtual scattering event in the regime $k\sigma \ll 1, k\xi \ll 1$	93
4.7. Relative correction of the dispersion relation (at $k = 0$)	95
4.8. Speckle potential and ground-state density profile	97
4.9. Histograms of the correction to the speed of sound	98
4.10. Correction to the speed of sound as function of the disorder strength	99
4.11. Increase of the non-condensed density n_{nc} due to disorder	101
4.12. Relative disorder correction $M_N = (\bar{\epsilon}_k - \epsilon_k)\mu/V_0^2$ (at $k\xi = 10$)	104
4.13. Real part of the self-energy for individual atoms	106
4.14. Transition from the Bogoliubov regime to free-particle plane waves	107

5.1. Localized Bogoliubov quasiparticles in three dimensions . . .	112
6.1. Schematic representation of the setting for Bloch oscillations	115
6.2. Sketch of the dispersion relation in a lattice	116
6.3. Sketch of the intensity of two counter-propagating laser beams	117
6.4. Typical initial state for Bloch oscillations	119
6.5. Time evolution of stable Bloch oscillations	123
6.6. Real-space portraits of Bloch oscillations for several modulations $g(t)$	125
6.7. Key quantities of the Bloch oscillation with double Bloch period	127
6.8. Contraction of the Bloch oscillating wave packet	128
6.9. Drift and damping of the centroid motion	129
6.10. Growth of the most unstable mode	133
6.11. Rigid and breathing soliton under harmonic perturbation $g_1 \sin(Ft)$	134
6.12. Stability map	135

List of Tables

1.1. Typical temperatures and particle densities in BEC experiments	7
6.1. Collective-coordinates parameters for Gaussian and soliton-shaped wave packets	126

List of Boxes

2.1. Feynman diagrams of the condensate function Φ	27
3.1. Feynman rules: drawing and computing irreducible diagrams	70

1. Interacting Bose Gases—Complex Dynamics in Lattices and Disorder

This work is dedicated to the intriguing interplay of *interaction* and *inhomogeneous potentials*. Often these elements tend to produce opposite physical effects. Each of them separately is in general well understood, but together, they lead to complicated physical problems. A good starting point is solving the problem of one competitor alone, and then adding the other one. In [part I](#), we start with the homogeneous interacting Bose gas and then add a disorder potential as perturbation. In [part II](#), we proceed the other way around: We start with the non-interacting Bloch oscillation in a tilted lattice potential, and then switch on the particle-particle interaction.

The main ingredients *disorder* and *interaction* are ubiquitous in nature. Both of them have dramatic effects on transport properties. Disorder can induce Anderson localization of waves [\[1\]](#), which suppresses diffusion and conduction. In lattice systems, described by the Bose-Hubbard model, repulsive interaction drives the transition from superfluid to the Mott insulator [\[2–4\]](#).

The physical system of choice is a *Bose-Einstein condensate* (BEC) formed of an ultracold atomic gas. Bose-Einstein condensation is a quantum-statistical effect that occurs at high phase-space density: at sufficiently low temperature and high particle density, macroscopically many particles condense into the single-particle ground state. With some efforts, this exotic state of matter is achieved in the laboratory. The wave function of the condensate is a macroscopic quantum object and features macroscopic phase coherence. Thus, Bose-Einstein condensates can interfere coherently [\[5, 6\]](#), just like the matter wave of a single particle or coherent light in Young’s double-slit experiment.

Ultracold-atom experiments are not only a very interesting field of physics by themselves, but can also serve as model systems for problems from other fields of physics. For example, the Bose-Hubbard model [\[4\]](#), and the phenomenon of Bloch oscillation [\[7, 8\]](#) are realized experimentally. There are analogies with completely different fields of physics. For example, dilute Bose-Einstein condensates are well described by the Gross-Pitaevskii equation, a prototypical nonlinear wave equation, also known as the nonlinear

Schrödinger equation, which describes, for example, wave packets of water waves [9] and self-focusing laser pulses in nonlinear optical media [10].

After Anderson's discovery of localization [1], *disordered* systems of electrons and bosons have been studied for decades. A major difficulty comes from the interplay of disorder with *interactions*. At first, electronic systems were of interest [11], but with the experimental research on superfluid Helium, also bosons came into focus. Repulsive interaction among bosons prevents the condensation into the localized single-particle ground state and keeps the gas extended. Early works on the so-called *dirty boson problem* used renormalization techniques in one dimension [12, 13]. Others studied bosons on disordered lattices, the disordered Bose-Hubbard model [2, 14, 15], where a random on-site potential models disorder.

Because of to the complexity of the problem, there are still many open questions. There is a vast parameter space to cover: lattice vs. continuous systems, uncorrelated vs. correlated disorder, and the dimension of the system. The theoretical interest is kept alive by experimental progress in both lattice systems and continuous systems of ultracold atoms, where interaction, artificial disorder and the effective dimension can be controlled practically at will.

In the following, we consider the basic ingredients *lattice*, *disorder*, *interaction* and *cold-atom experiments* in some more detail.

1.1. Lattices

Physics in lattice potentials is very important for our understanding of solids. A typical question is, for example, why certain materials are electrical conductors, while others are insulators.

Many solids, like metals, ice or graphite, have a crystal structure, i.e. the atoms or molecules of the material are arranged on a lattice with perfect periodicity. The electrons experience this lattice as a periodic potential. Even weak lattice potentials have dramatic effects when the de Broglie wave length of the particle comes close to the lattice period. In momentum space, this point marks the edge of the Brillouin zone, where a *band gap* occurs (section 6.1). If the lattice potential is strong, the system is efficiently described with a tight-binding ansatz, i.e. a single-band description.

1.2. Disorder

Idealized models, like infinitely extended perfect crystals, can explain a great deal of physical phenomena, but some important features are missed. Disorder is nearly always present in nature and can have dramatic effects on transport properties in all kinds of media. In solid-state physics, disorder appears in the guise of impurities and displacements in crystals, which influence the dynamics of electrons and phonons.

Anderson localization and weak localization

Disorder can lead to coherent localization of waves, which means the suppression of diffusion [1, 17]. In the case of electrons, this implies the suppression of electrical conductivity. Localization relies on the interference of waves and occurs also for other types of waves, like microwaves [18], light [19, 20], ultrasound [21], water waves [17, Sec. 3.5], and atomic matter waves [22–26].

Localization phenomena depend crucially on dimension [17, 27]. Scaling theory [28] allows general statements on localization. In one dimension, all states are exponentially localized, no matter how weak the disorder. Also in two dimensions, all states are in principle localized, but the localization lengths are exponentially large and often exceed the relevant length scales of experimental setups. In three dimensions, localized and delocalized states coexist. Phonons are delocalized at low energies, separated by the so-called mobility edge from high-energy localized states [29, 30]. Electron states are localized at both upper and lower band edge, with delocalized states in the center of the band [11, 29].

Originally, Anderson localization is a linear phenomenon, without interactions between the particles playing a role. For electrons, things are complicated by the Coulomb interaction [11]. Pure localization without interaction effects can, for example, be observed for light propagating through a cold gas, with the disorder realized by the random positions of the atoms [19, 20]. In cold-atom experiments, one can reverse the roles of light and atoms: in the speckle field of a laser, the atoms are subject to a random potential proportional to the laser intensity [22, 23]. In both settings, the constructive interference of paths along closed scattering paths survives the disorder average and leads to enhanced backscattering. This regime of enhanced return probability is termed weak localization.

Quantum heat transport

Chains of harmonic oscillators are a simple model for the heat conductivity by phonons. Due to the integrability of the linear equations of motion, the heat transport is ballistic and the temperature gradient vanishes. Apart from the introduction of nonlinearities, *disorder* contributes to a finite heat resistance in such systems, because the eigenstates of the chain become localized. Indeed, in the disordered harmonic chain, a finite temperature gradient is found [31], however, the heat resistance does not scale linearly with the length of the chain as one would expect according to Fourier's law.

1.3. Interaction

Interaction effects among the particles can dramatically change the properties of physical systems. In contrast to fermions, bosons are not subject to the Pauli exclusion principle. They can come much closer to each other, such that interaction effects are more relevant.

Interaction and disorder

The problem of interacting disordered bosonic systems is known as the *dirty boson problem*. Historically, it emerged in the context of superfluid Helium in aerosol glasses (Vycor) [32] and has been subject of theoretical research for a long time [2, 13]. In absence of interactions, bosons in disordered environments will condense into the lowest-energy state, which is a localized state. This phase is known as the Lifshits glass. A repulsive interaction among the particles causes them to delocalize and finally leads to the disordered BEC phase [33]. The non-interacting Bose gas is extremely sensitive to external inhomogeneities like disorder. Thus, the non-interacting ground state is not a good starting point for perturbation theory. For this reason, the strategy in [part I](#) of this work is to start with a homogeneous interacting system and then to introduce disorder perturbatively.

Interaction and lattices

The Hubbard model describes interacting fermions or bosons (Bose-Hubbard model) on a lattice within the tight-binding approximation. The interaction drives the transition from the superfluid to the Mott insulator. At integer filling factor, i.e. with the same number of particles at each lattice site, the interaction causes an energy gap that suppresses the motion of the particles.

Even without disorder, the Bose-Hubbard model offers rich physics and its phase diagram is still a subject of very active research [34].

In [part II](#) of this work, an interacting bosonic system will be studied in the mean-field version of the Bose-Hubbard model, which is known as the discrete Gross-Pitaevskii equation.

1.4. Cold-atoms—Universal model systems

In experiments with ultracold atoms, lattice potentials, disorder and interactions are brought together. Ultracold atoms are a very exciting topic for their own sake, but they are also very useful to model problems from different fields of physics [35–37]. In solid-state physics it is difficult to access and to manipulate system parameters directly. Let us, for example, consider electrons in a metal. There is no way of changing the lattice spacing, the lattice strength and the Coulomb interaction. In addition, the experimental access is limited.

Thanks to the experimental progress in the past years, cold atoms in magnetic and optical traps have become very well controllable. They can be used to model solid-state systems, with the system parameters selectively tunable and a more flexible access for measurements.

Tailoring potentials

By virtue of the Zeeman effect, atomic energy levels are shifted by magnetic fields, depending on the magnetic quantum number. The Zeeman shift is proportional to the magnitude of the magnetic field. This allows trapping a spin-polarized gas in suitable magnetic configurations [38].

The trapped atoms can then be manipulated by optical means. If the field of a laser couples to an internal transition of the atoms, it induces a *light shift* of the energy levels [39]. This results in a potential proportional to the intensity of the laser field, and allows the potential to be controlled on length scales of the laser wave length. Optical lattice potentials can be realized with two counter-propagating laser beams. This allows producing optical crystals that are much cleaner than real crystals. The phenomenon of Bloch oscillations in tilted lattices, for example, is so sensitive to dephasing that it cannot be observed in real solids. In ultracold atoms in optical lattices, however, Bloch oscillations can be observed [40, 41]. In highly anisotropic traps, the dynamics in certain directions can be completely frozen. This allows effectively one-dimensional and two-dimensional experiments to be realized [42].

Tuning the interactions

In contrast to electrons, the atoms are neutral and have only short-range interactions. Typically, the average particle distance is much larger than the scattering length, a length that describes the strength of s-wave scattering. For many atom species used in cold-atom experiments, the scattering length for atom-atom scattering can be tuned by means of a Feshbach resonance [43–46]. The basic idea is to tune the unbound scattering state into resonance with a bound state (molecule). This is done using the Zeeman shift induced by an external magnetic field. At the resonance, the scattering length has a pole. Together with the background scattering length, this allows the scattering length to be tuned to arbitrary positive or negative values. It is even possible to switch off the atom-atom interactions.

1.5. Cold atoms—History and key experiments

Bose-Einstein condensation

Bose and Einstein established the theory of Bose-Einstein statistics in 1924 and 1925 [47, 48]. The key idea is that quantum particles are indistinguishable, i.e., two states that differ only by the interchange of two particles are actually the same state. Considering a non-interacting Bose gas in three dimensions, Einstein realized that at a given temperature only a finite number of particles can populate the excited states. When more particles are added to the system, they condense into the lowest energy state, whose occupation number diverges (section 2.1). The critical particle number, however, turned out to be so large that for many decades it was impossible to reach sufficiently low temperatures and sufficiently high densities without the particles forming a liquid or a solid, due to their interactions.

The first experiments that came close to Bose-Einstein condensation were experiments with superfluid helium [49]. However, neither ^3He nor ^4He can be regarded as a direct realization of Einstein’s condensate of the non-interacting gas. ^3He atoms are fermions and have to be described by BCS theory [50], and ^4He is dominated by interactions, which makes it more a liquid than an ideal gas.

In the nineteen-eighties and nineties, a lot of effort was made to create a weakly interacting BEC of spin-polarized hydrogen and of gases of alkali atoms. In 1995, the alkali experiments were successful: a sodium BEC was realized at MIT [51], a rubidium BEC at JILA [38] and a lithium BEC at Rice University [52]. A few years later, also the hydrogen experiment was successful [53]. In the past years, alkali BECs have become the workhorses

Table 1.1.: Typical temperatures and particle densities in BEC experiments

	$T[\mu\text{K}]$	$\rho[\text{cm}^{-3}]$
Sodium, [51, MIT]	2	10^{14}
Rubidium, [38, JILA]	0.17	2.5×10^{12}
Lithium, [52, Rice]	~ 0.2	not measured
atmosphere	300×10^6	3×10^{19}

for all kinds of experiments. In 2001, E. A. Cornell (JILA), C. E. Wieman (JILA), and W. Ketterle (MIT) were awarded the Nobel prize in physics “for the achievement of Bose-Einstein condensation in dilute gases of alkali atoms, and for early fundamental studies of the properties of the condensates”.

The atom densities in BEC experiments are very limited because most elements form liquids or a solids at low temperatures, due to their interactions. At reduced densities, the temperatures required for Bose-Einstein condensation become even lower and demand sophisticated trapping and cooling techniques (evaporative cooling) [38, 51, 52]. Compared with atmospheric conditions, temperatures and densities in the alkali BECs are incredibly low (table 1.1).

With these experiments, the phenomenon of Bose-Einstein condensation predicted 70 years earlier became directly accessible. The population of the ground state can be observed rather directly by taking time-of-flight absorption images [38, 51]. The trapping potential is switched off and the condensate expands, converting its momentum distribution to a real-space distribution, which can be observed by taking absorption images. In these images, a bi-modal distribution consisting of the condensate fraction around

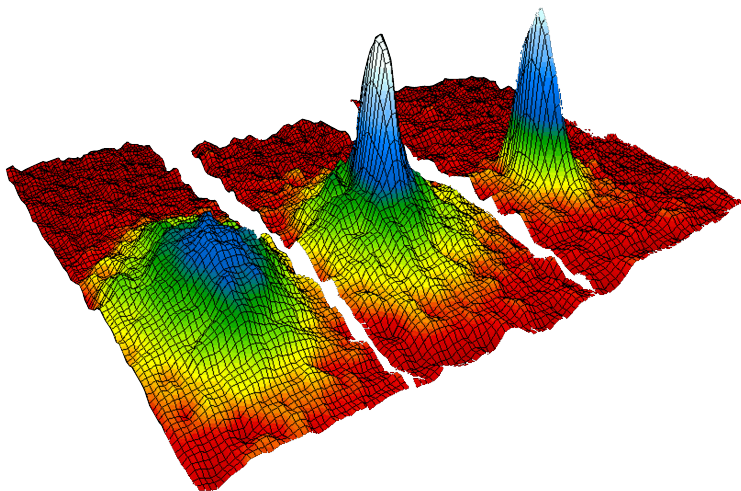
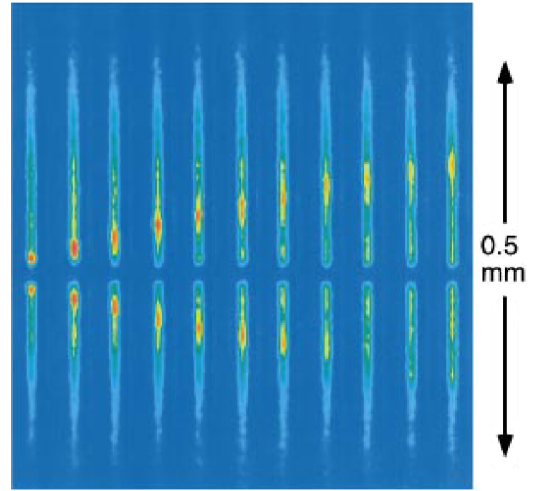


Figure 1.1: The time-of-flight images from [51] (taken from [JILA web page](#)) show the momentum-space portrait of the rubidium cloud: thermal cloud (left), bi-modal distribution (middle), condensate (right).

Figure 1.2: Observation of sound propagation in a condensate by nondestructive rapid phase-contrast imaging. An image was taken every 1.3 ms, beginning 1 ms after switching on the repulsive laser in the center. Two pulses travel outward with the speed of sound. Taken from [57].



$k = 0$ and the thermal cloud marks the transition from the thermal cloud to the Bose-Einstein condensate, [figure 1.1](#).

Interaction in BECs

In dilute alkali condensates, the atoms interact only weakly. Nevertheless, interactions play a crucial role. They deform the condensate compared with the single-particle ground state. In a harmonic trap, the shape of the condensate changes from the harmonic-oscillator ground state to the Thomas-Fermi inverted parabola density-profile ([subsection 2.2.3](#)). In presence of disorder, repulsive interaction stabilizes the condensate against fragmentation and condensation into the localized lowest-energy state.

Bogoliubov excitations

The low-energy excitations differ significantly from the non-interacting condensate. Instead of single particles excited from zero momentum to some finite momentum, the low-energy excitations are collective, similar to a classical sound wave, where all the particles oscillate back and forth. As function of momentum, the excitation spectrum begins linearly. The slope defines the speed of sound c , which, according to Landau's criterion, implies superfluidity [54, 55]. Objects moving relative to the condensate with velocities lower than $v_c = c$ cannot create any excitations and the dynamics is completely dissipationless. This principle was used in one of the early measurements of the speed of sound in a BEC [56]. There, the condensate was stirred with a repulsive laser beam and a rapid heating was observed as soon as the stirring speed exceeded the critical velocity.

More directly, the speed of sound in a BEC was measured by locally perturbing the condensate with a repulsive laser beam and by observing the ensuing propagation in real space [57] (figure 1.2).

A very powerful method is Bragg spectroscopy [58–64]. In a two-photon process, the response to a given momentum and energy transfer is measured. This allows determining the static and dynamic structure factors, which contain the dispersion relation of the excitations, in particular the speed of sound.

Disorder expansion-experiments

Cold-atom experiments offer the opportunity for the direct observation of Anderson localization of matter waves [65]. For this purpose, artificial disorder is created in the clean experimental setup. Such a disorder potential can be attained using the speckle field of the random superposition of coherent waves from a laser [66, 67] (section 3.1). In the expansion experiments in Palaiseau [25, 67–69] and in Florence [70], a BEC was released from a tight trap to a one-dimensional wave guide superposed with a disorder potential. The initial interaction energy is converted into kinetic energy. After the initial expansion, the interaction energy is negligible and the phenomenon of Anderson localization of non-interacting particles can be observed. The atoms populate localized states and the expansion stops. The localization length is determined from the envelope of the density profile.

Optical lattices

The standing wave of counter-propagating laser beams can be used as a lattice potential for modeling solid-state systems. This allows implementing and investigating solid-state models like the Bose-Hubbard model [4]. The wave phenomenon of Bloch oscillation is very sensitive to dephasing (section 6.1). Because of that, Bloch oscillations are not observable in usual solids, but cold-atom experiments offer very clean conditions, such that the observation of Bloch oscillations became possible [8]. By taking advantage of a Feshbach resonance, i.e. by tuning the s-wave scattering length to zero, it is possible to observe very long-living Bloch oscillations over more than 10 000 cycles [40].

1.6. Standing of this work

This thesis consists of two main parts. Both of them try to shed some light on open questions in the field defined by the corner stones *lattice dynamics*, *disorder*, and *interactions*.

Part I: The disordered Bogoliubov problem

In the first part, the Bogoliubov excitations [71] of a disordered Bose-Einstein condensate are studied. These excitations are essential for the properties of the Bose gas. They determine, for example, the critical velocity of superfluidity and thermodynamical properties like the heat capacity. Bogoliubov excitations are the Goldstone modes [72] associated to the $U(1)$ symmetry breaking of the BEC phase transition. They are intimately connected to that phase transition and have a great importance for the phase diagram of disordered Bose gases [73–75]. The question about the impact of disorder on the properties and the phase diagram of interacting Bose gases can thus be phrased “How does the disorder potential influence the elementary excitations of the system?”

After the experiment-oriented point of view in the previous section, let us now have a look at fundamental theoretical work. The concepts of Bose-Einstein statistics were derived in the nineteen-twenties by Bose [47] and Einstein [48], including the prediction of Bose-Einstein condensation. A milestone in the study of *interacting* bosons was Bogoliubov’s approach [71], where the classical treatment of the condensate mode leads to the concept of quasiparticles, which interpolate between collective low-energy excitations and free-particle excitations at high energies (subsection 2.3.1). More detailed studies of the interacting Bose gas followed and took into account the depletion of the condensate mode due to interactions [76].

What is known about disordered Bogoliubov excitations, what is not?

The works mentioned above aimed mainly on the bulk properties of superfluid helium. Some time later, *disordered* interacting Bose gases came into focus. Much of our present knowledge on disordered BEC traces back to Huang and Meng [77] and Giorgini, Pitaevskii and Stringari [78]. In both works, uncorrelated disorder in three dimensions was considered and quantities like the superfluid fraction and the depletion of the zero-momentum mode due to disorder and interaction were calculated.

Many other different aspects of disordered interacting bosons were studied, but the picture is still far from complete in the details. Many approaches

are restricted to a particular parameter range. There are several works dealing with Bogoliubov excitations and disorder, using methods that are restricted to one dimension, like the transfer-matrix approach [79] or the phase formalism [33, 79]. Often, the disorder is approximated by an uncorrelated white-noise disorder. In present-day experiments, however, the situation is usually different. For speckle potentials (section 3.1), the finite correlation length can in general not be neglected.

One of the central quantities of interest is the *speed of sound* in disordered Bose gases. I.e. the dispersion relation at low energies, entering the Landau criterion of superfluidity. The question how the speed of sound is influenced by disorder has been investigated in different parameter regimes and dimensions with different methods leading to different predictions. Using perturbation theory, Giorgini *et al.* [78] find a positive correction for uncorrelated disorder in three dimensions, which has been reproduced by Lopatin *et al.* [75] and Falco *et al.* [80]. Within a self-consistent non-perturbative approach, Yukalov and Graham [81, 82] report a *decrease* of the sound velocity in three dimensions, even in the case of δ -correlated disorder, which is in clear contradiction to [78]. For disordered hard-core bosons on a lattice, Zhang [83] finds a decrease of c to fourth order in disorder strength, without information on the second-order effect.

Thus, the knowledge of the speed of sound in disordered systems is far from comprehensive. A major goal of this work is to provide a formalism for describing the excitations of disordered BEC, that covers a range of parameters as wide as possible. In particular, different dimensions and arbitrary types of disorder should be covered.

The disordered Bogoliubov problem is not expected to be simple. Concerning the spectrum of the non-uniform Bose gas, Nozières and Pines write in their book *Theory of Quantum Liquids* [84, chapter 10]:

In practice, one faces enormous mathematical difficulties, except in the case of the ground state, for which $\Phi(\mathbf{r})$ is constant ... The coupled equations (...) [equation (2.65) in this work], though certainly complex in character, are rich in physical content. It may be expected that detailed study of these and similar equations will yield much new information concerning the non-uniform superfluid Bose liquid.

In this work, this very problem is tackled, in the case where the condensate is non-uniform due to a *disorder* potential.

Strategy of this work and a short peek at the main results

We are interested in the disordered problem, where the particular potential is unknown. This makes it impossible and also undesirable to compute the spectrum and the eigenstates explicitly. Instead, the spectrum is computed in the disorder average, by means of a diagrammatic approach. The structure of [part I “The Disordered Bogoliubov Problem”](#) is as follows.

In [chapter 2](#), the general framework is set up for the treatment of a Bose-Einstein condensate and its Bogoliubov excitations in presence of a weak external potential. Starting from the very concepts of Bose statistics and Bose-Einstein condensation, we derive the Gross-Pitaevskii mean-field framework ([subsection 2.2.2](#)). Subsequently, the ground state is treated in a mean-field manner, but the excited particles are described fully quantized. The expansion of the many-particle Hamiltonian around the mean-field ground state leads to the inhomogeneous Hamiltonian for Bogoliubov excitations ([section 2.3](#)). Via the Gross-Pitaevskii equation, this Hamiltonian depends nonlinearly on the external potential. As a first application, the scattering of Bogoliubov quasiparticles at a single impurity is discussed in detail ([section 2.4](#)). Finally, the general structure of the Bogoliubov Hamiltonian is discussed, in particular the orthogonality relations of its eigenstates.

[Chapter 3](#) is dedicated to the disordered Bogoliubov problem. The experimentally relevant speckle disorder potential and its statistical properties are discussed in [section 3.1](#). Then, in [section 3.2](#), a suitable basis for the disordered Bogoliubov problem is found. All findings then enter in the diagrammatic perturbation theory of [section 3.3](#), which leads to the concept of the effective medium with the disorder-averaged dispersion relation $\bar{\epsilon}_k$, determined by the self energy Σ . In physical terms, this yields corrections to quantities like the density of states, the speed of sound and the mean free path.

The theory derived is indeed valid in a large parameter space: the excitations considered can be particle-like or sound-like, the disorder potential can be correlated or uncorrelated on the length scale of the wave length, and the condensate can be in the Thomas-Fermi regime or in the smoothing regime, depending on the ratio of condensate healing length and disorder correlation length.

The discussion of the results in the different regimes of the parameter space deserves a separate chapter, which is given in [chapter 4](#). Concerning the speed of sound, the main results are:

- The correction due to uncorrelated disorder depends on the dimension. The leading correction is positive in three dimensions and negative in one dimension. In two dimensions, the speed of sound remains unaffected.
- For *correlated* disorder, the speed of sound is *reduced*, independent of the dimension.

In the case of uncorrelated disorder in three dimensions, the result of this work reproduces previous results [[75](#), [78](#), [80](#)]. To my knowledge, the results in lower dimensions and in correlated disorder are new.

The corrections to the speed of sound depend non-monotonically on the disorder correlation length. In the density of states, this results in an interesting signature. In one dimension, a sharp peak in the density of states is found at $k\sigma = 1$.

The “condensate depletion” computed by Huang and Meng and Giorgini *et al.* [[77](#), [78](#)] is interpreted as a mere deformation of the Gross-Pitaevskii condensate. We compute numerically the “Beyond-Huang-Meng” non-condensed fraction ([subsection 2.5.6](#) and [4.3.3](#)).

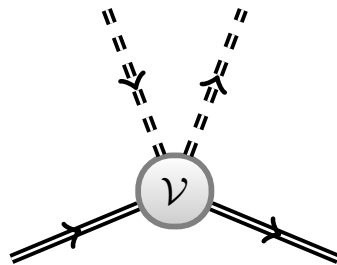
Part II: Bloch oscillations with time dependent interactions

In [part II](#), lattice dynamics are discussed, more precisely Bloch oscillations of Bose-Einstein condensates in tilted lattice potentials with time-dependent interactions. This topic might appear rather exotic and far-fetched at this point, but as pointed out above, all experimental requirements are available and interesting new physics waits to be discovered. The main finding of this part is, that by modulating the interaction in a suitable way it is not only possible to maintain the Bloch oscillation, but also to make it more robust against certain perturbations.

A more detailed introduction to the subject is given in [section 6.1](#).

Part I.

The Disordered Bogoliubov Problem



2. The Inhomogeneous Bogoliubov Hamiltonian

In this chapter, the framework for describing dilute Bose gases in weak external potentials is derived. Before starting with the actual problem of the interacting gas in a given external potential, we shortly review the mechanism of Bose-Einstein condensation at the example of the ideal Bose gas (section 2.1). Then, in section 2.2, we formulate the interacting many-particle problem and perform the mean-field approximation, which allows the Gross-Pitaevskii ground state to be computed.

The essential of this chapter is the saddlepoint expansion around the disorder-deformed condensate state (section 2.3). This yields the Hamiltonian and the equations of motion for Bogoliubov excitations in presence of the external potential. For illustration and as a numerical test, scattering of a Bogoliubov excitation at a single impurity is discussed analytically and compared to a numerical integration (section 2.4).

The Bogoliubov excitations disclose information beyond the mean-field ground-state, in particular the fraction of non-condensed atoms that are present even in the ground state. In section 2.5, important properties of Bogoliubov eigenstates, in particular their orthogonality relations, are discussed. The orthogonality to the zero-frequency mode will be of particular importance when choosing the basis for the disordered problem in chapter 3.

In order to be self-contained, this chapter reports some basic topics that can be found in books and review articles. For more details, the reader is referred to the reviews by Dalfovo, Giorgini, Pitaevskii and Stringari [85] and by Leggett [86], and the books by Pethick and Smith [54] and Pitaevskii and Stringari [55].

2.1. Bose-Einstein condensation of the ideal gas

In the following, the basic ideas of the phenomenon of Bose-Einstein condensation are presented, using the example of the ideal Bose gas. For the ideal gas, the partition function can be calculated analytically, which leads to the derivation of Bose-Einstein statistics.

2. The Inhomogeneous Bogoliubov Hamiltonian

As a matter of principle, quantum particles and quasiparticles, like electrons, photons, nucleons or atoms, are indistinguishable. Interchanging two particles may only change the many-particle wave function by a phase factor e^{ia} , but all physical quantities stay invariant. Interchanging the particles twice recovers the initial state, such that $e^{i2a} = 1$. The only two possibilities are $e^{ia} = \pm 1$, i.e. to change or not to change sign when interchanging two particles. The former possibility is realized for fermions. For them, the anti-symmetry results in the Pauli exclusion principle, forbidding more than one particle in the same single-particle state. The other possibility is realized for bosons, whose wave functions are symmetric under permutation of particles. Compared with classical statistics, the statistical weight of permutations is lost, such that the agglomeration of particles is preferred, although there is no attractive interaction present. For the basic idea, see also [figure 2.1](#).

2.1.1. Partition function and Bose statistics

Let us quantitatively investigate the phenomenon of preferred agglomeration by considering the grand canonical partition function $Z = \text{tr} \left\{ \exp \left[-\beta (\hat{H} - \mu \hat{N}) \right] \right\}$ of an ideal Bose gas. Here, \hat{H} is the Hamilton operator, \hat{N} is the total particle-number operator, $\beta = (k_B T)^{-1}$ is the inverse thermal energy, and the chemical potential μ controls the particle number as a Lagrange multiplier. The trace is taken in the Fock representation ([subsection 2.2.1](#)), where every many-particle state is defined by the occupation numbers of the single-particle states of a certain basis. Choosing the energy states of the non-interacting Hamiltonian as basis, we can express the Hamiltonian and the total number operator in terms of the number operator \hat{n}_i : $\hat{H} = \sum_i \epsilon_i \hat{n}_i$, $\hat{N} = \sum_i \hat{n}_i$. The number operator $\hat{n}_i = \hat{a}_i^\dagger \hat{a}_i$ consists of the bosonic creation

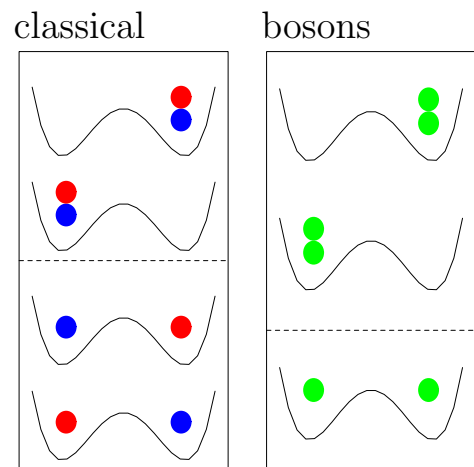


Figure 2.1: Bunching of bosons in a minimal system.

In contrast to classical particles, quantum particles are *indistinguishable*. The two classical states “red particle left, blue particle right” and vice versa are merged to a single state “one particle left and one particle right”. The probability of finding both particles at the same site is enhanced from $1/2$ to $2/3$.

and annihilation operators \hat{a}_i^\dagger and \hat{a}_i of the corresponding state. These fulfill the bosonic commutator relations

$$[\hat{a}_i, \hat{a}_j^\dagger] = \delta_{ij} \quad [\hat{a}_i, \hat{a}_j] = 0 = [\hat{a}_i^\dagger, \hat{a}_j^\dagger]. \quad (2.1)$$

For an ideal gas of non-interacting bosons, the single-particle energy eigenstates are occupied independently and the grand canonical partition function factorizes into single-state partition functions

$$Z = \sum_{\{n\}} \langle \{n\} | e^{-\beta(\hat{H} - \mu\hat{N})} | \{n\} \rangle = \prod_i \sum_{n_i=0}^{\infty} e^{-\beta(\epsilon_i - \mu)n_i} = \prod_i \frac{1}{1 - e^{-\beta(\epsilon_i - \mu)}}. \quad (2.2)$$

From the partition function, thermodynamic quantities like the average energy or the average particle number can be derived. From the total number of particles

$$N = k_B T \frac{\partial}{\partial \mu} \ln(Z) = \sum_i \frac{1}{e^{\beta(\epsilon_i - \mu)} - 1}, \quad (2.3)$$

the Bose occupation number n_i for the state with energy ϵ_i is obtained as

$$n_i = \frac{1}{e^{\beta(\epsilon_i - \mu)} - 1}. \quad (2.4)$$

The chemical potential μ has to be lower than the lowest energy level, otherwise unphysical negative occupation numbers would occur. Without loss of generality, the lowest energy level is chosen as the origin of energy $\epsilon_0 = 0$. All occupation numbers increase monotonically with μ , and the chemical potential determines $\sum_i n_i = N$.

2.1.2. Bose-Einstein condensation

The Bose occupation numbers n_i (2.4) diverge, when the chemical potential μ approaches the respective energy level ϵ_i from below. The chemical potential has to be lower than all energy levels, so this divergence can only happen to the occupation of the ground state. This suggests separating the total particle number N in the ground-state population n_0 and the number of thermal particles N_T

$$N = n_0 + N_T, \quad (2.5)$$

with $n_0 = (e^{\beta|\mu|} - 1)^{-1}$ and $N_T = \sum_{i \neq 0} n_i$. Already in 1925, Einstein pointed out, that under certain conditions, the population of the thermal states N_T

2. The Inhomogeneous Bogoliubov Hamiltonian

is bounded [48]. When even more particles are added to the system, the only choice to place them is to put them into the ground state. The population of this single quantum state with a macroscopic number of particles is called Bose-Einstein condensation.

Let us estimate the maximum number of particles in excited states. This is reached for the maximum possible value of the chemical potential $\mu = \epsilon_0 = 0$. As we treat the ground state separately, it is adequate to compute the maximum number of thermal particles at a given temperature in the continuum approximation

$$N_T^{\max} = \int d\epsilon \frac{\rho(\epsilon)}{e^{\beta\epsilon} - 1}, \quad (2.6)$$

where the density of states $\rho(\epsilon)$ typically follows a power law $\rho(\epsilon) = C_\alpha \epsilon^{\alpha-1}$, at least for the most relevant low-energy range. If the parameter α is large enough, the integral (2.6) converges. For $\alpha > 1$, the integral can be evaluated as

$$N_T^{\max} = C_\alpha (k_B T)^\alpha \Gamma(\alpha) \zeta(\alpha), \quad (2.7)$$

where the product of the gamma function $\Gamma(\alpha) = \int_0^\infty dx x^{\alpha-1} e^{-x}$ and the Riemann zeta function $\zeta(\alpha) = \sum_{n=1}^\infty n^{-\alpha}$ is a number of order one. The critical particle number at a given temperature is defined by $N_c = N_T^{\max}(T)$.

For free particles in a box with volume L^d , the density of states is given as

$$\rho(\epsilon) = L^d \frac{S_d}{2(2\pi)^d} (2m/\hbar^2)^{\frac{d}{2}} \epsilon^{\frac{d}{2}-1}, \quad (2.8)$$

with the surface of the d -dimensional unit sphere S_d . That means, the parameter $\alpha = d/2$ depends on the dimension. True Bose-Einstein condensation cannot occur in one or two dimensions, where the integral (2.7) diverges. In contrast, in three dimensions the critical particle density is $n_c = N_c/L^3 = \zeta(\frac{3}{2}) \lambda_T^{-d}$, where $\lambda_T = \sqrt{\frac{2\pi\hbar^2}{mk_B T}}$ is the thermal de Broglie wave length. As $\zeta(\frac{3}{2}) \approx 2.612$ is of order one, this condition states that Bose-Einstein condensation occurs, when the average particle spacing comes close to the thermal de Broglie wave length, $n_c(T) \lambda_T^d = \mathcal{O}(1)$. Remarkably, ideal Bose-Einstein condensation can occur at any temperature if the particle density is high enough, or conversely, at any particle density if the temperature is low enough.

In harmonic traps, the density of states is different from that of free-space, namely $\rho(\epsilon) \propto \epsilon^{d-1}$. Consequently, Bose-Einstein condensation occurs also

in two dimensions. The considerations so far are valid in the thermodynamic limit. For experimental applications, the concept has to be adapted to a finite system size and a finite particle number. This leads to corrections of the critical temperature [87, 88]. In the thermodynamic limit no Bose-Einstein condensation is predicted in 1D traps and low-dimensional boxes. Nevertheless, macroscopic ground-state populations are found in finite systems [87]. Also particle-particle interactions should enhance the phase coherence. In experiments, the coherence length is often larger than the largest length scale and the Bose gas is regarded as quasi-condensate.

Note that the critical temperature of Bose-Einstein condensation is determined by the particle density. The condensation typically occurs already for temperatures much higher than the energy gap to the first excited state ϵ_1 . Thus, it is fundamentally different from the behavior predicted by the classical Boltzmann factor $e^{-\epsilon/k_B T}$. Bose-Einstein condensation is a statistical effect, resulting from the indistinguishability and is not caused by attractive interactions.

2.1.3. Order parameter and spontaneous symmetry breaking

There is more to Bose-Einstein condensation than just the distribution of particle numbers. The single-particle state with the macroscopic particle number defines the condensate function $\Phi(\mathbf{r})$ (more precisely, the state associated with the only macroscopic eigenvalue of the density matrix). This wave function exists only in the condensed Bose gas and takes the role of the order parameter of the phase transition to the Bose-Einstein condensate. The order parameter spontaneously takes a particular phase, breaking the $U(1)$ symmetry of the non-condensed phase. By virtue of the Goldstone theorem [72], this *spontaneously broken symmetry* implies the existence of Goldstone bosons. Goldstone bosons are excitations related to the broken symmetry, in this case to a homogeneous phase diffusion with zero frequency [89]. It will turn out that the Bogoliubov excitations are the Goldstone bosons of Bose-Einstein condensation.

Experimentally, the phase of the condensate becomes accessible in interference experiments, where the phase of one condensate with respect to that of another condensate determines the position of the interference pattern.

2.2. Interacting BEC and Gross-Pitaevskii mean-field

With the concept of Bose-Einstein condensation (section 2.1) in mind, we now consider interacting Bose gases. For interacting particles, genuine many-body theory is the starting point. In a mean-field manner, the so-called Gross-Pitaevskii theory [55, 90] takes advantage of the macroscopically occupied ground state of the Bose-Einstein condensate. Fluctuations are neglected and the condensate wave function is computed.

2.2.1. Basic many-body theory

The state of N indistinguishable bosons is described by a N -particle wave function $\Psi_N(\mathbf{r}_1, \mathbf{r}_2, \dots, \mathbf{r}_N)$, which is symmetric with respect to the exchange of two particles. In order to avoid the explicit symmetrization, it is convenient to use the Fock representation. The Fock space is the direct sum of correctly symmetrized N -particle Hilbert spaces. It is only specified how many particles are in each single-particle state. The unphysical information, which of the particles is which, is not included. Starting from the vacuum state with no particles, general Fock states are constructed by means of creation operators that create a particle in a certain single-particle state. Bosonic (fermionic) commutation relations of the creation and annihilation operators guarantee that any Fock state is symmetric (antisymmetric). In real-space, the creators and annihilators are called field operators and are denoted by $\hat{\Psi}(\mathbf{r})$. They obey the bosonic commutator relations

$$[\hat{\Psi}(\mathbf{r}), \hat{\Psi}^\dagger(\mathbf{r}')] = \delta(\mathbf{r} - \mathbf{r}'), \quad [\hat{\Psi}(\mathbf{r}), \hat{\Psi}(\mathbf{r}')] = 0 = [\hat{\Psi}^\dagger(\mathbf{r}), \hat{\Psi}^\dagger(\mathbf{r}'). \quad (2.9)$$

For fermions, the commutator $[\cdot, \cdot]$ is replaced with the anticommutator. Physically, expectation values containing field operators, like the particle density $n(\mathbf{r}, t) = \langle \hat{\Psi}^\dagger(\mathbf{r}, t) \hat{\Psi}(\mathbf{r}, t) \rangle$ or the single-particle density matrix $\rho(\mathbf{r}, \mathbf{r}', t) = \langle \hat{\Psi}^\dagger(\mathbf{r}, t) \hat{\Psi}(\mathbf{r}', t) \rangle$ are the quantities of interest.

The time-evolution of any physical observable is given by the Heisenberg equation of motion for operators

$$i\hbar \frac{d}{dt} \hat{A} = [\hat{A}, \hat{H}] + i\hbar \frac{\partial}{\partial t} \hat{A}, \quad (2.10)$$

with the Hamiltonian [85]

$$\hat{H} = \int d^d r \hat{\Psi}^\dagger(\mathbf{r}) \left[\frac{-\hbar^2}{2m} \nabla^2 + V(\mathbf{r}) \right] \hat{\Psi}(\mathbf{r}) + \frac{g}{2} \int d^d r \hat{\Psi}^\dagger(\mathbf{r}) \hat{\Psi}^\dagger(\mathbf{r}) \hat{\Psi}(\mathbf{r}) \hat{\Psi}(\mathbf{r}). \quad (2.11)$$

The first part contains the kinetic energy and the potential energy due to the external potential $V(\mathbf{r})$. The interaction potential $V_{\text{int}} = g\delta(\mathbf{r} - \mathbf{r}')$ in the second part represents two-body collisions. As the atoms are neutral, this interaction is short range and the actual physical interaction has been replaced by a point interaction. In three dimensions, the parameter g depends on the s-wave scattering length a_s as $g = 4\pi\hbar^2 a_s/m$. This approximation is good in the dilute-gas limit, where the average particle distance $n^{-1/3}$ is much larger than the scattering length a_s . The external potential $V(\mathbf{r})$ is typically given by the harmonic trapping potential, possibly superposed with scattering impurities or a disorder potential.

In the Fock representation it is specified how many atoms are in each single-particle state. From the start, the Fock representation is capable of handling variable particle numbers. Thus, it is straightforward to relax the constraint of a fixed particle number by Legendre-transforming to the grand canonical Hamiltonian $\hat{E} = \hat{H} - \mu\hat{N}$. Here, the chemical potential μ controls the average particle number. In the grand canonical picture, the equation of motion of the field operator reads

$$i\hbar\frac{d}{dt}\hat{\Psi}(\mathbf{r}) = \left[-\frac{\hbar^2}{2m}\nabla^2 + V(\mathbf{r}) - \mu\right]\hat{\Psi}(\mathbf{r}) + g\hat{\Psi}(\mathbf{r})^\dagger\hat{\Psi}(\mathbf{r})\hat{\Psi}(\mathbf{r}), \quad (2.12)$$

according to equation (2.10) with \hat{H} replaced by $\hat{E} = \hat{H} - \mu\hat{N}$.

2.2.2. Gross-Pitaevskii energy functional and equation of motion

The description in terms of the many-particle Hamilton operator (2.11) holds very generally, but suitable approximations are desirable for practical use.

At sufficiently low temperatures, also the interacting Bose gas is expected to Bose-Einstein condense. In three dimensions, this can be proven rigorously [91, 92]. In one and in two dimensions, at least a quasi-condensate [93] should exist, where the phase coherence is not truly long-range, but should extend over the experimentally relevant length scales.

The macroscopically populated single-particle state is called the condensate state $\Phi(\mathbf{r})$. It is defined as the eigenstate associated to the only macroscopic eigenvalue of the single particle density matrix. The condensate wave function takes a particular phase and spontaneously breaks the $U(1)$ symmetry of the non-condensed system, such that $\Psi(\mathbf{r}) = \langle\hat{\Psi}(\mathbf{r})\rangle$ is non-zero. One can separate the field operator into its mean value and its fluctuations

$$\hat{\Psi}(\mathbf{r}) = \Psi(\mathbf{r}) + \delta\hat{\Psi}(\mathbf{r}) \quad (2.13)$$

2. The Inhomogeneous Bogoliubov Hamiltonian

and expand the problem in the quantum fluctuations $\delta\hat{\Psi}(\mathbf{r})$.¹ Later, in [subsection 2.5.6](#), we will see that the small parameter of this expansion is the gas parameter $\sqrt{na_s^3}$ [95], i.e. the range of the interaction a_s compared with the average particle spacing $n^{-\frac{1}{3}}$.

The Gross-Pitaevskii mean-field approximation consists in neglecting the quantum fluctuations $\delta\hat{\Psi}(\mathbf{r})$, i.e. the field operators in (2.11) are replaced by a complex field $\Psi(\mathbf{r})$. Equivalently, the Gross-Pitaevskii approximation is obtained from the Hamiltonian $\hat{E} = \hat{H} - \mu\hat{N}$ by a Hartree-Fock ansatz of the many-particle wave function as a pure product $\Psi_N(\mathbf{r}_i) = N^{-N/2} \prod_i \Psi(\mathbf{r}_i)$. Then, the operator (2.11) reduces to the Gross-Pitaevskii energy functional

$$E[\Psi, \Psi^*] = \int d^d r \left\{ \frac{\hbar^2}{2m} |\nabla\Psi(\mathbf{r})|^2 + [V(\mathbf{r}) - \mu] |\Psi(\mathbf{r})|^2 + \frac{g}{2} |\Psi(\mathbf{r})|^4 \right\}. \quad (2.14)$$

The equation of motion can be derived from the variation of the action $\int d^d r dt L$ with the Lagrangian

$$L = \int d^d r \frac{i\hbar}{2} \left[\Psi^* \frac{\partial\Psi}{\partial t} - \Psi \frac{\partial\Psi^*}{\partial t} \right] - E[\Psi, \Psi^*], \quad (2.15)$$

see e.g. [54, Chapter 7]. The so-called Gross-Pitaevskii equation describes the time evolution in terms of a functional derivative with respect to the conjugate field

$$i\hbar \frac{\partial}{\partial t} \Psi = \frac{\delta E}{\delta\Psi^*} = \left[-\frac{\hbar^2}{2m} \nabla^2 + V(\mathbf{r}) - \mu \right] \Psi(\mathbf{r}) + g |\Psi(\mathbf{r})|^2 \Psi(\mathbf{r}). \quad (2.16)$$

Alternatively to the Lagrangian prescription, which might appear a bit *ad hoc* at this place, the Gross-Pitaevskii equation is obtained straightforwardly from the Heisenberg equation of motion (2.12) of the many-particle problem by inserting equation (2.13) and neglecting the fluctuations. Formally, the Gross-Pitaevskii equation is very similar to the Schrödinger equation of a single particle. Kinetic and potential energy appear in the same manner, the only modification is the interaction term $g|\Psi|^2$. The Gross-Pitaevskii equation is also called nonlinear Schrödinger equation and appears in many different fields of physics [9, 10].

¹The non-vanishing expectation value of the field operator $\hat{\Psi}(\mathbf{r})$ can be rigorously defined in a coherent state: The macroscopic population of the ground state, together with the grand canonical ensemble with variable particle number, allows the construction of coherent states from superpositions of states with different particle numbers in the condensate state [94].

Formulation in terms of density and phase

For the physical interpretation it is useful to express the Gross-Pitaevskii energy functional and the corresponding equation of motion in terms of the condensate density and its complex phase. The local condensate density $n(\mathbf{r}) = |\Psi(\mathbf{r})|^2$ is normalized to the total particle number $\int d^d r n(\mathbf{r}) = N$. The complex phase of the GP wave-function $\Psi(\mathbf{r}, t) = \sqrt{n(\mathbf{r}, t)} \exp\{i\varphi(\mathbf{r}, t)\}$ is given by $\varphi(\mathbf{r}, t)$. The energy functional (2.14) then becomes

$$E[n, \varphi] = \int d^d r \left\{ \frac{\hbar^2}{2m} \left[(\nabla \sqrt{n})^2 + n(\nabla \varphi)^2 \right] + (V(\mathbf{r}) - \mu)n + \frac{g}{2}n^2 \right\}. \quad (2.17)$$

The time evolution (2.16) is rephrased and yields the equations of motion for density and phase

$$\frac{\partial}{\partial t} n = \frac{1}{\hbar} \frac{\delta E}{\delta \varphi} = -\frac{\hbar}{m} \nabla \cdot (n \nabla \varphi) =: -\nabla \cdot (n \mathbf{v}_s) \quad (2.18a)$$

$$-\hbar \frac{\partial}{\partial t} \varphi = \frac{\delta E}{\delta n} = -\frac{\hbar^2}{2m} \frac{\nabla^2 \sqrt{n_0(\mathbf{r})}}{\sqrt{n_0(\mathbf{r})}} + \frac{\hbar^2}{2m} (\nabla \varphi)^2 + g n_0(\mathbf{r}) + V(\mathbf{r}) - \mu. \quad (2.18b)$$

The first equation is the continuity equation of an irrotational fluid with superfluid velocity proportional to the phase gradient $\mathbf{v}_s = \frac{\hbar}{m} (\nabla \varphi)$ (the term *superfluid* is explained on page 31). The second equation (2.18b) describes the time evolution of the phase, whose gradient determines the velocity field. The term containing the derivatives of the density stems from the quantum mechanical kinetic energy. As it has no classical analog, it is often called quantum pressure.

The superfluid velocity is proportional to the gradient of the phase of the condensate wave function and is thus *irrotational*, i.e. a superfluid cannot rotate freely. The only possibility to rotate the superfluid is to create *vortices* in the superfluid [96, 97].

2.2.3. Ground state

In the following, the dynamics of excitations close to the ground state are of interest. The ground state $\Phi(\mathbf{r}) = \sqrt{n_0(\mathbf{r})}$, $\varphi_0(\mathbf{r}) = 0$ minimizes the energy functional (2.14) and is a stationary solution of the equations of motion (2.18). Obviously, the phase has to be homogeneous, i.e. there is no

2. The Inhomogeneous Bogoliubov Hamiltonian

superfluid flow. The density profile fulfills the stationary Gross-Pitaevskii equation

$$-\frac{\hbar^2}{2m} \frac{\nabla^2 \Phi(\mathbf{r})}{\Phi(\mathbf{r})} + g |\Phi(\mathbf{r})|^2 = \mu - V(\mathbf{r}). \quad (2.19)$$

In a flat potential $V(\mathbf{r}) = 0$, the density $n(\mathbf{r}) = n_\infty = \mu/g$ is constant. Interaction and kinetic energy define the characteristic length scale of the BEC, the *healing length* $\xi = \hbar/\sqrt{2mgn_\infty}$. The condensate changes its density on this length scale. In presence of an external potential $V(\mathbf{r})$, the solution of the nonlinear equation (2.19) is non-trivial. The limits of very strong interaction and no interaction are understood as follows:

- In the *Thomas-Fermi* (TF) regime, the kinetic energy (quantum pressure) is negligible compared with the interaction energy. The density profile is determined by the balance of the external potential and the interaction:

$$n_{\text{TF}}(\mathbf{r}) = (\mu - V(\mathbf{r}))/g \quad \text{for } \mu > V(\mathbf{r}), \text{ otherwise zero.} \quad (2.20)$$

Often, the Thomas-Fermi approximation is a reasonable approximation. However, special care has to be taken at the edges of the trap, where the condensate density seems to vanish abruptly.

- In the opposite case of a non-interacting system $g = 0$, the Gross-Pitaevskii equation reduces to the linear Schrödinger equation. In a harmonic trap, the ground state is given by the Gaussian wave function of the harmonic-oscillator ground state. In the homogeneous system, the ground state is the $\mathbf{k} = 0$ mode with homogeneous density. However, this state is very sensitive to weak perturbations, like a weak disorder potential, because there is no interaction that counteracts the localization of the wave function. Thus, the unstable non-interacting gas is not a convenient starting point for perturbation theory of the ground state.

2.2.4. The smoothed potential

In the case of an extended condensate that is modulated by a weak potential, one can perform a *weak disorder expansion* in the small parameter V/μ [99]

$$\sqrt{n_0(\mathbf{r})} = \Phi(\mathbf{r}) = \Phi_0 + \Phi^{(1)}(\mathbf{r}) + \Phi^{(2)}(\mathbf{r}) + \dots \quad (2.21)$$

With this expansion, the stationary Gross-Pitaevskii equation (2.19) is solved order by order. There are two mechanisms: (i) scattering of atoms

Box 2.1: Feynman diagrams of the condensate function (2.21)

The constituents of the diagrams are

- particles from the $\mathbf{k} = 0$ mode \vdash
- response function $S(k) = \text{---}$ from (2.22)
- potential scattering $V_q = \vdots$
- particle-particle scattering $g = \asymp$

Drawing Feynman diagrams. Starting from $\Phi^{(0)} = \vdash$, diagrams of order n are constructed from diagrams of order $n' < n$ by

- attaching a potential scattering, e.g.

$$\vdash \cdot \vdots \cdot \text{---} = \vdash \overset{\vdots}{\bullet} \text{---}$$

- by combination of several diagrams, e.g.

$$\vdash \overset{\vdots}{\bullet} \text{---} \cdot \vdash \overset{\vdots}{\bullet} \text{---} \cdot \vdash \cdot \asymp \cdot \text{---} = 3 \vdash \overset{\vdots}{\bullet} \text{---} \overset{\vdots}{\bullet} \text{---}$$

The combinatorial factor three comes from permutations.

The first diagrams read

$$\Phi = \underbrace{\vdash}_{\Phi^{(0)}} + \underbrace{\vdash \overset{\vdots}{\bullet} \text{---}}_{\Phi^{(1)}} + \underbrace{\vdash \overset{\vdots}{\bullet} \text{---} \overset{\vdots}{\bullet} \text{---} + 3 \vdash \overset{\vdots}{\bullet} \text{---} \overset{\vdots}{\bullet} \text{---}}_{\Phi^{(2)}} + \dots$$

Computing the diagrams. Each potential contributes to the momentum. At the vertices, the momentum is conserved, so the outgoing momentum (open end) is the sum of all momentum transfers by the external potentials.

$$\Phi_q^{(2b)} = \vdash \overset{\vdots}{\bullet} \text{---} \overset{\vdots}{\bullet} \text{---} = \frac{1}{L^{\frac{d}{2}}} \sum_{q'} V_{q'} S(q') V_{q-q'} S(|\mathbf{q} - \mathbf{q}'|) g S(q)$$

Finally, all free momenta are summed over.

The diagrams presented in this box are equivalent to the real-space diagrams in [98], when taken in the case of a real ground-state wave function.

2. The Inhomogeneous Bogoliubov Hamiltonian

at the external potential and (ii) scattering processes between atoms. The above expansion can be nicely written in terms of Feynman diagrams, see [box 2.1](#).

The first-order correction reads

$$\Phi_{\mathbf{k}}^{(1)} = \frac{-V_{\mathbf{k}}}{2\mu + \epsilon_{\mathbf{k}}^0} \Phi_0 =: S(k) V_{\mathbf{k}} \Phi_0, \quad (2.22)$$

where the linear response function $S(k)$ contains the kinetic energy of a free particle $\epsilon_{\mathbf{k}}^0 = \hbar^2 k^2 / (2m)$ and the chemical potential μ . Atoms from the originally homogeneous condensate are scattered once by the external potential (first-order diagram in [box 2.1](#)). The condensate wave function shows an imprint of the external potential, similar to the one described by the Thomas-Fermi formula (2.20), but variations on length scales shorter than the healing length ξ are suppressed. This smoothing is due to the cost of the kinetic energy $\epsilon_{\mathbf{k}}^0$ that was neglected in the Thomas-Fermi formula. In [figure 2.2](#), the density depression of a rather narrow impurity potential is shown. The density dip of the first-order result (2.22) is broader and shallower than that predicted by the Thomas-Fermi formula. The real-space representation is given as the convolution of the bare potential with a smoothing kernel given by the d -dimensional inverse Fourier transform of $[2\mu + \epsilon_{\mathbf{k}}^0]^{-1}$.

The second order contains double scattering processes and reads

$$\Phi_{\mathbf{k}}^{(2)} = S(k) \frac{1}{L^{\frac{d}{2}}} \sum_{\mathbf{q}} \left[V_{\mathbf{k}-\mathbf{q}} + 3g\Phi_0\Phi_{\mathbf{k}-\mathbf{q}}^{(1)} \right] \Phi_{\mathbf{q}}^{(1)}. \quad (2.23)$$

The processes contained in this formula are double scattering at the external potential and interaction of two single-scattered particles, see [box 2.1](#). In [figure 2.2](#) it is demonstrated, that the second order leads to a very satisfying agreement with the exact solution of the Gross-Pitaevskii equation, even for a rather strong potential.

Rephrasing in terms of density and smoothed potential

Motivated by the Thomas-Fermi formula (2.20), one can cast the imprint of the potential into a smoothed potential $\tilde{V}(\mathbf{r})$, which is expanded in orders of the small parameter

$$n_0(\mathbf{r}) = \frac{1}{g} \left[\mu - \tilde{V}^{(1)}(\mathbf{r}) - \tilde{V}^{(2)}(\mathbf{r}) + \dots \right]. \quad (2.24)$$

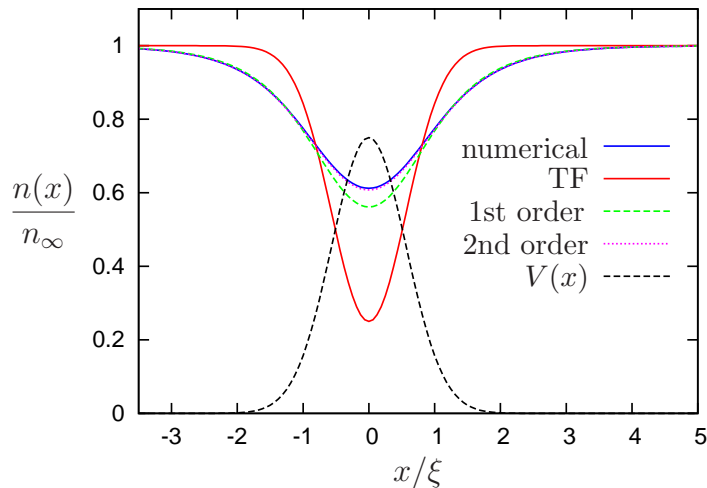


Figure 2.2.: The condensate density profile in presence of an impurity $V(x) = V_0 \exp(-x^2/r_0^2)$. For the parameters $V_0 = 0.75\mu$ and $r_0 = 0.8\xi$, the numerically obtained Gross-Pitaevskii ground state (solid blue) differs significantly from the simple Thomas-Fermi formula (2.20) (solid red).

The leading orders of the smoothed potential can be obtained from (2.22) and (2.23)

$$\tilde{V}_{\mathbf{k}}^{(1)} = \frac{2\mu}{2\mu + \epsilon_k^0} V_{\mathbf{k}}, \quad \tilde{V}_{\mathbf{k}}^{(2)} = -\frac{1}{L^{\frac{d}{2}}} \sum_{\mathbf{q}} \frac{\epsilon_k^0 + 2\epsilon_q^0}{2\mu + \epsilon_k^0} \frac{\tilde{V}_{\mathbf{q}}^{(1)} \tilde{V}_{\mathbf{k}-\mathbf{q}}^{(1)}}{4\mu}. \quad (2.25)$$

2.3. Bogoliubov Excitations

The Gross-Pitaevskii formalism from the previous section yields the mean-field ground-state. We now consider quantum fluctuations around this ground state by separating the fluctuations from the mean-field wavefunction $\hat{\Psi}(\mathbf{r}) = \Phi(\mathbf{r}) + \delta\hat{\Psi}(\mathbf{r})$. Taking advantage of the macroscopic population of the ground state, we consider the Hamiltonian (2.11) only to leading order in the fluctuations. Again, we use representation in terms of density and phase

$$\hat{n}(\mathbf{r}) = n_0(\mathbf{r}) + \delta\hat{n}(\mathbf{r}), \quad \hat{\varphi}(\mathbf{r}) = \varphi_0(\mathbf{r}) + \delta\hat{\varphi}(\mathbf{r}), \quad (2.26)$$

where the phase and density operators are

$$\delta\hat{n}(\mathbf{r}) = \Phi(\mathbf{r}) \left\{ \delta\hat{\Psi}^\dagger(\mathbf{r}) + \delta\hat{\Psi}(\mathbf{r}) \right\}, \quad \delta\hat{\varphi}(\mathbf{r}) = \frac{i}{2\Phi(\mathbf{r})} \left\{ \delta\hat{\Psi}^\dagger(\mathbf{r}) - \delta\hat{\Psi}(\mathbf{r}) \right\}, \quad (2.27)$$

up to higher orders in the fluctuations. Density and phase operators are conjugate fields, fulfilling the commutator relation $[\delta\hat{n}(\mathbf{r}), \delta\hat{\varphi}(\mathbf{r}')] = i\delta(\mathbf{r} - \mathbf{r}')$

2. The Inhomogeneous Bogoliubov Hamiltonian

\mathbf{r}'). With this, we expand the grand canonical Hamiltonian $\hat{E} = \hat{H} - \mu\hat{N}$ (2.11) in orders of $\delta\hat{\Psi}$ and $\delta\hat{\Psi}^\dagger$. The linear part vanishes, because $\Phi(\mathbf{r})$ is the ground-state of the Gross-Pitaevskii equation. The relevant part is then the quadratic part \hat{F} of the Hamiltonian \hat{E}

$$\hat{E} = E_0 + \hat{F}[\delta\hat{n}, \delta\hat{\varphi}]. \quad (2.28)$$

Third-order and fourth-order terms in the fluctuations are neglected. Here, $E_0 = E[n_0(\mathbf{r}), \varphi_0(\mathbf{r})]$ is the Bogoliubov ground-state energy. The quadratic Hamiltonian is found as

$$\hat{F} = \int d^d r \left\{ \frac{\hbar^2}{2m} \left[\left(\nabla \frac{\delta\hat{n}}{2\Phi(\mathbf{r})} \right)^2 + \frac{[\nabla^2 \Phi(\mathbf{r})]}{4\Phi^3(\mathbf{r})} \delta\hat{n}^2 + \Phi^2(\mathbf{r}) (\nabla \delta\hat{\varphi})^2 \right] + \frac{g}{2} \delta\hat{n}^2 \right\}. \quad (2.29)$$

The potential $V(\mathbf{r})$ does not appear directly in the equations of motion for the excitations. Instead, it enters via the condensate function $\Phi(\mathbf{r})$, according to the nonlinear equation (2.19).

With (2.29), the problem is reduced to a Hamiltonian that is quadratic in the excitations. To this order, there are no mixed terms of $\delta\hat{n}$ and $\delta\hat{\varphi}$, but the Heisenberg equations of motion (2.10) for $\delta\hat{\varphi}$ and $\delta\hat{n}$

$$\frac{\partial \delta\hat{\varphi}}{\partial t} = \frac{1}{i\hbar} [\delta\hat{\varphi}, \hat{F}], \quad \frac{\partial \delta\hat{n}}{\partial t} = \frac{1}{i\hbar} [\delta\hat{n}, \hat{F}] \quad (2.30)$$

are coupled, because $[\delta\hat{n}(\mathbf{r}), \delta\hat{\varphi}(\mathbf{r}')] = i \delta(\mathbf{r} - \mathbf{r}')$.

2.3.1. The free Bogoliubov problem

Before including the external potential, we consider the excitations of the homogeneous system $V(\mathbf{r}) = 0$, $n_0(\mathbf{r}) = \mu/g$. In this case, the Bogoliubov Hamiltonian (2.29) reduces to

$$\begin{aligned} \hat{F}^{(0)} &= \int d^d r \left\{ \frac{\hbar^2}{2m} \left[\left(\nabla \frac{\delta\hat{n}}{2\sqrt{n_\infty}} \right)^2 + (\nabla \sqrt{n_\infty} \delta\hat{\varphi})^2 \right] + 2g n_\infty \left(\frac{\delta\hat{n}}{2\sqrt{n_\infty}} \right)^2 \right\} \\ &= \sum_{\mathbf{k}} \left[\epsilon_{\mathbf{k}}^0 n_\infty \delta\hat{\varphi}_{\mathbf{k}} \delta\hat{\varphi}_{-\mathbf{k}} + (2\mu + \epsilon_{\mathbf{k}}^0) \frac{\delta\hat{n}_{\mathbf{k}} \delta\hat{n}_{-\mathbf{k}}}{4n_\infty} \right], \end{aligned} \quad (2.31)$$

with $\epsilon_{\mathbf{k}}^0 = \hbar^2 k^2 / (2m)$. The Fourier representation is already diagonal in \mathbf{k} , but the equations of motion (2.30) are still coupled. This can be resolved by the Bogoliubov transformation [71], a transformation that couples density

and phase fluctuations to quasiparticle creation and annihilation operators $\hat{\gamma}_{\mathbf{k}}^\dagger$ and $\hat{\gamma}_{\mathbf{k}}$

$$\begin{pmatrix} \hat{\gamma}_{\mathbf{k}} \\ \hat{\gamma}_{-\mathbf{k}}^\dagger \end{pmatrix} = \begin{pmatrix} a_k & a_k^{-1} \\ -a_k & a_k^{-1} \end{pmatrix} \begin{pmatrix} i\sqrt{n_\infty}\delta\hat{\varphi}_{\mathbf{k}} \\ \frac{\delta\hat{n}_{\mathbf{k}}}{2\sqrt{n_\infty}} \end{pmatrix}. \quad (2.32)$$

A transformation of this kind, with the free parameter a_k , guarantees that the quasiparticles obey bosonic commutation relations analogous to (2.1). Inserting the inverse of the above transformation

$$\begin{pmatrix} i\sqrt{n_\infty}\delta\hat{\varphi}_{\mathbf{k}} \\ \frac{\delta\hat{n}_{\mathbf{k}}}{2\sqrt{n_\infty}} \end{pmatrix} = \frac{1}{2} \begin{pmatrix} a_k^{-1} & -a_k^{-1} \\ a_k & a_k \end{pmatrix} \begin{pmatrix} \hat{\gamma}_{\mathbf{k}} \\ \hat{\gamma}_{-\mathbf{k}}^\dagger \end{pmatrix} \quad (2.33)$$

into the Hamiltonian (2.31), we find off-diagonal terms $\hat{\gamma}_{\mathbf{k}}^\dagger\hat{\gamma}_{-\mathbf{k}}^\dagger$ and $\hat{\gamma}_{-\mathbf{k}}\hat{\gamma}_{\mathbf{k}}$. These can be eliminated by choosing the free parameter as $a_k = \sqrt{\epsilon_k^0/\epsilon_k}$ with $\epsilon_k = \sqrt{\epsilon_k^0(2\mu + \epsilon_k^0)}$. Then the Hamiltonian takes its diagonal form

$$\hat{F}^{(0)} = \sum_{\mathbf{k}} \epsilon_k \hat{\gamma}_{\mathbf{k}}^\dagger \hat{\gamma}_{\mathbf{k}}. \quad (2.34)$$

The famous Bogoliubov dispersion relation [71]

$$\epsilon_k = \sqrt{\epsilon_k^0(2\mu + \epsilon_k^0)} \quad (2.35)$$

replaces the kinetic energy of free particles ϵ_k^0 (figure 2.3). In the high-energy regime, the chemical potential μ is negligible compared with ϵ_k^0 and the free dispersion relation, shifted by the chemical potential, is recovered

$$\epsilon_k = \epsilon_k^0 + \mu + \mathcal{O}(\mu/\epsilon_k^0). \quad (2.36)$$

Superfluidity

In the low-energy regime, the interaction $gn = \mu$ dominates over the kinetic energy. A single excitation involves many individual particles, comparable to classical sound waves. The dispersion relation is linear $\epsilon_k = ck$, with sound velocity $c = \sqrt{\mu/m}$. According to Landau's argument [54, chapter 10.1], this linear dispersion at low energies implies superfluidity:

In general, an obstacle moving through a fluid with velocity \mathbf{v} can dissipate energy by creating elementary excitations. By a Galilei transformation to the reference frame of the obstacle, the energy of the excitation ϵ_k is

2. The Inhomogeneous Bogoliubov Hamiltonian

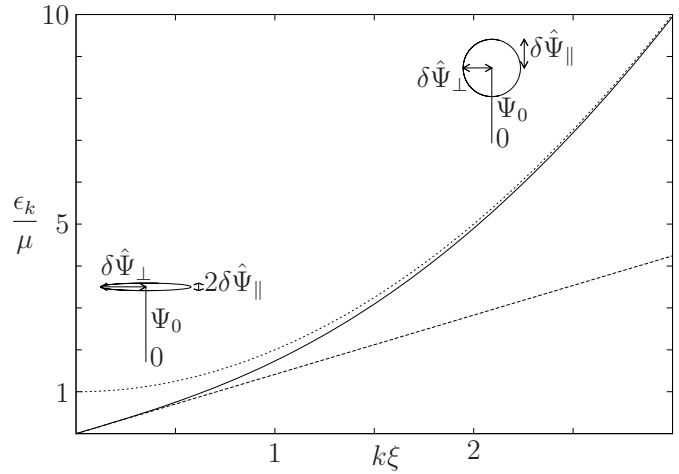


Figure 2.3: Bogoliubov dispersion relation (2.35). Insets: schematic representation of the amplitudes $\delta\Psi_{\perp}$ and $\delta\Psi_{\parallel}$ (2.37).

transformed to $\epsilon_k - \hbar\mathbf{k}\cdot\mathbf{v}$. The static obstacle cannot transfer energy, so excitations can only be created if $v > \epsilon_k/(\hbar k)$. Thus, there is a critical velocity $v_c = \min_k \epsilon_k/\hbar k = c$.

Superfluid flow is one of the key features of Bose-Einstein condensates and has been subject of many experiments. For example stirring experiments, where dissipation was observed when the condensate was stirred with velocities above the critical velocity [56], or persistent flow in a toroidal trap [100].

In the ideal Bose gas (section 2.1), the excitations are still bare particles with dispersion relation ϵ_k^0 and zero critical velocity. The phase transition to the Bose-Einstein condensate phase, *together* with the interactions, results in superfluidity.

Signature of a Bogoliubov excitation

Let us split the fluctuation operator $\delta\hat{\Psi}(\mathbf{r}) = \hat{\Psi}(\mathbf{r}) - \Phi(\mathbf{r})$ into its components parallel and perpendicular to the order parameter $\Phi(\mathbf{r})$

$$\delta\hat{\Psi}_{\parallel} = \frac{1}{2}(\delta\hat{\Psi} + \delta\hat{\Psi}^{\dagger}), \quad \delta\hat{\Psi}_{\perp} = \frac{1}{2i}(\delta\hat{\Psi} - \delta\hat{\Psi}^{\dagger}). \quad (2.37)$$

With equation (2.27) and the Bogoliubov transformation (2.33), the components take the form

$$\begin{aligned} \delta\hat{\Psi}_{\parallel} &= \frac{1}{L^{\frac{d}{2}}} \sum_{\mathbf{k}} \frac{a_k}{2} (e^{i\mathbf{k}\cdot\mathbf{r}} \hat{\gamma}_{\mathbf{k}} + e^{-i\mathbf{k}\cdot\mathbf{r}} \hat{\gamma}_{\mathbf{k}}^{\dagger}), \\ \delta\hat{\Psi}_{\perp} &= \frac{1}{L^{\frac{d}{2}}} \sum_{\mathbf{k}} \frac{1}{2ia_k} (e^{i\mathbf{k}\cdot\mathbf{r}} \hat{\gamma}_{\mathbf{k}} - e^{-i\mathbf{k}\cdot\mathbf{r}} \hat{\gamma}_{\mathbf{k}}^{\dagger}), \end{aligned}$$

again with the coefficient $a_k = \sqrt{\epsilon_k^0/\epsilon_k}$. The signature of a Bogoliubov excitation is a plane wave with amplitudes a_k and a_k^{-1} , respectively.

At high energies, the coefficient a_k tends to one and the components of the wave parallel and perpendicular to the order parameter are equal. Then, the Bogoliubov wave resembles the plane wave of a free particle $\delta\Psi \propto \exp[i(\mathbf{k}_0 \cdot \mathbf{r} - \epsilon_{k_0} t/\hbar)]$ (inset in figure 2.3).

At low energies, the spectrum (2.35) changes from quadratic to linear, but it is still *gapless*: at low momenta, excitations with arbitrarily low energy exist. The coefficient a_k tends to zero, which means, that the Bogoliubov excitation γ_k has hardly any signature in the density, but all the more in the phase [see inset in figure 2.3]. In the limit $k \rightarrow 0$, the Bogoliubov excitations pass over to a homogeneous shift of the condensate phase. This connects the Bogoliubov excitations to the broken $U(1)$ symmetry of Bose-Einstein condensate. The Bogoliubov excitations are the Goldstone modes [72] associated to this broken symmetry.

2.3.2. The inhomogeneous Bogoliubov problem

Let us come back to the Hamiltonian (2.29) and include the external potential $V(\mathbf{r})$ and its imprint of the external potential in the condensate density $n_0(\mathbf{r})$. This inhomogeneity breaks translation invariance, which allowed the diagonalization by the Bogoliubov transformation (2.33) in the free problem, with two consequences: Firstly, there will be scattering among the Bogoliubov modes, and secondly, the anomalous terms $\hat{\gamma}_{\mathbf{k}}^\dagger \hat{\gamma}_{-\mathbf{k}'}^\dagger$ and their Hermitian conjugates do not vanish, which leads to anomalous coupling.

As the Hamiltonian (2.29) is quadratic in the fluctuations without any term mixing $\delta\hat{n}$ and $\delta\hat{\varphi}$, the general structure of the disorder part $F^{(V)} = F - F^{(0)}$ is

$$\hat{F}^{(V)}[\delta\hat{n}, \delta\hat{\varphi}] = \frac{1}{2L^{\frac{d}{2}}} \sum_{\mathbf{k}, \mathbf{k}'} \left\{ n_\infty \delta\hat{\varphi}_{\mathbf{k}'}^\dagger S_{\mathbf{k}'\mathbf{k}} \delta\hat{\varphi}_{\mathbf{k}} + \frac{\delta\hat{n}_{\mathbf{k}'}^\dagger R_{\mathbf{k}'\mathbf{k}} \delta\hat{n}_{\mathbf{k}}}{4n_\infty} \right\}. \quad (2.38)$$

The density and phase coupling matrices S and R vanish in absence of disorder. Comparing with (2.29), we find that both the phase coupling-element and the density coupling element are related to the imprint of the external potential in the condensate wave-function $\sqrt{n_0(\mathbf{r})} = \Phi(\mathbf{r})$.

Non-perturbative couplings

The phase coupling is proportional to the condensate density $n_0(\mathbf{r}) = \Phi(\mathbf{r})^2$ and can be written as

$$S_{\mathbf{k}'\mathbf{k}} = \frac{1}{L^{\frac{d}{2}}} \sum_{\mathbf{q}} \frac{\hbar^2}{m} \mathbf{k}' \cdot \mathbf{k} \Phi_{\mathbf{k}'-\mathbf{q}} \Phi_{\mathbf{q}-\mathbf{k}}. \quad (2.39)$$

2. The Inhomogeneous Bogoliubov Hamiltonian

According to the equations of motion (2.30), this is a coupling between phase and density fluctuations, mediated by particles in the non-uniform condensate Φ . The density coupling has a different dependence on the non-uniform condensate. Indeed, by expressing the non-uniform condensate Φ in terms of the inverse imprint $\bar{\Phi}(\mathbf{r}) = \Phi_0^2/\Phi(\mathbf{r})$, we can write the density coupling in a form analogous to (2.39)

$$R_{\mathbf{k}'\mathbf{k}} = \frac{1}{L^{\frac{d}{2}}} \sum_{\mathbf{q}} \tilde{r}_{\mathbf{k}'\mathbf{k}\mathbf{q}} \bar{\Phi}_{\mathbf{k}'-\mathbf{q}} \bar{\Phi}_{\mathbf{q}-\mathbf{k}}, \quad (2.40)$$

with $\tilde{r}_{\mathbf{k}'\mathbf{k}\mathbf{q}} = \hbar^2 \{q^2 - 2(\mathbf{k}' - \mathbf{q}) \cdot (\mathbf{q} - \mathbf{k}) + [(\mathbf{k}' - \mathbf{q})^2 + (\mathbf{k} - \mathbf{q})^2] / 2\} / m$.

Both formulae (2.39) and (2.40) are non-perturbative. That means they hold for arbitrary external potentials, if only the condensate wave function Φ and its inverse $\bar{\Phi}$ are determined correctly.

Inhomogeneous Bogoliubov Hamiltonian in the free Bogoliubov basis

For the further analysis, it is useful to transform to Bogoliubov quasiparticles $\hat{\gamma}_{\mathbf{k}}$, such that the free Hamiltonian takes its diagonal form (2.34). We use the Bogoliubov transformation (2.33) of the homogeneous problem. In this basis every mode is still characterized by its momentum \mathbf{k} . Only the saddle point $(n_0)_{\mathbf{k}}$, from where the fluctuations $\delta\hat{n} = \hat{n} - n_0$ are measured, is shifted by the external potential. A detailed discussion about this choice of basis is found in section 3.2.

Thus, the couplings are transformed in the following way

$$\begin{pmatrix} W_{\mathbf{k}'\mathbf{k}} & Y_{\mathbf{k}'\mathbf{k}} \\ Y_{\mathbf{k}'\mathbf{k}} & W_{\mathbf{k}'\mathbf{k}} \end{pmatrix} = \frac{1}{4} \begin{pmatrix} a_{\mathbf{k}'}^{-1} & a_{\mathbf{k}'} \\ -a_{\mathbf{k}'}^{-1} & a_{\mathbf{k}'} \end{pmatrix} \begin{pmatrix} S_{\mathbf{k}'\mathbf{k}} & 0 \\ 0 & R_{\mathbf{k}'\mathbf{k}} \end{pmatrix} \begin{pmatrix} a_{\mathbf{k}}^{-1} & -a_{\mathbf{k}}^{-1} \\ a_{\mathbf{k}} & a_{\mathbf{k}} \end{pmatrix} =: \mathcal{V}_{\mathbf{k}'\mathbf{k}}, \quad (2.41)$$

and the Bogoliubov Hamiltonian (2.29) takes the form

$$\hat{F}[\hat{\gamma}, \hat{\gamma}^\dagger] = \sum_{\mathbf{k}} \epsilon_{\mathbf{k}} \hat{\gamma}_{\mathbf{k}}^\dagger \hat{\gamma}_{\mathbf{k}} + \frac{1}{2L^{\frac{d}{2}}} \sum_{\mathbf{k}, \mathbf{k}'} \begin{pmatrix} \hat{\gamma}_{\mathbf{k}'}^\dagger & \hat{\gamma}_{-\mathbf{k}'} \end{pmatrix} \begin{pmatrix} W_{\mathbf{k}'\mathbf{k}} & Y_{\mathbf{k}'\mathbf{k}} \\ Y_{\mathbf{k}'\mathbf{k}} & W_{\mathbf{k}'\mathbf{k}} \end{pmatrix} \begin{pmatrix} \hat{\gamma}_{\mathbf{k}} \\ \hat{\gamma}_{-\mathbf{k}}^\dagger \end{pmatrix}. \quad (2.42)$$

This Hamiltonian for the inhomogeneous Bogoliubov problem is the central achievement of the whole chapter. The equation of motion for the bosonic Bogoliubov quasiparticles $\hat{\gamma}_{\mathbf{k}}$ reads

$$i\hbar \frac{\partial}{\partial t} \hat{\gamma}_{\mathbf{k}'} = [\hat{\gamma}_{\mathbf{k}'}, \hat{F}] = \epsilon_{\mathbf{k}'} \hat{\gamma}_{\mathbf{k}'} + \frac{1}{L^{\frac{d}{2}}} \sum_{\mathbf{k}} \left\{ W_{\mathbf{k}'\mathbf{k}} \hat{\gamma}_{\mathbf{k}} + Y_{\mathbf{k}'\mathbf{k}} \hat{\gamma}_{-\mathbf{k}}^\dagger \right\}. \quad (2.43)$$

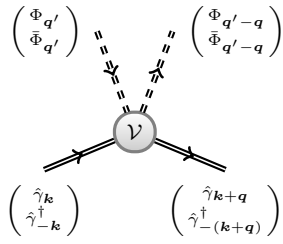


Figure 2.4: Universal Bogoliubov scattering vertex (2.41). The pseudo-spinor $(\hat{\gamma}_{\mathbf{k}}, \hat{\gamma}_{-\mathbf{k}}^\dagger)^T$ scatters with the condensate wave-function Φ and its inverse profile $\bar{\Phi}$.

The matrix $W_{\mathbf{k}'\mathbf{k}}$ contains the usual scattering between different momentum states, induced by the inhomogeneous potential. The anomalous scattering element $Y_{\mathbf{k}'\mathbf{k}}$ allows the creation or annihilation of excitation pairs. The reason for the anomalous coupling Y , between $\hat{\gamma}_{\mathbf{k}}$ and the conjugate operators $\hat{\gamma}_{-\mathbf{k}}^\dagger$, lies in the expansion of the nonlinear term and the Bogoliubov approximation.

The anomalous coupling can be handled in a linear manner by defining a pseudo-spinor $\hat{\Gamma}_{\mathbf{k}} = (\hat{\gamma}_{\mathbf{k}}, \hat{\gamma}_{-\mathbf{k}}^\dagger)^T$, which leads to the equation of motion

$$i\hbar \frac{\partial}{\partial t} \hat{\Gamma}_{\mathbf{k}'} = \begin{pmatrix} 1 & 0 \\ 0 & -1 \end{pmatrix} \left\{ \epsilon_{\mathbf{k}'} \hat{\Gamma}_{\mathbf{k}'} + \frac{1}{L^{\frac{d}{2}}} \sum_{\mathbf{k}} \mathcal{V}_{\mathbf{k}'\mathbf{k}} \hat{\Gamma}_{\mathbf{k}} \right\}. \quad (2.44)$$

The product of the matrix $\text{diag}(1, -1)$ and \mathcal{V} from equation (2.41) makes the time evolution non-Hermitian, which is discussed in more detail in section 2.5. As depicted in figure 2.4, the pseudo-spinor $\hat{\Gamma}_{\mathbf{k}}$ is scattered by the matrix-valued potential \mathcal{V} , with the momentum transfer provided by the condensate wave function Φ and the inverse profile $\bar{\Phi}$ (c.f. equations (2.39), (2.40) and (2.41)).

In order to keep track of the momentum balance, the momentum of the creator in the second component of the pseudo-spinor $\hat{\Gamma}_{\mathbf{k}}$ has been chosen reversed. This concept of a pseudo-spinor containing $\hat{\gamma}_{\mathbf{k}}$ and $\hat{\gamma}_{-\mathbf{k}}^\dagger$ has been adopted from the Nambu formalism, employed in the BCS theory of superconductivity [16, Section 18.5] and will be particularly useful later in section 3.3.

2.3.3. Disorder expansion of the Bogoliubov Hamiltonian

The coupling elements depend non-perturbatively on the condensate wave-function, which is the solution of the stationary Gross-Pitaevskii equation (2.16). In practice this solution is either obtained numerically [cf. subsection 2.4.4, section 4.3] or by the systematic perturbative expansion of subsection 2.2.4. For the analytical treatment, we choose the perturbative expansion (2.21) of Φ and $\bar{\Phi}$, and expand the scattering elements in orders of the inhomogeneous potential.

The first-order scattering amplitudes read

$$S_{\mathbf{k}'\mathbf{k}}^{(1)} = -4\xi^2 \mathbf{k}' \cdot \mathbf{k} \frac{V_{\mathbf{k}'-\mathbf{k}}}{2 + \xi^2(\mathbf{k}' - \mathbf{k})^2}, \quad (2.45a)$$

$$R_{\mathbf{k}'\mathbf{k}}^{(1)} = -4\xi^2(\mathbf{k}' \cdot \mathbf{k} - k^2 - k'^2) \frac{V_{\mathbf{k}'-\mathbf{k}}}{2 + \xi^2(\mathbf{k}' - \mathbf{k})^2}, \quad (2.45b)$$

$$\begin{aligned} W_{\mathbf{k}'\mathbf{k}}^{(1)} &= \frac{V_{\mathbf{k}'-\mathbf{k}}}{2 + \xi^2(\mathbf{k}' - \mathbf{k})^2} \left[\sqrt{\frac{\epsilon_k^0 \epsilon_{k'}^0}{\epsilon_k \epsilon_{k'}}} (k^2 + k'^2 - \mathbf{k}' \cdot \mathbf{k}) - \sqrt{\frac{\epsilon_k \epsilon_{k'}}{\epsilon_k^0 \epsilon_{k'}^0}} \mathbf{k}' \cdot \mathbf{k} \right] \xi^2 \\ &=: w_{\mathbf{k}'\mathbf{k}}^{(1)} V_{\mathbf{k}'-\mathbf{k}}, \end{aligned} \quad (2.45c)$$

$$\begin{aligned} Y_{\mathbf{k}'\mathbf{k}}^{(1)} &= \frac{V_{\mathbf{k}'-\mathbf{k}}}{2 + \xi^2(\mathbf{k}' - \mathbf{k})^2} \left[\sqrt{\frac{\epsilon_k^0 \epsilon_{k'}^0}{\epsilon_k \epsilon_{k'}}} (k^2 + k'^2 - \mathbf{k}' \cdot \mathbf{k}) + \sqrt{\frac{\epsilon_k \epsilon_{k'}}{\epsilon_k^0 \epsilon_{k'}^0}} \mathbf{k}' \cdot \mathbf{k} \right] \xi^2 \\ &=: y_{\mathbf{k}'\mathbf{k}}^{(1)} V_{\mathbf{k}'-\mathbf{k}}. \end{aligned} \quad (2.45d)$$

The most important feature of all first-order couplings is that the potential factorizes from an envelope function that contains interaction, kinetic energy and the scattering geometry. The first-order scattering event can be written as

$$\mathcal{V}_{\mathbf{k}'\mathbf{k}}^{(1)} = \begin{pmatrix} w_{\mathbf{k}'\mathbf{k}}^{(1)} & y_{\mathbf{k}'\mathbf{k}}^{(1)} \\ y_{\mathbf{k}'\mathbf{k}}^{(1)} & w_{\mathbf{k}'\mathbf{k}}^{(1)} \end{pmatrix} V_{\mathbf{k}'-\mathbf{k}} = v_{\mathbf{k}'\mathbf{k}}^{(1)} V_{\mathbf{k}'-\mathbf{k}} = \begin{matrix} \vdots \\ \boxtimes \\ \vdots \end{matrix}. \quad (2.46)$$

Second-order scattering-amplitudes. The phase coupling element $S_{\mathbf{k}'\mathbf{k}}$ is proportional to the momentum transfer by the ground-state density $(n_0)_{\mathbf{k}'-\mathbf{k}}$. According to equations (2.24) and (2.25), the second-order contains a convolution of the disorder potential with itself and an envelope function. The density coupling element $R^{(2)}$ has the same structure with a different envelope function

$$S_{\mathbf{k}',\mathbf{k}}^{(2)} = \frac{1}{\mu L^{\frac{d}{2}}} \sum_{\mathbf{q}} V_{\mathbf{k}'-\mathbf{q}} V_{\mathbf{q}-\mathbf{k}} s_{\mathbf{k}'\mathbf{q}\mathbf{k}}^{(2)} \quad R_{\mathbf{k}',\mathbf{k}}^{(2)} = \frac{1}{\mu L^{\frac{d}{2}}} \sum_{\mathbf{q}} V_{\mathbf{k}'-\mathbf{q}} V_{\mathbf{q}-\mathbf{k}} r_{\mathbf{k}'\mathbf{q}\mathbf{k}}^{(2)}. \quad (2.47)$$

The explicit form of the second-order envelope functions is found as

$$s_{\mathbf{k}'\mathbf{q}\mathbf{k}}^{(2)} = 2\xi^2 \mathbf{k}' \cdot \mathbf{k} \frac{(\mathbf{k}' - \mathbf{k})^2 + (\mathbf{q} - \mathbf{k}')^2 + (\mathbf{q} - \mathbf{k})^2}{[2\xi^{-2} + (\mathbf{k}' - \mathbf{k})^2] [2\xi^{-2} + (\mathbf{q} - \mathbf{k}')^2] [2\xi^{-2} + (\mathbf{q} - \mathbf{k})^2]}, \quad (2.48a)$$

$$\begin{aligned}
 r_{\mathbf{k}'\mathbf{q}\mathbf{k}}^{(2)} &= \xi^2 \left\{ k'^2 + k'^2 + k^2 + \frac{3}{2} [(\mathbf{q} - \mathbf{k}')^2 + (\mathbf{q} - \mathbf{k})^2] \right. \\
 &\quad \left. + (k'^2 + k^2 - \mathbf{k}' \cdot \mathbf{k}) \frac{2\xi^{-2} - (\mathbf{q} - \mathbf{k}')^2 - (\mathbf{q} - \mathbf{k})^2}{2\xi^{-2} + (\mathbf{k}' - \mathbf{k})^2} \right\} / \left\{ 2 \left[1 + \frac{\xi^2(\mathbf{q} - \mathbf{k}')^2}{2} \right] \left[1 + \frac{\xi^2(\mathbf{q} - \mathbf{k})^2}{2} \right] \right\}.
 \end{aligned} \tag{2.48b}$$

Again, the scattering elements are transformed according to equation (2.41), which brings us to the structure of the second-order scattering matrix

$$\mathcal{V}_{\mathbf{k}'\mathbf{k}}^{(2)} = \frac{1}{L^{\frac{d}{2}}} \sum_{\mathbf{q}} \begin{pmatrix} w_{\mathbf{k}'\mathbf{q}\mathbf{k}}^{(2)} & y_{\mathbf{k}'\mathbf{q}\mathbf{k}}^{(2)} \\ y_{\mathbf{k}'\mathbf{q}\mathbf{k}}^{(2)} & w_{\mathbf{k}'\mathbf{q}\mathbf{k}}^{(2)} \end{pmatrix} \frac{V_{\mathbf{k}'-\mathbf{q}} V_{\mathbf{q}-\mathbf{k}}}{\mu} =: \frac{1}{\mu L^{\frac{d}{2}}} \sum_{\mathbf{q}} V_{\mathbf{k}'-\mathbf{q}} v_{\mathbf{k}'\mathbf{q}\mathbf{k}}^{(2)} V_{\mathbf{q}-\mathbf{k}} = \begin{matrix} \vdots \\ \boxtimes \\ \vdots \end{matrix}. \tag{2.49}$$

In particular, the diagonal element of $W^{(2)}$ is needed later. In this case, the envelope function simplifies to

$$w_{\mathbf{k}\mathbf{k}+\mathbf{p}\mathbf{k}}^{(2)} = \frac{k\xi}{\sqrt{2 + k^2\xi^2}} \frac{(2k^2 + 3p^2 + \mathbf{k} \cdot \mathbf{p})\xi^2}{(2 + p^2\xi^2)^2}. \tag{2.50}$$

Higher orders. If needed, higher-order scattering vertices $\mathcal{V}^{(n)}$ can be derived systematically with the following prescription.

1. Compute the ground state (2.21) to the desired order, using the expansion shown in box 2.1.
2. Compute the inverse field $\bar{\Phi}_{\mathbf{q}} = (\Phi_0^2/\Phi)_{\mathbf{q}}$.
3. $S^{(n)}$ and $R^{(n)}$ are obtained by collecting all terms of order n in equations (2.39) and (2.40).
4. Finally, apply the transformation (2.41) in order to obtain $W^{(n)}$ and $Y^{(n)}$.

$$\begin{aligned}
 \mathcal{V} &= \begin{matrix} \vdots \\ \text{---} \circ \text{---} \\ \vdots \end{matrix} = \begin{matrix} \vdots \\ \text{---} \boxtimes \text{---} \\ \vdots \end{matrix} + \begin{matrix} \vdots \\ \text{---} \boxtimes\boxtimes \text{---} \\ \vdots \end{matrix} + \begin{matrix} \vdots \\ \text{---} \boxtimes\boxtimes\boxtimes \text{---} \\ \vdots \end{matrix} + \dots \\
 &= \mathcal{V}^{(1)} + \mathcal{V}^{(2)} + \mathcal{V}^{(3)} + \dots
 \end{aligned} \tag{2.51}$$

The inhomogeneous Bogoliubov Hamiltonian is an essential cornerstone for this entire work. It will be essential for both the single scattering in section 2.4 and the disordered problem in chapter 3.

2.3.4. Bogoliubov mean-field

So far, the excitations on top of the mean-field condensate $\Phi(\mathbf{r})$ have been treated in a quantized manner. The canonically quantized Bogoliubov Hamiltonian (2.29) is basal for the rest of [part I](#). It is necessary for the condensate depletion in [section 2.5](#) and will be fruitful in the diagrammatic perturbation theory in disordered problem [subsection 3.3.2](#).

For many purposes, however, it is sufficient and useful to treat the Bogoliubov excitations $\hat{\gamma}_{\mathbf{k}}$ in a mean-field manner as a complex field $\gamma_{\mathbf{k}}$. This is analogous to the mean-field approximation for the condensate and justified for strongly populated Bogoliubov modes. The mean-field approximation is equivalent to the excitations on top of the Gross-Pitaevskii ground-state in the scope of the time dependent Gross-Pitaevskii equation (2.16). The commutators in the equations of motion (2.30) pass over to functional derivatives of the energy functional F that is obtained from (2.29) by replacing the operators $\delta\hat{\varphi}$ and $\delta\hat{n}$ with their respective classical fields:

$$\frac{\partial\delta\varphi}{\partial t} = -\frac{1}{\hbar}\frac{\delta F}{\delta(\delta n)}, \quad \frac{\partial\delta n}{\partial t} = \frac{1}{\hbar}\frac{\delta F}{\delta(\delta\varphi)}. \quad (2.52)$$

This mean-field framework allows very efficient numerical computations. It will be employed in the single-scattering setup of [section 2.4](#) and in the disordered setup of [section 4.3](#).

2.4. Single scattering event

In the previous section, we have seen that the plane-wave Bogoliubov excitations are no eigenstates of the inhomogeneous Bogoliubov problem, but are scattered with scattering amplitudes $W_{\mathbf{k}'\mathbf{k}}$ and coupled to their adjoint via $Y_{\mathbf{k}'\mathbf{k}}$. One could try to find the exact eigenstates in presence of some disorder or impurity potential, an approach discussed later in [section 2.5](#). Here, however, a scattering process is considered in the momentum basis. A plane-wave excitation enters a scattering region, where an impurity potential deforms the local condensate density. The elastically scattered wave is determined both analytically and numerically within the full time-dependent Gross-Pitaevskii equation. This elastic scattering event can be regarded as a building block for the disordered problem in [chapter 3](#). The contents of this section have been published in [\[101\]](#).

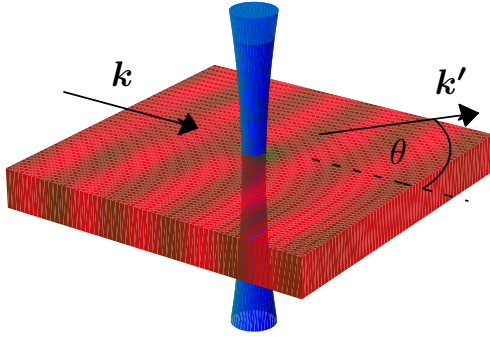


Figure 2.5: 2D single-scattering setup. A blue-detuned laser beam focused perpendicularly through a 2D BEC provides an impurity potential $V(\mathbf{r}) = V(0) \exp(-\mathbf{r}^2/r_0^2)$, which scatters an incident Bogoliubov wave with wave vector \mathbf{k} into modes \mathbf{k}' at scattering angle θ .

2.4.1. Single scattering setting

The following experimental setting is proposed for observing the scattering of a Bogoliubov excitation off a potential impurity. The basic idea is to create a BEC in a shallow trap with an impurity and then to imprint a single plane-wave Bogoliubov excitation. After some time, the wave scattered at a certain angle is measured.

The experiment should be realized in two dimensions for the following reasons. In an experiment in one dimension, there is only forward and backscattering. Thus, no angular dependence is observable. In contrast, a two-dimensional setup allows observing the angular dependence of the scattered wave, and the impurity can be realized easily by means of a blue-detuned laser penetrating perpendicularly through the center of the condensate. The two-dimensional setup is sketched in [figure 2.5](#). In three dimensions, things would become more complicated, because the impurity cannot be realized using a single laser beam as in $d = 2$. Moreover, simple time-of-flight images are more complicated to evaluate, because they show the integrated density along the vertical dimension.

The trap should be shallow enough, such that the condensate can be considered as homogeneous around the impurity. Thus, the potential appearing in the formalism of [section 2.3](#) is given by the impurity potential alone. The light-shift potential of the laser beam forming the impurity potential takes the shape of the Gaussian intensity profile of the beam $V(\mathbf{r}) = V(0) \exp(-\mathbf{r}^2/r_0^2)$. As discussed in [subsection 2.2.3](#), this potential causes a depression in the ground-state density of the BEC [see [figure 2.2](#)]. Next, a plane-wave Bogoliubov excitation is imprinted by a Bragg-spectroscopy technique [[60](#), [61](#)]. Two laser beams with a certain detuning are radiated onto the condensate at a certain angle. By absorption of a photon from the one beam and stimulated emission of a photon into the other, the energy and the momentum for a Bogoliubov quasiparticle are provided. By

this process, a particular Bogoliubov mode is excited very strongly², which allows treating the Bogoliubov excitations in the mean-field manner of [subsection 2.3.4](#). Equivalently, the time-dependent Gross-Pitaevskii equation (2.16) can be integrated numerically.

During its propagation, the wave is scattered at the impurity and the scattered wave is detected at scattering angle θ . For the experimental detection, again a Bragg-spectroscopy technique should be used in order to separate the excitation from the condensate background making it observable in a time-of-flight image. This technique has already been used experimentally for the excitation and detection of Bogoliubov excitations by Vogels *et al.* [61], following a proposal by Brunello *et al.* [60]. The only thing to change is to detect the scattered wave at an angle θ with respect to the imprinted wave.

2.4.2. Limiting cases of the elastic scattering amplitude

The Bogoliubov dispersion relation (2.35) interpolates between the sound-wave regime at low energies and the particle regime at high energies. Before considering the scattering amplitude in the entire energy range, it is instructive to consider the limiting cases from a separate point of view.

Scattering of particles

In the single-particle regime of the Bogoliubov spectrum, excitations are plane matter waves with dispersion relation $\epsilon_k^0 = \hbar^2 k^2 / 2m$. From the momentum representation of the Schrödinger equation it follows that the amplitude of a single-scattering process $\mathbf{k} \mapsto \mathbf{k}' = \mathbf{k} + \mathbf{q}$ is proportional to the Fourier component $V_{\mathbf{q}} = L^{-\frac{d}{2}} \int d^d r V(\mathbf{r}) e^{-i\mathbf{q}\cdot\mathbf{r}}$ of the scattering potential. If the potential $V(\mathbf{r})$ varies on a characteristic length r_0 , the scattering may be anisotropic if the wave can resolve this structure, $qr_0 \geq 1$ [22, 23]. In the opposite case of a small obstacle such that $qr_0 \ll 1$, also known as the s-wave scattering regime, the scattering amplitude is simply proportional to V_0 and can therefore only be *isotropic*.

Scattering of sound waves

In the other limit, the characteristics of sound waves are very different. Similar to classical sound waves in air, many particles oscillate collectively

²This technique was employed in an experiment [61], where the number of 40 000 excited atoms corresponds to about 20 000 Bogoliubov quasiparticles at $k\xi = p/(\sqrt{2}mc) \approx 0.27$.

back and forth. In the regime $k\xi \ll 1$ and $\xi \ll r_0$, the Thomas-Fermi formula (2.20) applies.

Excitations of the superfluid ground state in the regime $k\xi \ll 1$ are longitudinal sound waves with density fluctuations $\delta n = n - n_{\text{TF}}$ and phase fluctuations $\delta\varphi$. The phase is the potential for the local superfluid velocity $\mathbf{v}_s = (\hbar/m)\nabla\delta\varphi$. The superfluid hydrodynamics is determined by the continuity equation (2.18a) $\partial_t n + \nabla \cdot (n\mathbf{v}_s) = 0$ and by the Euler equation for an ideal compressible fluid, $m[\partial_t \mathbf{v}_s + (\mathbf{v}_s \cdot \nabla)\mathbf{v}_s] = -\nabla(gn + V)$, derived from (2.18b) in the present limit. To linear order in δn and $\delta\varphi$, these two equations can be combined to a single wave equation

$$m [c^2 \nabla^2 - \partial_t^2] \delta n = \nabla \cdot (V(\mathbf{r}) \nabla \delta n), \quad (2.53)$$

with the sound velocity $c = \sqrt{\mu/m}$ from subsection 2.3.1. The gradient-potential operator on the right-hand side then causes scattering with an amplitude proportional to $-(\mathbf{k} \cdot \mathbf{k}')V_{\mathbf{k}'-\mathbf{k}}$. Hence, the potential component $V_{\mathbf{k}'-\mathbf{k}}$ from above, which must appear in all cases to satisfy momentum conservation, is multiplied with a dipole (or p-wave) characteristic $A(\theta) = -\cos\theta$. This scattering cross-section with a node at $\theta_0 = \pm\pi/2$ can be understood, in the frame of reference where the local fluid velocity is zero, as the dipole radiation pattern of an impurity that oscillates to and fro, quite similar to the case of classical sound waves scattered by an impenetrable obstacle [102].

2.4.3. Analytical prediction for arbitrary $k\xi$

Now, the opposite characteristics of the limiting cases discussed above have to be unified by the Bogoliubov theory that interpolates between both regimes. Starting point is the equation of motion (2.43) for Bogoliubov excitations in the mean-field framework. Transforming from time to frequency domain, equation (2.43) can be written as

$$\gamma_{\mathbf{k}'}(\omega) = G_0(k', \omega) \frac{1}{L^{\frac{d}{2}}} \sum_{\mathbf{k}''} [W_{\mathbf{k}'\mathbf{k}''} \gamma_{\mathbf{k}''}(\omega) + Y_{\mathbf{k}'\mathbf{k}''} \gamma_{-\mathbf{k}''}^*(-\omega)], \quad (2.54)$$

where $G_0(k', \omega) = [\hbar\omega - \epsilon_{k'} + i0]^{-1}$ designates the retarded Green function of the homogeneous condensate, the infinitesimal shift $+i0$ being due to causality. The Bogoliubov field $\gamma_{\mathbf{k}'} = \gamma_{\mathbf{k}'}^{(0)} + \gamma_{\mathbf{k}'}^{(s)}$ is separated into the initially imprinted wave $\gamma_{\mathbf{k}'}^{(0)}(\omega) = \gamma_0(\omega) \delta_{\mathbf{k}'\mathbf{k}}$ with $\gamma_0(\omega) \propto \delta(\hbar\omega - \epsilon_k)$ and the scattered wave $\gamma_{\mathbf{k}'}^{(s)}$, which is of order V . The stationary scattering state is

2. The Inhomogeneous Bogoliubov Hamiltonian

now determined within the Born approximation, i.e. on the right hand side of (2.54), $\gamma_{\mathbf{k}''}$ is replaced with $\gamma_{\mathbf{k}''}^{(0)}$.

In order to single out the elastically scattered wave, which is the most relevant part, we apply the Sokhatsky-Weierstrass theorem [103] $[x+i0]^{-1} = \text{P} x^{-1} - i\pi\delta(x)$ to the Green function, with P denoting the Cauchy principal value. We consider the imaginary part of the Green function

$$\text{Im}G_0(k', \omega_k) = -\pi\delta(\hbar\omega_k - \epsilon_{k'}) = -\pi \left| \frac{\partial\epsilon_{k'}}{\partial k'} \right|^{-1} \delta(|\mathbf{k}'| - k). \quad (2.55)$$

From the first equality, it is seen that there is no contribution (to order V) from the anomalous scattering term, because $(\gamma_{-\mathbf{k}''}^{(0)})^*$ has a negative frequency. Only elastic scattering to \mathbf{k}' with $|\mathbf{k}'| = k$ is permitted (second equality). In order to account for the finite system size, the Dirac δ -function has to be averaged over the k -space resolution $\Delta k = 2\pi/L$, which yields a factor $L/(2\pi)$. Thus, the elastic scattering amplitude at angle θ is given by

$$\text{Im} \frac{\gamma^{(s)}(\theta)}{\gamma_0} = -\frac{1}{2} L^{\frac{2-d}{2}} W_{\mathbf{k}'\mathbf{k}} \left| \frac{\partial\epsilon_k}{\partial k} \right|^{-1}. \quad (2.56)$$

The derivative of the dispersion relation can be expressed in terms of the density of states (3.63) and evaluates as follows

$$\left| \frac{\partial\epsilon_k}{\partial k} \right|^{-1} = 2\pi \frac{\rho_0(\epsilon_k)}{\hbar k} = \frac{1}{2\mu\xi} \frac{\sqrt{2 + k^2\xi^2}}{1 + k^2\xi^2}. \quad (2.57)$$

The other quantity needed for the elastic scattering formula (2.56) is the scattering element $W_{\mathbf{k}'\mathbf{k}}$. For consistency with the Born approximation, the first order in the impurity strength is sufficient.

First-order scattering element

The first-order scattering element (2.45c) is the product of the momentum transfer of the external potential $V_{\mathbf{k}'-\mathbf{k}}$ and an envelope function $w_{\mathbf{k}'\mathbf{k}}^{(1)}$. The potential factor is the same as for free particles scattered at the potential and provides the momentum transfer for scattering from \mathbf{k} to \mathbf{k}' . The envelope function comprises the Bogoliubov dynamics and interaction effects. It depends only on the dimensionless momenta $\mathbf{k}\xi$ and $\mathbf{k}'\xi$. Remarkably, the envelope function features a node which separates forward scattering from backscattering with opposite sign, figure 2.6(a). Let us come back to elastic scattering. For $\epsilon_k = \epsilon_{k'}$ and $\epsilon_k^0 = \epsilon_{k'}^0$, the scattering amplitude (2.45c)

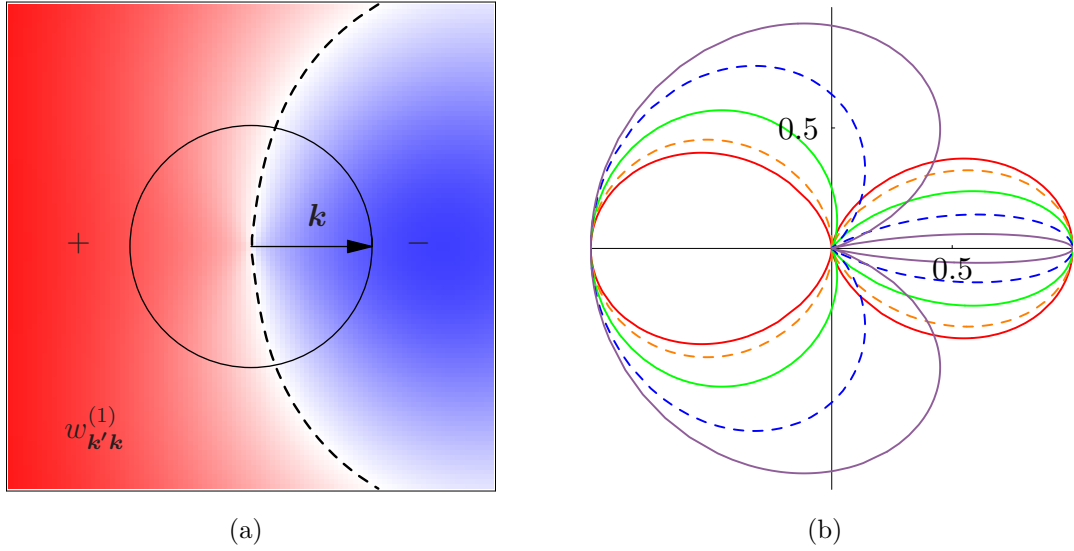


Figure 2.6.: First-order scattering envelope functions. (a) Envelope function $w_{\mathbf{k}'\mathbf{k}}^{(1)}$ of the first-order scattering element (2.45c), plotted in the \mathbf{k}' -plane. The circle of elastic scattering is shown as a solid line. There is a node in the scattering amplitude (dashed line) that separates forward scattering from backscattering with opposite signs. (b) Polar plot $[A(k\xi, \theta)]^2$ of the angular envelope function (2.59) of elastic scattering for $k\xi = 0.2$ (red), 0.5, 1, 2, 5 (violet). The envelope is close to a dipole-radiation (p-wave) pattern for sound waves $k\xi \ll 1$, and tends to an isotropic (s-wave) pattern for single-particle excitations $k\xi \gg 1$. In the intermediate regime, backscattering is favored over forward scattering.

simplifies significantly. As function of the momentum k and the scattering angle $\theta = \angle(\mathbf{k}, \mathbf{k}')$, the elastic scattering amplitude writes

$$W_{\mathbf{k}'\mathbf{k}}^{(1)} \Big|_{k'=k} = \frac{\epsilon_k^0}{\epsilon_k} A(k\xi, \theta) V_{\mathbf{k}'-\mathbf{k}}, \quad (2.58)$$

with a remarkably simple angular envelope

$$A(k\xi, \theta) = \frac{k^2\xi^2(1 - \cos \theta) - \cos \theta}{k^2\xi^2(1 - \cos \theta) + 1}, \quad (2.59)$$

see figure 2.6(b). The node of vanishing scattering amplitude of this envelope is found to be at

$$\cos \theta_0 = \frac{k^2\xi^2}{1 + k^2\xi^2}. \quad (2.60)$$

In the deep sound-wave regime $k\xi \rightarrow 0$, the envelope $A(\theta) = -\cos(\theta)$ presents the dipole radiation pattern. In the opposite limit $k\xi \rightarrow \infty$, the nodes move to the forward direction. Finally, when the healing length ξ becomes larger than the system size L , the node angle $\theta_0 \approx \sqrt{2}/k\xi$ becomes

2. The Inhomogeneous Bogoliubov Hamiltonian

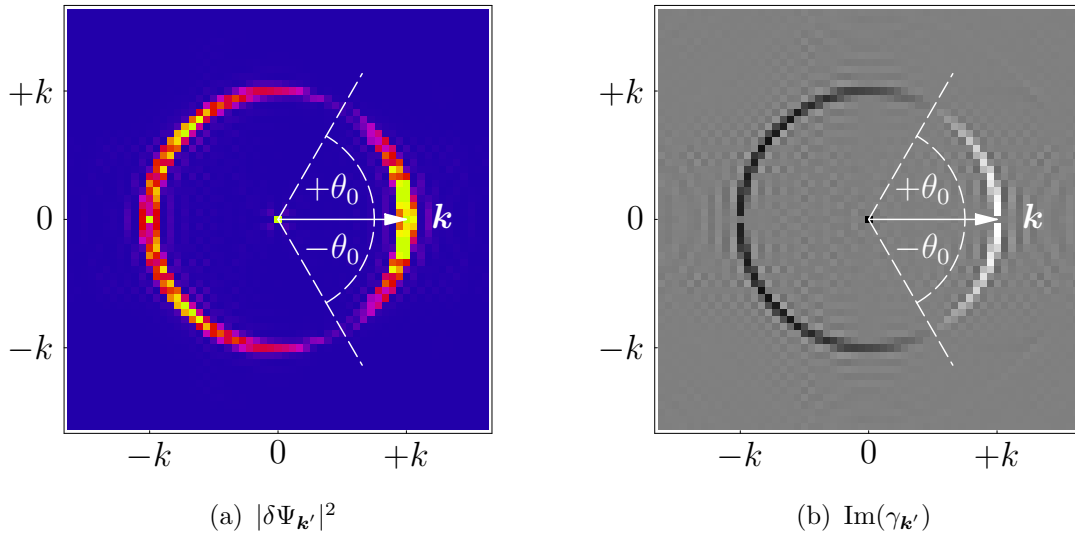


Figure 2.7.: Fourier analysis of the stationary scattering state obtained by numerical integration of the GP equation. (a) Density plot $|\delta\Psi_{\mathbf{k}'}|^2$. The components of the scattered wave are distributed on the elastic circle $|\mathbf{k}'| = k$ with characteristic nodes at $\pm\theta_0$. (b) Scattering state in terms of the Bogoliubov amplitude $\text{Im}(\gamma_{\mathbf{k}'})$. This figure is more distinct than (a), because the interference of Bogoliubov waves with $\pm\mathbf{k}'$ is eliminated. The sign change across the scattering node θ_0 is clearly visible. For the numerical parameters $V(0) = 0.25\mu$, $k\xi = 1$, $kr_0 = 0.5$, scattering is suppressed around $\theta_0 \approx \pi/3$.

smaller than the angular k -space resolution $1/kL$. Then, the last contribution with negative $A(k\xi, \theta)$ is the forward scattering element, which can be absorbed by shifting the origin of the single-particle energy ϵ_k , and we recover the Hamiltonian for the potential scattering of free matter waves [22, 23].

Finally, we insert the elastic scattering amplitude (2.58) into equation (2.56) and find for the two-dimensional scattering problem³

$$\text{Im}[\gamma^{(s)}(\theta)/\gamma_0] = -\frac{1}{4\mu\xi} \frac{k\xi}{1 + k^2\xi^2} A(k\xi, \theta) V_{2k \sin(\theta/2)}. \quad (2.61)$$

2.4.4. Numerical verification

The predicted elastic scattering amplitude (2.61) is an ideal opportunity for a numerical check of the formalism so far. The numerical simulation follows the experimental proposal from above, recall figure 2.5. In the numerics, the time-dependent Gross-Pitaevskii equation (2.16) is integrated. It relies neither on the linearization of small excitation amplitudes, nor on perturbation

³Note that in two dimensions the system size L does not enter explicitly in the formula. In general, there is a factor $L^{\frac{2-d}{2}}$ on the right hand side. The Fourier transforms $f_{\mathbf{k}} = L^{-\frac{d}{2}} \int d^d r e^{-i\mathbf{k}\cdot\mathbf{r}} f(\mathbf{r})$ of the quantities $f = \gamma^{(0)}, \gamma^{(s)}, V$ scale differently with L : $V_k \propto L^{-\frac{d}{2}}$, $\gamma^{(0)} \propto L^{\frac{d}{2}}$, and $\gamma^{(s)} \propto L^{1-\frac{d}{2}}$.

theory for a weak potential. The trapping potential is neglected, instead, the impurity potential is placed into a finite homogeneous system with periodic boundary conditions. In order to investigate the interesting envelope function (2.59) in the scattering amplitude (2.61), the potential factor $V_{\mathbf{k}'-\mathbf{k}}$ should allow scattering in all directions. That means, the impurity should be pointlike in the sense that its extension r_0 should be much smaller than the wave length $kr_0 \ll 1$. First, the Gross-Pitaevskii ground state is calculated by imaginary-time propagation, using the forth-order Runge-Kutta method [104]. Then a plane-wave Bogoliubov excitation of the unperturbed system is superposed. During the real-time evolution, the wave propagates and is scattered at the impurity. After some time t , the stationary scattering state should be reached in a square with edge length $L \approx ct$ around the impurity. This part of the system is Fourier transformed and compared to the condensate ground state without the excitation. In the density plot of the scattered wave $|\delta\Psi_{\mathbf{k}'}|^2$, figure 2.7(a), one can already observe the node of vanishing scattering amplitude (2.60) very clearly.

The data shown in figure 2.7(a) still shows the Gross-Pitaevskii wave function. One can get more insight in terms of Bogoliubov amplitudes $\gamma_{\mathbf{k}'} = u_{\mathbf{k}'}\delta\Psi_{\mathbf{k}'} + v_{\mathbf{k}'}\delta\Psi_{-\mathbf{k}'}$, with $u_k = (\epsilon_k + \epsilon_k^0)/(2\sqrt{\epsilon_k\epsilon_k^0})$ and $v_k = (\epsilon_k - \epsilon_k^0)/(2\sqrt{\epsilon_k\epsilon_k^0})$. The corresponding plot of the imaginary part of the Bogoliubov-transformed amplitude in figure 2.7(b) clearly shows the amplitude sign change across the scattering node. Note that figure 2.7(b) is much clearer than figure 2.7(a), because there Bogoliubov excitations with opposite $\pm\mathbf{k}'$ interfere in the wave function densities $|\delta\Psi_{\mathbf{k}'}|^2$. One may wonder why the superposition of nodes stemming from opposite wave vectors still gives a density dip as clear as in figure 2.7(a). In fact, in the single-particle case $k\xi \gg 1$, v_k/u_k tends to zero such that only the node of one component is observed, whereas for sound waves $k\xi \ll 1$ both components contribute equally, but now with symmetric nodes at $\pm\frac{\pi}{2}$ that superpose exactly. This node robustness should facilitate the experimental observation.

We extract the scattering amplitude from the data on the elastic scattering circle in figure 2.7(b) and plot it together with the analytical prediction (2.61) as function of the scattering angle θ at various wave vectors $k\xi$, as shown in figure 2.8. The agreement is very good, with residual numerical scatter due to transients and boundary effects.

Equation (2.61) and figure 2.8 show that the overall magnitude of scattering peaks at $k\xi \approx 1$, at the crossing from waves to particles. Physically, this results from two competing scalings in (2.56):

- The Bogoliubov scattering amplitude $W(k, \theta) \propto \epsilon_k^0/\epsilon_k$ is proportional to k for $k\xi \ll 1$ and saturates to a constant for $k\xi \gg 1$.

2. The Inhomogeneous Bogoliubov Hamiltonian

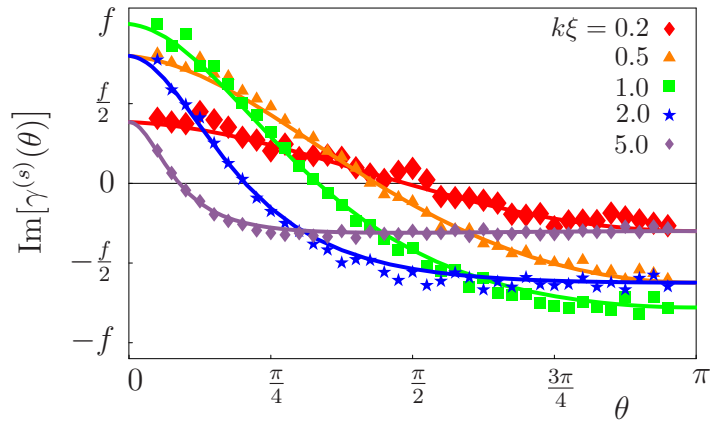


Figure 2.8.: Elastic scattering amplitude (2.61) in units of $f = \gamma_0 V_0 / (8\xi\mu)$ for different values of $k\xi$, at fixed potential radius $kr_0 = 0.5$. Symbols: Results from numerical integration of the full GP equation. Solid curves: analytical prediction (2.61). With increasing k , the node moves to the left, according to (2.60). The overall amplitude has a maximum at $k\xi \approx 1$.

- The inverse group velocity ($\partial k / \partial \epsilon_k$) behaves like the constant c^{-1} for sound waves ($k\xi \ll 1$) and decreases as k^{-1} for particles ($k\xi \gg 1$).

The product of both contributions therefore has limiting behavior k and k^{-1} , respectively, with a maximum around the crossover $k\xi \approx 1$ from phonons to particles.

2.4.5. One-dimensional setting

In a one-dimensional setting, only forward scattering and backscattering are present. This allows easily computing the transmission of a Bogoliubov excitation across an impurity. Now we consider the reflection of an incident Bogoliubov excitation $\gamma_{k'}^{(0)} = \delta_{k'k} \gamma_0$ and compute the elastically reflected wave $\gamma_{k'}^{(r)} = \delta_{k'(-k)} \gamma_r$ in the Born approximation. The elastically scattered wave is again singled out by the imaginary part of the Green function, such that (2.61) applies

$$\text{Im} \frac{\gamma_r}{\gamma_0} = \frac{L^{\frac{1}{2}} V_{-2k}}{4\mu\xi} \frac{k\xi}{k^2\xi^2 + 1}. \quad (2.62)$$

For a point like scatterer, the right hand side is proportional to the weight of the impurity $L^{\frac{1}{2}} V_k \approx \int dx V(x) =: 8\mu\xi B$. From the elastically reflected wave, we obtain the reflection amplitude $r = 2\text{Im}\gamma_r / \gamma_0$. The factor 2 is because the reflected wave exists only on one side of the impurity. For a narrow potential, the transmission intensity $T = 1 - |r|^2$ is shown in figure 2.9. The impurity is perfectly transparent at long wave lengths. At the

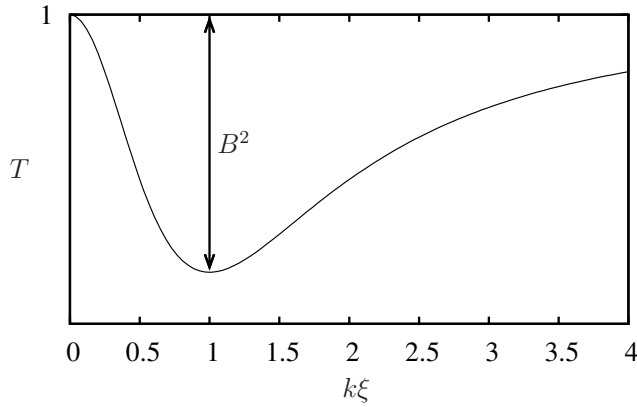


Figure 2.9: One-dimensional transmission T of Bogoliubov excitations across a narrow impurity $V(x)$ with dimensionless impurity strength $B = \int dx V(x)/(8\mu\xi)$.

crossover from sound waves to particles, there is a backscattering maximum, and at high energies the reflection decreases again. The findings of (2.62) and figure 2.9 are in quantitative agreement with the results of Bilas and Pavloff [79] in the limit of a weak impurity. Given the tools from section 2.3, the formalism works very straightforwardly and the problem reduces to the coupling element $W_{-k,k}$. In contrast to Bilas and Pavloff, we do not require the explicit knowledge of Bogoliubov eigenstates, including propagating and evanescent modes.

To some extent, our result in figure 2.9 can be compared to the work of Kagan, Kovrizhin, and Maksimov [105], who consider tunneling across an impurity that suppresses the condensate density very strongly. We agree in the aspect of perfect transmission at low energies. At high energies, however, Kagan *et al.* do not find a revival of transmission. This is reasonable, because they consider a different regime, where the strong impurity deeply depresses the condensate. For long wave-length excitations, this depression is on a short scale and practically invisible, but for wave lengths shorter than the width of the depression, transmission becomes impossible.

2.5. Exact diagonalization of the Bogoliubov problem

In this section, the properties of the Bogoliubov eigenbasis are discussed. The equations of motion for the small excitations derived in section 2.3 stem from the Bogoliubov expansion of the nonlinear Hamiltonian (2.11). Although the equations of motion for the excitations are linear, the expansion of the nonlinear term implies a fundamental difference compared with the Schrödinger equation, namely a non-Hermitian time evolution. This has consequences for the orthogonality properties of the eigenstates and the spectrum [106]. Especially the orthogonality relation to the condensate

function is important for the choice of a suitable Bogoliubov basis for the disorder average in [section 3.2](#).

The explicit knowledge of the Bogoliubov eigenstates reveals more about the condensate than the Gross-Pitaevskii ground state: The condensate depletion, i.e. the number of particles that are not in the Gross-Pitaevskii state, can be computed.

2.5.1. Analogy to other bosonic systems

The commutator relation of density and phase fluctuations $[\delta\hat{n}(\mathbf{r}), \delta\hat{\varphi}(\mathbf{r}')] = i\delta(\mathbf{r} - \mathbf{r}')$ [see [section 2.3](#)] is analogous to the commutator of coordinate q and momentum p of a particles $[x_i, p_j] = i\hbar\delta_{ij}$. The Hamiltonian (2.38) can schematically be written as

$$F = \frac{1}{2} (\mathbf{p}^T, \mathbf{q}^T) \begin{pmatrix} M & C \\ C^T & K \end{pmatrix} \begin{pmatrix} \mathbf{p} \\ \mathbf{q} \end{pmatrix}, \quad (2.63)$$

which is the general quadratic bosonic Hamiltonian [107]. It describes a particle or a set of particles in a harmonic potential. The mass matrix and the matrix of spring constants are given as $M = \epsilon^0 + S$ and $K = 2\mu + \epsilon^0 + R$, respectively. In the general Hamiltonian, off-diagonal blocks C may be present. Their absence in the Bogoliubov problem (2.38) corresponds to time-reversal symmetry, which is compatible with the absence of magnetic fields or rotations. The quadratic ‘‘potential’’ $\mathbf{q}^T K \mathbf{q}$ is harmonic, which is suitable for describing phonons in random elastic media [31, 107].

By defining creation and annihilation operators of the harmonic oscillators, the Hamiltonian (2.63) takes a structure analogous to the Bogoliubov Hamiltonian (2.42)

$$F = \frac{1}{2} (\hat{\gamma}^\dagger, \hat{\gamma}) \begin{pmatrix} \Gamma & \Delta \\ \Delta^\dagger & \Gamma^T \end{pmatrix} \begin{pmatrix} \hat{\gamma} \\ \hat{\gamma}^\dagger \end{pmatrix}. \quad (2.64)$$

Note the different sign convention for the second component of the pseudo-spinors, such that $\Gamma_{\mathbf{k}'\mathbf{k}} = W_{\mathbf{k}'\mathbf{k}}$, but $\Delta_{\mathbf{k}'\mathbf{k}} = Y_{\mathbf{k}'(-\mathbf{k})}$.

From the structure of (2.64), rather general properties follow, like the chiral symmetry (i.e. the occurrence of frequencies in pairs $\pm\omega$) [107]. In the following, we will derive this and some more properties at the concrete Bogoliubov problem.

2.5.2. Bogoliubov-de-Gennes equations

How can the general Bogoliubov Hamiltonian (2.63) or (2.64) be diagonalized? For this task, the representation in terms of the field operator $\delta\hat{\Psi}$ is

used, instead of density $\delta\hat{n}$ and phase $\delta\hat{\varphi}$. This makes the structure better comparable with the Schrödinger equation and helps to point out the differences. The expansion of the grand canonical Hamiltonian (2.11) reads

$$\hat{F} = \frac{1}{2} \int d^d r (\delta\hat{\Psi}^\dagger(\mathbf{r}), \delta\hat{\Psi}(\mathbf{r})) \begin{pmatrix} \mathcal{L} & G \\ G^* & \mathcal{L} \end{pmatrix} \begin{pmatrix} \delta\hat{\Psi}(\mathbf{r}) \\ \delta\hat{\Psi}^\dagger(\mathbf{r}) \end{pmatrix} + \text{cst.}, \quad (2.65)$$

with the Hermitian operator $\mathcal{L} = -\frac{\hbar^2}{2m}\nabla^2 + V(\mathbf{r}) - \mu + 2g|\Phi(\mathbf{r})|^2$ and $G = g\Phi(\mathbf{r})^2$. The goal is now to find a transformation to quasiparticles $\hat{\beta}_\nu$, such that the Bogoliubov Hamiltonian \hat{F} takes the diagonal form

$$\hat{F} = \sum_\nu \hbar\omega_\nu \hat{\beta}_\nu^\dagger \hat{\beta}_\nu. \quad (2.66)$$

The Bogoliubov Hamiltonian was obtained by the expansion around the saddlepoint. It turns out that the saddlepoint is indeed an energy minimum, not only in the homogeneous problem (2.3.1), but also in inhomogeneous systems. Therefore, the spectrum $\hbar\omega_\nu$ is positive. The transformation mixes $\delta\hat{\Psi}(\mathbf{r})$ and $\delta\hat{\Psi}^\dagger(\mathbf{r})$, similar to the homogeneous Bogoliubov transformation in subsection 2.3.1. Furthermore, the inhomogeneous potential and its density imprint will mix the plane waves, such that the eigenstates will have some unknown shape. The general transformation to a set of eigenmodes reads

$$\delta\hat{\Psi}(\mathbf{r}) = \sum_\nu [u_\nu(\mathbf{r})\hat{\beta}_\nu - v_\nu^*(\mathbf{r})\hat{\beta}_\nu^\dagger], \quad (2.67)$$

with a set of initially unknown functions $u_\nu(\mathbf{r})$ and $v_\nu(\mathbf{r})$ [106]. Note that there are different conventions concerning the sign in front of v_ν^* . Here and e.g. in [54, 105, 106], the minus sign is used, with $v_{\mathbf{k}}(\mathbf{r}) = v_{\mathbf{k}}e^{i\mathbf{k}\cdot\mathbf{r}}$ in the homogeneous case. In other literature, $v_\nu(\mathbf{r})$ is defined with opposite sign [55, 79, 85, 86]. The quasiparticle annihilators $\hat{\beta}_\nu$ appearing in equation (2.67) and their creators obey bosonic commutator relations, as will be verified below.

The equation of motion for $\delta\hat{\Psi}(\mathbf{r})$ is set up using both forms of the Hamiltonian (2.65) and (2.66). By equating the coefficients, we find the following equation on the $u_\nu(\mathbf{r})$ and $v_\nu(\mathbf{r})$

$$\eta \underbrace{\begin{pmatrix} \mathcal{L} & -G \\ -G^* & \mathcal{L} \end{pmatrix}}_{=:Q} \begin{pmatrix} u_\nu(\mathbf{r}) \\ v_\nu(\mathbf{r}) \end{pmatrix} = \hbar\omega_\nu \begin{pmatrix} u_\nu(\mathbf{r}) \\ v_\nu(\mathbf{r}) \end{pmatrix}, \quad (2.68)$$

where $\eta = \text{diag}(1, -1)$. This equation is known as the Bogoliubov-de-Gennes equation for the Bogoliubov eigenmodes [86]. Although both operators Q

and η are self-adjoint (Hermitian), their product is not, $(\eta Q)^\dagger = Q\eta \neq \eta Q$. But ηQ is intimately connected with its adjoint: $(\eta Q)^\dagger = Q\eta = \eta(\eta Q)\eta = \eta(\eta Q)\eta^{-1}$. This property is called pseudo-Hermiticity with respect to η [108].

In presence of an arbitrary potential with a corresponding ground-state density, the determination of the eigenstates is possible only numerically. However, some analytical statements on their properties can be made.

2.5.3. Zero-frequency mode

The relation of the excitations to the ground state $\Phi(\mathbf{r})$ is of particular interest. A special solution of (2.68) is given by an excitation, where both $u(\mathbf{r})$ and $v(\mathbf{r})$ are proportional to the ground state, $u_0(\mathbf{r}) = v_0(\mathbf{r}) = \alpha\Phi(\mathbf{r})$, $\alpha \in \mathbb{C}$. This solution has zero frequency, as can be seen from $(\mathcal{L} - G)\Phi = 0$, because Φ is a stationary solution of the Gross-Pitaevskii equation (2.16). The contribution of this “excitation” to the field operator (2.67) is given as $2i\text{Im}(\alpha)\Phi(\mathbf{r})$, i.e. it consists only in a global phase shift of the wave function. Due to the gauge symmetry, there is no restoring force, so it is not an excitation in the strict sense. This zero-mode is the Goldstone mode related to the $U(1)$ symmetry breaking of the order parameter [72, 89].

The fact that the zero-mode takes place only in the phase of the condensate and not in the density is perfectly compatible with the observation made in subsection 2.3.1 that the low-energy Bogoliubov-excitations oscillate mainly in the phase and hardly in the density (figure 2.3).

2.5.4. Eigenstates of non self-adjoint operators

Before considering the proper excitations with finite frequencies, it is useful to discuss some general properties of the eigenstates of non-Hermitian operators [109]. Let us assume the eigenstates of a non-Hermitian operator $\mathcal{U} \neq \mathcal{U}^\dagger$ to be known and investigate their orthogonality relations. In the following, the orthonormal basis \mathbf{e}_k , which will in general not be the eigenbasis of the operator \mathcal{U} , will be employed. The standard scalar product $(\mathbf{a}, \mathbf{b}) = \mathbf{a}^\dagger \mathbf{b}$ is defined by the conventional matrix product of the adjoint vector \mathbf{a}^\dagger with \mathbf{b} . The orthonormality then reads $\mathbf{e}_j^\dagger \mathbf{e}_k = \delta_{j,k}$. Now we consider the effect of \mathcal{U} on the basis vectors:

$$\mathcal{U} \mathbf{e}_k = \sum_j U_{jk} \mathbf{e}_j \quad \mathcal{U} = \sum_{j,k} \mathbf{e}_j U_{jk} \mathbf{e}_k^\dagger \quad U_{jk} = \mathbf{e}_j^\dagger \mathcal{U} \mathbf{e}_k \quad (2.69)$$

The eigenvalues λ_m and the (right) eigenvectors \mathbf{a}_m of \mathcal{U} are defined by

$$\sum_j [U_{ij} - \lambda_m \delta_{ij}] (\mathbf{a}_m)_j = 0 \quad \Leftrightarrow \quad \det (U_{ij} - \lambda_m \delta_{ij}) = 0. \quad (2.70)$$

Analogously the eigenvectors of the adjoint operator $\mathcal{U}^\dagger = \sum_{j,k} \mathbf{e}_j U_{kj}^* \mathbf{e}_k^\dagger$ (or left eigenvectors of \mathcal{U}) can be defined

$$\sum_j [U_{ji}^* - \mu_n \delta_{i,j}] (\mathbf{b}_n)_j = 0 \quad \Leftrightarrow \quad \det (U_{ji}^* - \mu_n \delta_{i,j}) = 0. \quad (2.71)$$

Taking the complex conjugate and interchanging the indices, we see, that μ_n^* and λ_m satisfy the same equation. Thus, the eigenvalues can be enumerated such that $\mu_n^* = \lambda_n$. Finally, we compute the scalar product $\mathbf{b}_n^\dagger \mathcal{U} \mathbf{a}_m$ and let \mathcal{U} act both to the right and to the left

$$\mathbf{b}_n^\dagger \mathcal{U} \mathbf{a}_m = \sum_{i,j} (\mathbf{b}_n^\dagger)_i U_{ij} (\mathbf{a}_m)_j \stackrel{(2.70)}{=} \sum_i (\mathbf{b}_n^\dagger)_i \lambda_m (\mathbf{a}_m)_i \stackrel{(2.71)}{=} \sum_j \mu_n^* (\mathbf{b}_n^\dagger)_j (\mathbf{a}_m)_j .$$

From this, it follows the bi-orthogonality relation

$$(\lambda_m - \lambda_n) (\mathbf{b}_n, \mathbf{a}_m) = 0. \quad (2.72)$$

Thus, the eigenvector \mathbf{a}_m is orthogonal to the adjoints of eigenvectors with different eigenvalues \mathbf{b}_m . This, however, does not imply that the eigenvectors themselves are pairwise orthogonal. Only in the case of a Hermitian operator with $U_{ij} = U_{ji}^*$, the left equations of (2.70) and (2.71) imply that $\mathbf{a}_n = \mathbf{b}_n$, which then restores the usual orthogonality of eigenvectors.

2.5.5. Bogoliubov eigenstates with non-zero frequency

Let us express the bi-orthogonality relation derived above in terms of the Bogoliubov eigenstates. Let $\mathbf{a}_\nu = \begin{pmatrix} u_\nu \\ v_\nu \end{pmatrix}$ be an eigenvector of ηQ with eigenvalue ω_ν : $\eta Q \mathbf{a}_\nu = \hbar \omega_\nu \mathbf{a}_\nu$. With $\eta^2 = 1$, it can be seen that the matrix η relates the eigenvectors to those of the adjoint operator $Q\eta$

$$Q\eta(\eta \mathbf{a}_\nu) = \eta(\eta Q) \mathbf{a}_\nu = \hbar \omega_\nu \eta \mathbf{a}_\nu \quad \Rightarrow \quad \mathbf{b}_\nu = \eta \mathbf{a}_\nu. \quad (2.73)$$

With this, the bi-orthogonality relation (2.72) reads

$$0 = (\omega_\nu - \omega_\mu) \mathbf{b}_\nu^\dagger \mathbf{a}_\mu = (\omega_\nu - \omega_\mu) \int d^d r [u_\nu^*(\mathbf{r}) u_\mu(\mathbf{r}) - v_\nu^*(\mathbf{r}) v_\mu(\mathbf{r})] \quad (2.74)$$

2. The Inhomogeneous Bogoliubov Hamiltonian

for the Bogoliubov states. This condition on the eigenstates takes the place of the orthogonality in the Schrödinger problem. For Bogoliubov modes with different frequencies $\omega_\nu \neq \omega_\mu$, the integral in equation (2.74) has to vanish. For degenerate modes, the choice of the eigenbasis is not unique, but can be chosen such that the integral vanishes for different members of the same eigenspace as well. Together with a proper normalization (needed for $\mu = \nu$), equation (2.74) takes the form

$$\int d^d r [u_\nu^*(\mathbf{r})u_\mu(\mathbf{r}) - v_\nu^*(\mathbf{r})v_\mu(\mathbf{r})] = \delta_{\mu,\nu} \quad (2.75)$$

for all modes except for the zero-frequency mode. At this point, we forestall that the normalization constant is +1. Below, we will show that this corresponds to the bosonic character of the $\hat{\beta}_\nu$.

The zero-mode from subsection 2.5.3 cannot be normalized. However, condition (2.74) still holds, thus all Bogoliubov modes with finite frequency fulfill

$$\int d^d r \Phi^*(\mathbf{r}) [u_\nu(\mathbf{r}) - v_\nu(\mathbf{r})] = 0, \quad (2.76)$$

the orthogonality condition with respect to the ground state.

Mean-field total particle number

In the mean-field interpretation of Bogoliubov excitations (subsection 2.3.4), the Hilbert space representing the excitations has doubled from one complex function $\delta\Psi$, to a pseudo-spinor containing u and v . When expanding a given initial state in the Bogoliubov mean-field framework (subsection 2.3.4) into Bogoliubov eigenmodes, one has to determine the coefficients α_ν in $\Psi = \Phi + \sum_\nu [\alpha_\nu u_\nu(\mathbf{r}) - \alpha_\nu^* v_\nu^*(\mathbf{r})]$. If the ground state has no superfluid flow (i.e. no vortices, no 1D flow like e.g. in [110]), then the ground-state wave function and the Bogoliubov modes $u_\nu(\mathbf{r})$ and $v_\nu(\mathbf{r})$ can be chosen real. The deviation from the ground state then reads

$$\begin{aligned} \delta\Psi(\mathbf{r}, t) &= u_\nu(\mathbf{r})e^{-i\omega_\nu t} - v_\nu(\mathbf{r})e^{i\omega_\nu t} \\ &= [u_\nu(\mathbf{r}) - v_\nu(\mathbf{r})] \cos(\omega_\nu t) - i[u_\nu(\mathbf{r}) + v_\nu(\mathbf{r})] \sin(\omega_\nu t). \end{aligned} \quad (2.77)$$

The real part shifts the local condensate density by $\delta n(\mathbf{r}) = 2\Phi(\mathbf{r})\text{Re}\delta\Psi(\mathbf{r})$. The orthogonality condition (2.76) with respect to the ground state has a simple interpretation: it simply states that the total particle number is not changed by the excitations. This is reasonable, because the Gross-Pitaevskii ground state is computed with the particle number given by the initial state

$\Psi(\mathbf{r}, t = 0)$. There is no reason why the deviations from the ground state should affect the number of particles, they merely deform the wave function. This relation between the phase-related zero-mode and the particle number does not come as a surprise, as phase and density are conjugate variables.

Frequency pairs

Due to the time-inversion symmetry, solutions of equation (2.68) occur in pairs. Defining $\hat{\tau} = \begin{pmatrix} 0 & 1 \\ 1 & 0 \end{pmatrix}$ and using the commutation relations $\eta\hat{\tau} = -\hat{\tau}\eta$, $\hat{\tau}Q = (Q\hat{\tau})^*$, we find

$$\eta Q(\hat{\tau}\mathbf{a}_\nu^*) = \eta\hat{\tau}Q^*\mathbf{a}_\nu^* = -\hat{\tau}(\eta Q\mathbf{a}_\nu)^* = -\hbar\omega_\nu\hat{\tau}\mathbf{a}_\nu^* \quad \mathbf{a}_\nu^- = \hat{\tau}\mathbf{a}_\nu^* \quad (2.78a)$$

$$Q\eta(\hat{\tau}\mathbf{b}_\nu^*) = -Q\hat{\tau}\eta\mathbf{b}_\nu^* = -\hat{\tau}(Q\eta\mathbf{b}_\nu)^* = -\hbar\omega_\nu\hat{\tau}\mathbf{b}_\nu^* \quad \mathbf{b}_\nu^- = \hat{\tau}\mathbf{b}_\nu^*. \quad (2.78b)$$

From these solutions with negative frequencies, another orthogonality relation follows from equation (2.72) with $(\mathbf{b}_\nu^-, \mathbf{a}_\mu) = 0$

$$\int d^d r [v_\nu(\mathbf{r})u_\mu(\mathbf{r}) - u_\nu(\mathbf{r})v_\mu(\mathbf{r})] = 0. \quad (2.79)$$

Together with (2.75), this identity is used to invert the transformation (2.67) and express the quasiparticle operators in terms of the field operator

$$\hat{\beta}_\nu = \int d^d r [u_\nu^*(\mathbf{r})\delta\hat{\Psi}(\mathbf{r}) + v_\nu^*(\mathbf{r})\delta\hat{\Psi}^\dagger(\mathbf{r})]. \quad (2.80)$$

The identity (2.80) clarifies the meaning of the negative frequencies. The quasiparticle annihilator $\hat{\beta}_\nu^-$ of the negative-frequency mode reads

$$\hat{\beta}_\nu^- = \int d^d r [v_\nu(\mathbf{r})\delta\hat{\Psi}(\mathbf{r}) + u_\nu(\mathbf{r})\delta\hat{\Psi}^\dagger(\mathbf{r})] = \hat{\beta}_\nu^\dagger, \quad (2.81)$$

which coincides with the quasiparticle creator $\hat{\beta}_\nu^\dagger$. Thus, negative Bogoliubov frequencies have nothing to do with negative excitation energies, but simply swap the roles of creators and annihilators. They are not necessary for the completeness of the Bogoliubov eigenbasis and will be excluded in the following.

Properties of Bogoliubov eigenstates summed up

- The zero-frequency mode comes from the broken $U(1)$ symmetry and is not a Bogoliubov excitation in the proper sense.
- Only the excitations with positive frequencies are physically relevant.

2. The Inhomogeneous Bogoliubov Hamiltonian

- All finite-frequency modes fulfill the orthogonality (2.76) with respect to the ground state. This excludes a real overlap of $\delta\Psi$ with the ground state Φ .
- All eigenstates pairwise fulfill the bi-orthogonality relation (2.74).

Bogoliubov ground state

The Bogoliubov quasiparticles satisfy the bosonic commutator relations

$$[\hat{\beta}_\mu, \hat{\beta}_\nu^\dagger] = \delta_{\mu,\nu}, \quad [\hat{\beta}_\mu^\dagger, \hat{\beta}_\nu^\dagger] = [\hat{\beta}_\mu, \hat{\beta}_\nu] = 0, \quad (2.82)$$

which are easily verified using equations (2.75), (2.79) and (2.80). The operators $\hat{\beta}_\nu^\dagger$ and $\hat{\beta}_\nu$ create and annihilate Bogoliubov excitations. In particular, the Bogoliubov ground state is the Bogoliubov vacuum $|\text{vac}\rangle$, defined by the absence of Bogoliubov excitations

$$\hat{\beta}_\nu |\text{vac}\rangle = 0. \quad (2.83)$$

2.5.6. Non-condensed atom density

Bogoliubov quasiparticles can be excited thermally or by external perturbations. But even in the ground state, not all particles are in the (Gross-Pitaevskii) condensate state. We are interested in the number of non-condensed atoms

$$n_{\text{nc}} = \frac{1}{L^d} \int d^d r \langle \text{vac} | \delta\hat{\Psi}^\dagger(\mathbf{r}) \delta\hat{\Psi}(\mathbf{r}) | \text{vac} \rangle. \quad (2.84)$$

It is important to distinguish this density n_{nc} of atoms that are not in the condensate $\Phi(\mathbf{r})$ from the number of particles that are not in the state $k = 0$. The latter is sometimes referred to as “condensate depletion” [77, 78], but it is more a condensate *deformation*.

The “condensate depletion due to disorder” n_R in [77, Eq. (9)] is only due to the first-order smoothing correction (2.22) of the Gross-Pitaevskii wave function.

The shift of the non-condensed density due to disorder, which we are going to compute now, is beyond Huang’s and Meng’s work [77]. In order to evaluate the non-condensed density, the field operator $\delta\hat{\Psi}(\mathbf{r})$ is expressed in terms of the Bogoliubov creators and annihilators, using equation (2.67)

$$n_{\text{nc}} = \sum_\nu \frac{1}{L^d} \int d^d r |v_\nu(\mathbf{r})|^2. \quad (2.85)$$

In this form, the non-condensed density requires the Bogoliubov eigenstates to be computed explicitly. This will be done in the numerical study of the disordered Bogoliubov problem in [subsection 4.3.3](#).

Non-condensed density in the homogeneous BEC

In the homogeneous Bogoliubov problem ([subsection 2.3.1](#)), we use equation (2.27) and (2.33) and write

$$\delta\hat{\Psi}(\mathbf{r}) = \frac{1}{L^{\frac{d}{2}}} \sum_{\mathbf{k}} \left[u_k e^{i\mathbf{k}\cdot\mathbf{r}} \hat{\gamma}_{\mathbf{k}} - v_k e^{-i\mathbf{k}\cdot\mathbf{r}} \hat{\gamma}_{\mathbf{k}}^\dagger \right], \quad v_k = \frac{\epsilon_k - \epsilon_k^0}{2\sqrt{\epsilon_k \epsilon_k^0}}. \quad (2.86)$$

Inserting this into equation (2.84), we find the density of non-condensed atoms as

$$n_{\text{nc}} = \frac{1}{L^d} \sum'_{\mathbf{k}} |v_k|^2. \quad (2.87)$$

The prime indicates that the homogeneous condensate mode $\mathbf{k} = 0$ is excluded from the summation.

Because of the asymptotics $|v_k|^2 \sim (k\xi)^{-4}$, there is no UV divergence in the dimensions $d = 1, 2, 3$. In three dimensions, the sum is approximated by an integral, which leads to

$$n_{\text{nc}} = \frac{1}{6\sqrt{2}\pi^2} \frac{1}{\xi^3}, \quad \frac{n_{\text{nc}}}{n} = \frac{8}{3\sqrt{\pi}} \sqrt{na_s^3}. \quad (2.88)$$

The fraction of non-condensed particles scales with the gas parameter $\sqrt{na_s^3}$ [77], where $a_s = mg/(4\pi\hbar^2)$ is the s-wave scattering length.

The non-condensed density n_{nc} (2.88) is a function of the healing length $\xi = \hbar/\sqrt{2mgn}$. It depends on the product of total density n and interaction parameter g . In the ratio n_{nc}/n this is converted to the gas parameter $\sqrt{na_s^3}$. This is the small parameter that ensures the applicability of Gross-Pitaevskii theory ([subsection 2.2.2](#)). The above reasoning is true not only in the present homogeneous case, but also for inhomogeneous condensates.

For low momenta, the summand in (2.87) diverges like $1/(k\xi)$. In one dimension, this IR divergence forbids evaluating the sum (2.87) in the continuum approximation. This is consistent with the fact that there is no true Bose-Einstein condensate in one dimension ([subsection 2.1.2](#)). The long-range order is destroyed by the long wave-length fluctuations. However, in finite systems, where the quasi-condensate concept holds, the sum can always be evaluated.

2.6. Conclusions on Gross-Pitaevskii and Bogoliubov

The basic idea of the formalism employed in this chapter is splitting the bosonic field operator into the mean-field Gross-Pitaevskii ground state and the quantized fluctuations. The Gross-Pitaevskii ground state $\Phi(\mathbf{r}) = \langle \hat{\Psi}(\mathbf{r}) \rangle$ is equivalent to a Hartree-Fock ansatz of a product state.⁴ This approximation is good for Bose condensed systems. Due to inhomogeneous external potentials, the condensate function $\Phi(\mathbf{r})$ gets deformed, but within Gross-Pitaevskii theory the system is still fully condensed. As discussed in [subsection 2.1.2](#), there actually is no true Bose-Einstein condensate in one and two dimensions, which is in agreement with general theorems [111] forbidding true long-range order in $d = 1, 2$. For practical purposes, however, it is usually meaningful to consider the Bose gas as a quasi-condensate with phase coherence on a sufficiently long scale.

Within the Gross-Pitaevskii framework, there is no information about those particles that are not in the product state of the condensate. This is where Bogoliubov theory takes over. Starting with the Gross-Pitaevskii wave function, it describes those particles that are outside of the condensate in a quantized manner. The Bogoliubov quasiparticles are characterized by the functions $u_\nu(\mathbf{r})$ and $v_\nu(\mathbf{r})$, which are simply plane waves in the homogeneous case. In presence of an external potential and the corresponding imprint in the condensate density, however, the eigenstates can in general only be determined numerically.

The Bogoliubov ground state is conceptually different from the Gross-Pitaevskii ground state. It is defined abstractly as the vacuum of quasiparticles $\hat{\beta}_\nu |\text{vac}\rangle = 0$. Together with the transformation (2.67), this allows computing the fraction of non-condensed particles (2.84). This condensate depletion needs to be low in order to verify *a posteriori* the validity of the Gross-Pitaevskii approximation. In the homogeneous system, the fraction of the non-condensed particles scales with the gas parameter $\sqrt{na_s^3}$. Thus, the Gross-Pitaevskii approximation is applicable in the dilute Bose gas $\sqrt{na_s^3} \ll 1$. The question how the non-condensed fraction is influenced by an external disorder potential will be addressed in [subsection 4.3.3](#).

⁴In this work, the standard symmetry breaking formulation is used, where the condensate takes a definite phase, such that $\langle \hat{\Psi} \rangle$ is finite. More precisely, the system is in a coherent state, i.e. an eigenstate of the annihilator $\hat{\Psi}$ with an uncertain number of particles. Other formulations are possible, like Castin's and Dum's number conserving formulation [112]. For the practical purposes within the scope of this work, however, the symmetry breaking approach is sufficient.

3. Disorder

In the previous chapter, we have set up the general formalism for describing Bogoliubov excitations in a weak external potential, and, as a first application, we have applied it to the scattering of Bogoliubov waves at a single impurity. Now it is time to enter the disordered world by specifying the potential $V(\mathbf{r})$ as a disordered potential with certain statistical properties. The disorder potential causes an imprint in the condensate density, which forms an inhomogeneous background for the excitations (figure 3.1).

In section 3.1, the experimentally relevant optical speckle potential is presented, and its statistical properties are derived. The speckle disorder will be used throughout this work. In the final results, the two-point correlation function of the speckle disorder can be replaced with the correlation function of any other kind of disorder.

The goal of this chapter is to give a useful characterization of the dynamics of Bogoliubov excitations in presence of disorder. Of course, the results should not depend on the particular realization of disorder, so suitable disorder averages are necessary. Before doing so, some considerations about the choice of the basis for the excitations have to be made. Until now, the free Bogoliubov basis in terms of density and phase fluctuations has been used rather intuitively. In section 3.2, it is discussed in detail, why this basis actually is the only reasonable choice for the disordered Bogoliubov problem.

All considerations made so far meet in section 3.3, the essential of this chapter. The propagation of Bogoliubov excitations in the disorder averaged *effective medium* is described by the average Green function, which reveals the disorder-broadened dispersion relation, with a finite lifetime and a renormalized propagation speed of the excitations. The optical analog of this is the index of refraction and the absorption coefficient in a medium like glass or water.

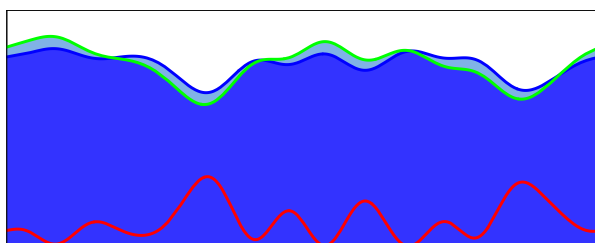


Figure 3.1: Schematic representation of the disordered Bogoliubov setting. The disorder potential (red) leaves an imprint in the condensate (blue). On top of that, wave excitations (green) are considered.

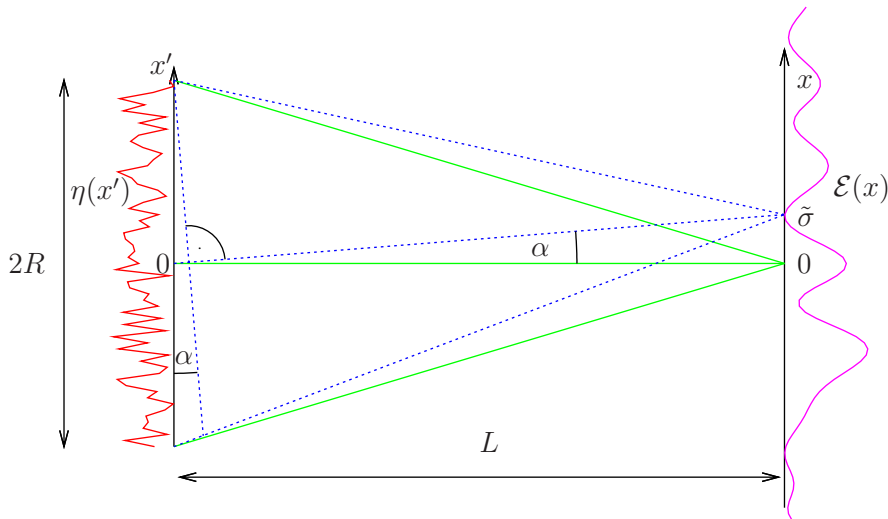


Figure 3.2.: Principle of the speckle phenomenon. Waves with random phase originating from the rough surface on the left interfere and create a speckle pattern $\mathcal{E}(x)$ on the right. The finite correlation length of the speckle pattern can be understood as follows. Let the interference be constructive at $r = 0$. What is the shortest scale, where destructive interference can occur? This distance $\tilde{\sigma}$ can be estimated by the condition that at least the waves from the outermost points interfere destructively, i.e. their path difference increases from zero at $x = 0$ to $2R\alpha = 2R\tilde{\sigma}/L = \lambda_L/2$ at $r = \tilde{\sigma}$, where λ_L is the laser wave length. Thus, the correlation length $\tilde{\sigma}$ is given by the laser wave length λ_L over the numerical aperture $\tilde{\sigma} = \lambda_L L / (4R)$. In the following, the conventional definition of the correlation length $\sigma = \frac{\lambda_L}{2\pi} \frac{L}{R}$ [23, 115] will be used, which differs by a numerical factor.

3.1. Optical speckle potential

Disorder potentials with very well controlled statistical properties can be created experimentally with optical laser-speckle fields. The coherent light of a laser is directed on a rough surface or through a diffusor plate, such that the elementary waves originating from each point have a random phase. In the far field, their interference creates a random intensity pattern with well known statistical properties. In particular, it has a finite correlation length, which is related to the laser wave length and the aperture of the speckle optics [66, 67]. Depending on the detuning of the laser frequency with respect to an internal resonance of the atoms, the speckle intensity is translated into a repulsive or attractive *light shift potential* for the atoms. Speckle disorder has been used in many cold-atoms experiments, for example the expansion experiments in Palaiseau [25, 67–69] and in Hannover [113], experiments at Rice University [114] and in Florence [70].

3.1.1. Speckle amplitude

The coherent light from a laser is widened and directed on a rough surface or through a milky plate (diffusor). The roughness is assumed to be larger than the laser wave length, such that the phases of the emitted elementary waves are totally random. According to Huygens' principle, each point on the diffusor emits elementary waves proportional to $e^{ik_L|\mathbf{r}'|}/|\mathbf{r}'| =: h(\mathbf{r}')$. The electric field $\mathcal{E}(\mathbf{r})$ in the plane of observation in some distance L is the superposition of these elementary waves with phase factors $\eta(\mathbf{r}')$

$$\mathcal{E}(\mathbf{r}) = \int d^d r' \eta(\mathbf{r}') h(\mathbf{r} - \mathbf{r}'), \quad (3.1)$$

see [figure 3.2](#). The complex random field $\eta(\mathbf{r}')$ has zero mean $\overline{\eta(\mathbf{r}')} = 0$ and is uncorrelated in the sense that its spatial correlation is much shorter than the laser wave length $\overline{\eta^*(\mathbf{r})\eta(\mathbf{r}')} \propto \delta(\mathbf{r} - \mathbf{r}')\Theta(R - |\mathbf{r}'|)$. Here, the finite radius R of the diffusor is expressed using the Heaviside step function Θ . The integral over the random numbers can be regarded as a random walk in the complex plane. According to the central limit theorem, the local probability distribution is Gaussian

$$P(\text{Re } \mathcal{E}, \text{Im } \mathcal{E}) = \frac{1}{\pi I_0} e^{-\frac{|\mathcal{E}|^2}{I_0}}, \quad \text{with } I_0 = \overline{|\mathcal{E}|^2}. \quad (3.2)$$

Due to the finite laser wave length and the finite optical aperture, there is a spatial correlation length σ . The speckle intensity cannot vary on length scales shorter than σ , because elementary waves from different points have to acquire a certain path difference in order to switch from constructive to destructive interference, see [figure 3.2](#). Let us consider in more detail the speckle interference pattern in the far-field. If the distance L is sufficiently large, the Fresnel approximation [[116](#), Chapter 4] can be made. It consists in an expansion of $|\mathbf{r} - \mathbf{r}'|$ in $h(\mathbf{r} - \mathbf{r}')$ in the small parameter $|\mathbf{x} - \mathbf{x}'|/L$, where \mathbf{x} and \mathbf{x}' denote the components of \mathbf{r} and \mathbf{r}' in the diffusor plane and the plane of observation, respectively:

$$h(\mathbf{r} - \mathbf{r}') \approx \frac{1}{L} e^{ik_L L} \exp\left(ik_L \frac{(\mathbf{x} - \mathbf{x}')^2}{2L}\right) \quad (3.3)$$

Inserting [\(3.3\)](#) into [\(3.1\)](#) and expanding the quadratic term in the exponent, one finds

$$\tilde{\mathcal{E}}(\mathbf{x}) = \frac{1}{L} \int d^2 x' \exp\left(-i \frac{k_L}{L} \mathbf{x} \cdot \mathbf{x}'\right) \tilde{\eta}(\mathbf{x}'). \quad (3.4)$$

3. Disorder

The quadratic terms have been absorbed as phase factors in

$$\tilde{\mathcal{E}}(\mathbf{x}) = e^{-i\frac{k_L}{2L}x^2} e^{-ik_L L} \mathcal{E}(\mathbf{r}) \quad \text{and} \quad \tilde{\eta}(\mathbf{x}') = e^{i\frac{k_L}{2L}x'^2} \eta(\mathbf{x}'). \quad (3.5)$$

The mixed term in (3.4) connects $\tilde{E}(\mathbf{x})$ and $\tilde{\eta}(\mathbf{x}')$ as a Fourier transform. Up to a complex phase, the field (3.1) is identified as the Fourier transform of the random field $\tilde{\eta}(\mathbf{x}')$, evaluated at $\mathbf{k} = k_L \mathbf{x}/L$. Accordingly, the Fourier components of the field $\tilde{\mathcal{E}}_{\mathbf{k}}$ are given by the random field $\tilde{\eta}(\mathbf{x}')$ evaluated at $\mathbf{x}' = -L\mathbf{k}/k_L$. The Fourier components inherit all statistical properties from the surface of the diffusor:

$$\overline{\tilde{\mathcal{E}}_{\mathbf{k}} \tilde{\mathcal{E}}_{\mathbf{k}'}} \propto \overline{\tilde{\eta}^*(-L\mathbf{k}/k_L) \tilde{\eta}(-L\mathbf{k}'/k_L)} \propto \delta(\mathbf{k} - \mathbf{k}') \Theta(\sigma^{-1} - |\mathbf{k}|), \quad (3.6)$$

with the disorder correlation length $\sigma = L/(Rk_L)$. As only the intensity of the electric fields is relevant for the light-shift potential [see below], we identify \mathcal{E} with $\tilde{\mathcal{E}}$ in the following. In terms of the average intensity in the plane of observation $I_0 = \overline{|\mathcal{E}(\mathbf{x})|^2}$, the field correlator reads

$$\overline{\mathcal{E}_{\mathbf{k}}^* \mathcal{E}_{\mathbf{k}'}} = \frac{(2\pi\sigma)^d}{\text{Vol}(d)} I_0 \Theta(1 - k\sigma) (2\pi)^d \delta(\mathbf{k} - \mathbf{k}') =: \gamma(k) (2\pi)^d \delta(\mathbf{k} - \mathbf{k}'), \quad (3.7)$$

which defines the so-called complex degree of coherence $\gamma(k)$ [23]. Here, $\text{Vol}(d)$ is the volume of the d -dimensional unit sphere. All modes with $k < 1/\sigma = Rk_L/L$ are statistically independent with a common Gaussian probability distribution.

3.1.2. Generalization to 3D

In the preceding derivation of the speckle correlations, a two-dimensional or one-dimensional diffusor plate and a corresponding plane of observation was considered (figure 3.2). The third dimension was needed for the distance L between both. How can this setup be generalized to three dimensions? Also in the third dimension, the speckle field has a certain grain size, but this axial correlation length is typically an order of magnitude longer [66, 67]. Such a 3D speckle field with an anisotropic correlation function has been used e.g. in an experiment on the 3D Bose-Hubbard model [117]. There, the transverse correlation length was shorter than the lattice spacing, and the axial correlation length was of the order of the lattice spacing. In a lattice, variations on a scale shorter than the lattice spacing do not matter, so the disorder was effectively uncorrelated in all three dimensions, fulfilling the demands of the disordered Bose-Hubbard problem.

In continuous systems, however, there is no spacing, and the actual correlation length is important, so similar correlation lengths in all directions are desirable. This could be achieved by the superposition of several speckle fields, where at least a second speckle field for the third dimension is needed. This would achieve similar correlation lengths in all directions, but with an anisotropic correlation function. Ideally, the speckle pattern should be obtained in a closed cavity [23, 24], which restores the isotropy. In this case, the complex degree of coherence reads $\gamma(\mathbf{k}) = 2\pi^2\sigma^2\delta(|\mathbf{k}| - k_L)$, which results in a k -space correlator $C_3(k\sigma) = (8\pi k\sigma)^{-1}\Theta(2 - |k\sigma|)$ with a divergence at $k = 0$.

Lacking a simple experimentally realized model, we prefer to follow Pilati *et al.* [118] and define the three-dimensional speckle disorder from a more abstract point of view. Independently of a possible experimental realization, we declare Eq. (3.7) the definition of the speckle field also in dimension three. This preliminary isotropic three-dimensional speckle field grasps the important features of laser speckles: the asymmetric intensity distribution (3.10) and the finite support of the correlator in k -space (3.12), see below. Like the two-dimensional speckle it might have to be adjusted to the experimental details of future experimental setups, in particular to anisotropies.

3.1.3. Intensity and potential correlations

In typical experimental setups, the laser frequency ω_L is chosen to be close to an internal resonance ω_0 of the atom such that $\omega_L/\omega_0 \approx 1$, but far-detuned in the sense that the detuning $\Delta = \omega_L - \omega_0$ is larger than the line width Γ of the transition or the inverse lifetime of the excited state. Then, the energy levels of the atoms are shifted due to the interaction of their induced dipole moment with the electric laser field [39]. This shift is proportional to the laser intensity $I(\mathbf{r}) = |\mathcal{E}(\mathbf{r})|^2$, where the sign and the magnitude depend on the detuning

$$\Delta E(\mathbf{r}) = \frac{3\pi c_L^2}{2\omega_0^3} \frac{\Gamma}{\Delta} 2\epsilon_0 c_L I(\mathbf{r}). \quad (3.8)$$

In this formula, ϵ_0 is the vacuum permittivity and c_L is the speed of light. The origin of energy is shifted such that the potential has zero mean

$$V(\mathbf{r}) = V_0(I(\mathbf{r}) - I_0)/I_0. \quad (3.9)$$

Here, the signed disorder strength is defined as $V_0 = 3\pi c_L^3 \epsilon_0 \Gamma I_0 / (\omega_0^3 \Delta)$. The magnitude of the parameter V_0 is the rms value of $V(\mathbf{r})$, $V_0^2 = \overline{V(\mathbf{r})^2}$. Its sign is determined by the detuning of the laser frequency and states

3. Disorder

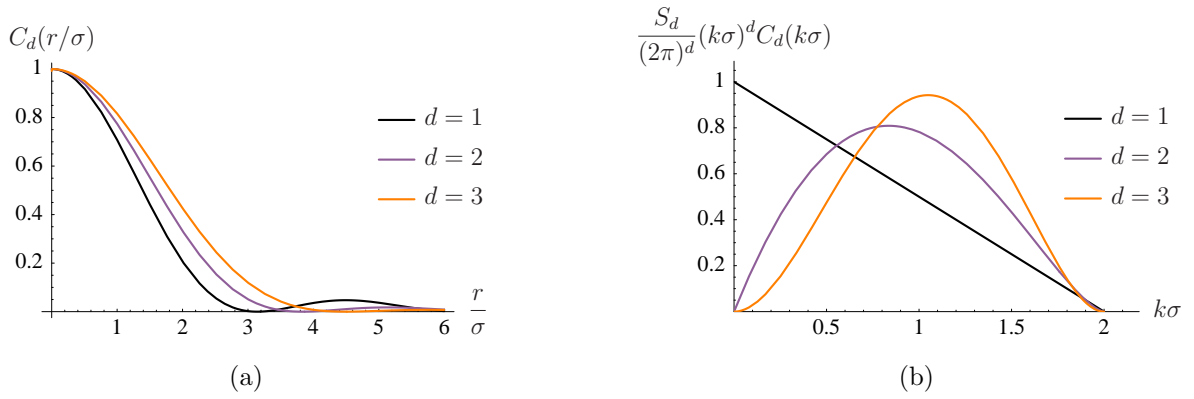


Figure 3.3.: Speckle correlation functions in $d = 1, 2, 3$. (a) real-space representation. (b) k -space representation. For the sake of comparable scales, $S_d(k\sigma)^d C_d(k\sigma)/(2\pi)^d$ is plotted.

whether the speckle potential is repulsive or attractive, see [figure 4.8](#) on page [97](#). Because of Eq. (3.2), the intensity probability distribution is a negative exponential with a baseline at zero intensity and arbitrarily high peaks in the exponential tail. Then, the potential has the skewed probability distribution with zero mean

$$P(w)dw = \Theta(w + 1)e^{-(w+1)}dw, \quad \text{with } w = V(\mathbf{r})/V_0. \quad (3.10)$$

When computing the two-point correlator of the intensity, the convolution of the field correlator $\gamma(k)$ with itself occurs. The potential correlator

$$\overline{V_{\mathbf{k}}V_{-\mathbf{k}'}} = (2\pi)^d \delta(\mathbf{k} - \mathbf{k}') \sigma^d V_0^2 C_d(k\sigma) \quad (3.11)$$

defines the dimensionless k -space correlation function $C_d(k\sigma)$. Being the convolution of two d -dimensional spheres of radius σ^{-1} , $C_d(k\sigma)$ is centered at $k = 0$ and vanishes for $k > 2\sigma^{-1}$, see [figure 3.3\(b\)](#). In one dimension, the speckle correlation function

$$C_1(k\sigma) = \pi(1 - k\sigma/2) \Theta(1 - k\sigma/2) \quad (3.12a)$$

has the particularly simple shape of a triangle, the convolution of a 1D box with itself. In two and three dimensions, the convolutions of disks and balls, respectively, are slightly more complicated

$$C_2(k\sigma) = \left[8 \arccos(k\sigma/2) - 2k\sigma \sqrt{4 - k^2\sigma^2} \right] \Theta(1 - k\sigma/2) \quad (3.12b)$$

$$C_3(k\sigma) = \frac{3\pi^2}{8} (k\sigma - 2)^2 (4 + k\sigma) \Theta(1 - k\sigma/2). \quad (3.12c)$$

The dimensionless correlators (3.12) are normalized such that $\int \frac{d^d \alpha}{(2\pi)^d} C_d(\alpha) = 1$ in any dimension. At $k\sigma = 2$, they vanish like $(2 - k\sigma)^{\frac{d+1}{2}}$. The real-space correlation function $C_d(r/\sigma) = \overline{V(\mathbf{r})V(0)}/V_0^2$ decays on the length scale of the correlation length σ , see figure 3.3(a).

Because of its experimental relevance, the speckle potential will be the model of choice for most of the rest of this work.

3.2. A suitable basis for the disordered problem

Before applying the Bogoliubov Hamiltonian (2.29) to the disordered problem, we should think about the basis to work with. In presence of the disorder potential, one could in principle compute the Bogoliubov eigenbasis $\{u_\nu(\mathbf{r}), v_\nu(\mathbf{r})\}$ (section 2.5), which fulfills the bi-orthogonality relation (2.75) and the orthogonality to the ground state (2.76). However, for each realization of the disorder potential $V(\mathbf{r})$, this basis would be different, precluding any meaningful disorder average. Thus, we want to construct a basis from momentum states, which satisfies the orthogonality relations (2.75) and (2.76) as well as possible. In absence of disorder, it should reduce to the usual plane-wave Bogoliubov basis (2.32). The price for using a momentum basis instead of the eigenbasis will be the coupling among the Bogoliubov modes in the time evolution, similar to equation (2.76).

In the homogeneous Bogoliubov problem (subsection 2.3.1), the field operator can be written in terms of density and phase fluctuations or in terms of Bogoliubov quasiparticles

$$\delta\hat{\Psi}(\mathbf{r}) \stackrel{(2.27)}{=} \frac{\delta\hat{n}(\mathbf{r})}{2\Phi(\mathbf{r})} + i\Phi(\mathbf{r})\delta\hat{\varphi}(\mathbf{r}) \quad \Phi(\mathbf{r}) = \Phi_0 \quad (3.13a)$$

$$\stackrel{(2.32)}{=} \frac{1}{L^{\frac{d}{2}}} \sum_{\mathbf{k}} e^{i\mathbf{k}\cdot\mathbf{r}} \left(u_k \hat{\gamma}_{\mathbf{k}} - v_k \hat{\gamma}_{-\mathbf{k}}^\dagger \right), \quad (3.13b)$$

with $u_k = (\epsilon_k + \epsilon_k^0)/(2\sqrt{\epsilon_k \epsilon_k^0})$, $v_k = (\epsilon_k - \epsilon_k^0)/(2\sqrt{\epsilon_k \epsilon_k^0})$ and $u_k^2 - v_k^2 = 1$.

When the disorder is switched on, the ground state is deformed $\Phi(\mathbf{r}) \neq \Phi_0$, and equation (3.13a) and (3.13b) are not equivalent any more. Basically there are two options how to define Bogoliubov quasiparticles in the disordered system:

- Using quasiparticles defined by equation (3.13b)
- Introducing the disorder in equation (3.13a) and then applying the Bogoliubov transformation (2.32)

The difference resides in the order of switching on the disorder and applying the transformation (2.32). Let us investigate which option better fulfills the orthogonality conditions (2.75) and (2.76).

3.2.1. Bogoliubov basis in terms of free particle states

Let us start with the simpler looking option (3.13b). By comparison with equation (2.67), we directly identify the functions $\tilde{u}_{\mathbf{k}}(\mathbf{r}) = L^{-\frac{d}{2}}u_{\mathbf{k}}e^{i\mathbf{k}\cdot\mathbf{r}}$ and $\tilde{v}_{\mathbf{k}}(\mathbf{r}) = L^{-\frac{d}{2}}v_{\mathbf{k}}e^{i\mathbf{k}\cdot\mathbf{r}}$. These are exactly the same functions as in the homogeneous case, and obviously all Bogoliubov modes $\mathbf{k} \neq 0$ fulfill the bi-orthogonality (2.75).

In presence of an external potential, however, the condensate state Φ is deformed and is not orthogonal to the plane waves $u_{\mathbf{k}}(\mathbf{r})$ and $v_{\mathbf{k}}(\mathbf{r})$ any more. Testing the condition (2.76), we indeed find

$$\int d^d r \Phi(\mathbf{r}) [u_{\mathbf{k}}(\mathbf{r}) - v_{\mathbf{k}}(\mathbf{r})] = (u_{\mathbf{k}} - v_{\mathbf{k}})\Phi_{-\mathbf{k}} \neq 0.$$

This overlap with the ground state mixes the modes $\mathbf{k} \neq 0$ with the zero-frequency mode that cannot be treated as a proper Bogoliubov mode (subsection 2.5.3). If one tries nevertheless to work with operators $\hat{b}_{\mathbf{k}} = \int d^d r [\tilde{u}_{\nu}^*(\mathbf{r})\delta\hat{\Psi}(\mathbf{r}) + \tilde{v}_{\nu}^*(\mathbf{r})\delta\hat{\Psi}^\dagger(\mathbf{r})]$, the inelastic coupling matrices $W_{\mathbf{k}'\mathbf{k}}$ are found to diverge for $k \rightarrow 0$. Due to this diverging coupling to low-energy modes, perturbation theory will break down, even for small values of the external potential.

3.2.2. Bogoliubov basis in terms of density and phase

Let us try the other option (3.13a), where the disorder is switched on before the transformation (2.32) is applied. $\Phi(\mathbf{r})$ is the disorder-deformed ground-state and the field operator is expressed in terms of $\hat{\gamma}_{\mathbf{k}}$ and $\hat{\gamma}_{\mathbf{k}}^\dagger$

$$\begin{aligned} \delta\hat{\Psi}(\mathbf{r}) &= \frac{\Phi_0}{\Phi(\mathbf{r})} \frac{\delta\hat{n}(\mathbf{r})}{2\Phi_0} + \frac{\Phi(\mathbf{r})}{\Phi_0} i \Phi_0 \delta\hat{\varphi}(\mathbf{r}) \\ &\stackrel{(2.32)}{=} \frac{1}{2L^{\frac{d}{2}}} \sum_{\mathbf{k}} e^{i\mathbf{k}\cdot\mathbf{r}} \left\{ \left[\frac{\Phi(\mathbf{r})}{\Phi_0 a_{\mathbf{k}}} + \frac{\Phi_0 a_{\mathbf{k}}}{\Phi(\mathbf{r})} \right] \hat{\gamma}_{\mathbf{k}} - \left[\frac{\Phi(\mathbf{r})}{\Phi_0 a_{\mathbf{k}}} - \frac{\Phi_0 a_{\mathbf{k}}}{\Phi(\mathbf{r})} \right] \hat{\gamma}_{-\mathbf{k}}^\dagger \right\}, \end{aligned} \quad (3.14)$$

with $a_k = \sqrt{\epsilon_k^0/\epsilon_k}$. By comparison to equation (2.67), we identify the functions

$$u_{\mathbf{k}}(\mathbf{r}) = \frac{1}{2} \left(\frac{\Phi(\mathbf{r})}{\Phi_0 a_k} + \frac{\Phi_0 a_k}{\Phi(\mathbf{r})} \right) \frac{e^{i\mathbf{k}\cdot\mathbf{r}}}{L^{d/2}}, \quad v_{\mathbf{k}}(\mathbf{r}) = \frac{1}{2} \left(\frac{\Phi(\mathbf{r})}{\Phi_0 a_k} - \frac{\Phi_0 a_k}{\Phi(\mathbf{r})} \right) \frac{e^{i\mathbf{k}\cdot\mathbf{r}}}{L^{d/2}} \quad (3.15)$$

as disorder-deformed plane-waves. Now we can check their bi-orthogonality (2.75), which is indeed fulfilled:

$$\int d^d r [u_{\mathbf{k}}^*(\mathbf{r})u_{\mathbf{k}'}(\mathbf{r}) - v_{\mathbf{k}}^*(\mathbf{r})v_{\mathbf{k}'}(\mathbf{r})] = \int \frac{d^d r}{2L^d} \left(\frac{a_k}{a_{k'}} + \frac{a_{k'}}{a_k} \right) e^{-i(\mathbf{k}-\mathbf{k}')\cdot\mathbf{r}} = \delta_{\mathbf{k}\mathbf{k}'}. \quad (3.16)$$

Also the orthogonality with respect to the ground state (2.76) is fulfilled, because $\Phi(\mathbf{r}) [u_{\mathbf{k}}(\mathbf{r}) - v_{\mathbf{k}}(\mathbf{r})]$ is a plane wave with zero average for all $\mathbf{k} \neq 0$.

In the sense of the paragraph “[Mean-field total particle number](#)” in [subsection 2.5.5](#), this compliance was expected, because the Bogoliubov modes (2.32) are constructed from plane-wave density modulations with zero spatial average, which cannot affect the mean-field particle number.

Conclusion

Only the Bogoliubov quasiparticles (2.32) in terms of density and phase

$$\hat{\gamma}_{\mathbf{k}} = \frac{1}{a_k} \frac{\delta \hat{n}_{\mathbf{k}}}{2\Phi_0} + i a_k \Phi_0 \delta \hat{\varphi}_{\mathbf{k}} \quad (3.17)$$

fulfill the requirements for the study of the disordered Bogoliubov problem. They are labeled by their momentum \mathbf{k} , which is independent of the disorder realization $V(\mathbf{r})$. Only the ground state $\Phi(\mathbf{r})$, from where the fluctuations are measured, is shifted. The Bogoliubov quasiparticles (2.32) fulfill the bi-orthogonality relation (2.75), which is necessary for using them as basis, but most importantly, they decouple from the zero-frequency mode.

The equations of motion (2.43) for the $\hat{\gamma}_{\mathbf{k}}$ for $\mathbf{k} \neq 0$ are coupled, which will be subject of the perturbation theory in the next section.

3.3. Effective medium and diagrammatic perturbation theory

Finally, all preparations for tackling the disordered Bogoliubov problem have been made. In [section 2.3](#), the Bogoliubov Hamiltonian (2.42) has been derived and in the previous sections, we have discussed the statistical properties of the disorder potential. Now it is time to characterize the dynamics of Bogoliubov excitations in presence of disorder. The key idea is to average over the disorder and to understand the disordered Bose-Einstein condensate as an effective medium for the propagation of Bogoliubov excitations. The effective medium is characterized by quantities like the index of refraction [[subsection 3.4.5](#)] describing the propagation speed, the mean free path [[subsection 3.4.2](#)] or the diffusion constant [Boltzmann transport length, [subsection 3.4.2](#)]. The main information is contained in the single-(quasi)particle Green-function, also called propagator or resolvent, of the system.

3.3.1. Green functions

The Bogoliubov excitations are bosonic quasiparticles with the commutator relations

$$[\hat{\gamma}_{\mathbf{k}}, \hat{\gamma}_{\mathbf{k}'}^\dagger] = \delta_{\mathbf{k}\mathbf{k}'}, \quad [\hat{\gamma}_{\mathbf{k}}, \hat{\gamma}_{\mathbf{k}'}] = [\hat{\gamma}_{\mathbf{k}}^\dagger, \hat{\gamma}_{\mathbf{k}'}^\dagger] = 0. \quad (3.18)$$

We define the single-(quasi)particle Green-function [[16](#), Chapter 8]

$$G_{\mathbf{k}\mathbf{k}'}(t) := \frac{1}{i\hbar} \langle [\hat{\gamma}_{\mathbf{k}}(t), \hat{\gamma}_{\mathbf{k}'}^\dagger(0)] \rangle \Theta(t). \quad (3.19)$$

The average $\langle \cdot \rangle$ denotes the thermal average. Here, $T = 0$ is considered, so it is simply the expectation value in the ground state. The Green function contains information, how a quasiparticle created at time 0 in some state \mathbf{k}' propagates to some state \mathbf{k} where it is destroyed at time t .

Before starting with the disordered problem, let us determine the unperturbed Green function, which is the starting point for the perturbation theory. In absence of the perturbation terms in (2.43), the time evolution of the Bogoliubov operators

$$\hat{\gamma}_{\mathbf{k}}(t) = \exp(-i\epsilon_{\mathbf{k}}t/\hbar)\hat{\gamma}_{\mathbf{k}}(0) \quad (3.20)$$

is trivial and the free Green function $(G_0(t))_{\mathbf{k}\mathbf{k}'} = G_0(k, t)\delta_{\mathbf{k}\mathbf{k}'}$ is found as

$$G_0(k, t) = \frac{1}{i\hbar} \exp(-i\epsilon_{\mathbf{k}}t/\hbar)\Theta(t). \quad (3.21)$$

For the Fourier transform to frequency domain, we introduce a convergence ensuring parameter $\eta > 0$, which appears as an infinitesimal shift of the pole

$$G_0(k, \omega) = \lim_{\eta \rightarrow 0} \frac{1}{\hbar\omega - \epsilon_k + i\eta} =: \frac{1}{\hbar\omega - \epsilon_k + i0}. \quad (3.22)$$

In the disordered problem, the equation of motion (2.43) for $\hat{\gamma}_{\mathbf{k}}$ mixes with $\hat{\gamma}_{-\mathbf{k}'}$. Thus, we define the anomalous Green function [49]

$$F_{\mathbf{k}\mathbf{k}'} := \frac{1}{i\hbar} \langle [\hat{\gamma}_{-\mathbf{k}}^\dagger(t), \hat{\gamma}_{\mathbf{k}'}^\dagger(0)] \rangle \Theta(t). \quad (3.23)$$

The equations of motion for the Green functions are coupled

$$\begin{aligned} i\hbar \frac{d}{dt} G_{\mathbf{k}\mathbf{k}'}(t) &= \epsilon_k G_{\mathbf{k}\mathbf{k}'}(t) + \frac{1}{L^{\frac{d}{2}}} \sum_{\mathbf{k}''} [W_{\mathbf{k}\mathbf{k}''} G_{\mathbf{k}''\mathbf{k}'} + Y_{\mathbf{k}\mathbf{k}''} F_{\mathbf{k}''\mathbf{k}'}] + \delta(t) \delta_{\mathbf{k}'\mathbf{k}} \\ i\hbar \frac{d}{dt} F_{\mathbf{k}\mathbf{k}'}(t) &= -\epsilon_k F_{\mathbf{k}\mathbf{k}'}(t) - \frac{1}{L^{\frac{d}{2}}} \sum_{\mathbf{k}''} [W_{\mathbf{k}\mathbf{k}''} F_{\mathbf{k}''\mathbf{k}'} + Y_{\mathbf{k}\mathbf{k}''} G_{\mathbf{k}''\mathbf{k}'}]. \end{aligned} \quad (3.24)$$

Here, the commutator (3.18) and $\partial_t \Theta(t) = \delta(t)$ were used. In absence of disorder, the anomalous Green function F vanishes, at least within the Bogoliubov approximation, i.e. to order $\mathcal{O}(\hat{\gamma}^2)$.

It is useful to combine these two coupled equations of motion to one matrix valued equation. This can be achieved by setting up the equations of motion for the Hermitian conjugate of the propagators

$$G_{\mathbf{k}\mathbf{k}'}^\dagger(t) = \frac{1}{i\hbar} \langle [\hat{\gamma}_{\mathbf{k}}^\dagger(t), \hat{\gamma}_{\mathbf{k}'}(0)] \rangle \Theta(t), \quad F_{\mathbf{k}\mathbf{k}'}^\dagger(t) = \frac{1}{i\hbar} \langle [\hat{\gamma}_{-\mathbf{k}}(t), \hat{\gamma}_{\mathbf{k}'}(0)] \rangle \Theta(t) \quad (3.25)$$

and combining them to the generalized propagator

$$\mathcal{G} = \begin{pmatrix} G & F^\dagger \\ F & G^\dagger \end{pmatrix}. \quad (3.26)$$

The Hermitian conjugates of the propagators are closely related to the advanced propagators. In frequency domain, the relation $G_{\mathbf{k}\mathbf{k}'}^\dagger(\omega) = G_{\mathbf{k}'\mathbf{k}}^A(-\omega)$ holds. Similar pseudo-spinor structures appear also in other field of physics. Examples are the Nambu formalism of the BCS theory [16, Chapter 18.5], where electrons and holes are combined in a spinor, or applications in particle physics [119].

The equation of motion for the generalized propagator reads

$$i\hbar \frac{d}{dt} \mathcal{G} = \eta \left\{ \left[\begin{pmatrix} \epsilon & 0 \\ 0 & \epsilon \end{pmatrix} + \begin{pmatrix} W & Y \\ Y & W \end{pmatrix} \right] \mathcal{G} + \begin{pmatrix} \mathbf{1} & 0 \\ 0 & \mathbf{1} \end{pmatrix} \delta(t) \right\}. \quad (3.27)$$

3. Disorder

In this compact notation, the matrix multiplication implies the sum over the free momentum $L^{-\frac{d}{2}} \sum_{\mathbf{k}'}$. The matrix η is given as $\text{diag}(\mathbf{1}, -\mathbf{1})$ and $\mathbb{1}_{\mathbf{k}\mathbf{k}'} = \delta_{\mathbf{k}\mathbf{k}'}$.

Transforming to frequency space and multiplying by η from the left gives a compact form amenable to perturbation theory

$$[\mathcal{G}_0^{-1} - \mathcal{V}] \mathcal{G} = \mathbb{1}. \quad (3.28)$$

The unperturbed generalized propagator \mathcal{G}_0 contains (3.22) and its conjugate

$$\mathcal{G}_0(k, \omega) = \begin{pmatrix} \frac{1}{\hbar\omega - \epsilon_k + i0} & 0 \\ 0 & \frac{1}{-\hbar\omega - \epsilon_k - i0} \end{pmatrix} = \begin{pmatrix} G_0(k, \omega) & 0 \\ 0 & G_0^*(k, -\omega) \end{pmatrix}. \quad (3.29)$$

Again, the infinitesimal shifts $\pm i0$ come from the convergence ensuring factors in the Fourier transform, their sign being determined by the causality factor $\Theta(t)$ in the definition of the propagators. The perturbations are contained in the Bogoliubov scattering operator $\mathcal{V} = \begin{pmatrix} W & Y \\ Y & W \end{pmatrix}$, which was introduced in subsection 2.3.2.

3.3.2. The self-energy

With equation (3.28) we can now set up a usual diagrammatic perturbation theory [16, 23, 120]. Equation (3.28) is solved for the full propagator \mathcal{G} by writing the inverse of operators in terms of a series expansion in powers of \mathcal{V} :

$$\begin{aligned} \mathcal{G} &= [\mathcal{G}_0^{-1} - \mathcal{V}]^{-1} = \mathcal{G}_0 [\mathbb{1} - \mathcal{V}\mathcal{G}_0]^{-1} \\ &= \mathcal{G}_0 \sum_{n=0}^{\infty} (\mathcal{V}\mathcal{G}_0)^n = \mathcal{G}_0 + \mathcal{G}_0\mathcal{V}\mathcal{G}_0 + \mathcal{G}_0\mathcal{V}\mathcal{G}_0\mathcal{V}\mathcal{G}_0 + \dots \end{aligned} \quad (3.30)$$

In order to get meaningful results on a random system, the disorder has to be averaged over. To this end, it is necessary to trace \mathcal{V} back to the speckle field amplitudes, because these are the basic quantities with known statistical properties and a Gaussian probability distribution. Remember subsection 2.3.3: The scattering operator depends nonlinearly on the external potential $\mathcal{V} = \mathcal{V}^{(1)} + \mathcal{V}^{(2)} + \mathcal{V}^{(3)} + \dots$, where $\mathcal{V}^{(n)}$ contains the disorder potential to the n -th power. At this point, the representation with Feynman diagrams is again instructive. We start with the expansion (2.51) and draw

$$\mathcal{V} = \begin{array}{c} \vdots \\ \boxed{\otimes} \\ \vdots \end{array} + \begin{array}{c} \vdots \\ \boxed{\otimes\otimes} \\ \vdots \end{array} + \begin{array}{c} \vdots \\ \boxed{\otimes\otimes\otimes} \\ \vdots \end{array} + \dots \quad (3.31)$$

Here, we have taken into account that each speckle potential $V_{\mathbf{k}}$ contributes the electrical fields $\mathcal{E}_{\mathbf{q}}$ and $\mathcal{E}_{\mathbf{k}-\mathbf{q}}^*$, which are drawn as \circ and $*$, respectively.

Together with the free propagator $\mathcal{G}_0 = \text{---}$, all contributions from (3.30) can be written as diagrams, for example

$$\mathcal{V}^{(1)}\mathcal{G}_0\mathcal{V}^{(1)} = \begin{array}{c} \vdots \\ \vdots \\ \boxed{*} \text{---} \boxed{*} \\ \vdots \\ \vdots \end{array}, \quad \mathcal{V}^{(1)}\mathcal{G}_0\mathcal{V}^{(1)}\mathcal{G}_0\mathcal{V}^{(1)} = \begin{array}{c} \vdots \\ \vdots \\ \boxed{*} \text{---} \boxed{*} \text{---} \boxed{*} \\ \vdots \\ \vdots \end{array}, \quad \mathcal{V}^{(1)}\mathcal{G}_0\mathcal{V}^{(2)} = \begin{array}{c} \vdots \\ \vdots \\ \boxed{*} \text{---} \boxed{**} \\ \vdots \\ \vdots \end{array}. \quad (3.32)$$

Now, equation (3.30) is averaged over the disorder, which yields the so-called Born series

$$\overline{\mathcal{G}} = \mathcal{G}_0 + \mathcal{G}_0\overline{\mathcal{V}}\mathcal{G}_0 + \mathcal{G}_0\overline{\mathcal{V}}\mathcal{G}_0\overline{\mathcal{V}}\mathcal{G}_0 + \dots \quad (3.33)$$

According to the Gaussian moment theorem [121], averages over a product of several Gauss-distributed random variables separate into averages of pairs, the so-called contractions. Each summand on the right hand side is obtained as the sum over its contractions, i.e. the fields (dotted lines) are pairwise connected using their pair correlation function (3.7), see also box 3.1 on page 70. Let us have a look at the disorder average of (3.31):

$$\overline{\mathcal{V}^{(1)}} = \begin{array}{c} \circ \\ \vdots \\ \boxed{*} \end{array} = 0 \quad \overline{\mathcal{V}^{(2)}} = \begin{array}{c} \circ \\ \vdots \\ \boxed{**} \end{array} =: \begin{array}{c} \circ \\ \vdots \\ \boxed{**} \end{array} \neq 0 \quad \overline{\mathcal{V}^{(3)}} = \begin{array}{c} \circ \\ \vdots \\ \boxed{***} \end{array} \neq 0 \quad (3.34)$$

The first-order term vanishes, because the potential $V(\mathbf{r})$ has been shifted such that its average vanishes [equation (3.9)]. Any other diagram, where a field correlator forms a simple loop $\begin{array}{c} \circ \\ \vdots \\ \boxed{*} \end{array}$, i.e. returns to the same sub-vertex, vanishes as well. The other diagrams in (3.34), however, are non-zero. In the second-order term, two field correlations (dotted lines) were combined to a single *potential* correlation (dashed line). In the non-zero diagram of $\mathcal{V}^{(3)}$, the field correlators form a ring. Similarly, the disorder averages of (3.32) translate into the following diagrams

$$\overline{\mathcal{V}^{(1)}\mathcal{G}_0\mathcal{V}^{(1)}} = \begin{array}{c} \text{---} \\ \vdots \\ \boxed{*} \text{---} \boxed{*} \\ \vdots \\ \text{---} \end{array}, \quad \overline{\mathcal{V}^{(1)}\mathcal{G}_0\mathcal{V}^{(1)}\mathcal{G}_0\mathcal{V}^{(1)}} = \begin{array}{c} \text{---} \\ \vdots \\ \boxed{*} \text{---} \boxed{*} \text{---} \boxed{*} \\ \vdots \\ \text{---} \end{array}, \quad \overline{\mathcal{V}^{(1)}\mathcal{G}_0\mathcal{V}^{(2)}} = \begin{array}{c} \text{---} \\ \vdots \\ \boxed{*} \text{---} \boxed{**} \\ \vdots \\ \text{---} \end{array}. \quad (3.35)$$

These averages consist of only one diagram each. Many diagrams of higher order are *reducible*, i.e. they separate into independent factors when a single propagator is removed. The forth-order diagram $\begin{array}{c} \text{---} \\ \vdots \\ \boxed{*} \text{---} \boxed{*} \text{---} \boxed{*} \text{---} \boxed{*} \\ \vdots \\ \text{---} \end{array}$, for example, separates into twice the first diagram in (3.35), connected with a free propagator. The redundant information of the reducible diagrams in $\overline{\mathcal{G}}$ can be

3. Disorder

Box 3.1: Feynman rules: drawing and computing irreducible diagrams

- Let us compute the self-energy Σ , i.e. the irreducible terms of (3.30), with $\mathcal{V} = \mathcal{V}^{(1)} + \mathcal{V}^{(2)} + \dots$. Exemplarily, we choose $\mathcal{G}_0 \mathcal{V}^{(1)} \mathcal{G}_0 \mathcal{V}^{(2)} \mathcal{G}_0$. We omit the first and last propagator and draw the “amputated diagram” in terms of vertices and internal propagators:

$$\mathcal{V}^{(1)} \mathcal{G}_0 \mathcal{V}^{(2)} = \begin{array}{c} \text{---} \square \text{---} \square \text{---} \\ \text{---} \square \text{---} \square \text{---} \\ \text{---} \square \text{---} \square \text{---} \end{array}$$

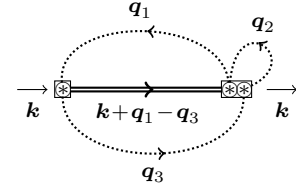
- The disorder average is done by connecting the field lines pairwise in all possible configurations:

$$\overline{\mathcal{V}^{(1)} \mathcal{G}_0 \mathcal{V}^{(2)}} = 2 \begin{array}{c} \text{---} \square \text{---} \square \text{---} \\ \text{---} \square \text{---} \square \text{---} \\ \text{---} \square \text{---} \square \text{---} \end{array} + 2 \begin{array}{c} \text{---} \square \text{---} \square \text{---} \\ \text{---} \square \text{---} \square \text{---} \\ \text{---} \square \text{---} \square \text{---} \end{array} + \begin{array}{c} \text{---} \square \text{---} \square \text{---} \\ \text{---} \square \text{---} \square \text{---} \\ \text{---} \square \text{---} \square \text{---} \end{array} + \begin{array}{c} \text{---} \square \text{---} \square \text{---} \\ \text{---} \square \text{---} \square \text{---} \\ \text{---} \square \text{---} \square \text{---} \end{array}$$

- The first diagrams have a combinatorial factor of two, because of the equivalence of the two sub-vertices in $\mathcal{V}^{(2)}$.
- The last two diagrams are reducible and do not belong to Σ .
- All diagrams containing a simple loop vanish, because $\overline{V} = 0$.

- We compute the only remaining diagram by

- Labeling each field line with an independent momentum \mathbf{q}_i
- Determining the momenta of the propagators by momentum conservation
- Translating the constituents:



$$\text{Field correlators (3.7)} \circ \overset{\mathbf{q}_i}{\curvearrowright} * = \gamma(\mathbf{q}_i)$$

$$\text{Bogoliubov propagators (3.29)} \overset{\mathbf{k}}{\rightleftarrows} = \mathcal{G}_0(\mathbf{k}, \omega)$$

$$\text{Envelope functions } \square = v_{\mathbf{k}_1 \mathbf{k}_2}^{(1)} \text{ (2.46) and } \square = v_{\mathbf{k}_1 \mathbf{q} \mathbf{k}_2}^{(2)} \text{ (2.49)}$$

The arguments \mathbf{k}_1 and \mathbf{k}_2 are given by the incoming and outgoing momentum of the respective vertex. There may also be internal momenta, like $\mathbf{q} = \mathbf{k} + \mathbf{q}_2 - \mathbf{q}_3$ in the second-order vertex.

- Finally, we sum over all free momenta \mathbf{q}_i . The diagram evaluates as

$$\frac{1}{L^{\frac{3d}{2}}} \sum_{\mathbf{q}_1, \mathbf{q}_2, \mathbf{q}_3} \gamma(\mathbf{q}_1) \gamma(\mathbf{q}_2) \gamma(\mathbf{q}_3) v_{\mathbf{k}(\mathbf{k}+\mathbf{q}_1-\mathbf{q}_3)}^{(1)} \mathcal{G}_0(\mathbf{k}+\mathbf{q}_1-\mathbf{q}_3, \omega) v_{(\mathbf{k}+\mathbf{q}_1-\mathbf{q}_3)(\mathbf{k}+\mathbf{q}_2-\mathbf{q}_3)\mathbf{k}}^{(2)},$$

with the external momentum \mathbf{k} and frequency ω .

avoided by reorganizing the Born series (3.33). The diagrams are sorted by the number of irreducible sub-diagrams they contain, and not by their order in \mathcal{V}/μ . The result is the Dyson equation

$$\bar{\mathcal{G}} = \mathcal{G}_0 + \mathcal{G}_0 \Sigma \bar{\mathcal{G}}, \quad (3.36)$$

where the self-energy Σ contains all irreducible contributions

$$\Sigma = \underbrace{\text{[diagram 1]} + \text{[diagram 2]}}_{\Sigma^{(2)}} + 2 \underbrace{\left[\text{[diagram 3]} + 2 \text{[diagram 4]} + \text{[diagram 5]} \right]}_{\Sigma^{(3)}} + \dots \quad (3.37)$$

Due to the disorder average, each block of Σ is diagonal in \mathbf{k} . The contributions to Σ are then sorted by their order in \mathcal{V}/μ . The first two terms are second order in the disorder potential, the others are of higher order. In principle, any desired order of the above series can be determined in a systematic way, see box 3.1. In practice, however, the complexity and the number of diagrams grows very rapidly.

Born approximation

In the following, we will restrict ourselves to the leading order V^2/μ^2 , i.e.

$$\Sigma^{(2)} = \text{[diagram 1]} + \text{[diagram 2]} = \overline{\mathcal{V}^{(2)}} + \overline{\mathcal{V}^{(1)} \mathcal{G}_0 \mathcal{V}^{(1)}}, \quad (3.38)$$

which is known as the Born approximation. Note that this leading-order approximation in the self-energy still implies an infinite number of diagrams in the correction to the averaged propagator $\bar{\mathcal{G}}$ via the recursive formula (3.36). This allows a shift of the pole of the propagator (3.22), which would be impossible in leading-order perturbation theory directly for \mathcal{G} .

3.3.3. Computing the self-energy in the Born approximation

In the Born approximation (3.38), the two field correlators in each diagram are combined to one intensity correlator $\text{[diagram 1]} = \int d^d q' \gamma(\mathbf{q} - \mathbf{q}') \gamma(\mathbf{q}') =$

3. Disorder

$V_0^2 \sigma^d C_d(q\sigma)$. We compute the first block of the Born approximation $\Sigma^{\text{B}} := \Sigma_{11}^{(2)}$

$$\begin{aligned} \Sigma^{\text{B}}(k, \hbar\omega) &= \left(V_0^2 \sigma^d \frac{1}{L^{\frac{d}{2}}} \sum_{\mathbf{q}} C_d(q\sigma) \left[v_{\mathbf{k}(\mathbf{k}+\mathbf{q})\mathbf{k}}^{(2)} + v_{\mathbf{k}\mathbf{k}+\mathbf{q}}^{(1)} \mathcal{G}_0(\mathbf{k} + \mathbf{q}) v_{\mathbf{k}+\mathbf{q}\mathbf{k}}^{(1)} \right] \right)_{11} \\ &= \frac{V_0^2 \sigma^d}{L^{\frac{d}{2}}} \sum_{\mathbf{q}} C_d(q\sigma) \left[w_{\mathbf{k}(\mathbf{k}+\mathbf{q})\mathbf{k}}^{(2)} + \frac{(w_{\mathbf{k}(\mathbf{k}+\mathbf{q})}^{(1)})^2}{\hbar\omega - \epsilon_{\mathbf{k}+\mathbf{q}} + i0} - \frac{(y_{\mathbf{k}(\mathbf{k}+\mathbf{q})}^{(1)})^2}{\hbar\omega + \epsilon_{\mathbf{k}+\mathbf{q}}} \right]. \end{aligned} \quad (3.39)$$

The infinitesimally shifted pole in the propagator $G_0(\epsilon_{\mathbf{k}})_{\mathbf{k}'}$ is split into real and imaginary part, using the Sokhatsky-Weierstrass theorem [103] $[\hbar\omega - \epsilon_{\mathbf{k}'} + i0]^{-1} = \text{P}[\hbar\omega - \epsilon_{\mathbf{k}'}]^{-1} - i\pi\delta(\hbar\omega - \epsilon_{\mathbf{k}'})$. Thus, elastic scattering enters in the imaginary part and inelastic processes are captured by the Cauchy principal value P of the integral (3.39). For the actual evaluation of the integral, the first-order and second-order envelope functions $w_{\mathbf{k}\mathbf{k}'}$ and $y_{\mathbf{k}\mathbf{k}'}$, given in (2.45c) (2.45d) and (2.50), are needed.

Transferring the results to other types of disorder

In the Born approximation, the self-energy (3.39) depends only on the two-point correlator of the disorder *potential*

$$\overline{V_{\mathbf{k}} V_{-\mathbf{k}'}} = (2\pi)^d \delta(\mathbf{k} - \mathbf{k}') V_0^2 \sigma^d C(k\sigma). \quad (3.40)$$

The field correlators (3.7) occur only in higher-order diagrams. The self-energy in the Born approximation is valid also for other types of disorder, like for example a Gaussian model $C_d^{\text{G}}(k\sigma) = (2\pi)^{d/2} \exp(-k^2\sigma^2/2)$, as employed e.g. in [122]. In subsection 4.1.4, we will come back to this and compare the effect of speckle disorder to the effect of Gaussian disorder on the disorder-averaged density of states.

3.4. Deriving physical quantities from the self-energy

The self-energy derived in the previous section is the central result of the present [chapter 3 “Disorder”](#). It allows deriving many physical quantities.

3.4.1. The physical meaning of the self-energy

In order to understand the meaning of the self-energy, it is useful to define the spectral function $S(k, \omega) = -2\text{Im}\bar{G}(k, \omega)$ [16], which contains all information about the frequency and lifetime of the excitations. In the unperturbed system, the spectral function is given by a Dirac δ -function

$$S_0(k, \omega) = -2\text{Im}G_0(k, \omega) = 2\pi\delta(\hbar\omega - \epsilon_k). \quad (3.41)$$

In presence of disorder, this function may get modified, but in any case it will stay normalized

$$\int dE \frac{S(k, E)}{2\pi} = 1, \quad (3.42)$$

such that the spectral function is the energy distribution of a quasiparticle with wave vector \mathbf{k} . Let us express the spectral function in terms of the self-energy $\text{Re}\Sigma + i\text{Im}\Sigma$. First, the Dyson equation (3.36) has to be solved for the average propagator, i.e. the 2×2 matrix $[\mathcal{G}_0^{-1} - \Sigma]$ has to be inverted. One finds

$$\bar{G}(k, \omega) = \left[G_0(\omega)^{-1} - \Sigma_{11}(k, \omega) - \frac{\Sigma_{12}(k, \omega)\Sigma_{21}(k, \omega)}{G_0^*(-\omega)^{-1} - \Sigma_{22}(k, \omega)} \right]^{-1}. \quad (3.43)$$

The numerator of the last term is quadratic in the self-energy, i.e. fourth order in V_0/μ , whereas $G_0^*(-\omega)^{-1} = -\hbar\omega - \epsilon_k \approx 2\epsilon_k$ is finite. In the scope of the Born approximation, i.e. to second order in V_0/μ , this term has to be dropped. Consequently equation (3.43) simplifies

$$\bar{G}(k, \omega) = [G_0(k, \omega)^{-1} - \Sigma^{\text{B}}(k, \omega)]^{-1}, \quad (3.44)$$

with $\Sigma_{11}^{(2)} = \Sigma^{\text{B}}$. This leads to

$$S^{\text{B}}(k, \omega) = \frac{-2\text{Im}\Sigma^{\text{B}}(k, \omega)}{[\hbar\omega - (\epsilon_k + \text{Re}\Sigma^{\text{B}}(k, \omega))]^2 + [\text{Im}\Sigma^{\text{B}}(k, \omega)]^2}. \quad (3.45)$$

The peak of the spectral function is shifted by the real part of the self-energy and broadened by the imaginary part (which will turn out to be negative, such that the spectral function is positive and fulfills (3.42)).

3. Disorder

The poles of the averaged Green function (3.44) define the complex dispersion relation

$$\hbar\omega = \epsilon_k + \Sigma^{\text{B}}(k, \hbar\omega). \quad (3.46)$$

In the Born approximation, the self-energy is of order V_0^2/μ^2 , and its energy argument $\hbar\omega$ can be consistently replaced with its on-shell value ϵ_k . In the following, we separate the self-energy into the real and the imaginary correction of the dispersion relation

$$\hbar\omega_k = \epsilon_k + \Sigma^{\text{B}}(k, \epsilon_k) = \epsilon_k \left[1 + \frac{V_0^2}{\mu^2} \Lambda(k) - i \frac{\gamma_k}{2\epsilon_k} \right]. \quad (3.47)$$

3.4.2. Mean free path

According to the reasoning in section 3.2 the Bogoliubov modes are expressed in a basis that is characterized by the momentum \mathbf{k} and is not the eigenbasis of the Bogoliubov Hamiltonian. Thus, \mathbf{k} is “not a good quantum number” and the Bogoliubov modes suffer scattering, which is reflected in a finite lifetime and the broadening of their dispersion relation.

Scattering rate and mean free path

A Bogoliubov excitation, which evolves like $e^{-i\epsilon_k t/\hbar}$ in the unperturbed case, evolves in the disordered case like $e^{-i(\epsilon_k + \text{Re}\Sigma)t/\hbar} e^{-|\text{Im}\Sigma|t/\hbar}$. That means, its intensity gets damped by elastic scattering events to other modes. The imaginary part of the self-energy defines the inverse lifetime or scattering rate

$$\hbar\gamma_k = -2\text{Im}\Sigma^{\text{B}}(k, \epsilon_k). \quad (3.48)$$

In equation (3.39), the only possibility for an imaginary part to occur is the imaginary part of the Green function $\text{Im}(\epsilon_k - \epsilon_{\mathbf{k}+\mathbf{q}} + i0)^{-1} = -\pi\delta(\epsilon_k - \epsilon_{\mathbf{k}+\mathbf{q}})$. This restricts the integral to the energy shell. Physically, this is not surprising. Because of energy conservation, a Bogoliubov quasiparticle can only be scattered to modes with the same energy. Other modes can only be virtually excited, but the quasiparticle has to come back. Such virtual scattering events will enter the real part of the self-energy, see subsection 3.4.5 below.

On the energy shell, the scattering element simplifies, section 2.4. Thus the scattering rate is given as the d -dimensional angular integral

$$\hbar\gamma_k = \frac{V_0^2}{2\mu^2} (k\sigma)^d \frac{k\xi}{\sqrt{2 + (k\xi)^2(1 + (k\xi)^2)}} \int \frac{d\Omega_d}{(2\pi)^{d-1}} C_d(2k\sigma \sin \theta/2) A^2(k\xi, \theta). \quad (3.49)$$

With the group velocity $v_g = \partial_k \epsilon_k / \hbar$, the scattering rate is converted to the scattering mean free path $l_s = v_g / \gamma_k$

$$\frac{1}{kl_s} = \frac{V_0^2}{4\mu^2} \frac{k^d \sigma^d}{(1 + k^2 \xi^2)^2} \int \frac{d\Omega_d}{(2\pi)^{d-1}} C_d(2k\sigma \sin \theta/2) A^2(k\xi, \theta). \quad (3.50)$$

The fraction in front of the integral assures that the mean free path diverges both for very low momenta $k\sigma \ll 1$ and for high momenta $k\xi \gg 1$. In-between, the mean free path scales with μ^2/V_0^2 . Thus, describing Bogoliubov excitations as plane waves also in the inhomogeneous case is well justified.

3.4.3. Boltzmann transport length

In equation (3.50), elastic scattering in all directions contributes to the inverse mean free path. The forward scattering events, however, do not randomize the direction of the quasiparticles and do not affect the diffusive transport. The relevant length for diffusion is the Boltzmann transport length l_B [22, 23], the length of randomization of direction. It is obtained from equation (3.50) by introducing a factor $[1 - \cos(\theta)]$, which suppresses forward scattering:

$$\frac{1}{kl_B} = \frac{V_0^2}{4\mu^2} \frac{k^d \sigma^d}{(1 + k^2 \xi^2)^2} \int \frac{d\Omega_d}{(2\pi)^{d-1}} [1 - \cos(\theta)] C_d(2k\sigma \sin \theta/2) A^2(k\xi, \theta), \quad (3.51)$$

In subsection 4.1.2, Boltzmann transport length and mean free path are compared in the regime of a hydrodynamic Bose-Einstein condensate.

3.4.4. Localization length

In order to determine the localization lengths of the Bogoliubov states in a disordered Bose-Einstein condensate, the single-particle Green functions of the previous section are not sufficient. Rather, the *intensity propagator* should be considered [22, 23, 123], in order to derive the weak-localization correction to the diffusion constant. This is beyond the scope of this work, but nevertheless, we can estimate the localization lengths of Bogoliubov excitations, based on general results on localization of particles and phonons.

In one-dimensional disordered systems, the backscattering process $k \mapsto -k$ that amounts to the inverse Boltzmann transport length (3.51) is known to induce strong, Anderson localization of the excitation in the disordered potential [17]. The inverse localization length $\Gamma_{\text{loc}} = 1/(2l_B)$, which describes exponential localization, is directly proportional to the inverse

backscattering length l_B^{-1} [124]. This holds very generally for particle-like and for phonon-like excitations. From (3.51) we deduce

$$\Gamma_{\text{loc}} = \frac{V^2}{8\mu^2} \sigma k^2 \frac{C_1(2k\sigma)}{(1 + k^2\xi^2/2)^2}, \quad (3.52)$$

which agrees with the findings of [33], and also with [79], where the limits $\sigma \rightarrow 0$ and $\xi \rightarrow 0$ have been investigated. It should be noted that these approaches employ the phase-formalism that is particularly suited for 1D systems, whereas our Green-function theory permits to go to higher dimensions without conceptual difficulties.

Also in two dimensions, the localization length is related to the Boltzmann transport length l_B , but it is not the same scale. By using scaling theory [17, chapter 8.2], it can be shown that the localization length depends exponentially on kl_B

$$l_{\text{loc}} = l_B \exp\left(\frac{\pi}{2}kl_B\right). \quad (3.53)$$

This result was derived for electrons, i.e. for particles, but also the localization length of phonons scales exponentially [29].

In three dimensions, the question of localization is less clear, because localized and delocalized states coexist and phonons and particles have different characteristics [29] (section 5.3).

3.4.5. Renormalization of the dispersion relation

In this subsection, the (real) shift of the Bogoliubov dispersion relation due to the disorder potential is derived. In the limit of small $k\xi$, this shift is the correction of the speed of sound.

In the grand canonical ensemble, which was employed so far, the correction is directly given by the self-energy, which is here taken in the on-shell Born approximation. From the real part of (3.46), the disorder-averaged dispersion relation is found as

$$\bar{\epsilon}_k = \epsilon_k + \text{Re}\Sigma^{\text{B}}(k, \epsilon_k). \quad (3.54)$$

We define the relative correction in units of V_0^2/μ^2 , i.e., we take the scaling of the Born approximation into account

$$\Lambda_\mu(k) := \frac{\mu^2}{V_0^2} \frac{\bar{\epsilon}_k - \epsilon_k}{\epsilon_k} = \frac{\mu^2}{V_0^2} \frac{\text{Re}\Sigma^{\text{B}}(k, \epsilon_k)}{\epsilon_k}. \quad (3.55)$$

The subscript μ indicates, that the disorder is ramped up at constant chemical potential μ .

Fixed particle number

Let us have a look at the density profile (2.24) of the condensate in presence of a disorder potential $V(\mathbf{r})$. In the disorder average the first-order contribution (2.25) vanishes because $\overline{V} = 0$. In contrast, the second-order contribution (2.25) survives the disorder average. With $\overline{V_{\mathbf{q}}V_{\mathbf{k}-\mathbf{q}}} = (2\pi)^d \delta(\mathbf{k}) V_0^2 \sigma^d C_d(q\sigma)$ (3.11) and $C_d(q\sigma) \geq 0$ (3.12), the shift of the mean density is found to be positive:

$$\frac{\overline{n(\mathbf{r})} - n_\infty}{n_\infty} = -\frac{\overline{\tilde{V}^{(2)}(\mathbf{r})}}{\mu} = \frac{\sigma^d V_0^2}{\mu^2} \int \frac{d^d q}{(2\pi)^d} C_d(q\sigma) \frac{q^2 \xi^2}{(2 + q^2 \xi^2)^2} > 0 \quad (3.56)$$

At constant chemical potential, the disorder attracts more particles from the grand canonical reservoir into the system. The integral (3.56) is significant for $\sigma \approx \xi$, because then, the fraction $q^2 \xi^2 / (2 + q^2 \xi^2)^2$ and the disorder correlation function overlap efficiently.

The counter-intuitive increase of the particle density can be understood more directly [14] from the spatial average of the stationary Gross-Pitaevskii equation (2.19). When the potential is switched on, the right hand side of equation (2.19) does not change, because $V(\mathbf{r})$ has zero mean. By integration by parts one sees that the kinetic energy term $-\frac{\hbar^2}{2m} \int \frac{d^d r}{\text{Vol}} (\nabla \sqrt{n_0(\mathbf{r})})^2 / n_0(\mathbf{r})$ has a negative average, which has to be compensated by a positive correction of the averaged interaction term, i.e. an increase of the average density.

For an experiment it appears very unnatural that the particle number should change while ramping up the disorder. Once the condensate is created, the atom number and the average condensate density should stay constant when the disorder potential is ramped up. For the rest of this work, we switch to the canonical ensemble with fixed atom number. The increase of the average density due to the disorder is compensated by an appropriate shift of the chemical potential $\Delta\mu$. Consider the disorder average of (2.24) with $\overline{\tilde{V}^{(1)}} = 0$ and $n_\infty = \mu/g$ replaced by $(\mu + \Delta\mu)/g$

$$\frac{\mu + \Delta\mu}{g} \left(1 - \frac{\overline{\tilde{V}^{(2)}(\mathbf{r})}}{\mu} \right) \stackrel{!}{=} \frac{\mu}{g}. \quad (3.57)$$

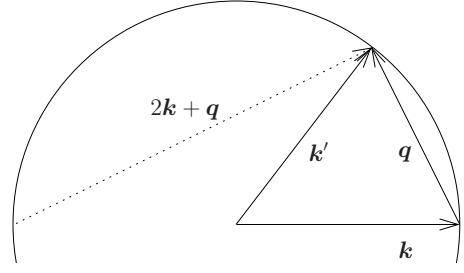
Consequently, the chemical potential is shifted by

$$\frac{\Delta\mu}{\mu} = \frac{\overline{\tilde{V}^{(2)}(\mathbf{r})}}{\mu} \stackrel{(3.56)}{=} -\frac{\sigma^d V_0^2}{\mu^2} \int \frac{d^d q}{(2\pi)^d} C(q\sigma) \frac{q^2 \xi^2}{(2 + q^2 \xi^2)^2} < 0, \quad (3.58)$$

up to higher orders in V_0^2/μ^2 . The correction to $\text{Re}\Sigma$ is of higher order, but the shift $\Delta\mu$ corrects also the clean dispersion relation ϵ_k by $\Delta\mu \frac{\partial \epsilon_k}{\partial \mu}$.

3. Disorder

Figure 3.4: Geometry of the scattering process. In terms of the momentum transfer \mathbf{q} , the elasticity condition $\mathbf{k}^2 = \mathbf{k}'^2$ becomes $\mathbf{q} \cdot (2\mathbf{k} + \mathbf{q}) = 0$, geometrically recognized in the Thales circle.

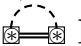


Altogether, the relative correction of the speed of sound at fixed particle number is given as

$$\Lambda_N(k) = \Lambda_\mu(k) - \frac{\sigma^d}{2 + k^2\xi^2} \int \frac{d^d q}{(2\pi)^d} \frac{C_d(q\sigma) q^2 \xi^2}{(2 + q^2 \xi^2)^2}. \quad (3.59)$$

Now, we can combine the above equation with the self-energy $\text{Re}\Sigma(k, \epsilon_k)$ (3.39) to a single integral over the disorder correlator

$$\Lambda_N(k) = \text{P} \int \frac{d^d q \sigma}{(2\pi)^d} \frac{C_d(q\sigma)}{(2 + q^2 \xi^2)^2} \left[2 \frac{k^2 \xi^2 + q^2 \xi^2}{2 + k^2 \xi^2} + h(\mathbf{k}\xi, \mathbf{q}\xi) \right]. \quad (3.60)$$

The first part in the brackets comes from the $W^{(2)}$ term and the transformation to the canonical ensemble. The other part is due to virtual scattering processes, which are momentum conserving but not energy conserving. The function $h(\mathbf{k}\xi, \mathbf{q}\xi)$ collects the first-order envelope functions and the propagators from the  part in (3.39)

$$h(\mathbf{k}, \mathbf{q}) = \frac{\text{num}(\mathbf{k}, \mathbf{q})}{\text{den}(\mathbf{k}, \mathbf{q}) + i0}. \quad (3.61)$$

After some algebra, numerator and denominator are found as

$$\begin{aligned} \text{num}(\mathbf{k}, \mathbf{q}) &= 2(2 + k^2)(2 + k^2 + q^2 + 2\mathbf{k} \cdot \mathbf{q})(k^2 + \mathbf{k} \cdot \mathbf{q})^2 / k^2 \\ &\quad + 2(k^2 + q^2 + 2\mathbf{k} \cdot \mathbf{q})(k^2 + q^2 + \mathbf{k} \cdot \mathbf{q})^2 \\ &\quad - 4(2 + k^2)(k^2 + q^2 + \mathbf{k} \cdot \mathbf{q})(k^2 + \mathbf{k} \cdot \mathbf{q}) \end{aligned} \quad (3.62a)$$

$$\begin{aligned} \text{den}(\mathbf{k}, \mathbf{q}) &= (\epsilon_k^2 - \epsilon_{\mathbf{k}+\mathbf{q}}^2)(2 + k^2) \\ &= -\mathbf{q} \cdot (2\mathbf{k} + \mathbf{q})(2 + 2k^2 + q^2 + 2\mathbf{k} \cdot \mathbf{q})(2 + k^2). \end{aligned} \quad (3.62b)$$

The denominator exhibits an elastic-scattering pole at $\epsilon_k = \epsilon_{\mathbf{k}+\mathbf{q}}$. Geometrically, the first scalar product $\mathbf{q} \cdot (2\mathbf{k} + \mathbf{q})$ expresses the elasticity condition on the Thales circle, [figure 3.4](#).

The correction (3.60) to the dispersion relation $\bar{\epsilon}_k$ in will be discussed in detail in [chapter 4](#).

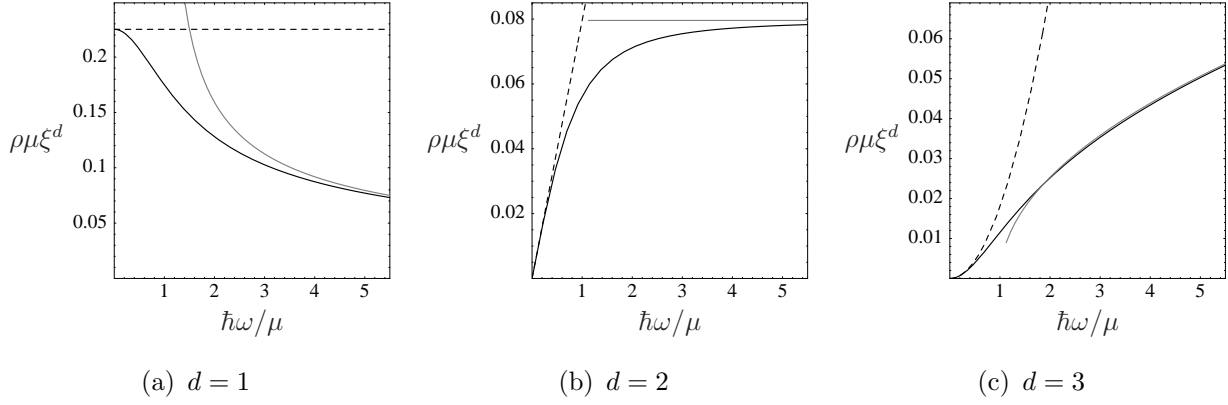


Figure 3.5.: Bogoliubov density of states (solid line). At low energies $\hbar\omega \ll \mu$, the density of states is phonon-like $\rho \propto \omega^{d-1}$ (dashed line), whereas at high energies $\hbar\omega \gg \mu$ it is particle like $\rho \propto (\hbar\omega - \mu)^{\frac{d}{2}-1}$ (gray line).

3.4.6. Density of states

The spectral function (3.45) can be regarded as the probability of a Bogoliubov quasiparticle in state \mathbf{k} to have energy $\hbar\omega$. By integrating over all possible states, we obtain the average density of states, i.e. the probability to find a state at a given energy $\hbar\omega$

$$\bar{\rho}(\omega) = \int \frac{d^d k}{(2\pi)^d} \frac{S(\mathbf{k}, \omega)}{2\pi}. \quad (3.63)$$

The spectral function is modified by the corrections to the free dispersion relation (3.47), i.e. by $\text{Im}\Sigma^B$ and $\text{Re}\Sigma^B = V_0^2 \Lambda / \mu^2$.

Clean density of states

Already in absence of disorder, the density of states shows an interesting feature, namely the transition from sound-wave like excitations to particle-like excitations. This implies a transition from $\rho_{\text{sw}}(\omega) \propto \omega^{d-1}$ to $\rho_{\text{particle}}(\omega) \propto \omega^{\frac{d}{2}-1}$. According to equation (3.41), the clean density of states is found as

$$\rho_0(\omega) = \frac{S_d}{(2\pi)^d} k_\omega^{d-1} \left| \frac{\partial k}{\partial \omega} \right|_{k_\omega}, \quad \hbar\omega = \mu k_\omega \xi \sqrt{k_\omega^2 \xi^2 + 2}. \quad (3.64)$$

For low-energy excitations with $\hbar\omega = ck$, this reduces to a phonon-like dispersion relation $\rho \propto \omega^{d-1}$, and for high energies it passes over to the free-particle density of states $\rho \propto \omega^{\frac{d}{2}-1}$, see figure 3.5.

Disorder correction

What is the impact of the self-energy Σ^B on the spectral function (3.45)? The imaginary part broadens the Lorentzian

$$S^B(k, \omega) = \frac{-2\text{Im}\Sigma^B(k, \epsilon_k)}{[\hbar\omega - \bar{\epsilon}_k]^2 + [\text{Im}\Sigma^B(k, \epsilon_k)]^2}. \quad (3.65)$$

This merely has an effect on the density of states (3.64), because as function of ω , the Lorentzian is still normalized. For the evaluation of the integral (3.63), we can approximate the Lorentzian with a Dirac δ -distribution at the corrected dispersion relation $\bar{\epsilon}_k = \epsilon_k(1 + \frac{V_0^2}{\mu^2}\Lambda_N(k))$:

$$\bar{\rho}(\omega) = \int \frac{d^d k}{(2\pi)^d} \delta(\hbar\omega - \bar{\epsilon}_k) = \frac{S_d}{(2\pi)^d} \left[k^{d-1} \left| \frac{\partial \bar{\epsilon}_k}{\partial k} \right|^{-1} \right]_{k=k_0}. \quad (3.66)$$

Here, k_0 is defined by $\hbar\omega = \epsilon_{k_0}(1 + \frac{V_0^2}{\mu^2}\Lambda_N(k_0))$. To leading order in the disorder strength, equation (3.66) can be expressed as

$$\bar{\rho}(\omega) = \rho_0(\omega) \left\{ 1 - \frac{V_0^2}{\mu^2} \left[d + k \frac{\partial}{\partial k} \right] \frac{v_{\text{ph}}(k)}{v_{\text{g}}(k)} \Lambda(k) \right\}_{k=k_\omega}, \quad (3.67)$$

with $\hbar\omega = \epsilon_{k_\omega}$, the phase velocity $v_{\text{ph}}(k) = \epsilon_k/(\hbar k)$, and the group velocity $v_{\text{g}} = \partial_k \epsilon_k/\hbar$. The velocity ratio $v_{\text{g}}/v_{\text{ph}} = \frac{1+k^2\xi^2/2}{1+k^2\xi^2}$ is one in the linear sound-wave part of the spectrum and approaches 1/2 in the regime of the quadratic particle spectrum.

A detailed study of the disorder-averaged density of states in the hydrodynamic regime will be presented in [section 4.1](#).

4. Disorder—Results and Limiting Cases

The disordered Bogoliubov problem contains three different length scales: the excitation wave length $\lambda = 2\pi/k$, the healing length ξ , and the disorder correlation length σ . The physics is not determined by the absolute values of these length scales, but rather by their values relative to each other. The three relevant dimensionless parameters are the following:

- The ratio σ/ξ indicates, whether the disordered condensate is in the Thomas-Fermi regime ($\sigma \gg \xi$) or in the smoothing regime ($\sigma \ll \xi$), see [subsection 2.2.3](#).
- The parameter $k\xi$ indicates, whether the excitations are sound-wave like ($k\xi \ll 1$) or particle like ($k\xi \gg 1$), see [subsection 2.3.1](#).
- The parameter $k\sigma$ discriminates the point-scatterer regime ($k\sigma \ll 1$) from a very smooth scattering potential $k\sigma \gg 1$.

These three relevant parameters are not independent, two of them fix the third one, e.g. $\sigma/\xi = (k\sigma)/(k\xi)$. The dimension of the parameter space is reduced from three to two dimensions. This is analog to RGB color space at fixed lightness. Each of the three dimensionless parameters can be mapped to one of the three RGB channels. The parameter $k\xi$, for example, determines the red channel, where $k\xi \rightarrow 0$ is mapped to cyan and $k\xi \rightarrow \infty$ to red. Similarly, $k\sigma$ and σ/ξ define the green and the blue channel, respectively, which completes the color. The identity $(\sigma/\xi)(k\xi)/(k\sigma) = 1$

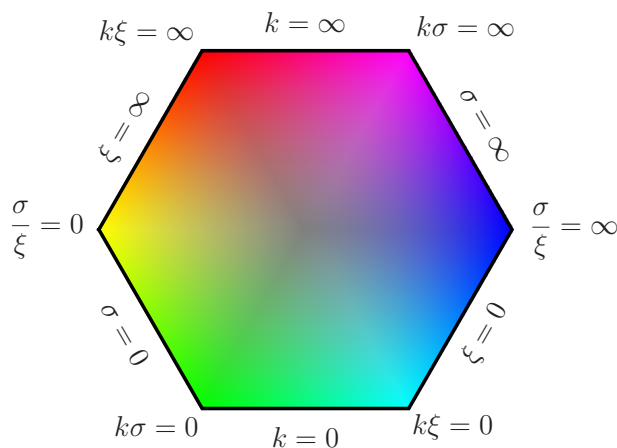


Figure 4.1: Illustration of the parameter space of the full Bogoliubov problem. The relevant dimensionless parameters σ/ξ , $k\xi$, $k\sigma$ are identified with the color space at fixed lightness. On the edges, the limiting cases of the following sections are found.

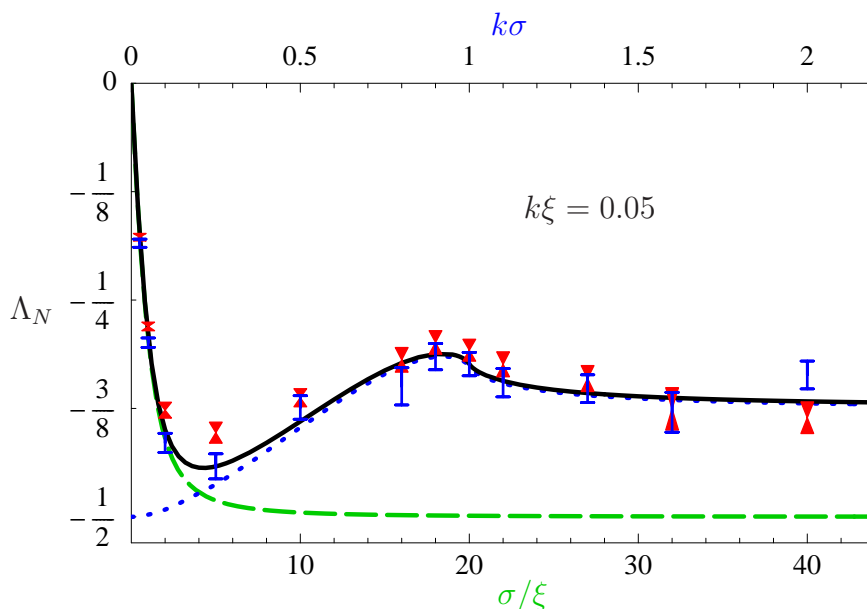


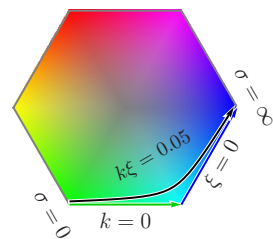
Figure 4.2.: Relative correction of the speed of sound $\Lambda_N = \Delta c \mu^2 / (c V_0^2)$ for 1D speckle disorder. Full formula (3.60) for $k\xi = 0.05$ (black line). Limiting formulae $\Lambda_N(k\sigma)|_{\xi=0}$ [section 4.1, (4.15)] (dotted blue) and $\Lambda_N(\sigma/\xi)|_{k=0}$ [section 4.2, (4.31)] (dashed green). Numerical results of a Gross-Pitaevskii integration, as discussed in section 4.3, are shown for $V_0/\mu = +0.03$ (blue straight marks) and $V_0/\mu = -0.03$ (red triangular marks).

fixes the value of the lightness, leaving the two-dimensional space of hue and saturation, as shown in Fig. 4.1.

Limiting cases, where one of the length scales is zero or infinity, i.e. much shorter or much longer than the other length scales, are found on the edges. We focus mainly on the low-energy excitations $k\xi \ll 1$. Only in the last section, section 4.4, we consider the transition to particle-like excitations $k\xi \gg 1$.

Low-energy excitations

We are interested in the low-energy features, i.e. the sound-wave regime $k\xi \ll 1$. For practical purposes, we choose a small but finite value $k\xi = 0.05$. In the parameter space, the curve defined by $k\xi = 0.05$ appears as a smooth curve close to the $\xi = 0$ edge and the $k = 0$ edge, as shown in the illustration on the right. Let us consider



the speed of sound, which is a significant physical quantity. In figure 4.2, the correction (3.60) of the speed of sound due to a one-dimensional speckle disorder potential is shown. The curve is rather complicated with three different regimes: a linear increase at very short correlation lengths, a non-monotonic intermediate range and saturation at long correlation lengths. In

the following sections, we will illuminate the different regimes and elaborate limiting results.

In addition to excitation wave length and healing length, the disorder correlation length provides a third length scale σ with no *a priori* constraints. Thus, the sound limit $k\xi \rightarrow 0$ can be understood in two different ways:

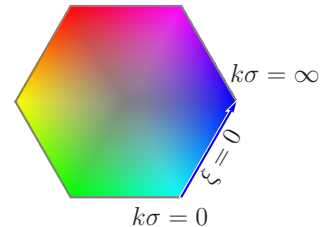
1. Interaction dominates, and the healing length is the shortest of all length scales and drops out, $\xi \rightarrow 0$. This so-called hydrodynamic limit leaves $k\sigma$ as free variable. It is found at the lower right edge in the parameter space [figure 4.1](#) and is discussed in detail in [section 4.1](#).
2. Conversely, the excitation wave length can be taken as the longest of all length scales, i.e. $k \rightarrow 0$, leaving σ/ξ as free variable. This limit is found at the lowermost edge of the parameter space and discussed in [section 4.2](#).

Analytical results from both limits reproduce the exact correction (3.60) for large σ/ξ and small $k\sigma$, respectively, cf. [figure 4.2](#). Finally, in [section 4.3](#), we verify the perturbative predictions in all regimes with a numerical integration of the time-dependent Gross-Pitaevskii equation in a one-dimensional disordered system.

4.1. Hydrodynamic limit I: $\xi = 0$

Here, the so-called hydrodynamic regime is discussed, where the interaction $gn = \mu$ dominates over the quantum pressure, i.e. kinetic energy. For the ground state this means that the Thomas-Fermi approximation (2.20) holds, and the excitations are in the sound-wave regime $k\xi \ll 1$. The fact that the interaction μ is the largest energy scale implies that the healing length $\xi = \hbar/\sqrt{2m\mu}$ is the shortest length scale. Thus, the physical results from [section 3.4](#) can be taken in the limit $\xi \rightarrow 0$. All results will then depend only on the ratio σ/λ of the remaining length scales, respectively on $k\sigma = 2\pi\sigma/\lambda$.

Physically, it is more instructive to perform the hydrodynamic limit in the very beginning and to derive the results from the much simpler hydrodynamic equations of motion [115].



4.1.1. Direct derivation from hydrodynamic equations of motion

We start from the equations of motion (2.18) for density and phase in the limit of negligible quantum pressure. For the ground state this means that the Thomas-Fermi formula (2.20) applies, $n_0(\mathbf{r}) = n_{\text{TF}} = (\mu - V(\mathbf{r}))/g$.¹ The speed of sound characterizes the dynamics of small deviations $\delta n(\mathbf{r}, t) = n(\mathbf{r}, t) - n_0(\mathbf{r})$ and $\delta\varphi(\mathbf{r}, t) = \varphi(\mathbf{r}, t) - \varphi_0$ from the ground state in the long wave-length regime $k\xi \ll 1$. In terms of density and superfluid velocity, the linearized equations of motion (2.18) read

$$\partial_t \delta n + \nabla \cdot [n_0(\mathbf{r})\mathbf{v}] = 0, \quad (4.1)$$

$$\partial_t \mathbf{v} = -\frac{g}{m} \nabla \delta n, \quad (4.2)$$

and are recognized as the linearized versions of continuity equation and Euler's equation for an ideal compressible fluid, respectively. These can be combined to a single classical wave equation

$$[c^2 \nabla^2 - \partial_t^2] \delta n = \frac{1}{m} \nabla \cdot [V(\mathbf{r}) \nabla \delta n]. \quad (4.3)$$

Translation invariance of the free equation suggests using a Fourier representation in space and time,

$$[\omega^2 - c^2 k^2] \delta n_{\mathbf{k}} = \int \frac{d^d k'}{(2\pi)^d} \tilde{V}_{\mathbf{k}\mathbf{k}'} \delta n_{\mathbf{k}'}. \quad (4.4)$$

The disorder potential causes scattering $\mathbf{k} \rightarrow \mathbf{k}'$ of plane waves with an amplitude

$$\tilde{V}_{\mathbf{k}\mathbf{k}'} = -\frac{1}{m} (\mathbf{k} \cdot \mathbf{k}') V_{\mathbf{k}-\mathbf{k}'}. \quad (4.5)$$

The factor $\mathbf{k} \cdot \mathbf{k}'$ originates from the mixed gradient in (4.3) and implies pure p-wave scattering of sound waves as discussed in section 2.4, in contrast to s-wave scattering of independent particles [23].

In contrast to the perturbation theory in section 3.3, the starting point (4.3) is a second-order equation of motion and does not have the block-matrix structure. Apart from that, the diagrammatic perturbation theory works exactly the same way. Analogously to (3.28), the following equation defines the Green function \tilde{G}

$$(\tilde{G}_0^{-1} - \tilde{V}) \tilde{G} = \mathbf{1}. \quad (4.6)$$

¹Note that within the Thomas-Fermi approximation, the average particle density does not change. Thus, we need not distinguish Λ_μ and Λ_N (section 3.4.5) in the present section 4.1.

The free Green function $\tilde{G}_0 = (2\pi)^d \delta(\mathbf{k} - \mathbf{k}') \tilde{G}_0(k, \omega)$ is diagonal in \mathbf{k} ,

$$\tilde{G}_0(k, \omega) = [\omega^2 - c^2 k^2 + i0]^{-1}. \quad (4.7)$$

The full Green function \tilde{G} is expanded in the same way as in equation (3.30), $\tilde{G} = \tilde{G}_0 + \tilde{G}_0 \tilde{V} \tilde{G}_0 + \dots$. Again, we take the disorder average and find

$$\overline{\tilde{G}}(k, \omega) = \left[\tilde{G}_0(k, \omega)^{-1} - \tilde{\Sigma}(k, \omega) \right]^{-1}. \quad (4.8)$$

The poles of this average Green function at $\omega^2 = c^2 k^2 + \tilde{\Sigma}(k, \omega)$ now determine the effective dispersion relation. In the Born approximation, the self-energy $\tilde{\Sigma}(k, \omega)$ evaluates as

$$\tilde{\Sigma}(k, \omega) = V_0^2 \sigma^d \int \frac{d^d k'}{(2\pi)^d} C_d(|\mathbf{k} - \mathbf{k}'| \sigma) \frac{(\mathbf{k}' \cdot \mathbf{k})^2}{m^2} \tilde{G}_0(k', \omega). \quad (4.9)$$

The self-energy corrects the quadratic dispersion relation $(\hbar\omega)^2 = c^2 k^2 + \tilde{\Sigma}(k, \omega)$. To leading order, we can use the on-shell approximation and replace $\tilde{\Sigma}(k, \omega)$ with $\tilde{\Sigma}(k, ck)$, such that $\omega = ck [1 + \tilde{\Sigma}(k, ck)/(2ck)]$. This converts to the inverse mean free path $(kl_s)^{-1} = -\text{Im}\tilde{\Sigma}(k, ck)/(c^2 k^2)$ and the relative correction of the speed of sound $\Lambda = \text{Re}\tilde{\Sigma}(k, ck)\mu^2/(2c^2 k^2 V_0^2)$.

Before discussing these results in detail, we verify that these results are in agreement with the result (3.39) from section 3.4 in the limit $\xi \rightarrow 0$. The envelope functions reduce to $w^{(2)} = \mathcal{O}(k\xi)$, $w_{\mathbf{k}'\mathbf{k}}^{(1)} = -\mathbf{k}' \cdot \mathbf{k} \xi / \sqrt{2kk'} = -y_{\mathbf{k}'\mathbf{k}}^{(1)}$. With this, we indeed find

$$\lim_{\xi \rightarrow 0} \Sigma^{\text{B}}(k, \epsilon_k) = \hbar \frac{\tilde{\Sigma}(k, ck)}{2ck}. \quad (4.10)$$

Next, let us consider the central results inverse mean free path and correction to the speed of sound.

4.1.2. Transport length scales

Mean free path

The imaginary part of the self-energy $\tilde{\Sigma}$ leads to the inverse mean free path

$$\frac{1}{kl_s} = \frac{V_0^2}{4\mu^2} (k\sigma)^d \int \frac{d\Omega_d}{(2\pi)^{d-1}} C_d(2k\sigma \sin \theta/2) \cos^2(\theta). \quad (4.11)$$

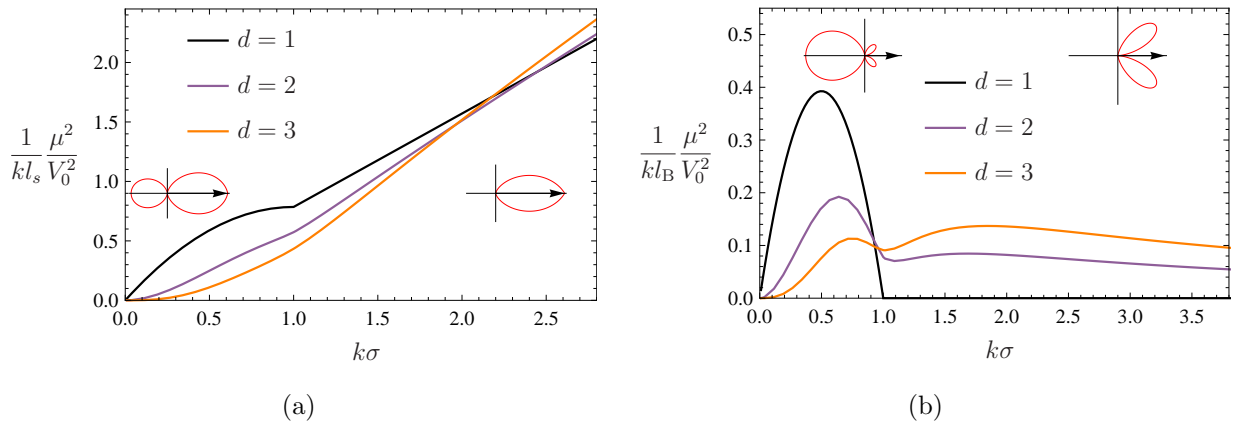


Figure 4.3.: (a) inverse mean free path (4.11) and (b) inverse Boltzmann transport length (3.51) in the hydrodynamic limit $\xi = 0$ for a speckle disorder (3.12). The insets show schematically the angular dependence of elastic scattering.

Equivalently, this result is obtained from (3.50) with the elastic envelope function $A^2 = \cos^2(\theta)$ from section 2.4. This result is a function of $k\sigma$ and is shown in figure 4.3(a).

For small values of $k\sigma$, the correlator C_d can be approximated by $C_d(0)$. Then, the d -dimensional angular average of $\cos^2(\theta)$ gives $1/d$. This result is due to the “concentration of measure phenomenon” [125]: With increasing dimension, the measure of the sphere is concentrated at the equator, where $\cos\theta$ vanishes. Altogether we find

$$\frac{1}{kl_s} \approx \frac{V_0^2}{4\mu^2} (k\sigma)^d C_d(0) \frac{S_d}{(2\pi)^{d-1}} \frac{1}{d} \quad (4.12)$$

Thus, the inverse mean free path, measured in units of the wave length, scales like $(k\sigma)^d$.

For large values of $k\sigma$, the potential allows practically only forward scattering. That means, $\cos^2(\theta)$ can be evaluated as 1 and the angular integral (4.11) over the correlator $C_d(2k\sigma \sin(\theta/2)) \approx C_d(k\sigma\theta)$ scales like $(k\sigma)^{-(d-1)}$, leading to a linear scaling $(kl_s)^{-1} \propto k\sigma$.

Boltzmann transport length and localization length

By adding a factor $1 - \cos\theta$ under the angular integral (4.11), we obtain the inverse Boltzmann transport length (3.51), see figure 4.3(b). At large $k\sigma$, where forward scattering dominates, this suppresses $1/(kl_B)$ compared with $1/(kl_s)$, see insets of figure 4.3.

In one dimension, there is only the backscattering contribution $k \rightarrow -k$

$$\frac{1}{kl_B} = \frac{V_0^2}{2\mu^2} \frac{k\sigma}{(1 + k^2\xi^2)^2} C_1(2k\sigma). \quad (4.13)$$

Due to the finite support of the speckle correlation function $C_d(2k)$ (3.12a), there is no backscattering at all for $k\sigma > 1$, and the inverse Boltzmann mean free path goes to zero, at least within the scope of the Born approximation. In dimensions $d \geq 2$, there are still contributions from scattering angles between 0 and $\pi/2$ [see insets of figure 4.3(b)], thus the inverse Boltzmann transport length does not go abruptly to zero at $k\sigma = 1$, figure 4.3(b).

Conclusion

How strongly are the Bogoliubov excitations affected by elastic scattering? In order to justify the description in terms of plane-wave states with a well-defined sound velocity, the Boltzmann length l_B and the localization length l_{loc} should be much larger than the wave length $\lambda = 2\pi/k$. This is easily fulfilled for the Boltzmann length (3.51). The curves shown in figure 4.3(b) are bounded and the scaling with V_0^2/μ^2 guarantees $l_B \gg \lambda$. The localization lengths are equal to or even exponentially larger than the Boltzmann length. The only thing to keep in mind is that for large values of $k\sigma$, forward scattering events, which produce incoherence in the phase, may occur frequently.

4.1.3. Speed of sound

We compute the relative correction of the speed of sound $\Lambda = \frac{\text{Re}\tilde{\Sigma}(k,ck)\mu^2}{2c^2k^2V_0^2}$ from the self-energy (4.9)

$$\Lambda = -\frac{1}{2} \text{P} \int \frac{d^d k' \sigma}{(2\pi)^d} C_d(|\mathbf{k} - \mathbf{k}'|\sigma) \frac{(\mathbf{k} \cdot \mathbf{k}')^2}{k^2(k'^2 - k^2)}. \quad (4.14)$$

This formula has simplified significantly compared with the principal-value integral (3.60).

1D speckle potential

In the 1D speckle case, the correlation function (3.12a) is piecewisely linear, and the integral (4.14) yields [115, 126]

$$\begin{aligned}\Lambda &= - \left\{ \frac{1}{2} + \frac{k\sigma}{8} \ln \left| \frac{1 - k\sigma}{1 + k\sigma} \right| - \frac{k^2\sigma^2}{8} \ln \left| \frac{1 - k^2\sigma^2}{k^2\sigma^2} \right| \right\} \\ &= -\frac{1}{2} \left\{ 1 + \frac{k\sigma}{4} [2k\sigma \ln k\sigma - (k\sigma + 1) \ln(k\sigma + 1) - (k\sigma - 1) \ln |k\sigma - 1|] \right\}.\end{aligned}\tag{4.15}$$

From the last term in the second form, it is apparent that Λ is non-analytic at $k\sigma = 1$, the value beyond which elastic backscattering is suppressed. The correction (4.15) is a negative correction to the dispersion relation, as shown schematically in figure 4.4(a).

Limits in d dimensions

In higher dimensions, the integral (4.14) over the correlation functions gets more complicated, so that analytical solutions like (4.15) are not available in general. But in all cases, the principle-value integral (4.14) can be evaluated numerically. figure 4.4(b) shows the corresponding curves. Short-range correlated potentials ($k\sigma \ll 1$) affect low dimensions more than high dimensions and vice versa.

For smooth potentials with k -space correlators $C_d(k\sigma)$ that decrease sufficiently fast, the limits $k\sigma \rightarrow 0$ and $k\sigma \rightarrow \infty$ can be calculated analytically as follows. It is useful to rewrite equation (4.14) in terms of $\eta = 1/k\sigma$ as

$$\Lambda = -\frac{1}{2} \text{P} \int \frac{d^d q}{(2\pi)^d} \frac{C_d(q) [1 + \eta q \cos \beta]^2}{2\eta q \cos \beta + \eta^2 q^2}.\tag{4.16}$$

Denoting the angular part of the integral by $A_d(\eta q)$, one arrives at the radial integral $\int_0^\infty dq q^{d-1} C_d(q) A_d(\eta q)$. In the limit $k\sigma \ll 1$, the parameter ηq tends to infinity nearly everywhere under the integral. Then

$$A_d(\infty) = \int \frac{d\Omega_d}{(2\pi)^d} (\cos \beta)^2 = \frac{S_d}{(2\pi)^d} d^{-1},\tag{4.17}$$

and with $\int \frac{d^d q}{(2\pi)^d} C_d(q) = C_d(\mathbf{r} = 0) = 1$, we arrive at $\Lambda = -1/2d$. In the limit $k\sigma \rightarrow \infty$ we proceed similarly with $\eta \rightarrow 0$. The angular integrand reduces to $1 + [2\eta \cos \beta + \eta^2]^{-1}$, whose principle-value integral evaluates after some algebra to

$$A_d(0) = \frac{S_d}{(2\pi)^d} \frac{d+2}{4},\tag{4.18}$$

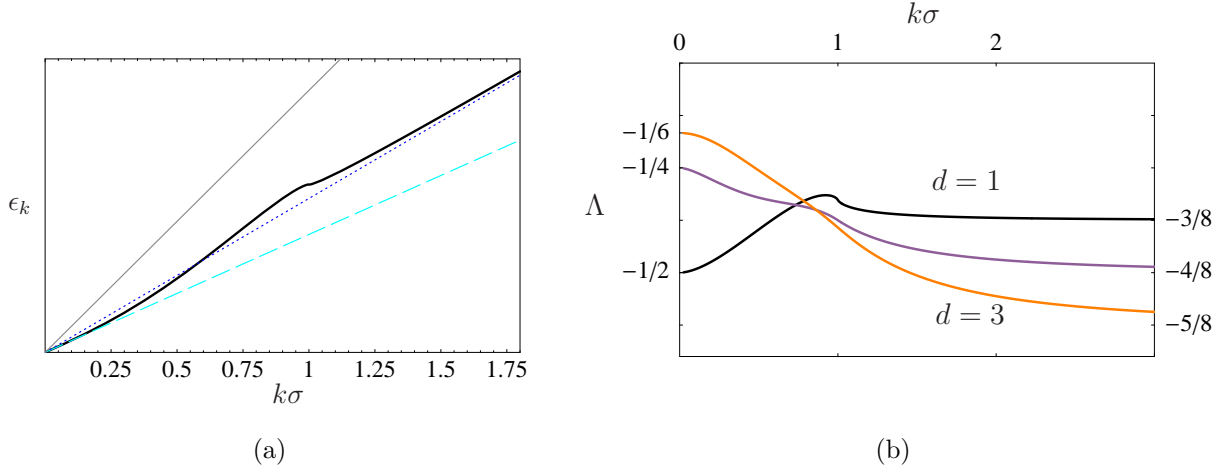


Figure 4.4.: (a) Schematic representation of the disorder-averaged dispersion relation (4.15) in one dimension. According to (4.19) the relative correction to ck (gray) is $-\frac{1}{2}V_0^2/\mu^2$ for small $k\sigma$ (dashed cyan) and $-\frac{3}{8}V_0^2/\mu^2$ for large $k\sigma$ (dotted blue). The full correction (4.15) interpolates between the limits (solid black). This plot corresponds to the linear regime of the Bogoliubov dispersion relation in figure 2.3. (b) Relative correction (4.14) to the speed of sound in a d -dimensional speckle potential. The limits (4.19) are met at the edges.

which leads to $\Lambda = -\frac{2+d}{8}$. Summarized, the limits are

$$\Lambda = -\frac{1}{2} \times \begin{cases} d^{-1}, & k\sigma \ll 1, \\ \frac{1}{4}(2+d), & k\sigma \gg 1. \end{cases} \quad (4.19a)$$

$$\Lambda = -\frac{1}{2} \times \begin{cases} d^{-1}, & k\sigma \ll 1, \\ \frac{1}{4}(2+d), & k\sigma \gg 1. \end{cases} \quad (4.19b)$$

In figure 4.4(b), these limits are shown together with the full curves (4.14) for speckle disorder. Note, however, that the limiting values are independent of the particular type of disorder.

2D speckle disorder

In the case of a two-dimensional speckle disorder, the angular part of equation (4.14) is solved analytically as a closed-path integral in the complex plane $z = e^{i\beta}$, $\beta = \angle(\mathbf{k}, \mathbf{k} - \mathbf{k}')$, using the residue theorem

$$A_2(q) = 1 - \left(\frac{q}{2k}\right)^2 + \left(1 - \frac{q^2}{2k^2}\right) \frac{k^2}{q\sqrt{q^2 - (2k)^2}}, \quad q = |\mathbf{k} - \mathbf{k}'|. \quad (4.20)$$

The last term is imaginary for $q < 2k$ and real for $q > 2k$. If $k\sigma > 1$, there is no overlap of the correlator $C_d(q)$ with the real part, such that the correction of the speed of sound (4.14) takes the form

$$\Lambda_2 = -\frac{1}{4\pi} \text{Re} \int dq\sigma C_2(q\sigma) A_2(q) = -\frac{1}{2} \left(1 - \frac{1}{8k^2\sigma^2}\right), \quad \text{for } k\sigma > 1. \quad (4.21)$$

Concordance with Goldstone theorem

It is important to notice that the relative correction of the Bogoliubov dispersion relation (4.14) has been found to be finite for any value of $k\sigma$ and in any dimension. That means, it is indeed possible to cast $\text{Re}\Sigma$ into a correction of the speed of sound, $ck + \text{Re}\Sigma = c'k$. The spectrum remains gapless. This is a necessity, because disorder does not affect the $U(1)$ symmetry of the (quasi)condensate and the Bogoliubov excitations *must* remain gapless Goldstone modes [72].

4.1.4. Density of states

In the present sound-wave regime, phase velocity and group velocity coincide. Thus the average density of states (3.67) reduces to [115]

$$\bar{\rho}(\omega) = \rho_0(\omega) \left\{ 1 - \frac{V_0^2}{\mu^2} \left[d + k \frac{\partial}{\partial k} \right] \Lambda(k) \right\}, \quad (4.22)$$

with $\rho_0(\omega) = S_d(2\pi c)^{-d}\omega^{d-1}$. Similarly to [127], we consider the scaling function $g_d(\omega\sigma/c) = \bar{\rho}(\omega)/\rho_0(\omega) - 1$, which is computed from the correction (4.14) of the speed of sound shown in figure 4.4(b). The limiting values from (4.19) translate to

$$g_d(\kappa) = \frac{V^2}{2\mu^2} \times \begin{cases} 1, & \kappa \ll 1, \\ \frac{d}{4}(2+d), & \kappa \gg 1. \end{cases} \quad (4.23)$$

Gurarie and Altland [127] suggested that one should be able to deduce from the asymptotic values and the curvatures of this scaling function whether the average density of state exhibits a “boson peak” at intermediate frequency $\omega \approx c/\sigma$. The asymptotics of the scaling function in our case allow for a smooth, monotonic transition between the limiting values in any dimension d . Thus one has no reason to expect any extrema in-between.

In figure 4.5(a), numerical results of the full scaling function (4.22), derived from the speed-of-sound correction Λ due to speckle disorder, are shown. In three dimensions, the scaling function is indeed smooth and monotonic.

In *one dimension*, however, the scaling function shows a strikingly non-monotonic behavior. Using (4.15) and (4.22), we can write down this function analytically

$$g_1(\kappa) = \frac{v^2}{2} \left(1 + \frac{\kappa}{2} \ln \left| \frac{\kappa - 1}{\kappa + 1} \right| - \frac{3\kappa^2}{4} \ln \left| \frac{1 - \kappa^2}{\kappa^2} \right| \right), \quad \kappa = \omega\sigma/c. \quad (4.24)$$

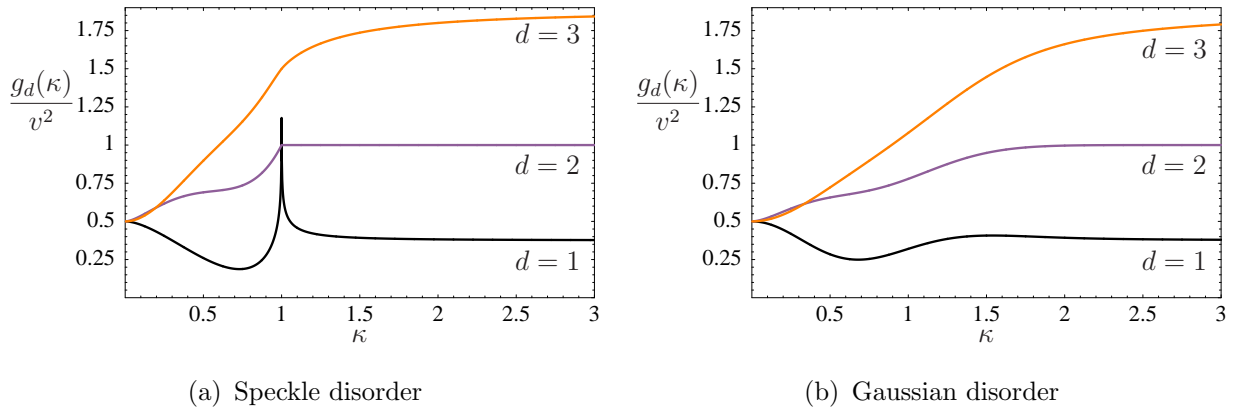


Figure 4.5.: Correction of the density of states $g_d(\kappa) = (\bar{\rho} - \rho_0)/\rho_0$ divided by the squared disorder strength $v = V/\mu$ as function of reduced momentum $\kappa = \omega\sigma/c$ in dimension $d = 1, 2, 3$. (a) Speckle disorder. At $\kappa = 1$, the momentum beyond which elastic backscattering becomes impossible in the Born approximation, there is a logarithmic divergence in $d = 1$, a kink in $d = 2$, and a curvature discontinuity in $d = 3$. (b) Gaussian model of disorder with spatial correlation $\overline{V(\mathbf{r})V(0)} = V_0^2 \exp[-r^2/(2\sigma^2)]$ and $C_1^G(k\sigma) = \sqrt{2\pi} \exp(-k^2\sigma^2/2)$ as used in [122]. The sharp features of the speckle disorder are washed out, but the structure of a local minimum followed by a local maximum in $d = 1$ still exists.

It shows a pronounced dip around $\kappa \approx 0.7$ and a sharp logarithmic divergence at $\kappa = 1$. This particular structure is a consequence of the Born approximation, more specifically the non-analyticity of the speckle pair correlation function (3.12a) at the boundary of its support. The existence of this “boson moat” could not be inferred from the asymptotics of $g_1(\kappa)$ alone [127]. Indeed, expanding the asymptotic behavior as

$$g_d(\kappa) = v^2 \times \begin{cases} \beta_d^<(1 + \alpha_d^<\kappa^2 + \dots), & \kappa \ll 1, \\ \beta_d^>(1 + \alpha_d^>\kappa^{-2} + \dots), & \kappa \gg 1, \end{cases} \quad (4.25)$$

we find $\alpha_1^< = -1 - \frac{3}{2}|\ln \kappa| < 0$ and $\alpha_1^> = \frac{1}{18} > 0$ of opposite sign. Together with the fact that $\beta_1^<$ is larger than $\beta_1^>$, these asymptotics would be compatible with a monotonic behavior and thus are not sufficient to infer the existence of intermediate extrema.

In *two dimensions*, a kink separates a monotonic range for $\kappa < 1$ from a totally flat plateau for $k\sigma > 1$ figure 4.5(a). This can be traced back to the exact formula for the correction of the speed of sound (4.21), where the k^{-2} term cancels when (4.22) is applied. The coefficient $\alpha_2^> = 0$ vanishes, which seems to happen also in other two-dimensional cases [127].

In *three dimensions*, the logarithmic singularity has moved to the second derivative of $g_3(\kappa)$, which is hardly resolvable in the figure. The asymptotics

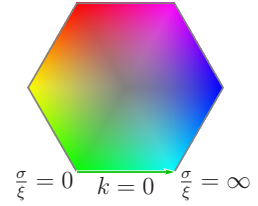
$\alpha_3^> < 0$ leaves an all but structureless average density of state, as expected [127].

As a rule, specific correlation-related features, like the non-analyticities at $\kappa = 1$, tend to be washed out by integration in higher dimensional k -space. Thus we expect arguments on general grounds [127] to hold more reliably in higher dimensions. Conversely, the low-dimensional behavior may escape a bird's-view approach and require detailed calculations. We have presented such a calculation for spatially correlated speckle disorder, so that our results should be of immediate use for cold-atom experiments.

The non-analyticities at $\kappa = 1$ are particular features of speckle disorder. The limiting values (4.23) and the asymptotics, however, are generic and hold also for other models of disorder, like the Gaussian model [122]. In figure 4.5(b), the correction of the density of states due to such a Gaussian disorder is shown. The sharp features of the speckle disorder are washed out, but limiting values, asymptotics and even the structure of an intermediate minimum and maximum in one dimension are the same.

4.2. Hydrodynamic limit II: towards δ -disorder

The low-energy regime is defined by excitation energies ϵ_k much smaller than the chemical potential μ . In terms of length scales, this is phrased as $\xi/\lambda \propto k\xi \ll 1$. In the previous section, this has been achieved by setting the healing length ξ to zero. For the third length scale of the system, the disorder correlation length σ , this implied $\xi \ll \sigma$. In order to cover also the low-energy excitations in truly uncorrelated disorder $\sigma < \xi$, we change the point of view in this section and realize $k\xi \ll 1$ by setting k to zero. This allows describing the low-energy excitations of a disordered BEC with arbitrary ratio σ/ξ of correlation length and healing length. The price to pay is that $k\sigma$ is constrained to be small. Compared with the Bogoliubov wave length, the bare disorder potential is uncorrelated. The effective potential, i.e. the density profile, is smoothed to different degrees, depending on the ratio of ξ and σ .



4.2.1. Mean free path

In the present limit $k \ll \sigma^{-1}, \xi^{-1}$, the inverse mean free path (4.11) evaluates exactly the same way as in the limit (4.12), where $\xi \ll \sigma, k^{-1}$ and $k\sigma \ll 1$ implied $k\xi \ll 1$ and $k\sigma \ll 1$. According to (4.12), the inverse mean free path $(kl_s)^{-1}$ scales like $(V_0/\mu)^2(k\sigma)^d$. Note that the scaling $l_s^{-1} \propto k^{d-1}$ is

proportional to the surface of the energy shell, equivalently to the density of states counting the states available for elastic scattering, see equation (3.64). In the limit $k \rightarrow 0$, the elastic energy shell shrinks and the scattering mean free path diverges, even when measured in units of k^{-1} .

4.2.2. Speed of sound

In the momentum integration of the self-energy (3.39) [equivalently in (3.60)], an effective cutoff is provided either by the disorder correlator $C_d(q\sigma)$ at $q = \sigma^{-1}$ or by the smoothing functions included in $w^{(1)}$, $y^{(1)}$ and $w^{(2)}$ at $q = \xi^{-1}$. Both cutoffs are much larger than k , such that the accessible k -space volume of virtual states is much larger than the volume enclosed by the elastic scattering shell (figure 3.4). A typical virtual scattering event is sketched in figure 4.6.

Let us now consider the relative correction of the dispersion relation (3.60) in the limit $k = 0$. The first part in the bracket reduces to $q^2\xi^2$ and the function $h(\mathbf{k}\xi, \mathbf{q}\xi)$ simplifies to

$$h(0, \mathbf{q}\xi) = - \left[2 \cos^2 \beta + \frac{(q\xi)^4}{2 + (q\xi)^2} \right], \quad (4.26)$$

with $\beta = \angle(\mathbf{k}, \mathbf{q})$. Altogether, equation (3.60) becomes

$$\Lambda_N = 2\sigma^d \int \frac{d^d q \sigma}{(2\pi)^d} \frac{C_d(q)}{(2 + q^2\xi^2)^2} \left[\frac{q^2\xi^2}{2 + q^2\xi^2} - \cos^2 \beta \right]. \quad (4.27)$$

The elastic-scattering pole, which was originally present in (3.39), has disappeared from the formula, because practically all relevant virtual scattering states $\mathbf{k}' = \mathbf{k} + \mathbf{q}$ are outside the elastic scattering sphere, see figure 4.6. Also, the angle $\beta = \angle(\mathbf{k}, \mathbf{q})$ becomes equivalent to the angle $\theta = \angle(\mathbf{k}, \mathbf{k}')$. So, $\cos^2 \beta$ represents the p-wave scattering of sound waves, again. In contrast to the hydrodynamic case in the previous section, where the correction to the speed of sound is found to be always negative, there are now two competing

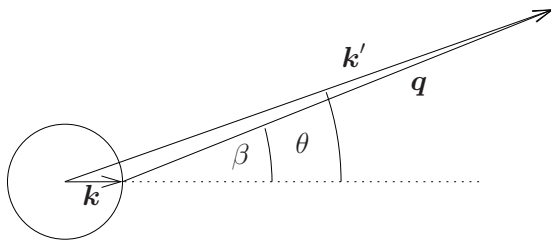


Figure 4.6: Typical virtual scattering event in the regime $k\sigma \ll 1$, $k\xi \ll 1$. The cutoffs σ^{-1} and ξ^{-1} given by the correlator and by the smoothing factor, respectively, are much larger than k . So, most of the virtual scattering states $\mathbf{k}' = \mathbf{k} + \mathbf{q}$ are far outside the elastic scattering shell $|\mathbf{k}'| = k$.

contributions in (4.27). The positive part comes from the $W^{(2)}$ contribution, whereas the negative parts enter via (4.26) and stems from the $\overline{\mathcal{V}\mathcal{G}_0\mathcal{V}}$ part.

The first step in evaluating equation (4.27) is to compute the angular integral over $\cos^2(\beta)$, where β is taken as polar angle in d -dimensional spherical coordinates. The angular average of $\cos^2(\beta)$ decreases with the dimension and is found as $1/d$, cf. discussion before (4.12). Thus, in higher dimensions the negative contribution to the integral (4.27) loses weight with respect to the positive contribution. The remaining radial integral reads

$$\Lambda_N = 2 \frac{S_d}{(2\pi)^d} \int dq q^{d-1} \sigma^d \frac{C_d(q\sigma)}{(2 + q^2\xi^2)^2} \left[\frac{q^2\xi^2}{2 + q^2\xi^2} - \frac{1}{d} \right]. \quad (4.28)$$

This result is plotted in figure 4.7(a) for speckle disorder in $d = 1, 2, 3$ dimensions.

Limits

The limit $(\frac{\sigma}{\xi} \rightarrow \infty)_{k=0}$ touches the limit $(k\sigma \rightarrow 0)_{\xi=0}$ of the previous section in the lower right corner $\xi \ll \sigma \ll k^{-1}$ of the parameter space represented in figure 4.1. Thus, the result (4.19a) is recovered.

In the other limit of δ -correlated disorder, new results are found: For $\xi \gg \sigma$, the smoothing factor $(2 + q^2\xi^2)^{-2}$ in (4.28) is sharply peaked at $q = 0$ with a width of ξ^{-1} , so that the correlator $C_d(q\sigma)$ can be evaluated as $C_d(0)$. Substituting $y = q\xi$ and integrating the first part in the bracket of (4.28) by parts, we find

$$\begin{aligned} \Lambda_N(k = 0, \sigma = 0) &= 2 \frac{S_d}{(2\pi)^d} \frac{\sigma^d C_d(0)}{\xi^d} \left[\frac{d}{4} - \frac{1}{d} \right] \int_0^\infty dy \frac{y^{d-1}}{(2 + y^2)^2} \\ &= \frac{\sigma^d C_d(0)}{\xi^d} \times \begin{cases} -\frac{3}{16\sqrt{2}}, & d = 1 \\ 0, & d = 2 \\ +\frac{5}{48\sqrt{2}\pi}, & d = 3. \end{cases} \end{aligned} \quad (4.29)$$

Remarkably, the correction is negative in one dimension, vanishes in two dimensions and is positive in three dimensions. In the scaling with V_0/μ fixed, used so far, the correction vanishes for $\sigma \rightarrow 0$, figure 4.7(a). The limit of uncorrelated disorder becomes well-defined, when $P_d(0) = V_0^2 \sigma^d C_d(0)$ is kept fixed while σ is decreased, figure 4.7(b). The 1D result will be studied in detail by means of a numerical integration of the Gross-Pitaevskii equation in section 4.3. As expected, the 3D result coincides exactly with the findings of Giorgini, Pitaevskii and Stringari [78], which have been confirmed by Lopatin and Vinokur [75] and by Falco *et al.* [80], but have been contradicted by Yukalov *et al.* [82].

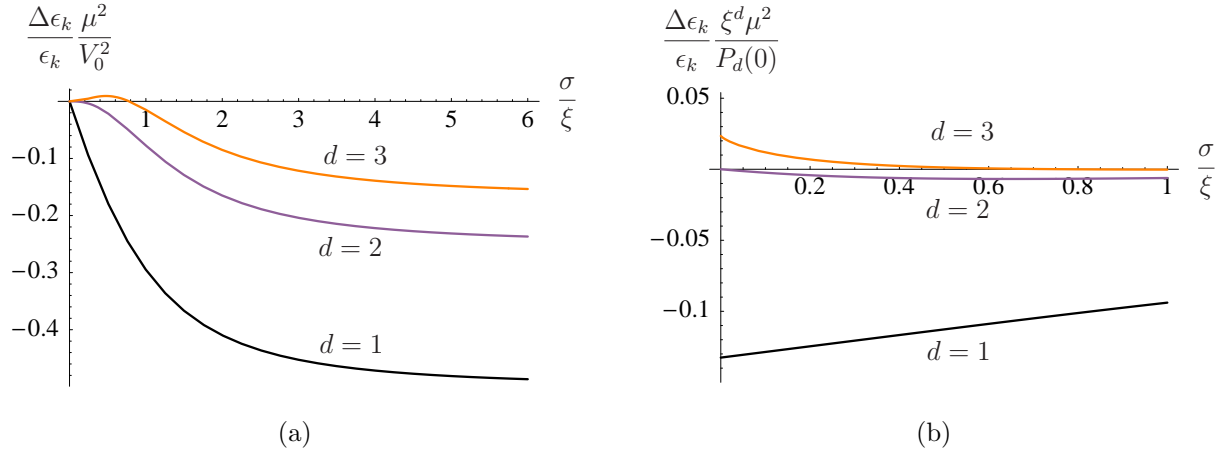


Figure 4.7.: Relative correction of the dispersion relation in the limit $k \rightarrow 0$ in $d = 1, 2, 3$.

In (a), the scaling is chosen as in the previous section, $\Lambda_N = \frac{\Delta \epsilon_k \mu^2}{\epsilon_k V_0^2}$. For large values of σ/ξ , the limit $\xi \ll \sigma \ll \lambda$ from equation (4.19a) and the left end of figure 4.4(b) is recovered. In (b) the scaling in units of $(\sigma/\xi)^d (V_0/\mu)^2$ is suitable for the limit of δ -correlated disorder. The limiting results from (4.29) are reached on the left. Remarkably, the correction is negative in $d = 1$ and positive in $d = 3$. The latter recovers the result by Giorgini *et al.* [78].

Intermediate behavior

In one dimension the correction (4.28) reads

$$\Lambda = -\frac{4}{\pi} \int dq \sigma \frac{C_1(q\sigma)}{(2 + q^2 \xi^2)^3}. \quad (4.30)$$

Because of $C_d(k\sigma) \geq 0$ [equations (3.12)], this correction is negative.

In three dimensions, the limiting values (4.29) and (4.19a) imply a sign change. In two dimensions, the qualitative behavior is less clear. In the case of speckle disorder (3.12), it is possible to solve (4.28) explicitly:

$$\Lambda_N(d=1) = -\frac{3}{8} z \left(\operatorname{arccot}(z) + \frac{1}{3} \frac{z}{1 + (z)^2} \right), \quad (4.31)$$

$$\Lambda_N(d=2) = z^3 \frac{2z\sqrt{1+z^2} - 1 - 2z^2}{\sqrt{1+z^2}} \quad (4.32)$$

$$\Lambda_N(d=3) = 7z^4 + \frac{5}{2} z^3 \arctan(1/z) - z^4 (6 + 7z^2) \log \left(\frac{1+z^2}{z^2} \right) \quad (4.33)$$

with $z = \frac{\sigma}{\sqrt{2}\xi}$, see figure 4.7 and figure 4.2.

Speed of sound—summary

Let us recapitulate the disorder correction of the speed of sound shown in figure 4.7(a). The right edge of the plot corresponds to the limit $\xi \ll \sigma \ll \lambda$,

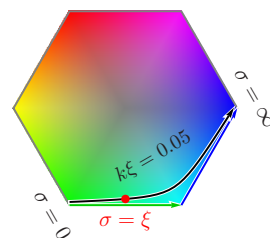
represented by the lower right corner in [figure 4.1](#), and coincides with the limit $k\sigma = 0$ in the previous section “[Hydrodynamic limit I: \$\xi = 0\$](#) ”. At this point, the correction is negative and proportional to $1/d$, which is typical for the angular integral over the p-wave scattering intensity $\cos^2 \theta$. Starting from this point $\sigma \gg \xi$, we decrease the disorder correlation length σ . The correction is described by [\(4.27\)](#), which reveals two facts: (a) The smoothing factor $[1 + q^2\xi^2/2]^{-1}$ weakens the effect of disorder. (b) There is also a positive correction (Mainly due to $W^{(2)}$ and beyond Thomas-Fermi effects), which does not diminish with d . In one dimension, the factor $-1/d$ is strong enough to keep the correction of the speed of sound negative. In three dimensions, however, the positive part takes over for $\sigma/\xi \lesssim 0.75$.

4.3. Numerical study of the speed of sound

In the previous two sections, we have worked out the low-energy behavior of the Bogoliubov excitations in the limits $\xi = 0$ and $k = 0$, which reproduce nicely the results of the full theory in the respective regimes. In this section, we confront the previous results with a direct numerical integration of the time-dependent Gross-Pitaevskii equation

[\(2.16\)](#). The numerical procedure is similar to the simulation of the single scattering process in [subsection 2.4.4](#). Essentially, the impurity is replaced by a disorder potential extending over the whole system and the setup is reduced from two dimensions to one dimension. Again, the simulation relies neither on the linearization in the excitations, nor on perturbation theory in the disorder potential. Thus, it is possible to go beyond leading-order perturbation theory for weak disorder. Also, we investigate the statistical distribution of the disorder average and the self-averaging properties of the speed of sound. As expected, the predictions from the Born approximation are confirmed very well for sufficiently weak disorder.

In the numerical integration of the original Gross-Pitaevskii equation [\(2.16\)](#) it is impossible to perform the strict limit $k = 0$ or $\xi = 0$ as it was done in the previous sections. Instead, the parameter $k\xi$ is fixed at a small but finite value. Then the ratio σ/ξ is varied, which allows reaching both regimes $\xi \ll \sigma, \lambda$ from [section 4.1](#) and $\lambda \gg \sigma, \xi$ from [section 4.2](#).



4.3.1. The numerical scheme

The integration is done in a one-dimensional system of length L with periodic boundary conditions. The discretization Δx is chosen smaller than

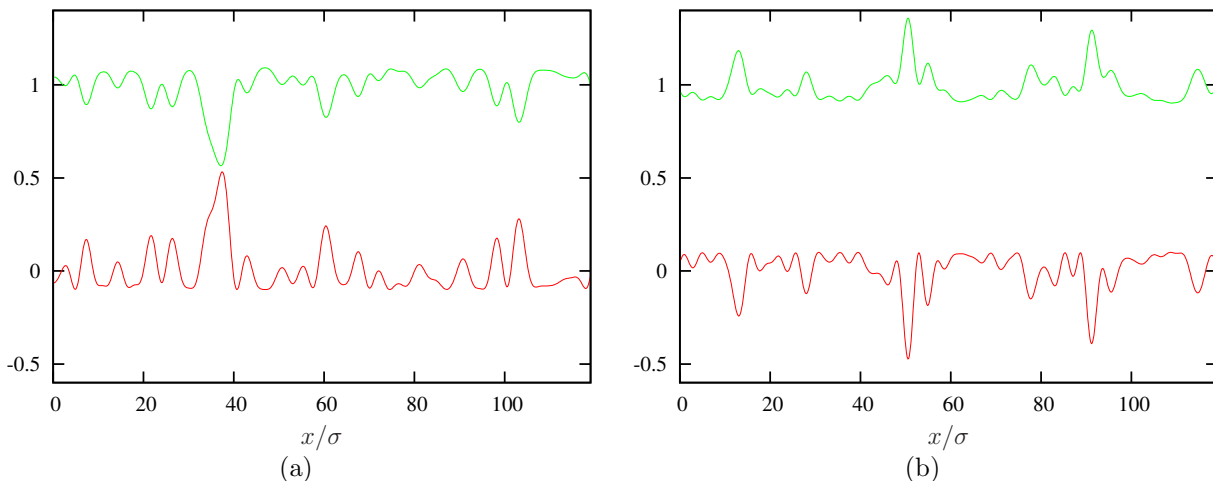


Figure 4.8.: Speckle potential $V(x)/\mu$ (red) and ground state density profile $n_0(x)/n_\infty$ (green) for (a) a repulsive speckle potential $V_0 = +0.1\mu$, (b) an attractive speckle potential $V_0 = -0.1\mu$. The asymmetric distribution (3.10) of the speckle potential can lead to occasional deep density depressions (a) or density peaks (b). At $\sigma = \xi$, the density profiles are slightly smoothed, compared with the Thomas-Fermi profile (2.20).

healing length, disorder correlation length and wave length. Due to the finite system size L , Fourier space becomes discrete, with $\Delta k = 2\pi/L$. The first step is to generate the speckle disorder potential. For all $k \leq \sigma^{-1}$, the independent complex field amplitudes E_k from (3.7) are populated using a Gaussian random number generator from the `gs1` library. In real space, the amplitudes are squared and the mean value is compensated, which gives the speckle disorder potential (3.9). Then the condensate ground-state is computed by imaginary time evolution, using the fourth-order Runge-Kutta algorithm [104]. Starting point is the homogeneous condensate, which adapts to the disorder potential during the imaginary time evolution, figure 4.8. The imaginary time evolution is not unitary, thus it violates the normalization of the wave function. This is compensated by re-normalizing the wave function after each imaginary time step, which corresponds to the shift of the chemical potential discussed in subsection 3.4.5.

Next, the disordered ground state is superposed with a plane-wave excitation γ_k of the homogeneous system. According to the Bogoliubov transformation (2.33) the imprints in density and phase read

$$\delta n(x) = 2\sqrt{n_\infty} \sqrt{\frac{\epsilon_k^0}{\epsilon_k}} \Gamma \cos(kx) \quad \delta\varphi(x) = \frac{1}{\sqrt{n_\infty}} \sqrt{\frac{\epsilon_k}{\epsilon_k^0}} \Gamma \sin(kx). \quad (4.34)$$

The amplitude of the phase modulation is much larger than the amplitude in the density, because of $\epsilon_k \gg \epsilon_k^0$ in the sound-wave regime. Thus, we choose a small value for the amplitude $\sqrt{\epsilon_k/\epsilon_k^0} \Gamma = 0.3\sqrt{n_\infty}V_0/\mu$. Then, the time

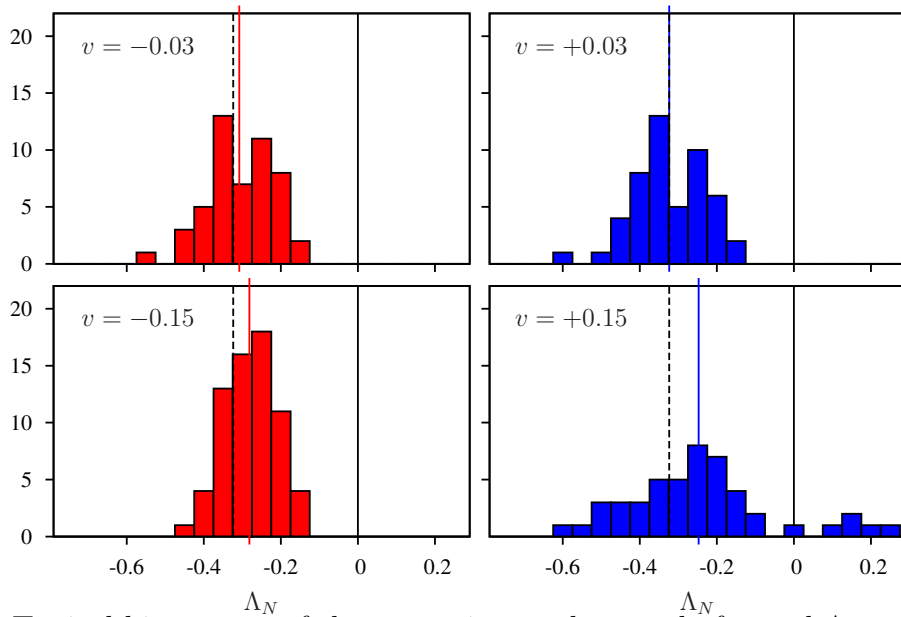


Figure 4.9.: Typical histograms of the correction to the speed of sound $\Lambda_N = \Delta c \mu^2 / (cV_0^2)$ at $k\xi = 0.05$, $k\sigma = 1$, $\sigma/\xi = 20$ over 50 realizations of disorder. The mean value of the respective distribution is marked with a solid line, and the Born prediction (4.15) $\Lambda_N = \frac{1}{4} \ln 2 - \frac{1}{2}$ is shown as a dashed line. For $V_0/\mu \lesssim 0.1$, the width of the distribution is clearly narrower than the mean value, i.e. the speed of sound shows self-averaging behavior. For $V_0 = +0.15\mu$, the distribution becomes very broad, extending even to positive values. The repulsive potential is so strong that the condensate density gets depressed nearly to zero below the highest peaks. Then, it is impossible to imprint a plane-wave density modulation (4.34). In two out of 50 realizations, no result could be obtained.

evolution is computed using again the fourth-order Runge-Kutta algorithm. The excitation propagates with a modified speed of sound and is slightly scattered at the same time. In order to extract the relevant information, the deviations of the wave function from the ground state are Bogoliubov transformed. Then the phase velocity is extracted from the complex phase of $\gamma_k \propto e^{-i\epsilon_k t/\hbar}$. This is done for many realizations of disorder and averaged over. By comparison with the phase velocity in the clean system, the change in the speed of sound is obtained. Furthermore, one can monitor the lifetime of the excitations by observing the elastically scattered amplitude γ_{-k} .

4.3.2. Disorder average and range of validity of the Born prediction

The numerical results for the speed of sound and other quantities (and experimental results as well) depend on the particular realization of disorder. For an infinite system, the results would be perfectly self-averaging. For practical reasons the size of the system was chosen to be 200 disorder corre-

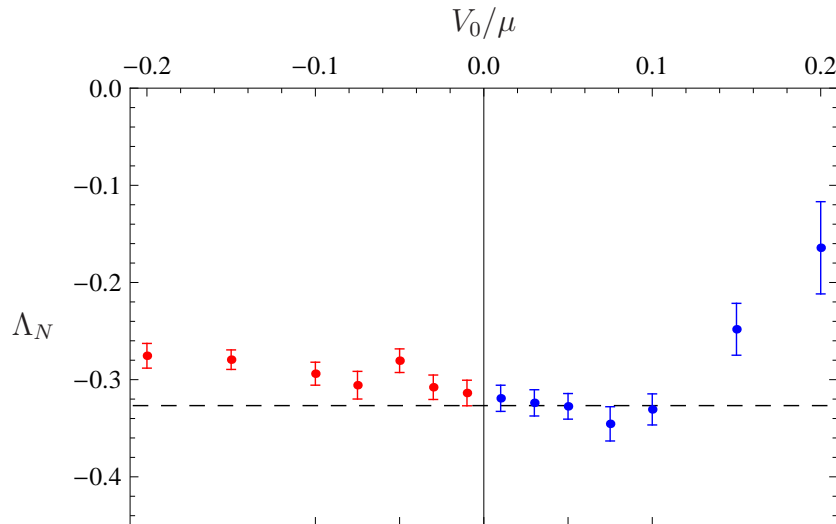


Figure 4.10.: Correction to the speed of sound at $k\xi = 0.05$, $k\sigma = 1$, $\sigma/\xi = 20$ as function of the disorder strength. The perturbative prediction appears as a horizontal line. The values were obtained by averaging over 50 realizations of disorder, the error bars show the estimated error of this mean value, which is given by the width of the distribution divided by the square root of the number of realizations. The histograms corresponding to the points at $v = \pm 0.03, \pm 0.15$ are shown in [figure 4.9](#). At large values of v , the potential is likely to fragment the condensate. At $v = 0.15$, this happened in two out of 50 realizations; At $v = 0.2$ it happened already in five out of 30 realizations, making the disorder average questionable.

lation lengths. In [figure 4.9](#) the distribution of results is shown for different disorder strengths V_0 at $k\xi = 0.05$ and $k\sigma = 1$. As long as the disorder is not too strong, the distributions are clearly single-peaked with well-defined averages. For larger values of $|V_0| \gtrsim 0.1\mu$, the highest potential peaks or wells reach the value of the chemical potential μ , which violates the assumptions of perturbation theory of the Born approximation from [chapter 3](#). In the case of an attractive (red-detuned) potential with deep wells, $V_0 < 0$, the effect is not very dramatic. In the opposite case of a repulsive (blue-detuned) speckle potential, however, the rare high peaks of the speckle potential may fragment the condensate. In the corresponding panel of $V_0 = +0.15\mu$, the distribution is strongly broadened, including even some points with opposite sign.

Also the mean values are shifted as function of the disorder strength V_0 . This is investigated in [figure 4.10](#), where the mean values of the distributions in [figure 4.9](#) are shown together with their estimated error. The correction is shown in units of $v^2 = V_0^2/\mu^2$, such that the Born approximation from [subsection 3.4.5](#) appears as the horizontal line as function of the disorder strength V_0 . At small values of $|V_0/\mu|$, the agreement is very good. Then there is a clear negative linear trend, which is due to the third moment of the speckle distribution function ([3.10](#)). At larger values $v \gtrsim 0.15$, the

condensate gets already fragmented, due to rare high potential peaks from the exponential tail in (3.10), see also figure 4.8. This is reflected in the positive deviation of the mean values and also in the increased width of the distribution. To sum things up: Beyond-Born effects are clearly visible, but the Born result remains useful in a rather wide range. The correction stays negative, even for nearly fragmented condensates.

4.3.3. Non-condensed fraction

Even in the ground state, there are particles that are not in the Gross-Pitaevskii condensate function Φ , but in excited states (subsection 2.5.6). In order to verify the preconditions for treating the one-dimensional disordered problem on grounds of the Gross-Pitaevskii equation, we compute the fraction of non-condensed particles. We start with the homogeneous (quasi)condensate and evaluate the sum (2.87). In the thermodynamic limit, this sum diverges in one dimension. Nonetheless, we can compute the sum for systems of finite size. For the system size $L = 200\xi$, used in the previous subsections, we find $n_{\text{nc}}|_{L=200\xi} = 0.3488/\xi$. Note that the non-condensed fraction diverges logarithmically with L : for $L = 10^5\xi$, for example, we find $n_{\text{nc}}|_{L=10^5\xi} = 1.046/\xi$.

We need to relate the non-condensed density to the total density $n_{1\text{D}}$ of the Bose gas. This non-condensed fraction scales like $(n_{1\text{D}}\xi)^{-1}$, i.e. the average particle spacing in relation to the healing length [55, chapter 17].

The numerical procedure for computing the non-condensed density in presence of disorder is as follows. In the same manner as in the Gross-Pitaevskii integration (subsection 4.3.1), the system is discretized into l points, the disorder potential is generated, and the Gross-Pitaevskii ground state is computed. Then, the $2l \times 2l$ real-space matrix (2.68) is set up and diagonalized numerically. As the matrix is not symmetric, the eigenvectors $(u_\nu(\mathbf{r}), v_\nu(\mathbf{r}))$ are not pairwise orthogonal. Instead, they satisfy the bi-orthogonality relation (2.74). The non-condensed density (2.85) is then evaluated from the relevant modes with positive frequency (section 2.5). In figure 4.11, results for the parameters used in the previous subsections are shown. The initial increase is quadratic in the reduced disorder strength V_0/μ . Strong deviations occur at $V_0 \gtrsim 0.1\mu$. At the disorder strength $V_0/\mu = 0.1$, the fraction of non-condensed atoms is increased by about 25%, i.e. the non-condensed fraction is still of the same order as in the homogeneous case.

In conclusion, the 1D validity condition for Gross-Pitaevskii theory in the homogeneous case is $n_{\text{nc}}/n_{1\text{D}} \propto (\xi n_{1\text{D}})^{-1} \ll 1$ [55, chapter 17] (with a

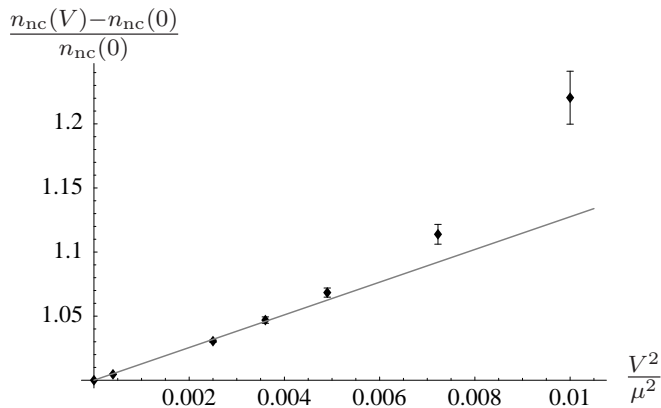


Figure 4.11: Relative increase of the non-condensed density n_{nc} due to disorder. With the parameters of the present section $\sigma = \xi = L/200$. Note that the increase and the reference $n_{nc}(V = 0)$ both depend on the system size L/ξ .

proportionality factor that depends logarithmically on L). As function of disorder strength, the non-condensed fraction *increases*, but it stays within the same order of magnitude, at least in the range of parameters of the present section.

4.3.4. Speed of sound as function of the correlation length

Having checked the prediction at one particular value of the disorder correlation length, we now investigate different regimes of length scales. Given the condition $k\xi = 0.05 \ll 1$, the correlation length σ can be the shortest of all length scales, larger than the healing length but shorter than the wave length, or the largest of all length scales.

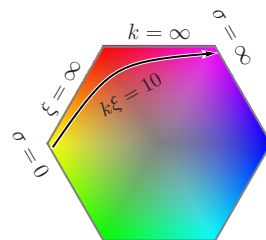
In the intermediate range, the full integral (3.60) interpolates between the hydrodynamic limit (4.15) and the limit of low-energy excitations (4.31).

In the first case, the prediction (4.31) from section 4.2 holds (green dashed line in figure 4.2). In the last case, the hydrodynamic limit (4.14) from section 4.1 is applicable (blue dotted line in figure 4.2). In-between, the full formula from subsection 3.4.5 has to be evaluated (solid line in figure 4.2). In figure 4.2 numerical data averaged over 50 realizations of disorder is shown together with the perturbative prediction from subsection 3.4.5. We find good agreement, both for $V_0 > 0$ and $V_0 < 0$.

4.4. Particle regime

In the previous sections of this chapter, we have investigated in detail the sound-wave excitations in the low-energy regime $k\xi \ll 1$. The predictions of the disordered Bogoliubov theory, however, hold more generally and allow the transition to the particle regime $k\xi \gg 1$. There, the interaction can be neglected with respect to the kinetic energy. The Hamiltonian (2.11) becomes non-interacting, and one could expect that the entire Bogoliubov problem passes over to the problem of free particles in disorder [22, 23]. However, in the non-interacting limit some subtleties occur because of assumptions made in the derivation of the Bogoliubov Hamiltonian.

In this section, we firstly discuss the predictions from section 3.4 in the particle regime $k\xi = 10 \gg 1$. In parameter space, the curve $k\xi = 10$ is opposite to that of section 4.3. The elastic scattering properties agree with those of free particles, but the real corrections to the spectrum turn out to differ. The leading order tends to a constant that can be absorbed in a shift of the chemical potential. In subsection 4.4.3, we compute the disorder averaged dispersion relation in the Schrödinger particle limit, where the condition $\mu \gg V$ from the Bogoliubov regime is reversed. Finally, we study numerically the transition between the two regimes.



4.4.1. Mean free path

Already in the single scattering problem [subsection 2.4.3], we have learned that in the limit $\xi \rightarrow \infty$, the first-order scattering element (2.45c) approaches the scattering amplitude of a free particle in disorder

$$W_{\mathbf{k}+\mathbf{q}\mathbf{k}}^{(1)} \approx \begin{cases} V_{\mathbf{q}} & q\xi \gg 1, \\ -V_{\mathbf{q}} & q\xi \ll 1. \end{cases} \quad (4.35a)$$

$$(4.35b)$$

Only the forward scattering element $W_{\mathbf{k}\mathbf{k}}^{(1)} = -V_0$ [cf. (2.58)] deviates, but can be absorbed in the chemical potential. Consequently, the imaginary part of the self-energy, which consists of the angular integral over the elastic scattering shell, passes over to the results of free particles in disorder. Equation (3.53) reduces to

$$\frac{1}{kl_s} = \left(\frac{V_0}{2\epsilon_k^0} \right)^2 (k\sigma)^d \int \frac{d\Omega_d}{(2\pi)^{d-1}} C_d \left(2k\sigma \sin \frac{\theta}{2} \right), \quad (4.36)$$

which coincides with [23, eq. (34)]. All quantities related to the interaction have disappeared. The energy scale μ has been replaced with the kinetic energy ϵ_k^0 of the particle and the only remaining length scales are combined in the reduced momentum $k\sigma$. In contrast to the sound-wave regime [subsection 4.1.2], the inverse mean free path of particles diverges at low energies. Slow particles are scattered strongly, and the perturbation theory breaks down [22, 23].

4.4.2. Renormalization of the dispersion relation in the Bogoliubov regime

Let us calculate the real part of the self-energy (3.39), i.e. the disorder correction of the dispersion relation, in the non-interacting limit $\mu \rightarrow 0$. Apart from $W^{(1)}$, we also need the anomalous scattering element $Y^{(1)}$ (2.45d), which does not vanish as one might expect for non-interacting particles. Instead, we find

$$Y_{\mathbf{k}+\mathbf{q}\mathbf{k}}^{(1)} \approx \begin{cases} V_{\mathbf{q}} [k^2 + (\mathbf{k} + \mathbf{q})^2] / q^2 & q\xi \gg 1, \\ V_{\mathbf{q}} (k\xi)^2 & q\xi \ll 1. \end{cases} \quad (4.37a)$$

$$(4.37b)$$

The real part of the self-energy (3.39), together with the correction fixing the particle number (3.59), is an integral over the momentum transfer \mathbf{q} . The correlator $C_d(q\sigma)$ provides a sharp cutoff at $q = 2/\sigma$, and also the smoothing factors contained in the envelope functions suppress the integrand for $q\xi \gg 1$. Thus, we can approximate the integrand for small q . Using (4.35b), (4.37b) and (2.50), we find

$$M_N^{(0)} := \frac{\epsilon_k}{\mu} \Lambda_N = \int \frac{d^d q}{(2\pi)^d} \sigma^d C_d(q\sigma) \frac{q^2 \xi^2}{(2 + q^2 \xi^2)^2}. \quad (4.38)$$

Only the anomalous coupling $y^{(1)}$ and the second order $w^{(2)}$ have contributed to this leading order, but not the normal scattering $w^{(1)}$. Equation (4.38) holds for $k\xi \gg 1$ and $k\sigma$ not too small. It is a strictly positive function of σ/ξ . In the leading order, there is no dependence on the momentum $k\xi$, thus it does not affect quantities like the group velocity and the effective mass (inverse of the second derivative of the dispersion relation). It is interpreted as a correction of the chemical potential in

$$\epsilon_k \stackrel{(2.36)}{=} \epsilon_k^0 + \mu \mapsto \epsilon_k^0 + \mu \left(1 + M_N^{(0)} V_0^2 / \mu^2 \right). \quad (4.39)$$

The integral (4.38) has the same form as the correction (3.59), due to fixing the particle number. However, it has the opposite sign. The correction

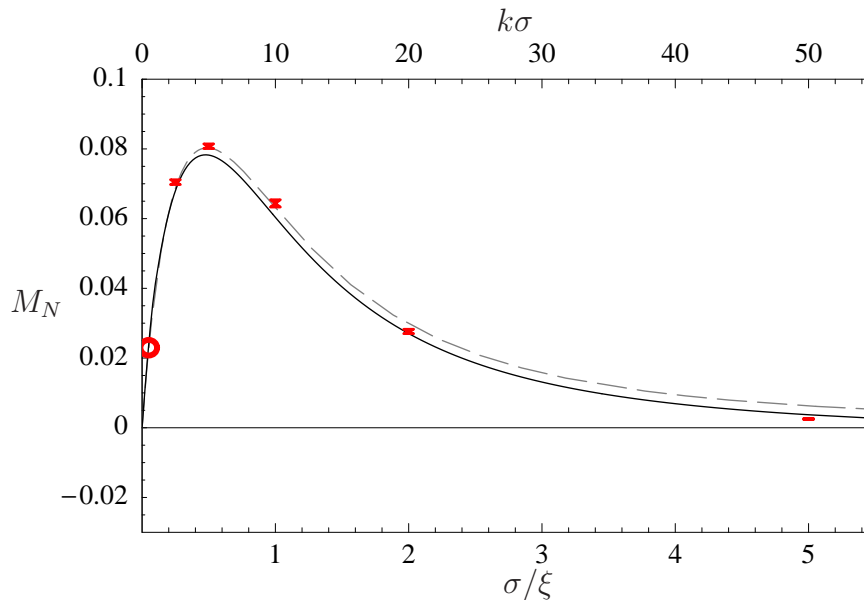


Figure 4.12.: Relative disorder correction $M_N = (\bar{\epsilon}_k - \epsilon_k)\mu/V_0^2$ of the dispersion relation at $k\xi = 10$, $V_0 = 0.03\mu$ in one dimension. Solid line: Full correction (3.60) for finite $k\xi = 10$. Dashed line: Limit (4.40) $M_N^{(0)}(\sigma/\xi)$ for $k\xi \rightarrow \infty$. Dots: Numerical integration in a system of size $L = 200\sigma$, averaged over 50 realizations of disorder [Each realization of disorder was normalized to mean value zero and rms value $|V_0|$]. The red circle marks $k\sigma = 0.5$, cf. figure 4.14

(4.38) is positive *although* the chemical potential has been lowered in order to keep the particle number constant. At fixed μ , the correction would be double, $\Lambda_\mu = 2\Lambda_N$.

For the 1D speckle potential, the integral (4.38) can be solved analytically

$$M_N^{(0)} = \frac{z}{2} \left[\arctan\left(\frac{1}{z}\right) - z \log\left(1 + \frac{1}{z^2}\right) \right], \quad z = \frac{\sigma}{\sqrt{2}\xi}. \quad (4.40)$$

In figure 4.12, this limit is compared to the full correction at a finite value $k\xi = 10$.

Numerical test: Bogoliubov quasiparticles at $k\xi = 10$. Analogously to the procedure in section 4.3, we determine numerically the correction to the dispersion relation in the particle regime $k\xi = 10$, as function of the correlation length σ . In figure 4.12, the numerical results are shown together with the full Born prediction (3.60) and the limit (4.40), showing good agreement. In contrast to the low-energy excitations, where the 1D correction [(4.15) and (4.30)] is always negative, it is here found to be positive. Only for $\sigma/\xi \gtrsim k\xi$, which is outside of the plot range, negative values are found. The correction $\Lambda_N = M_N\mu/\epsilon_k$ is much weaker than in the hydrodynamic

regime, because in the range of validity of the Bogoliubov perturbation theory, the disorder is weaker than the chemical potential, and the chemical potential is again much lower than the excitation energy ϵ_k^0 .

4.4.3. Transition to really free particles

How are the Bogoliubov excitations in the particle regime related to really free particles? In the limit of vanishing interaction $gn_\infty = \mu \rightarrow 0$, $\xi \rightarrow \infty$, the Gross-Pitaevskii energy functional (2.17) passes over to the usual Schrödinger energy functional and the Gross-Pitaevskii equation becomes the Schrödinger equation, which reads

$$[\hbar\omega - \epsilon_k^0] \Psi_{\mathbf{k}} = \int \frac{d^d k'}{(2\pi)^d} V_{\mathbf{k}-\mathbf{k}'} \Psi_{\mathbf{k}'} \quad (4.41)$$

in Fourier space. Also the Bogoliubov excitations seem to pass into free particles, as the coefficient $a_k = \sqrt{\epsilon_k^0/\epsilon_k}$ tends to one

$$\hat{\gamma}_{\mathbf{k}} \stackrel{(2.32)}{=} i\sqrt{n_\infty} \delta\hat{\varphi}_{\mathbf{k}} + \delta\hat{n}_{\mathbf{k}}/(2\sqrt{n_\infty}) \stackrel{(2.27)}{=} \delta\hat{\Psi}_{\mathbf{k}}. \quad (4.42)$$

The second equality relies on the fact that the condensate wave function $\Phi(\mathbf{r})$ is extended. It fails for strong disorder $V \gg \mu$, when the Bose-Einstein condensate becomes a fragmented Bose glass [74].

Self-energy in the Schrödinger regime

Before working out the difference between the Bogoliubov regime and the Schrödinger regime, let us consider the problem of the Schrödinger equation in presence of weak disorder. From equation (4.41), we write the Born approximation of the self-energy for the disordered Schrödinger problem

$$\text{Re}\Sigma_{\text{Sg}} = V_0^2 \text{P} \int \frac{d^d k'}{(2\pi)^d} \sigma^d \frac{C_d(|\mathbf{k} - \mathbf{k}'|, \sigma)}{\epsilon_k^0 - \epsilon_{k'}^0}. \quad (4.43)$$

For the 1D speckle potential, the correlator C_d is piecewisely linear and the Cauchy principal value can be computed analytically. Similarly to (4.15) we find

$$\text{Re}\Sigma_{\text{Sg}} = \frac{1}{4} \frac{V_0^2}{\sqrt{\epsilon_k^0 E_\sigma}} \left[\ln \left| \frac{1 + k\sigma}{1 - k\sigma} \right| + k\sigma \ln \left| \frac{1 - k^2\sigma^2}{k^2\sigma^2} \right| \right], \quad (4.44)$$

see figure 4.13. The self-energy scales like $V_0^2/\sqrt{\epsilon_k^0 E_\sigma}$, where $E_\sigma = \hbar^2/(2m\sigma^2)$ is the energy scale defined by the disorder correlation length.

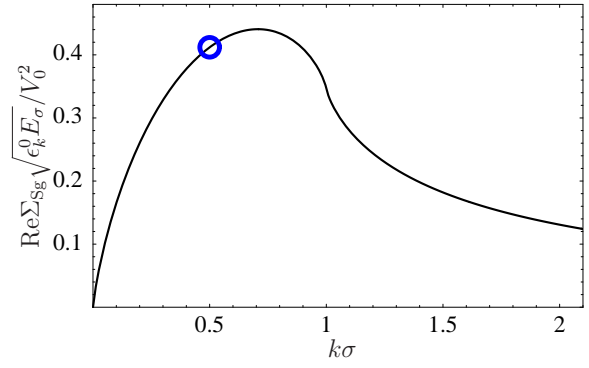


Figure 4.13: Real part of the self-energy (4.44) for individual atoms in a 1D speckle potential. The blue circle marks $k\sigma = 0.5$, cf. figure 4.14.

4.4.4. Closing the gap with a Gross-Pitaevskii integration

Although Bogoliubov excitations in the particle regime and free particles have the same dispersion relation and the same elastic scattering properties, the results obtained in the Bogoliubov regime [(4.40), figure 4.12] differ significantly from those of the Schrödinger regime [(4.44), figure 4.13]. The differences stem from the different presuppositions in the two regimes.

- In the Bogoliubov regime, plane-wave excitations with amplitude Γ are considered on top of the extended condensate function $\Phi(\mathbf{r})$. In the scope of the Bogoliubov approximation (section 2.3), the excitations have to be small $\Gamma \ll \Phi$. Conversely, in the Schrödinger regime, there is no background at all present, i.e. $\Gamma \gg \Phi$.
- In the Bogoliubov regime, the condensate wave function Φ provides an absolute reference for the complex phase of the excitations. The superposition of the plane-wave excitation with the condensate leads to a density modulation. In the Schrödinger regime, there is no condensate providing an absolute phase and consequently no signature in the density. The particles can only be tracked by the complex phase of $\delta\Psi_k$. In the following, we use $\delta\Psi_k \propto e^{-i\omega t}$ to obtain the phase velocity instead of the density and phase signature δn and $\delta\varphi$. We write M_{Sg} instead of M_N . In the Bogoliubov regime, these definitions are essentially equivalent, because the phase of the condensate changes only very slowly with time.
- The validity conditions for the disorder perturbation theories differ. In the Bogoliubov regime, the disorder must be weak in the sense that $V(\mathbf{r}) \ll \mu$. In the Schrödinger regime, μ vanishes and the validity condition is $V_0 \ll \sqrt{\epsilon_k^0 E_\sigma}$ [23]. When passing from the Bogoliubov regime to the Schrödinger regime, $V_0 \ll \mu$ has to be reversed $\mu \ll V_0$.

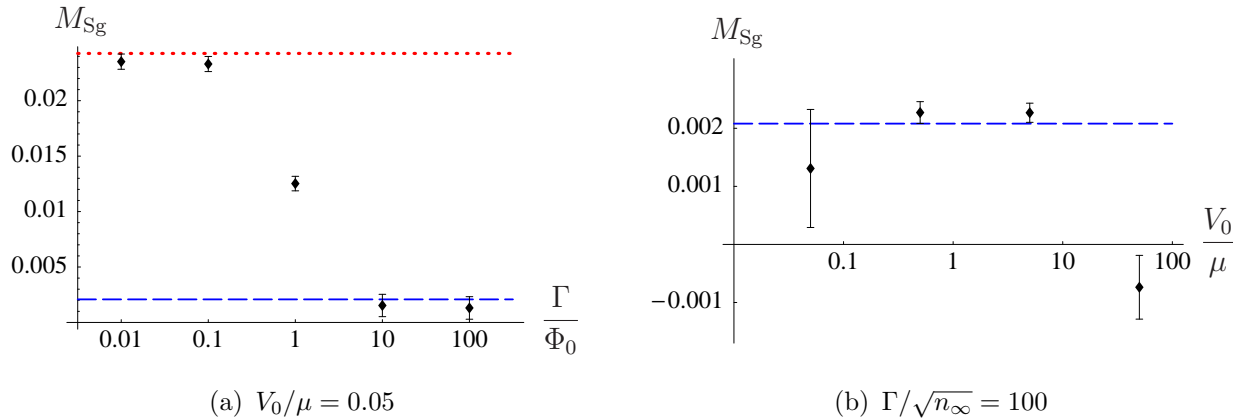


Figure 4.14.: Correction of the dispersion relation in the transition from the Bogoliubov regime to free-particle plane waves. Red dotted line: Bogoliubov limit (4.40), cf. figure 4.12; dashed line: Schrödinger limit (4.44), cf. figure 4.13; dots: results from the Gross-Pitaevskii integration. (a) Disorder correction at $V_0/\mu = 0.05$ as function of the wave amplitude Γ/Φ_0 ; (b) Disorder correction at $\Gamma/\sqrt{n_\infty} = 100$ as function of the ratio V_0/μ of disorder strength and chemical potential. For explanations, see main text. Parameters: $k\xi = 10$ and $k\sigma = 0.5$

We establish the connection between the Bogoliubov regime and the Schrödinger regime by means of a Gross-Pitaevskii integration and observe the disorder averaged propagation speed.

We proceed in two steps. Firstly, we increase the wave amplitude Γ with respect to the ground-state wave function Φ . We start with a plane wave with small amplitude on top of the extended Gross-Pitaevskii ground state and end at the opposite case of the whole condensate propagating as a plane wave in presence of a small fraction at rest. This transition is to be understood essentially as a formal transition. Physically, it is somewhat pathological, because the macroscopically populated traveling wave is a highly excited state and the Gross-Pitaevskii ansatz is questionable. However, interpreted as a single Schrödinger particle in a disordered environment, the problem is well defined [22, 23]. Results are shown in figure 4.14(a). As expected, they initially agree with the Bogoliubov prediction (4.40) and approach the Schrödinger prediction (4.44) for $\Gamma \gg \Phi_0$. The Schrödinger prediction is not met exactly, which is plausible because the chemical potential is still larger than the disorder potential.

In the Schrödinger regime, the chemical potential should be the lowest of all energy scales. Thus, in a second step, we increase the disorder strength V_0 beyond the chemical potential and the agreement gets better, figure 4.14(b). For very high values of V_0 , the validity condition $V_0 \ll \epsilon_k^0 = \mu k^2 \xi^2$ for the Born approximation in (4.43) is violated and the agreement gets worse again.

4.4.5. Conclusions on the particle limit

Bogoliubov quasiparticles at high energies and free particles without any condensate background have the same clean dispersion relation ϵ_k^0 and the same elastic scattering amplitude $W^{(1)}$.

Concerning the disorder correction to the dispersion relation, however, their respective behaviors appear contradictory. The correction derived in the Schrödinger regime (4.43) is not recovered by the correction in the Bogoliubov regime (4.38). The leading-order of the latter can be absorbed in an overall shift of the chemical potential (4.39), which leaves physical quantities like the effective mass, i.e. the curvature of the dispersion relation untouched. This is similar to section 2.4, page 44, where we also shifted the chemical potential in order to recover the equations of motion for free particles.

It is misleading to expect that the disordered Bogoliubov problem as treated in chapter 3 should pass over to the problem of single atoms in disordered potential [22, 23]. Though the underlying Hamiltonians are the same in the limit $g = 0$ (or $\mu = 0$, or $\xi = \infty$), differences occur because of the approximations made. In the expansion of the Bogoliubov Hamiltonian, the smoothed potential (2.21) was used, with the validity condition $\mu \gg V$. The interactions of Bogoliubov excitations with the condensate background scale like $gn_0(\mathbf{r}) \sim \mu$ and will never be negligible compared to the disorder potential.

After these problems with the real renormalization of the dispersion relation, it is astonishing that there are no differences in the elastic scattering processes. This can be understood in the following simplified reasoning: Schrödinger particles are subject to the external potential only, whereas Bogoliubov excitations in the particle regime see both, the external potential *and* the condensate background. At relevant wave numbers $k\xi \gg 1$, the condensate is so smooth that it cannot contribute to the scattering, thus, the elastic properties of Schrödinger particles and Bogoliubov excitations are the same. However, the homogeneous background does shift the mean energy, therefrom the shift of the chemical potential found in equation (4.39).

Beyond the leading correction (4.38), there should be k -dependent corrections, but these are at least one order $(k\xi)^{-1}$ smaller.

5. Conclusions and Outlook (Part I)

5.1. Summary

A general formalism for the description of the Bogoliubov excitations of inhomogeneous Bose-Einstein condensates has been set up. The difficulty of the inhomogeneous many-particle problem has been solved by means of an inhomogeneous Bogoliubov approximation. Taking advantage of the macroscopically populated condensate state, we have separated the problem into the mean-field condensate function $\Phi(\mathbf{r})$ and the quantized inhomogeneous Bogoliubov problem. Via the Gross-Pitaevskii equation (2.16), the external potential enters the condensate function $\Phi(\mathbf{r})$ nonlinearly. The condensate function then enters the Bogoliubov Hamiltonian and makes it inhomogeneous.

The Bogoliubov Hamiltonian (2.42) depends in a simple way on $\Phi(\mathbf{r})$ and $\bar{\Phi}(\mathbf{r}) = \Phi_0^2/\Phi(\mathbf{r})$, i.e., if one could solve the Gross-Pitaevskii equation exactly, one could write down the Bogoliubov Hamiltonian exactly, too. For practical purposes, however, the Bogoliubov Hamiltonian is expanded in powers of the external potential in a systematic way.

Already in the first order, interesting physics is observed, namely the transition from p-wave scattering characteristics in the sound-wave regime to s-wave scattering in the particle regime (section 2.4).

For the disordered problem, including the renormalization of the dispersion relation, some more efforts have been necessary. Firstly, the self-energy is of second order in the disorder potential, so also the second order of the Bogoliubov Hamiltonian had to be included in the correction. Secondly, the basis in presence of disorder had to be chosen correctly (section 3.2). With the reasoning of section 2.5 and section 3.2, this question has been answered once and for all: Bogoliubov modes (2.33) defined in terms of plane waves in density and phase are the only reasonable choice, unless one wants to exactly diagonalize the disordered Bogoliubov Hamiltonian (2.29).

With the disordered Bogoliubov formalism, physical quantities like the mean free path and the renormalized speed of sound can be calculated in the whole parameter space spanned by the excitation wave length, the condensate healing length and the disorder correlation length.

The mean free path is found to be sufficiently long, such that it makes sense to define a renormalized speed of sound. In three-dimensional uncorrelated disorder, the positive correction of the speed of sound predicted by Giorgini *et al.* [78] is recovered. Beyond that, the disorder-averaged speed of sound is computed for arbitrary correlation length and for arbitrary dimension. Interestingly, the positive correction for three-dimensional uncorrelated disorder changes its sign when going to correlated disorder or to one dimension.

Non-condensed fraction

The non-condensed fraction due to disorder (subsection 2.5.6 and subsection 4.3.3) goes beyond the condensate depletion calculated by Huang and Meng [77] and by Giorgini *et al.* [78]. There are two small parameters: the weak-disorder parameter V_0/μ and the gas parameter $\sqrt{na_s^3}$. The deformation of the Gross-Pitaevskii ground state scales with V_0/μ . This is the condensate depletion of [77, 78]. In this work, the Bogoliubov excitations are measured from the deformed Gross-Pitaevskii ground state. Consequently, the deformation of the ground state does not appear as a condensate depletion. The non-condensed fraction (2.85) is of the order $\sqrt{na_s^3}$, and its shift due to disorder is of the order $\sqrt{na_s^3} V_0^2/\mu^2$ (subsection 4.3.3).

The non-condensed fraction (2.85) has been computed numerically in a finite one-dimensional system, in order to verify that the validity of Gross-Pitaevskii theory is not destroyed by disorder.

5.2. Experimental proposals

From the studies presented in this work, the following proposals for experiments can be made.

Elastic single scattering

The first proposal follows the single scattering process discussed in section 2.4. The experimental procedure should essentially follow the numerical scheme. As pointed out in subsection 2.4.1, the setup should be two-dimensional. Apart from setups with a two-dimensional condensate in a magnetic trap with a superimposed optical lattice like in [5], the 2D experiment at MIT [42] with a sodium condensate in an optical trap consisting of a laser light sheet seems to be a particularly suitable starting point. An additional laser focused perpendicularly through the trap serves as impurity

potential. The imprint and the detection of the Bogoliubov waves follows Vogels *et al.* [61], using Bragg spectroscopy techniques. The crucial point is the detection of the scattered Bogoliubov wave, because it will be one or two orders of magnitudes smaller than the imprinted plane wave. In addition, the detection has to take place with angular sensitivity.

Despite these challenges, the continuous transition from a p-wave scattering amplitude in the sound-wave regime to an s-wave scattering amplitude in the particle regime promises to be an interesting object of experimental study.

Measurement of the speed of sound in disordered BEC

The predicted renormalization of the speed of sound due to disorder, as discussed in [chapter 4](#), can in principle be measured experimentally. However, in the perturbative regime of the predictions, the corrections scale quadratically with the disorder strength, and consequently they are very small. In a direct observation in real space, as in the experiment [57], the difference in the propagation speed should be hardly separable from the noise in the data. A more sophisticated ansatz is measuring the static structure factor by Bragg spectroscopy and to extract the dispersion relation, similar to the experiments [59, 62], but with a speckle disorder potential superposed to the trapping potential. In contrast to the first ansatz, it is possible to excite certain k values selectively, which allows also probing the transition from sound-like to particle-like excitations.

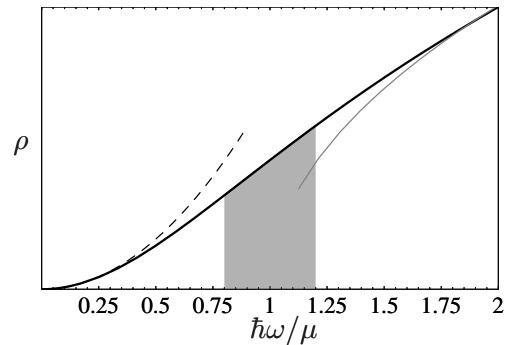
5.3. Theoretical outlook

With the inhomogeneous Bogoliubov Hamiltonian ([section 2.3](#)) and the block matrix notation ([subsection 3.3.2](#)) at hand, many other questions can be approached.

Localization

It should be particularly interesting to characterize the localization of Bogoliubov excitations across the transition from sound waves to particles. In three dimensions, phonon and particle regime have opposite characteristics concerning their localization [29]: Delocalized low-energy phonon states are separated by a mobility edge ω^* from localized high-energy states. Inversely, electrons are localized at the lower band edge, separated from extended states at the mobility edge E^* . The upper band edge does not apply in the case of bosons in a continuous system. Phonon regime and particle regime

Figure 5.1: Density of states in three dimensions (compare to figure 3.5(c)). For sufficiently strong disorder, the Bogoliubov excitations in the crossover region at $k\xi \approx 1$ are expected to localize (gray).



are now combined to the Bogoliubov dispersion relation (2.35), figure 2.3. Depending on the disorder strength, two regimes are possible:

1. Weak disorder $\mu < \omega^*$, $E^* < \mu$. Phonon and particle regime are combined without any localized states.
2. Strong disorder $\omega^* < \mu < E^*$. There is a range of localized states around the crossing from phonon to particle excitations.

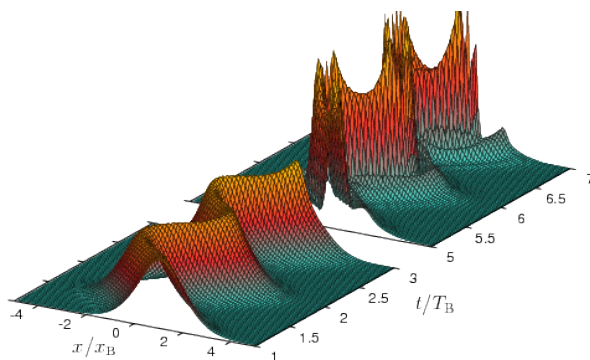
The characterization of these localized states between phonons and particles is an interesting topic for further research. A possible approach is a diagrammatic perturbation theory analogous to Vollhardt's and Wölfle's approach [123], which allows computing the weak-localization to the diffusion constant. This approach has already been applied to non-interacting cold atoms in speckle potentials [22, 128]. With the block-matrix notation employed in subsection 3.3.1, the Bogoliubov propagator follows equivalent equations of motion. It should be possible to compute the weak-localization correction to the diffusion constant analogously.

Finite temperature

With the Bogoliubov formalism set up in this work, it is in principle possible, to consider finite-temperature problems. Similar to the zero-temperature Green functions in the block-matrix formalism of subsection 3.3.2, also Matsubara Green functions could be set up and computed. However, the Bogoliubov formalism relies on the macroscopic occupation of the condensate mode and neglects the interactions between the Bogoliubov excitations. At higher temperatures, these interaction effects become relevant and one should take beyond-Bogoliubov terms into account. These interactions appear as additional perturbations and might be accessible with methods similar to those used by Hugenholtz and Pines [76]. However, two perturbations at once, disorder and the interaction among quasiparticles should make the problem extremely complicated.

Part II.

Bloch Oscillations



6. Bloch Oscillations and Time-Dependent Interactions

The second part of this work is somewhat separate from the Bogoliubov part, as now a lattice system is considered (figure 6.1), in contrast to the continuous system in part I. Instead of the disorder leading to scattering and localization, now the tilted lattice localizes the wave packet by the phenomenon of Bloch oscillation. The perturbation comes as a time-dependent interaction, which in general destroys the wave packet.

There are also strong links to part I. After the smooth-envelope approximation (6.7), the discrete Gross-Pitaevskii equation takes the form of the continuous Gross-Pitaevskii equation (which is also known as nonlinear Schrödinger equation), but now with a time-dependent effective mass.

Additionally to the time-dependent mass, also the interaction can be made time-dependent by means of a Feshbach resonance. Together they provide a source of energy for the growth of excitations (dynamical instability). These excitations are of the same type as the Bogoliubov excitations in part I. The growth of these excitations is the main mechanism for the destruction of the coherent wave packet.

The work of this part was done in collaboration with the group of Francisco Domínguez-Adame at Complutense University in Madrid. The essentials have been published in [129, 130].

6.1. Introduction

Historically, the interest in electrons and phonons in crystals has led to the investigation of lattice systems. Understanding quantum particles as waves is the key to understanding the dramatic effects a lattice can have

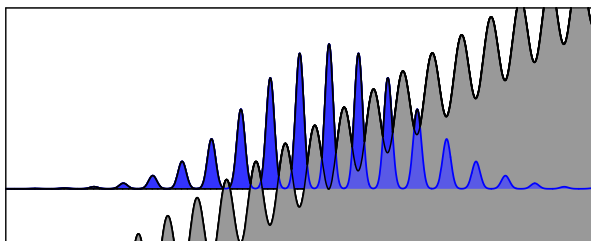
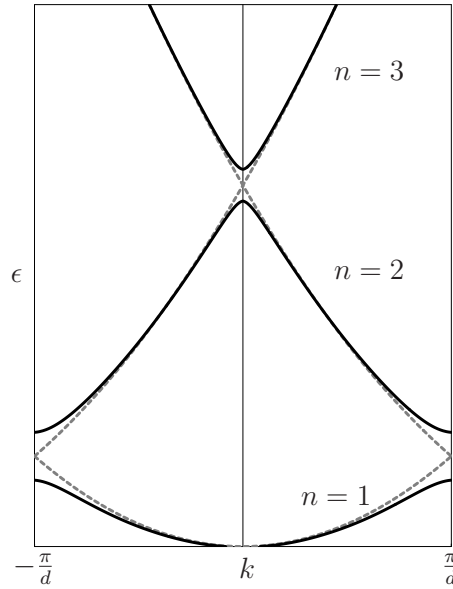


Figure 6.1: Schematic representation of the setting for Bloch oscillations. The wave packet (blue) is located in the wells of a deep tilted lattice potential (gray)

Figure 6.2: Sketch of the dispersion relation in a lattice. The dashed line shows the free dispersion $\epsilon_k^0 = \hbar^2 k^2 / (2m)$, folded back into the first Brillouin zone. The lattice with period d couples the degenerate states $k = +\pi/d$ and $k = -\pi/d$ at the edges of the Brillouin zone, which leads to band gaps (avoided crossings). In a deep lattice potential, the band gap becomes large and excitations from the lowest band to higher bands can be neglected at low temperatures.



on the particles. Even if the lattice is weak, in the sense that each site is only a weak scatterer, the coherent superposition of waves reflected at the periodic lattice can lead to total reflection if the scattered waves interfere constructively.

6.1.1. Bloch oscillation of a single particle

The lattice is symmetric under discrete translations by integer multiples of the lattice vectors. As a consequence, the Bloch theorem [131] states that every energy eigenstate $\psi(\mathbf{r})$ can be written as the product of a plane wave $e^{i\mathbf{k}\cdot\mathbf{r}}$ and a lattice-periodic function $u_{\mathbf{k}}^{(n)}(\mathbf{r})$. The energy states are organized in energy bands labeled with the index n (figure 6.2).

If the lattice potential is deep, the gap separating the lowest band from higher bands becomes large, such that tunneling to higher bands (Landau-Zener tunneling [132]) can be neglected and a description restricted to the lowest band is sufficient. The dispersion relation $\epsilon(k)$ is proportional to $-\cos(kd)$ (subsection 6.2.1).

The basic concept of Bloch oscillations can be understood within a semiclassical reasoning. Let us consider a wave packet with a narrow momentum distribution in a lattice. If the wave packet is accelerated by a uniform force $-F$ (like gravity or an electric field for charged particles), then its momentum $\hbar k = -Ft$ will increase linearly. In a lattice, however, momentum and velocity do not coincide. Indeed, the velocity is given by the *group velocity*, i.e. the first derivative of the dispersion relation $v_g = \partial_k \epsilon(k) \propto -\sin(kd) = \sin(Ft)$. Instead of accelerating uniformly, the

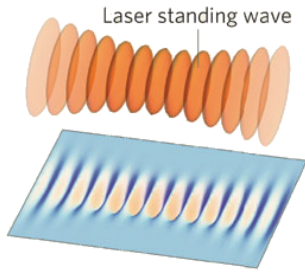


Figure 6.3: Sketch of the intensity of two counter-propagating laser beams, which creates the lattice potential for the ultracold atoms. Taken from [37].

wave packet oscillates in space. This phenomenon is known as *Bloch oscillation* and was predicted quite some time ago by Bloch and Zener [131, 133].

Notably, the edge of the Brillouin zone π/d coincides with the momentum, where the de Broglie wave length equals the lattice period. Simply speaking, Bragg reflection of the particle leads to the oscillating motion. In subsection 6.2.2, we will consider Bloch oscillations in a more rigorous way than in this introductory paragraph.

6.1.2. Experimental realization

Bloch oscillations rely on the coherent reflection of waves and are very sensitive to any kind of dephasing, as interaction effects or impurities in the lattice. In solid-state systems, the lattice spacing d is given by atomic distances, which is so short that the electrons suffer from scattering events long before they reach the edge of the Brillouin zone π/d . For the experimental observation of Bloch oscillations, it was necessary to increase artificially the lattice spacing, which was achieved in semiconductor superlattices [134, 135].

Later, Bloch oscillations were observed in cold atomic gases in optical lattice potentials [7, 8]. In cold-atom experiments, the atoms are trapped in the optical dipole potential (subsection 3.1.3, or [39]) of a laser standing wave, figure 6.3. The strength of the lattice can be adjusted via the laser intensity and detuning, and the lattice spacing can be selected via the laser wave length and the relative angle of the beams [136].

There is also an optical analog of Bloch oscillations. In the experiments [137, 138], an array of weakly coupled wave guides was prepared with an index of refraction that increased linearly across the array. Then, a light beam propagating along the wave-guide array oscillates along the transverse direction. The longitudinal direction of the array takes the role of the time axis ct .

6.1.3. Time dependent interaction $g(t)$

Via Feshbach resonances [43–46], ultracold-atom experiments open new possibilities. The s-wave scattering length can be tuned in a wide range, including negative values. In particular, a complete suppression of the interaction is possible. At zero scattering length, very long-living Bloch oscillations can be observed [40]. However, there are always residual experimental uncertainties, e.g. an interaction parameter $g(t)$ that fluctuates around zero. Thus, the question about the effect of such perturbations arises naturally.

We will consider perturbations that are commensurate with the Bloch frequency. It will turn out that their effect on the dynamics of the Bloch oscillation depends sensitively on their phase relative to the Bloch oscillation. Deliberately modulating the interaction can make the Bloch oscillation more robust against certain perturbations.

6.2. Model

Let us consider particles subjected to a lattice potential. For the description of Bloch oscillations, the starting point is the Gross-Pitaevskii equation

$$i\hbar\frac{\partial}{\partial t}\Psi = \left[-\frac{\hbar^2}{2m}\nabla^2 + V(\mathbf{r})\right]\Psi(\mathbf{r}) + g|\Psi(\mathbf{r})|^2\Psi(\mathbf{r}), \quad (6.1)$$

[subsection 2.2.2, equation (2.16)]. Here, we do not include the chemical potential because we work at fixed particle number. The setting differs from the Bogoliubov problem of the extended condensate ground state with the disorder imprint in part I. Here, the condensate is created in a harmonic trap and then transferred into an optical lattice, and the trap is switched off (figure 6.1). Obviously, this is not the ground-state configuration, and the condensate will have the tendency to spread, both due to repulsive interaction and due to the usual linear dispersion of matter waves.

The phenomenon of Bloch oscillation takes place in one direction. Thus, we consider a setup in which the transverse degrees of freedom are frozen. The transverse harmonic-oscillator ground state is integrated out, leading to a renormalized interaction parameter in the remaining dimension

$$g_{1D} = \frac{m\omega_{\perp}}{2\pi\hbar}g_{3D}. \quad (6.2)$$

Here, ω_{\perp} is the transverse oscillator frequency (or the geometric mean in anisotropic configurations). The usual three-dimensional interaction pa-

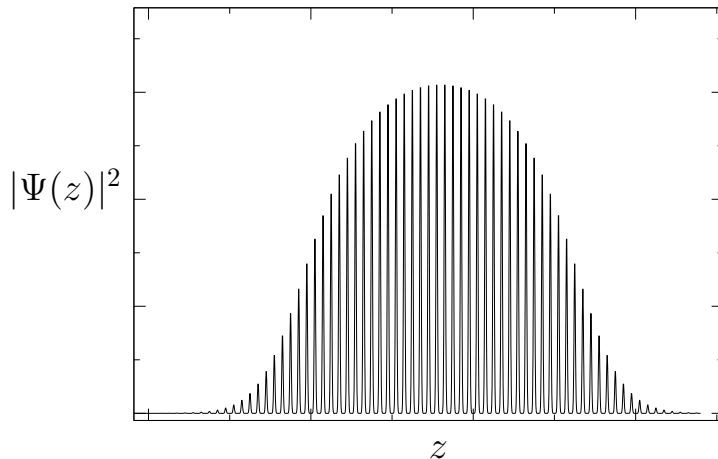


Figure 6.4: Typical initial state for Bloch oscillations. This density profile was obtained as the ground state of the continuous Gross-Pitaevskii equation (6.1) with $V_{1D} = V_0 \cos^2(\pi z/d) + \frac{1}{2}m\omega_z^2 z^2$. The trap ω_z is then switched off. This state is well described with a tight-binding ansatz.

parameter $g_{3D} = 4\pi\hbar^2 a_s/m$ is proportional to the s-wave scattering length a_s . In the one-dimensional Gross-Pitaevskii equation

$$i\hbar \frac{\partial}{\partial t} \Psi(z, t) = \left[-\frac{\hbar^2}{2m} \nabla^2 + V_{1D}(z) \right] \Psi(z, t) + g_{1D} |\Psi(z, t)|^2 \Psi(z, t), \quad (6.3)$$

the potential $V_{1D}(z)$ is given as a deep lattice potential $V_0 \cos^2(\pi x/d)$ with spacing d . Later-on, the lattice is accelerated in order to observe Bloch oscillations. This is done by tilting the lattice out of the horizontal plane, or by accelerating the lattice by optical means.

6.2.1. Tight binding approximation

In sufficiently deep lattice potentials, only the local harmonic-oscillator ground state in each lattice site is populated. This regime is called the tight-binding regime (figure 6.4). The condensate is represented by a single complex number $\Psi_n(t)$ at each lattice site [139]. Neighboring sites are weakly coupled by tunneling under the separating barrier with tunneling amplitude

$$J \approx \frac{4}{\sqrt{\pi}} (V_0/E_r)^{\frac{3}{4}} \exp(-2\sqrt{V_0/E_r}) E_r, \quad (6.4)$$

where $E = \hbar^2\pi^2/(2md^2)$ is the recoil energy [136]. Here, changes of the local oscillator function due to the interaction have been neglected. This assumption holds in deep lattices with $\hbar\omega_{\parallel} \gg g_{TB}|\Psi_n|^2$ (see below). Otherwise, the tunneling amplitude (6.4) gets modified already for slight deformations of the Wannier functions [140].

The tight-binding equation of motion thus reads

$$i\hbar\dot{\Psi}_n = -J(\Psi_{n+1} + \Psi_{n-1}) + Fdn\Psi_n + g_{\text{TB}}(t)|\Psi_n|^2\Psi_n. \quad (6.5)$$

Here, we have added a constant force F . The tight-binding interaction parameter g_{TB} is obtained from the one-dimensional interaction parameter $g_{1\text{D}}$ by integrating out also the harmonic-oscillator ground state in the longitudinal direction, $g_{\text{TB}} = N\sqrt{m\omega_{\parallel}}/2\pi\hbar g_{1\text{D}}$. The factor N comes from the convention that the discrete wave function Ψ_n is normalized to one instead of the particle number N .

Using an appropriate Feshbach resonance, the interaction parameter $g_{\text{TB}}(t)$ can be controlled by external magnetic fields. The validity of (6.5) is limited by the transverse trapping potential $|g_{\text{TB}}| \ll \hbar\omega_{\parallel}/n_0$, with $n_0 = \max_n |\Psi_n|^2$.

The dispersion relation of this single-band model reads $\epsilon(k) = -2J \cos(kd)$. Its curvature or inverse mass $m^{-1} = 2Jb^2 \cos(kd)/\hbar^2$ determines the dynamics of smooth wave-packets. The equation of motion (6.5) can be derived as $i\dot{\Psi}_n = \partial H/\partial \Psi_n^*$ from the nonlinear tight-binding Hamiltonian

$$H = \sum_n \left\{ -J(\Psi_{n+1}\Psi_n^* + \Psi_{n+1}^*\Psi_n) + Fnd|\Psi_n|^2 + \frac{g_{\text{TB}}(t)}{2}|\Psi_n|^4 \right\}. \quad (6.6)$$

6.2.2. Smooth-envelope approximation

Experimentally, the initial state is prepared by loading a Bose-Einstein condensate from an optical dipole trap into an optical lattice created by two counter-propagating laser beams [40]. If this is done adiabatically, the lowest oscillator states of the lattice are populated according to the profile of the condensate in the trap (figure 6.4).

In the following, we use J and d as units of energy and length, respectively. Furthermore, we set $\hbar = 1$ and omit the subscript TB of the interaction parameter. We tackle Eq. (6.5) by separating the rapidly varying Bloch phase $e^{ip(t)n}$ from a smooth envelope $A(z, t)$ comoving with the center of mass $x(t)$:

$$\Psi_n(t) = e^{ip(t)n} A(n - x(t), t) e^{i\phi(t)}. \quad (6.7)$$

With $p(t) = -Ft$, $x(t) = x_0 + 2 \cos(Ft)/F$, and $\phi = \phi_0 + 2 \sin(Ft)/F$, the envelope is found to obey the nonlinear Schrödinger equation

$$i\partial_t A = -\frac{1}{2m(t)} \partial_z^2 A + g(t)|A|^2 A, \quad (6.8)$$

with $1/m(t) = 2 \cos p(t)$. Higher spatial derivatives of A have been neglected. Note that we choose an immobile wave packet with $p(0) = 0$ as initial condition, which fixes the phase for the subsequent Bloch oscillations.

Let us consider solutions of (6.8) in two simple limits (a) and (b).

(a) Linear Bloch oscillation

In absence of the nonlinear term, a Schrödinger equation with a time-dependent mass is to be solved. This can be done easily in Fourier space with $A_k(t) \propto e^{-ik^2 \sin(Ft)/F}$. For an initial state of Gaussian shape with width σ_0 , this results in a breathing wave packet

$$A(z, t) = (2\pi)^{-\frac{1}{4}} \frac{\sqrt{\sigma_0}}{\sigma(t)} \exp\left(-\frac{z^2}{4\sigma^2(t)}\right) \quad \sigma^2(t) = \sigma_0^2 \left[1 + i \frac{\sin(Ft)}{F\sigma_0^2}\right]. \quad (6.9)$$

The time-dependent complex width $\sigma(t)$ implies a breathing of the width of the wave packet, as well as a gradient in the phase.

In the first quarter of the Bloch cycle, the mass is positive and the wave packet spreads, as expected for a free-particle dispersion. When the mass changes sign, the time evolution is reversed, and the wave packet recovers its original shape at the edge of the Brillouin zone. Thus, the wave packet shows perfectly periodic breathing on top of the Bloch oscillation. This behavior is independent of the particular initial shape of the wave packet.

(b) Rigid soliton

Let us consider the mass m and the interaction parameter g as constant for the moment. If both have opposite signs, then equation (6.8) admits a *soliton* solution

$$A(z, t) = \frac{1}{\sqrt{2\xi}} \frac{1}{\cosh(z/\xi)} e^{-i\omega t}, \quad (6.10)$$

with the quasistatic width $\xi = -2/(gm) > 0$. If the force F changes the effective mass as function of time, the interaction parameter can be tuned in such a way that the quasistatic width still exists or even is constant. A perfectly rigid soliton of width ξ_0 can be obtained by modulating the interaction like

$$g_r(t) = -2/[\xi_0 m(t)] = -|g_r| \cos(Ft) \quad \text{with} \quad g_r = -4/\xi_0 < 0. \quad (6.11)$$

More extensive studies based on this idea have been put forward in [141, 142]. If the quasistatic width $\xi(t) = -2/[g(t)m(t)]$ exists for all times but is not constant, then the soliton must be able to follow this width adiabatically in order not to decay. Otherwise its breathing mode will be driven, and other excitations may be created.

6.3. Periodic solutions

We can construct a class of functions $g(t)$ that allow a strictly periodic time evolution of the wave packet. Quite generally, a rigid wave packet is by no means necessary for persistent Bloch oscillations. Already in the linear case $g(t) = 0$ we have seen that the wave packet breathes. Also in the interacting case, one can find non-trivial functions $g(t)$ that are compatible with the time-reversal idea of the linear Bloch oscillation. Consider the class of periodic functions

$$g(t) = \cos(Ft)P(\sin(Ft)/F), \quad (6.12)$$

in which a factor $\cos(Ft)$ can be separated from a polynomial $P(\eta)$ in the bounded time variable

$$\eta(t) = \frac{1}{2} \int_0^t m(s)^{-1} ds = \frac{\sin(Ft)}{F}. \quad (6.13)$$

Because $\partial_t \eta(t) = 2m(t)^{-1}$, the explicit time dependence of the mass factorizes from all terms in the equation of motion (6.8) for $A(z, t) = \tilde{A}(z, \eta(t))$:

$$i\partial_\eta \tilde{A}(z, \eta) = -\partial_z^2 \tilde{A}(z, \eta) + P(\eta)|\tilde{A}|^2 \tilde{A}(z, \eta). \quad (6.14)$$

The ensuing dynamics for $\tilde{A}(z, \eta)$ as function of η may be quite complicated. However, as $\eta(t)$ itself is a *periodic function of time*, also the solution $A(z, t)$ must be periodic: any dynamics taking place in the first quarter of the Bloch period, while η runs from 0 to $1/F$, is exactly reversed in the next quarter, when η runs back. Figure 6.5 illustrates this argument by showing the time-dependence of several key quantities over one Bloch cycle, as well as a k -space density plot with clearly visible breathing dynamics.

The class of functions (6.12) covers all stable modulations that are Bloch periodic. The above argument can be generalized for periodic functions with frequencies commensurate with the Bloch frequency. Let us consider a modulation with the ν_2 -fold Bloch period. The fundamental frequency is then F/ν_2 , which suggests defining the time variable $\tau = Ft/\nu_2 + \tau_0$, such that $\cos(Ft) = \sin(\nu_2\tau)$. Trigonometric identities permit this to be expanded as $\cos(Ft) = \sin(\tau)M(\cos \tau)$, with some polynomial M . Now, if $g(t)$ is of the form $\sin(\tau)P(\cos(\tau))$, with some other polynomial P , we can define the bounded time $\eta' = -\nu_2 \cos(\tau)/F$ with $\partial_t = \sin(\tau)\partial_{\eta'}$. Then, the factor $\sin(\tau)$ factorizes from all terms of (6.8) and we find an equation similar to (6.14)

$$i\partial_{\eta'} \tilde{A}(z, \eta') = -M(\eta')\partial_z^2 \tilde{A}(z, \eta') + P(\eta')|\tilde{A}|^2 \tilde{A}(z, \eta'). \quad (6.15)$$

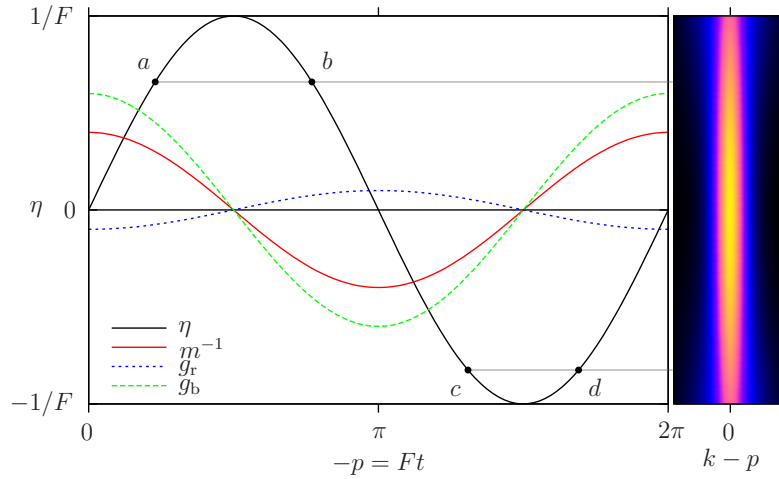


Figure 6.5.: Left panel: Time evolution scheme of stable Bloch oscillations. The inverse mass m^{-1} , the interaction parameter of the rigid soliton (6.11) as well as that of a breathing soliton $g_b(t) = g_0 \cos(Ft)$ are shown together with the bounded time $\eta = \sin(Ft)/F$ as function of time or momentum $-p = Ft$. Right panel: The k -space density [obtained by numerical integration of Eq. (6.5)] of a breathing wave packet is a function of η and thus strictly periodic in t : the points in time a and b as well as c and d show the same distribution, respectively.

Again, the time reversal argument applies. Equation (6.15) is solved as function of the bounded time η' , which implies that the wave packet is conserved under modulations given as

$$g(t) = \sin(\tau)P(\cos(\tau)) = \sum_n g_n \sin(n\tau) = \sum_n g_n \sin\left(\frac{n}{\nu_2} \left[Ft - \frac{\pi}{2}(2j+1) \right]\right). \quad (6.16)$$

With a different but equivalent derivation, we have published this result in [129].

6.4. Numerical examples

So far, we have made the following predictions on the basis of the continuous nonlinear Schrödinger equation (6.8) with time-dependent mass and interaction:

- The rigid soliton: With an initial state of soliton shape (6.10) and an interaction parameter modulated as $g(t) = -|g_r| \cos(Ft)$, the wave packet should completely conserve its shape.
- Modulations $g(t)$ that fulfill the simple time-reversal condition (6.12) or the generalized one (6.16) are predicted to lead to periodic solutions,

independently of the particular initial state. The internal dynamics of these solutions has not been characterized yet.

- For the largest part of the parameter space [$g(t)$ not fulfilling (6.16), for example $g(t) \propto \sin(Ft)$, $g(t) = g_0$], no periodicity is predicted. The wave packet is expected to decay, but we do not know how and how fast.

Let us start the investigations of the open question by directly integrating the discrete Gross-Pitaevskii equation (6.5), using the forth-order Runge-Kutta method [104]. As initial state, we choose the Gaussian wave packet, the ground state of the harmonic trap. For experimental applications, this appears more generic than the specific soliton shape. We then compute the time evolution with different functions $g(t)$. The resulting real-space plots are shown in figure 6.6. The linear Bloch oscillation shown in figure 6.6(a) is indeed long living. At constant interaction $g(t) = g_0$ (figure 6.6(b)) the wave packet decays.

Whenever the time-reversal condition (6.16) is fulfilled, the wave packet is long-living, (c) and (d). When equation (6.16) is not fulfilled [figure 6.6 (e) and (f)], we recognize two decay mechanisms:

- a smooth contraction (or spreading) of the wave packet, figure 6.6(e)
- the growth of perturbations on a short scale, figure 6.6(e) and figure 6.6(f)

We investigate these decay mechanisms and the internal dynamics in more detail by means of a collective-coordinates ansatz and a linear stability analysis in the following sections.

6.5. Collective coordinates

We employ a collective-coordinates ansatz [139] in order to describe the most important degrees of freedom of a Bloch oscillating wave packet. In this approach, we assume that the wave packet is essentially conserved and describe the dynamics of its center of mass (first moment) and its width (second moment).

Similarly to the smooth-envelope ansatz (6.7), the discrete wave function is cast into the form

$$\Psi_n(t) = e^{ip(t)n} \mathcal{A}(n - x(t), w(t), b(t)) e^{i\phi(t)}, \quad (6.17)$$

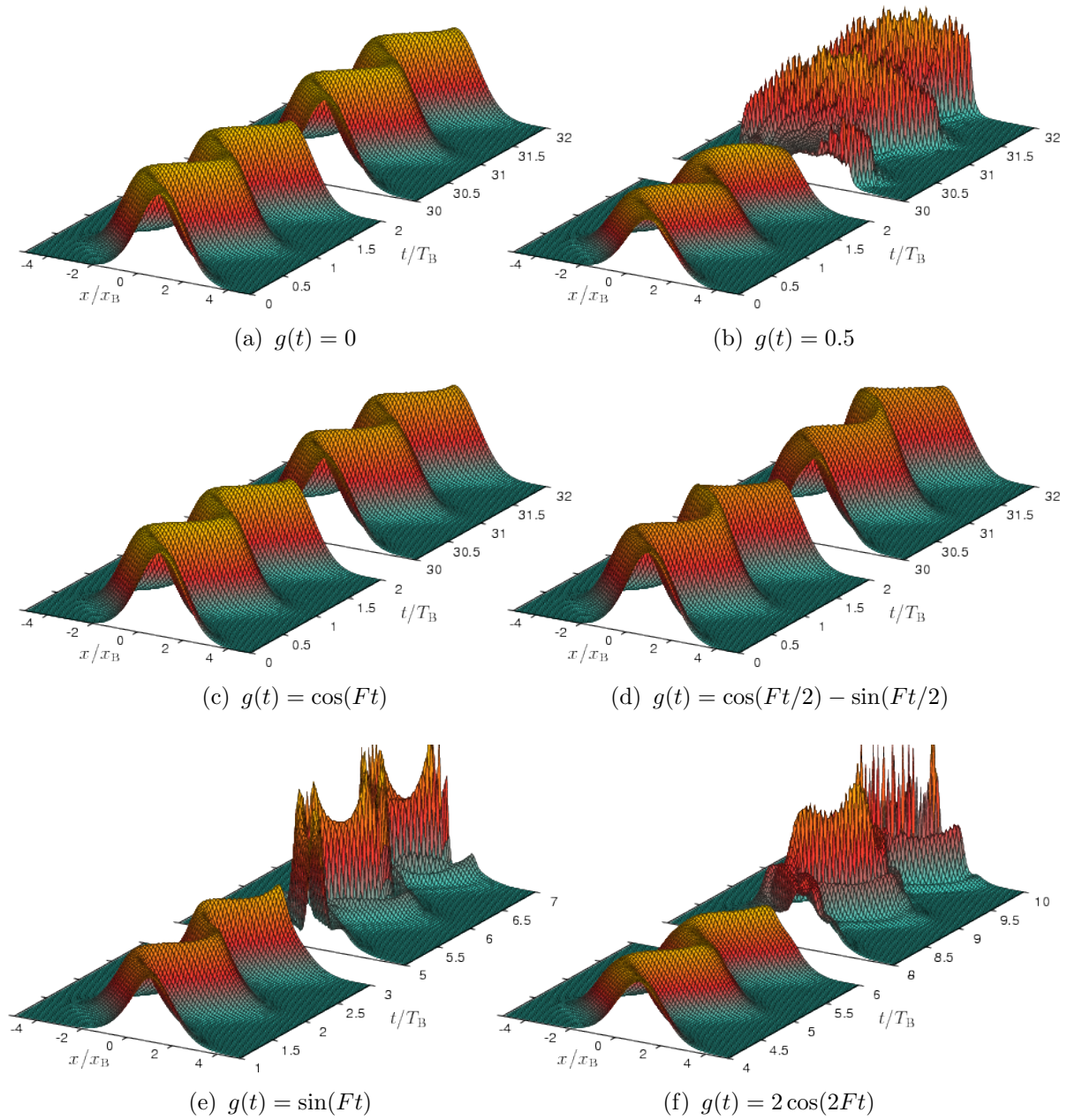


Figure 6.6.: Real-space portraits of Bloch oscillations for several modulations $g(t)$. In the linear case (a), the Bloch oscillation is very long-living. In presence of a constant interaction (b), the wave packet decays after a few Bloch cycles T_B . In (c) and (d), the interaction parameter is modulated according to (6.16) and the oscillations are indeed long-living. Only very slight deformations occur in (d). In (e) and (f), the modulation of the interaction parameter does not comply with (6.16). At $g(t) \propto \sin(Ft)$ (e), the wave packet is first contracted ($t \approx 3T_B$), then perturbations on a short scale grow. When modulating at double Bloch frequency (f), only short-scale perturbations are visible, but no contraction. Further parameters: $F = 0.2$, $\sigma_0 = 10$, Bloch amplitude $x_B = 2/F = 10$ sites.

6. Bloch Oscillations and Time-Dependent Interactions

Table 6.1.: Collective-coordinates parameters for Gaussian and soliton-shaped wave packets

shape	$\tilde{\mathcal{A}}(u)$	K	I
Gaussian	$(2\pi)^{-\frac{1}{4}} e^{-\frac{u^2}{4}}$	$\frac{1}{4}$	$\frac{1}{4\sqrt{\pi}}$
soliton	$\sqrt{\frac{\pi}{4\sqrt{3}}} \left[\cosh\left(\frac{\pi u}{2\sqrt{3}}\right) \right]^{-1}$	$\frac{1}{4} \left(\frac{\pi}{3}\right)^2$	$\frac{1}{4\sqrt{\pi}} \left(\frac{\pi}{3}\right)^{\frac{3}{2}}$

with the free variables center-of-mass position $x(t) = \langle n \rangle = \sum_n n |\Psi_n(t)|^2$ and variance $w(t) = \langle (n - x(t))^2 \rangle$ and their conjugate momenta $p(t)$ and $b(t)$, respectively. The momentum p is included in equation (6.17), according to its generating role $-i\partial_p \Psi_n = n \Psi_n$. Similarly, b is included in the wave function as

$$\mathcal{A}(z, w, b) = w^{-\frac{1}{4}} e^{ibz^2} \tilde{\mathcal{A}}(z/\sqrt{w}). \quad (6.18)$$

The even, real function $\tilde{\mathcal{A}}(u)$ is normalized to one with standard deviation one, $\int du |\tilde{\mathcal{A}}(u)|^2 = 1 = \int du u^2 |\tilde{\mathcal{A}}(u)|^2$.

The collective-coordinates ansatz (6.17) is inserted into the Hamiltonian (6.6). Taylor-expanding the discrete gradient to second order, the effective Hamiltonian is found as

$$H_{cc} = Fx - 2 \cos p \left[1 - \frac{K + 4b^2 w^2}{2w} \right] + I \frac{g(t)}{\sqrt{w}}, \quad (6.19)$$

with the kinetic integral $K = \int du |\tilde{\mathcal{A}}'(u)|^2$ and the interaction integral $I = \frac{1}{2} \int du |\tilde{\mathcal{A}}(u)|^4$. In table 6.1, these parameters are given for a Gaussian and for a soliton-shaped wave packet.

By construction, the collective coordinates obey the canonical equations of motion

$$\dot{p} = -\frac{\partial H_{cc}}{\partial x} = -F, \quad (6.20a)$$

$$\dot{x} = \frac{\partial H_{cc}}{\partial p} = 2 \sin p \left[1 - \frac{K + 4b^2 w^2}{2w} \right] = \sin p [2 - (\Delta k)^2], \quad (6.20b)$$

$$\dot{b} = -\frac{\partial H_{cc}}{\partial w} = \frac{K - 4w^2 b^2}{w^2} \cos p + \frac{1}{2} I g(t) w^{-\frac{3}{2}}, \quad (6.20c)$$

$$\dot{w} = \frac{\partial H_{cc}}{\partial b} = 8wb \cos p. \quad (6.20d)$$

Within the scope of collective coordinates, the momentum variance of the wave packet is given as $(\Delta k)^2 = K/w + 4b^2 w$. It appears in the Hamiltonian

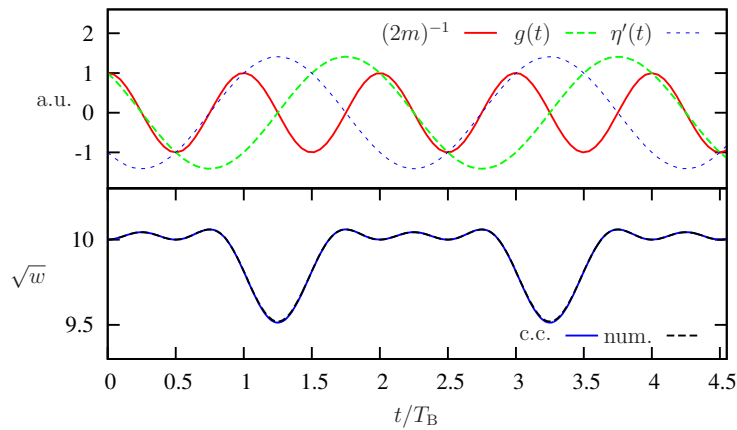


Figure 6.7.: Key quantities of the Bloch oscillation with double Bloch period $g(t) = \cos(Ft/2) - \sin(Ft/2)$ (figure 6.6(d)). Upper panel: The time dependence of mass m and interaction g allows the definition of a bounded time $\eta'(t)$, cf. (6.15). Lower panel: The width \sqrt{w} of the wave packet obtained from collective-coordinates (6.20) and from the full integration of (6.5), respectively.

(6.19) as part of the kinetic energy. The momentum variance is a good indicator for the decay of the wave packet. It is experimentally accessible in time-of-flight images.

6.5.1. Breathing dynamics in the stable cases

As a first application, we use the collective-coordinates equations of motion (6.20) to describe the breathing dynamics in the stable cases of (6.16). We choose the modulation with half Bloch frequency (figure 6.6(d)). In figure 6.7, the collective-coordinates prediction for the width \sqrt{w} is compared to the width extracted from the full integration of (6.5). The width shows a breathing with the double Bloch period, which is a combination of the free breathing of the linear Bloch oscillation [equation (6.9)] and the driven breathing due to the modulation of $g(t)$. The phase of the modulation $g(t)$ with respect to the Bloch oscillation complies with (6.16), which allows the definition of the bounded time η' , shown in the upper panel of (6.7). Similarly to figure 6.5, the width \sqrt{w} can be understood as function of η' .

6.5.2. Unstable cases—decay mechanisms and other dynamics

Now, we apply the collective-coordinates equations of motion (6.20) to the unstable cases shown in figure 6.6(e) and figure 6.6(f). The initial conditions are $w(0) = \sigma_0^2$ and $b(0) = 0$. In the very beginning of the dynamics, we can

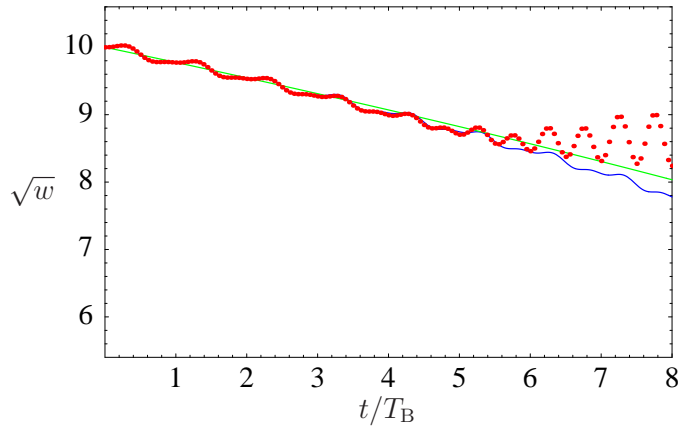


Figure 6.8: The initial contraction of the wave packet shown in (6.6(e)) (red dots) can be described by collective coordinates (blue). The green line shows the approximation (6.22). $F = 0.2$, $g_s = 1$, $\sigma_0 = 10$.

assume $w = \sigma_0^2$ as constant. Using (6.20c), we compute the change of the momentum b due to the interaction $g(t)$

$$\Delta b(t) = b(t) - b(t)|_{g=0} = \frac{I}{2} w_0^{-\frac{3}{2}} \int_0^t dt' g(t'). \quad (6.21)$$

Inserting this into the equation of motion (6.20d) for the width degree of freedom w , we understand that the modulation with double frequency from figure 6.6(f) has no average effect on the width.

Sine modulation

The modulation $g(t) = g_s \sin(Ft)$, considered in figure 6.6(e), however, leads to an average growth

$$w(t) \approx w_0 - 2 \frac{I g_s}{F \sqrt{w_0}} t. \quad (6.22)$$

This prediction is shown in figure 6.8, together with the full solution of (6.20) and the width extracted from the integration of the tight-binding equation of motion. A sine like modulation of the interaction contracts or broadens the wave packet, before destroying it.

Offset and cosine modulation

Let us consider an interaction parameter with a finite time average and a cosine modulation $g(t) = g_0 + g_c \cos(Ft)$. In the case $g_c = 0$, this covers the case of constant interaction shown in figure 6.6(b). The modulation is compatible with the time reversal, but the offset is expected to destroy the wave packet. We are interested in the centroid motion (6.20b). We expect a damping of the oscillation due to the momentum broadening term

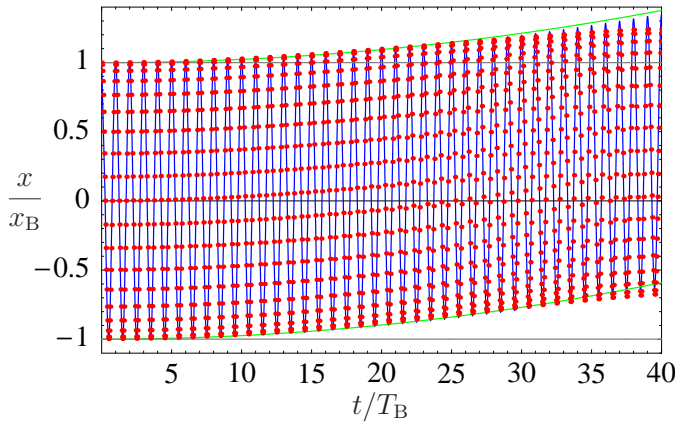


Figure 6.9: The centroid motion of a Gaussian wave packet under the interaction parameter $g(t) = g_0 + g_c \cos(Ft)$ shows a drift. The red dots are numerical results of (6.5), the blue line shows the collective-coordinates prediction (6.20), and the green lines show the estimate for the envelope (6.23). Parameters: $F = 0.2$, $g_0 = 0.1$, $g_c = 5$, $\sigma_0 = 10$.

$(\Delta k)^2 = K/w + 4b^2w$. Furthermore, if the product $\sin(p)(\Delta k)^2$ has a non-zero time average, a drift of the centroid can occur.

The perturbation $g(t)$ enters the k -space width via b^2 . We make a separation of time scales and write $\Delta b^2 = B_0(t) + B_c(t) \cos(Ft) + B_s(t) \sin(Ft) + \dots$. In this ansatz, the $B_x(t)$ vary on a much longer time scale than the Bloch period and their time derivatives are neglected. For equation (6.20b), only $B_0(t) = \frac{I^2 g_0^2}{4w_0^3} t^2$ and $B_s = \frac{I^2 g_0 g_s}{2Fw_0^3} t$ are relevant and lead to

$$x(t) \approx \frac{2}{F} \cos(Ft) \left[1 - \frac{K + I^2 g_0^2 t^2 / w_0}{2w_0} \right] + \frac{1}{2} \frac{I^2 g_0 g_c}{F w_0^2} t^2 \quad (6.23)$$

As expected, the offset causes damping. More remarkably, the modulated interaction induces a drift of the oscillating wave packet. In figure 6.9, the estimate (6.23) is plotted together with the full solution of the collective-coordinates equations of motion (6.20) and with the numerical results obtained from the integration of the tight-binding equation of motion (6.5). As expected, the agreement is initially very good, but deviations occur after about thirty Bloch periods, when the wave packet starts to decay and the collective-coordinates description breaks down.

Conclusion

The collective coordinates are useful for the description of the stable cases, where the wave packet is preserved, and for the description of the wave-packet decay in the very beginning. We have learned that the sine modulation directly contracts or broadens the wave packet and that a cosine modulation together with an offset makes the wave packet drift. Later, the wave packet loses its smooth shape, and the collective-coordinates description is bound to fail. In particular, collective coordinates cannot grasp the short-scale perturbations that occur in figure 6.6(e) and figure 6.6(f).

6.6. Dynamical instabilities

Time-dependent mass and interaction provide a source of energy for the growth of perturbations. In [section 6.4](#), we have seen that in some cases perturbations on a length scale much shorter than the width of the wave packet lead to the decay of the wave packet and k -space broadening. These perturbations cannot be described by the collective coordinates of [section 6.5](#). Instead, the sudden broadening shown in [figures 6.6\(e\)](#) and [6.6\(f\)](#) suggests an exponential growth of small perturbations.

6.6.1. Linear stability analysis of the infinite wave packet

In order to describe the growth of perturbations quantitatively, we perform a linear stability analysis on top of an infinitely extended wave function with density $|\Psi_n|^2 = n_0$

$$\Psi_n = [\sqrt{n_0} + \delta\Phi_n] e^{ip(t)n} e^{-i\varphi(t)}. \quad (6.24)$$

Inserting this into the discrete Gross-Pitaevskii equation ([6.5](#)), we determine the parameters $p(t) = -Ft$ and $\dot{\varphi} = -2 \cos(p) + \mu(t)$, $\mu(t) = g(t)n_0$ from the zeroth order in $\delta\Phi$.

With this, the first-order equation of motion for $\delta\Phi_n$ is derived. Similarly to the procedure in [subsection 6.2.2](#), we use a transformation to the moving reference frame $x(t) = 2 \cos(Ft)/F$ in order to eliminate the first derivative of the Taylor expansion of $\delta\Phi_{n\pm 1}$: $s(z) + id(z) = \delta\Phi_{x(t)+z}$. The Fourier-transformed equations of motion then read

$$\dot{d}_k = - [\epsilon_k^0(t) + 2n_0g(t)] s_k, \quad \dot{s}_k = \epsilon_k^0(t) d_k, \quad (6.25)$$

with $\epsilon_k^0(t) = k^2 \cos(Ft)$. The equations of motion ([6.25](#)) are linear, with real, time-periodic coefficients (provided, the frequency of the external modulation $\mu(t) = n_0g(t)$ is commensurate with the Bloch frequency F), which makes them accessible for Floquet theory [[143](#)]. The integration of two linearly independent initial conditions, e.g. $s_k^{(a)}(0) = 1$, $d_k^{(a)}(0) = 0$ and $s_k^{(b)}(0) = 0$, $d_k^{(b)}(0) = 1$, over one period T yields all information necessary for the time evolution over $n \in \mathbb{N}$ periods:

$$\begin{pmatrix} s_k(t + nT) \\ d_k(t + nT) \end{pmatrix} = M^n \begin{pmatrix} s_k(t) \\ d_k(t) \end{pmatrix}, \quad M = \begin{pmatrix} s_k^{(a)}(T) & s_k^{(b)}(T) \\ d_k^{(a)}(T) & d_k^{(b)}(T) \end{pmatrix}. \quad (6.26)$$

The eigenvalues ρ_k^\pm of the monodromy matrix M determine the growth of the perturbations. Liouville's theorem $\det M = 1$ fixes the product of the

eigenvalues $\rho_k^+ \rho_k^- = 1$, which allows computing the eigenvalues from the trace of the monodromy matrix $\rho_k^\pm = \Delta_k \pm \sqrt{\Delta_k^2 - 1}$:

$$\Delta_k = \frac{1}{2} \text{tr} M = \frac{1}{2} \left\{ s_k^{(a)}(T) + d_k^{(b)}(T) \right\}. \quad (6.27)$$

The logarithm $\lambda_k = \log[\max(\rho_k^+, \rho_k^-)]/T$ is called Lyapunov exponent and characterizes the exponentially growing amplitudes $s_k, d_k \sim e^{\lambda_k t}$.

For a given $g(t)$, each Fourier component (d_k, s_k) is integrated over the common period T of $g(t)$ and $\cos(Ft)$, which yields the Lyapunov exponents λ_k . This method turns out to be very efficient for interactions with zero time average. Unfortunately, it does not work correctly in the case of a finite offset. The constant interaction acts on the width degree of freedom, which is not included in the infinite wave packet.

6.6.2. Bloch periodic perturbations

For perturbations $\mu(t) = \mu_0 \cos Ft + \mu_1 \sin Ft$ modulated with the Bloch frequency, it is possible to solve the equations of motion (6.25) explicitly and to compute the Lyapunov exponent directly. From the criterion (6.16) we know that the cosine part alone leads to a periodic time evolution. Contrarily, the observations in section 6.4, figure 6.6(e) show that the sine part leads to the growth of perturbations. Thus, a perturbation theory in μ_1 will be performed in the following.

Considering for the moment only the part $\mu^{(0)}(t) = \mu_0 \cos(Ft)$, we can write the equations of motion (6.25) in terms of the bounded time $\eta(t) = \sin(Ft)/F$ (6.13)

$$i \frac{\partial d_k^{(0)}}{\partial \eta} = -[k^2 + \mu_0] s_k^{(0)} \quad i \frac{\partial s_k^{(0)}}{\partial \eta} = k^2 d_k^{(0)}. \quad (6.28)$$

The crossed coupling of d_k and s_k is the same as in the homogeneous Bogoliubov problem (subsection 2.3.1). We Bogoliubov transform the full equation of motion (6.25) using $\gamma_k = \sqrt{\epsilon_k/k^2} s_k + i\sqrt{k^2/\epsilon_k} d_k$ and $\epsilon_k = \sqrt{k^2(k^2 + 2\mu_0)}$, cf. equation (2.32)

$$i\gamma_k = \cos(Ft)\epsilon_k\gamma_k + \mu_1 \frac{k^2}{\epsilon_k} \sin(Ft) (\gamma_k + \gamma_{-k}^*). \quad (6.29)$$

As expected, the solution of the unperturbed part $\gamma_k^{(0)} = \gamma_0 e^{-i\epsilon_k \sin(Ft)/F}$ is periodic. In order to solve the first-order correction, we eliminate the

coupling to γ_{-k}^* by transforming to $\gamma_+ = \frac{1}{2}(\gamma_k + \gamma_{-k})$ and $\gamma_- = \frac{1}{2i}(\gamma_k - \gamma_{-k})$, which both obey the equation of motion

$$i\gamma = \cos(Ft)\epsilon_k\gamma + \mu_1 \frac{k^2}{\epsilon_k} \sin(Ft) (\gamma + \gamma^*) . \quad (6.30)$$

The unperturbed solution reads $\gamma^{(0)} = \gamma_0 e^{-i\epsilon_k \sin(Ft)/F}$ and suggests the ansatz $\gamma^{(1)} = \gamma_1(t) e^{-i\epsilon_k \sin(Ft)/F}$ for the first-order correction. The increase of $\gamma_1(t)$ is integrated over one period

$$\gamma_1(T) = \mu_1 \frac{k^2}{i\epsilon_k} \int_0^T dt \sin(Ft) \left(\gamma_0 + \gamma_0^* e^{2i\epsilon_k \sin(Ft)/F} \right) = \mu_1 \frac{k^2}{\epsilon_k} \frac{2\pi}{F} J_1(2\epsilon_k/F) \gamma_0^* , \quad (6.31)$$

with the Bessel function of the first kind J_1 . The growth per period is $\gamma_0 \rightarrow \gamma_0 + \gamma_1(T)$ and defines the Lyapunov exponent $\lambda T = \gamma_1(T)/\gamma_0$. The factor γ_0^*/γ_0 takes its extremal values $+1$ and -1 for $\gamma \in \mathbb{R}$ and $\gamma \in i\mathbb{R}$, respectively. Thus, the Lyapunov exponent is given as

$$\lambda_k = \left| \mu_1 \frac{k^2}{\epsilon_k} J_1\left(\frac{2\epsilon_k}{F}\right) \right| . \quad (6.32)$$

This result has been derived under the assumption $|\mu_1| \ll |k^2 + 2\mu_0|$ and holds for both real and imaginary Bogoliubov frequencies. (Imaginary frequencies appear for $\mu_0 < 0$ at $k^2 + 2\mu_0 < 0$.) Remarkably, it also holds at $k^2 + 2\mu_0 = 0$, where a calculation similar to the above one yields the result $\lambda = 2\pi\mu_1 k^2/F^2$, which is exactly the limiting value of (6.32). Also in the limit $\mu_0 = 0$, $k^2 \rightarrow 0$, the result $\lambda = 0$ found from (6.25) is reproduced correctly by the formula (6.32). In conclusion, the result (6.32) seems to be valid for all $\mu_1 < \max(k^2, k^2 + \mu_0)$, beyond the original validity condition.

6.6.3. Unstable sine

With the Lyapunov exponent (6.32), we understand the growth of the short-scale perturbations in the case of a sine-like perturbation, [figure 6.6\(e\)](#). With $\mu(t) = n_0 g_1 \sin(Ft)$, $n_0 = 1/(\sqrt{2\pi}\sigma_0)$, the Lyapunov exponent (6.32) reads $\lambda_k = |g_1 n_0 J_1(2k^2/F)|$. Its magnitude is proportional to the strength of the perturbation g_1 and its k dependence is solely determined by $J_1(2k^2/F)$, with a maximum $\lambda_{\max} \approx 0.582 g_1 n_0$ at $k_{\max}^2 \approx 0.921 F$. For a quantitative comparison, we choose a rather wide wave packet and a weak perturbation ([figure 6.10](#)). We find the predicted growth rate λ_{\max} of the most unstable mode in excellent agreement with the results from the numerical integration of the tight-binding equation of motion (6.5).

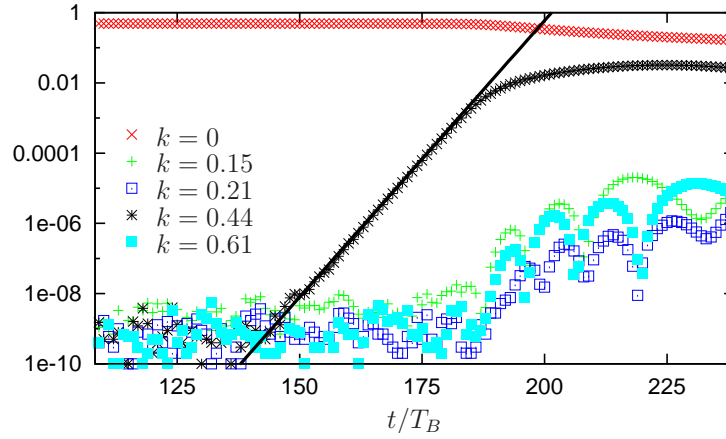


Figure 6.10.: Growth of the most unstable mode. Momentum density $|\Psi_k|^2$ for selected k -modes in the unstable case $g(t) = g_1 \sin(Ft)$. The original wave function is centered around $k = 0$. The solid line marks the growth rate λ_{\max} of the most unstable mode as predicted by equation (6.32). The growth of this mode precedes the damping of the centroid motion that sets in at $t \approx 200T_B$. Numerical parameters: $\sigma_0 = 100$, $g_1 n_0 = 0.01$, $F = 0.2$.

6.6.4. Robustness with respect to small perturbations

An important application for the linear stability analysis is the question “How sensitive are the long-living Bloch oscillations of (6.16) to small perturbations?”

Robustness of rigid and breathing wave packets

As shown in figure 6.6(c), the breathing wave packet with $g(t) = g_0 \cos(Ft)$ is long living, in accordance with the time-reversal condition (6.12). But its interaction parameter $g(t)$ always has the same sign as the mass m , thus, the stability criterion for solitons (6.11) is never fulfilled. The wave packet would decay if one stopped the Bloch oscillation by switching off the force F . It survives only because of the time-reversal argument of section 6.3.

How robust with respect to external perturbations can such a wave packet be? Should not a soliton that is stable at all times be more robust? Even cold-atom experiments suffer from slight imperfections, such as residual uncertainties in the magnetic field controlling the interaction term $g(t)$. For instance, in the Innsbruck experiment [40], the magnetic field is controlled up to 1 mG. The slope of $61a_0/\text{G}$ at the zero of the Feshbach resonance turns this into an uncertainty $\Delta a = 0.06a_0$ in the scattering length, $a_0 \approx 5.3 \cdot 10^{-11} \text{m}$ being the Bohr radius. This is converted to the uncertainty of the dimensionless tight-binding interaction $\Delta g \approx 0.4$. Note that this uncertainty Δg is larger than the interaction $g_r = -4/\xi_0$ needed to create a rigid soliton of only moderate width $\xi_0 \gtrsim 10$. From this point of

6. Bloch Oscillations and Time-Dependent Interactions

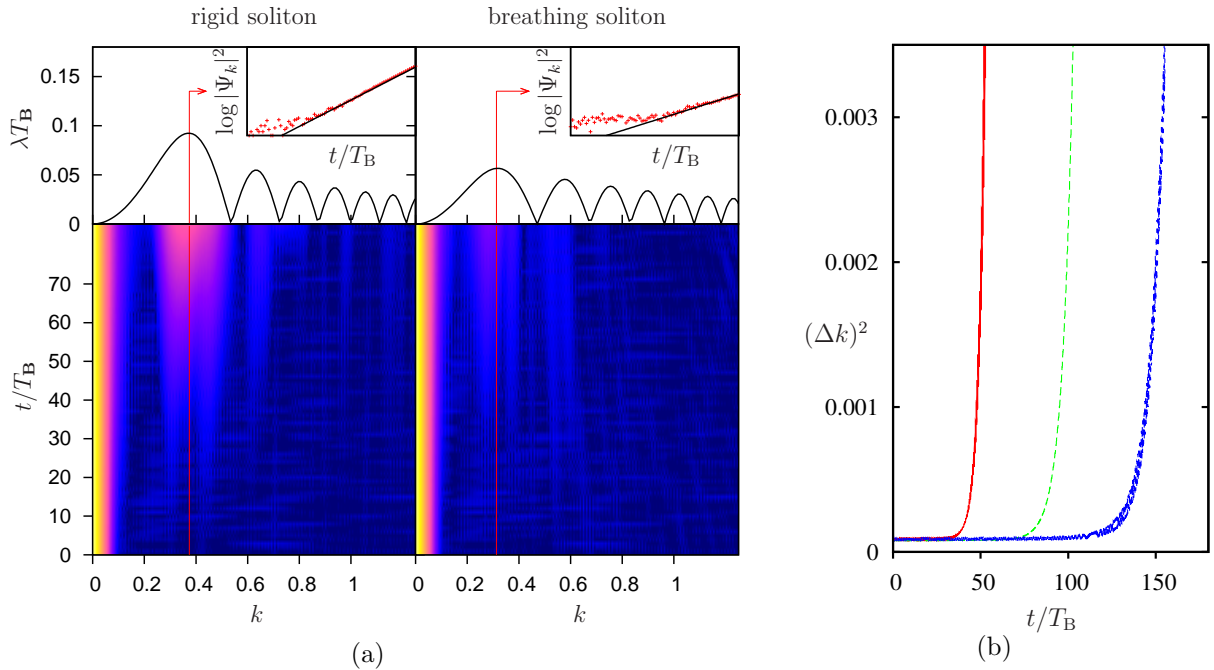


Figure 6.11.: (a) Decay of a rigid ($g_0 = g_r = -0.06$, left) and a breathing ($g_0 = 10$, right) soliton under the harmonic perturbation $g_1 \sin(Ft)$. Upper panel: growth rate (6.32) obtained by Floquet analysis of the linear-stability. Lower panel: Stroboscopic plot of the k -space density on a logarithmic color scale. The central peak of the initial wave packet is well separated from the excited fluctuations. Inset: Location and growth of the most unstable mode agree with the Floquet prediction. (b) The corresponding momentum variance of the breathing wave packet ($g_0 = 10$, blue), the rigid soliton ($g_0 = -0.06$, green dashed), and the antibreathing wave packet ($g = -10$, red). Parameters: $\sigma_0 = 60$, $F = 0.15$, $g_1 = 0.5$.

view, realizing a wide rigid soliton is practically equivalent to switching the interaction off altogether.

We choose to study in detail the effect of Bloch-periodic perturbations of $g(t)$, which are expected to have the largest impact. We take $g(t) = g_0 \cos(Ft) + g_1 \sin(Ft)$ with $g_0 = -|g_r|$ and $+10$ for the rigid soliton and the breathing wave packet, respectively. The off-phase perturbation $g_1 \sin(Ft)$ with an amplitude g_1 of order Δg makes the wave packet unstable. In both cases, we integrate equation (6.5) numerically. Rather than the strong force $F \approx 34$ in a vertical lattice [40], we choose a smaller force $F = 0.15$, corresponding to a slighter tilt. The Bloch period becomes much longer, making the wave packet more sensitive to dephasing.

For both cases of primary interest—the rigid and the breathing soliton—the upper panel of figure 6.11(a) shows the Lyapunov exponent (6.32), indistinguishable from the value obtained by numerical solution of equation (6.25), as function of k . Mainly the prefactor $k^2/|\epsilon_k| = |1 + 2g_0 n_0/k^2|^{-1}$ makes the Lyapunov exponents of the breathing wave packet ($g_0 = 10$)

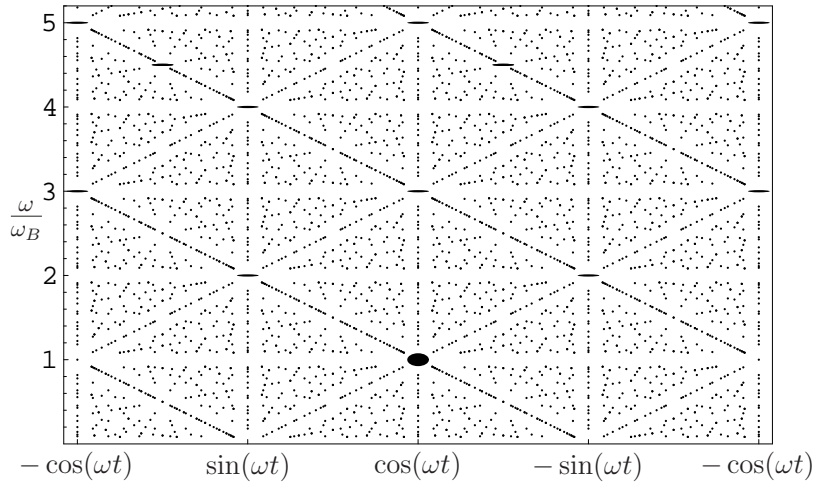


Figure 6.12.: Stability map showing the positions of the stable cases in the ω - δ -plane, according to (6.16). The size of the ellipses represents the robustness of the periodic cases against detuning in δ , and ω , respectively. At a given detuning of 10^{-4} the lifetime of the Bloch excitation is determined by $\min_k 1/\lambda_k$, which is mapped to the radii. The largest radii correspond to a lifetime of $5T_B$ or more, the smallest to $1T_B$ or less. On the ω -axis, all rational numbers ν_1/ν_2 with $\nu_2 < 12$ have been taken into account. Parameters: $F = 0.2$, $gn_0 = 1$.

smaller than those of the rigid soliton ($g_0 = g_r = -0.06$). The Lyapunov exponents provide a rather faithful portrait of the k -space evolution obtained by the numerics, plotted in the lower panels of figure 6.11(a) stroboscopically, i.e., at integer multiples of T_B . Notably, excitations grow exclusively in the intervals with the largest Lyapunov exponents. The predicted growth rate of the most unstable mode (indicated by the vertical line) agrees very well with the numerical data (inset in the upper panels of figure 6.11(a)). The growth of the Fourier components is directly reflected in the k -space broadening of the wave packet (figure 6.11(b)). The k -space broadening is an experimentally accessible quantity that signals the decay of the wave packet and the destruction of Bloch oscillations in real space. The rigid soliton shows greater resilience than the strongly antibreathing wave packet, but the breathing wave packet survives even longer.

Robustness map

Similarly to the above study, we also investigate the robustness of other stable modulations $g(t)$ from (6.16), namely monochromatic modulations $g(t) = g \cos(\omega t + \delta)$. In the ω - δ plane, there are only stable points, rather than regions of stability. How sensitive is the Bloch oscillation to slight experimental imperfections in frequency and phase?

We investigate the robustness of the stable points by varying both δ and ω slightly (by 10^{-4}) and determining the maximum Lyapunov exponent $\lambda = \max_k \lambda_k$ from a numerical integration of (6.25). The inverse Lyapunov exponent is a measure for the robustness and is mapped to the radius in the graphical representation in the parameter space [figure 6.12](#). In the dissymmetry of the points $+\cos(Ft)$ and $-\cos(Ft)$, we recover the result from above. The stable points are arranged on a regular pattern, with the most stable points arranged on lines. With increasing denominator ν_2 the robustness drops very rapidly.

6.7. Conclusions (Part II)

We have treated the problem of Bloch oscillations with a time-dependent interaction in the framework of the one-dimensional tight-binding model, i.e. for a deep lattice potential with a strong transverse confinement. For smooth wave packets, the bounded-time argument allows identifying a class of interactions $g(t)$ that lead to periodic dynamics.

Beyond the mere existence of these periodic solutions, we have set up two complementary methods for the quantitative description of stability and decay of the Bloch oscillating wave packet. The collective-coordinates approach is valid as long as the wave packet is essentially conserved. This approach is capable of describing on the one hand the centroid and the breathing dynamics in the periodic cases, and on the other hand the beginning of the decay in the unstable cases, for example at constant interaction.

The other approach, the linear stability analysis of the infinite wave packet, is suitable for the quantitative description of the decay of wide wave packets. More precisely, the relevant excitations have to be well decoupled in k -space from the original wave packet around $k = 0$. Perturbations like the off-phase perturbation in [subsection 6.6.4](#) are well described. Other perturbations, like a constant interaction, are missed, because the width of the wave packet is not properly included in the ansatz of an infinitely wide wave packet. Together, the two approaches provide a rather complete picture of the wave-packet dynamics.

The most remarkable physical results of this part are firstly the existence of long-living Bloch oscillations despite non-zero interaction if the interaction $g(t)$ respects the time-reversal symmetry (6.16). Secondly, a modulation of the interaction that enhances the breathing of the wave packet can make the Bloch oscillation more robust with respect to perturbations.

A. List of Symbols and Abbreviations

Bogoliubov part

- a_k Coefficient for Bogoliubov transformation (2.32), $a_k = \sqrt{\epsilon_k^0/\epsilon_k}$
- $A(k\xi, \theta)$ Elastic scattering envelope function
- $A_d(k)$ Angular integral in the self-energy in [section 4.1](#)
- BEC Bose-Einstein condensate
- β Inverse temperature $(k_B T)^{-1}$
- $\hat{\beta}_\nu$ Bogoliubov quasiparticle operator (in eigenbasis)
- C_d Disorder correlation function
- c Speed of sound
- n_{nc} Condensate depletion
- d Dimension
- ϵ_k Bogoliubov energy (2.35)
- ϵ_k^0 Kinetic energy of a free particle
- F Anomalous Green function
- \hat{F} Grand canonical Hamiltonian
- g Interaction parameter
- G Green function
- $\hat{\gamma}_k$ Bogoliubov mode
- γ_k Scattering rate
- $\gamma(k)$ Complex degree of coherence (only [section 3.1](#))

A. List of Symbols and Abbreviations

- \hat{H} Hamiltonian
- η Diagonal matrix $\text{diag}(1, -1)$, ([section 2.5, subsection 3.3.2](#))
- $\eta(\mathbf{r})$ Random field on rough surface (only [section 3.1](#))
- i Imaginary unit $i^2 = -1$
- \mathbf{k} Wave vector
- L Distance in speckle geometry (only [section 3.1](#))
- Λ Relative correction of the dispersion relation [in units of V^2/μ^2]
- λ Wave length
- μ Chemical potential
- n Condensate density
- P Cauchy principal value
- $\Phi(\mathbf{r})$ Gross-Pitaevskii ground-state
- $\hat{\varphi}$ Phase operator
- $\hat{\Psi}(\mathbf{r})$ Field operator
- R Diffusor radius in speckle geometry (only [section 3.1](#))
- $\rho(\omega)$ Density of states
- S_d Surface of the d -dimensional unit sphere
- $S(k, \omega)$ Spectral function [subsection 3.4.1](#)
- Σ Self-energy
- σ Disorder correlation length
- T Transmission coefficient ([subsection 2.4.5](#))
- TF Thomas-Fermi (page [26](#))
- t Time
- u_k Coefficient for Bogoliubov transformation $u_k = (\epsilon_k + \epsilon_k)/(2\sqrt{\epsilon_k \epsilon_k})$

- $u_\nu(r)$ Bogoliubov eigenstate, normal component
- V External potential
- $\tilde{V}^{(n)}$ n -th order of the smoothed potential (2.24)
- \tilde{V} Scattering amplitude (4.5) in the hydrodynamic regime
- $v_\nu(r)$ Bogoliubov eigenstate, anomalous component
- v_k Coefficient for Bogoliubov transformation $u_k = (\epsilon_k - \epsilon_k)/(2\sqrt{\epsilon_k \epsilon_k})$
- W Normal coupling element
- ξ Healing length
- Y Anomalous coupling element
- Z Partition function

Bloch part

- $\tilde{A}(z, t)$ Envelope function (6.7)
 - b Collective coordinates (section 6.5): conjugate momentum of the width degree of freedom w
 - d Lattice spacing
 - d_k Phase modulation with wavenumber k (section 6.6)
 - F Force
 - η Bounded time variable
 - Δ_k Quantity related to the Lyapunov exponent, equation (6.27)
 - J Tunneling amplitude (6.4)
 - λ Lyapunov exponent
 - M Monodromy matrix
 - p Momentum of the wave packet, equation (6.7)
 - s_k Density modulation with wavenumber k (section 6.6)

A. List of Symbols and Abbreviations

σ_0 Initial width of the wave packet

x Collective coordinates ([section 6.5](#)): centroid coordinate

ξ Soliton width ([6.10](#))

w Collective coordinates ([section 6.5](#)): width degree of freedom

Bibliography

- [1] P. W. Anderson, *Absence of diffusion in certain random lattices*, [Phys. Rev.](#) **109**, 1492 (1958).
- [2] M. P. A. Fisher, P. B. Weichman, G. Grinstein, and D. S. Fisher, *Boson localization and the superfluid-insulator transition*, [Phys. Rev. B](#) **40**, 546 (1989).
- [3] D. Jaksch, C. Bruder, J. I. Cirac, C. W. Gardiner, and P. Zoller, *Cold bosonic atoms in optical lattices*, [Phys. Rev. Lett.](#) **81**, 3108 (1998).
- [4] M. Greiner, O. Mandel, T. Esslinger, T. W. Hänsch, and I. Bloch, *Quantum phase transition from a superfluid to a Mott insulator in a gas of ultracold atoms*, [Nature](#) **415**, 39 (2002).
- [5] Z. Hadzibabic, P. Krüger, M. Cheneau, B. Battelier, and J. Dalibard, *Berezinskii-Kosterlitz-Thouless crossover in a trapped atomic gas*, [Nature](#) **441**, 1118 (2006).
- [6] T. Schumm, S. Hofferberth, L. M. Andersson, S. Wildermuth, S. Groth, I. Bar-Joseph, J. Schmiedmayer, and P. Krüger, *Matter-wave interferometry in a double well on an atom chip*, [Nature Physics](#) **1**, 57 (2005).
- [7] B. P. Anderson and M. A. Kasevich, *Macroscopic quantum interference from atomic tunnel arrays*, [Science](#) **282**, 1686 (1998).
- [8] M. Ben Dahan, E. Peik, J. Reichel, Y. Castin, and C. Salomon, *Bloch oscillations of atoms in an optical potential*, [Phys. Rev. Lett.](#) **76**, 4508 (1996).
- [9] V. E. Zakharov, *Stability of periodic waves of finite amplitude on the surface of a deep fluid*, [Journal of Applied Mechanics and Technical Physics](#) **9**, 190 (1968).
- [10] R. L. Sutherland, *Handbook of nonlinear optics*, Dekker, New York (1996).

- [11] P. A. Lee and T. V. Ramakrishnan, *Disordered electronic systems*, [Rev. Mod. Phys.](#) **57**, 287 (1985).
- [12] T. Giamarchi and H. J. Schulz, *Localization and interaction in one-dimensional quantum fluids*, [Europhys. Lett.](#) **3**, 1287 (1987).
- [13] —, *Anderson localization and interactions in one-dimensional metals*, [Phys. Rev. B](#) **37**, 325 (1988).
- [14] D. K. K. Lee and J. M. F. Gunn, *Bosons in a random potential: condensation and screening in a dense limit*, [Journal of Physics: Condensed Matter](#) **2**, 7753 (1990).
- [15] K. G. Singh and D. S. Rokhsar, *Disordered bosons: Condensate and excitations*, [Phys. Rev. B](#) **49**, 9013 (1994).
- [16] H. Bruus and K. Flensberg, *Many-body quantum theory in condensed matter physics*, Oxford Univ. Press (2004).
- [17] B. Kramer and A. MacKinnon, *Localization: theory and experiment*, [Reports on Progress in Physics](#) **56**, 1469 (1993).
- [18] P. Pradhan and S. Sridhar, *Correlations due to localization in quantum eigenfunctions of disordered microwave cavities*, [Phys. Rev. Lett.](#) **85**, 2360 (2000).
- [19] D. S. Wiersma, P. Bartolini, A. Lagendijk, and R. Righini, *Localization of light in a disordered medium*, [Nature](#) **390**, 671 (1997).
- [20] G. Labeyrie, D. Delande, C. A. Müller, C. Miniatura, and R. Kaiser, *Coherent backscattering of light by cold atoms: Theory meets experiment*, [Europhys. Lett.](#) **61**, 327 (2003).
- [21] H. Hu, A. Strybulevych, J. H. Page, S. E. Skipetrov, and B. A. van Tiggelen, *Localization of ultrasound in a three-dimensional elastic network*, [Nat Phys](#) **4**, 945 (2008).
- [22] R. C. Kuhn, C. Miniatura, D. Delande, O. Sigwarth, and C. A. Müller, *Localization of matter waves in two-dimensional disordered optical potentials*, [Phys. Rev. Lett.](#) **95**, 250403 (2005).
- [23] R. Kuhn, O. Sigwarth, C. Miniatura, D. Delande, and C. Müller, *Coherent matter wave transport in speckle potentials*, [New J. Phys.](#) **9**, 161 (2007).

- [24] R. Kuhn, *Coherent Transport of Matter Waves in Disordered Optical Potentials*, Ph.D. thesis, Universität Bayreuth & Université de Nice Sophia-Antipolis (2007), <http://opus.ub.uni-bayreuth.de/volltexte/2007/287/>.
- [25] J. Billy, V. Josse, Z. Zuo, A. Bernard, B. Hambrecht, P. Lugan, D. Clement, L. Sanchez-Palencia, P. Bouyer, and A. Aspect, *Direct observation of Anderson localization of matter waves in a controlled disorder*, *Nature* **453**, 891 (2008).
- [26] G. Roati, C. D'Errico, L. Fallani, M. Fattori, C. Fort, M. Zaccanti, G. Modugno, M. Modugno, and M. Inguscio, *Anderson localization of a non-interacting Bose-Einstein condensate*, *Nature* **453**, 895 (2008).
- [27] M. C. W. van Rossum and T. M. Nieuwenhuizen, *Multiple scattering of classical waves: microscopy, mesoscopy, and diffusion*, *Rev. Mod. Phys.* **71**, 313 (1999).
- [28] E. Abrahams, P. W. Anderson, D. C. Licciardello, and T. V. Ramakrishnan, *Scaling theory of localization: Absence of quantum diffusion in two dimensions*, *Phys. Rev. Lett.* **42**, 673 (1979).
- [29] S. John, H. Sompolinsky, and M. J. Stephen, *Localization in a disordered elastic medium near two dimensions*, *Phys. Rev. B* **27**, 5592 (1983).
- [30] S. John and M. J. Stephen, *Wave propagation and localization in a long-range correlated random potential*, *Phys. Rev. B* **28**, 6358 (1983).
- [31] C. Gaul and H. Büttner, *Quantum mechanical heat transport in disordered harmonic chains*, *Phys. Rev. E* **76**, 011111 (2007).
- [32] G. K. S. Wong, P. A. Crowell, H. A. Cho, and J. D. Reppy, *Superfluid critical behavior in ^4He filled porous media*, *Phys. Rev. Lett.* **65**, 2410 (1990).
- [33] P. Lugan, D. Clément, P. Bouyer, A. Aspect, and L. Sanchez-Palencia, *Anderson localization of Bogolyubov quasiparticles in interacting Bose-Einstein condensates*, *Phys. Rev. Lett.* **99**, 180402 (2007).
- [34] N. Teichmann, D. Hinrichs, M. Holthaus, and A. Eckardt, *Process-chain approach to the Bose-Hubbard model: Ground-state properties and phase diagram*, *Phys. Rev. B* **79**, 224515 (2009).

- [35] M. Lewenstein, A. Sanpera, V. Ahufinger, B. Damski, A. Sen, and U. Sen, *Ultracold atomic gases in optical lattices: mimicking condensed matter physics and beyond*, *Adv. Phys.* **56**, 243 (2007), [arXiv:cond-mat/0606771](#).
- [36] I. Bloch, J. Dalibard, and W. Zwerger, *Many-body physics with ultracold gases*, *Rev. Mod. Phys.* **80**, 885 (2008).
- [37] M. Greiner and S. Folling, *Condensed-matter physics: Optical lattices*, *Nature* **453**, 736 (2008).
- [38] M. H. Anderson, J. R. Ensher, M. R. Matthews, C. E. Wieman, and E. A. Cornell, *Observation of Bose-Einstein condensation in a dilute atomic vapor*, *Science* **269**, 198 (1995).
- [39] R. Grimm, M. Weidemüller, and Y. B. Ovchinnikov, *Optical dipole traps for neutral atoms*, *Advances in Atomic, Molecular, and Optical Physics* **42**, 95 (2000), preprint: [arXiv:physics/9902072](#).
- [40] M. Gustavsson, E. Haller, M. J. Mark, J. G. Danzl, G. Rojas-Kopeinig, and H.-C. Nägerl, *Control of interaction-induced dephasing of Bloch oscillations*, *Phys. Rev. Lett.* **100**, 080404 (2008).
- [41] T. Schulte, S. Drenkelforth, G. Kleine Büning, W. Ertmer, J. Arlt, M. Lewenstein, and L. Santos, *Dynamics of Bloch oscillations in disordered lattice potentials*, *Phys. Rev. A* **77**, 023610 (2008).
- [42] A. Görlitz, J. M. Vogels, A. E. Leanhardt, C. Raman, T. L. Gustavson, J. R. Abo-Shaeer, A. P. Chikkatur, S. Gupta, S. Inouye, T. Rosenband, and W. Ketterle, *Realization of Bose-Einstein condensates in lower dimensions*, *Phys. Rev. Lett.* **87**, 130402 (2001).
- [43] E. Tiesinga, B. J. Verhaar, and H. T. C. Stoof, *Threshold and resonance phenomena in ultracold ground-state collisions*, *Phys. Rev. A* **47**, 4114 (1993).
- [44] E. Timmermans, P. Tommasini, M. Hussein, and A. Kerman, *Feshbach resonances in atomic Bose-Einstein condensates*, *Physics Reports* **315**, 199 (1999).
- [45] T. Köhler, K. Góral, and P. S. Julienne, *Production of cold molecules via magnetically tunable Feshbach resonances*, *Rev. Mod. Phys.* **78**, 1311 (2006).

- [46] C. Chin, R. Grimm, P. Julienne, and E. Tiesinga, *Feshbach resonances in ultracold gases*, [arXiv:0812.1496](#) (2008).
- [47] S. N. Bose, *Plancks Gesetz und Lichtquantenhypothese*, [Zeitschrift für Physik A Hadrons and Nuclei](#) **26**, 178 (1924).
- [48] A. Einstein, *Quantentheorie des einatomigen idealen Gases*, Sitzungsberichte der Preussischen Akademie der Wissenschaften (1924) p. 261; Zweite Abhandlung (1925) p. 3.
- [49] A. Griffin, *Excitations in a Bose-Condensed Liquid*, Cambridge Univ. Press (1993).
- [50] J. Bardeen, L. N. Cooper, and J. R. Schrieffer, *Microscopic theory of superconductivity*, [Phys. Rev.](#) **106**, 162 (1957).
- [51] K. B. Davis, M. O. Mewes, M. R. Andrews, N. J. van Druten, D. S. Durfee, D. M. Kurn, and W. Ketterle, *Bose-Einstein condensation in a gas of sodium atoms*, [Phys. Rev. Lett.](#) **75**, 3969 (1995).
- [52] C. C. Bradley, C. A. Sackett, J. J. Tollett, and R. G. Hulet, *Evidence of Bose-Einstein condensation in an atomic gas with attractive interactions*, [Phys. Rev. Lett.](#) **75**, 1687 (1995).
- [53] D. G. Fried, T. C. Killian, L. Willmann, D. Landhuis, S. C. Moss, D. Kleppner, and T. J. Greytak, *Bose-Einstein condensation of atomic hydrogen*, [Phys. Rev. Lett.](#) **81**, 3811 (1998).
- [54] C. J. Pethick and H. Smith, *Bose-Einstein condensation in dilute gases*, Cambridge Univ. Press (2002).
- [55] L. Pitaevskii and S. Stringari, *Bose-Einstein condensation*, Clarendon Press, Oxford (2003).
- [56] C. Raman, M. Köhl, R. Onofrio, D. S. Durfee, C. E. Kulewicz, Z. Hadzibabic, and W. Ketterle, *Evidence for a critical velocity in a Bose-Einstein condensed gas*, [Phys. Rev. Lett.](#) **83**, 2502 (1999).
- [57] M. R. Andrews, D. M. Kurn, H.-J. Miesner, D. S. Durfee, C. G. Townsend, S. Inouye, and W. Ketterle, *Propagation of sound in a Bose-Einstein condensate*, [Phys. Rev. Lett.](#) **79**, 553 (1997), [Erratum: [Phys. Rev. Lett.](#) **80**, 2967 (1998)].

- [58] J. Stenger, S. Inouye, A. P. Chikkatur, D. M. Stamper-Kurn, D. E. Pritchard, and W. Ketterle, *Bragg spectroscopy of a Bose-Einstein condensate*, [Phys. Rev. Lett.](#) **82**, 4569 (1999).
- [59] D. M. Stamper-Kurn, A. P. Chikkatur, A. Görlitz, S. Inouye, S. Gupta, D. E. Pritchard, and W. Ketterle, *Excitation of phonons in a Bose-Einstein condensate by light scattering*, [Phys. Rev. Lett.](#) **83**, 2876 (1999).
- [60] A. Brunello, F. Dalfovo, L. Pitaevskii, and S. Stringari, *How to measure the Bogoliubov quasiparticle amplitudes in a trapped condensate*, [Phys. Rev. Lett.](#) **85**, 4422 (2000).
- [61] J. M. Vogels, K. Xu, C. Raman, J. R. Abo-Shaeer, and W. Ketterle, *Experimental observation of the Bogoliubov transformation for a Bose-Einstein condensed gas*, [Phys. Rev. Lett.](#) **88**, 060402 (2002).
- [62] J. Steinhauer, R. Ozeri, N. Katz, and N. Davidson, *Excitation spectrum of a Bose-Einstein condensate*, [Phys. Rev. Lett.](#) **88**, 120407 (2002).
- [63] J. Steinhauer, N. Katz, R. Ozeri, N. Davidson, C. Tozzo, and F. Dalfovo, *Bragg spectroscopy of the multibranch Bogoliubov spectrum of elongated Bose-Einstein condensates*, [Phys. Rev. Lett.](#) **90**, 060404 (2003).
- [64] R. Ozeri, N. Katz, J. Steinhauer, and N. Davidson, *Colloquium: Bulk Bogoliubov excitations in a Bose-Einstein condensate*, [Rev. Mod. Phys.](#) **77**, 187 (2005).
- [65] B. Shapiro, *Expansion of a Bose-Einstein condensate in the presence of disorder*, [Phys. Rev. Lett.](#) **99**, 060602 (2007).
- [66] J. W. Goodman, *Laser speckle and related phenomena*, chapter 2, p. 9, Springer-Verlag, Berlin, Heidelberg, New York (1975).
- [67] D. Clément, A. F. Varón, J. A. Retter, L. Sanchez-Palencia, A. Aspect, and P. Bouyer, *Experimental study of the transport of coherent interacting matter-waves in a 1D random potential induced by laser speckle*, [New J. Phys.](#) **8**, 165 (2006).
- [68] D. Clément, A. F. Varón, J. A. Retter, P. Bouyer, L. Sanchez-Palencia, D. Gangardt, G. V. Shlyapnikov, and A. Aspect, *Suppression of transport of an interacting elongated Bose-Einstein condensate in a random potential*, [Phys. Rev. Lett.](#) **95**, 170409 (2005).

- [69] L. Sanchez-Palencia, D. Clément, P. Lugan, P. Bouyer, G. V. Shlyapnikov, and A. Aspect, *Anderson localization of expanding Bose-Einstein condensates in random potentials*, [Phys. Rev. Lett.](#) **98**, 210401 (2007).
- [70] C. Fort, L. Fallani, V. Guarrera, J. E. Lye, M. Modugno, D. S. Wiersma, and M. Inguscio, *Effect of optical disorder and single defects on the expansion of a Bose-Einstein condensate in a one-dimensional waveguide*, [Phys. Rev. Lett.](#) **95**, 170410 (2005).
- [71] N. Bogoliubov, *On the theory of superfluidity*, *Journal of Physics (Moscow)* **11**, 23 (1947).
- [72] J. Goldstone, A. Salam, and S. Weinberg, *Broken symmetries*, [Phys. Rev.](#) **127**, 965 (1962).
- [73] M. Timmer, A. Pelster, and R. Graham, *Disorder-induced shift of condensation temperature for dilute trapped Bose gases*, [Europhys. Lett.](#) **76**, 760 (2006).
- [74] P. Lugan, D. Clement, P. Bouyer, A. Aspect, M. Lewenstein, and L. Sanchez-Palencia, *Ultracold Bose gases in 1D disorder: From Lifshits glass to Bose-Einstein condensate*, [Phys. Rev. Lett.](#) **98**, 170403 (2007).
- [75] A. V. Lopatin and V. M. Vinokur, *Thermodynamics of the superfluid dilute Bose gas with disorder*, [Phys. Rev. Lett.](#) **88**, 235503 (2002).
- [76] N. M. Hugenholtz and D. Pines, *Ground-state energy and excitation spectrum of a system of interacting bosons*, [Phys. Rev.](#) **116**, 489 (1959).
- [77] K. Huang and H.-F. Meng, *Hard-sphere Bose gas in random external potentials*, [Phys. Rev. Lett.](#) **69**, 644 (1992).
- [78] S. Giorgini, L. Pitaevskii, and S. Stringari, *Effects of disorder in a dilute Bose gas*, [Phys. Rev. B](#) **49**, 12938 (1994).
- [79] N. Bilas and N. Pavloff, *Anderson localization of elementary excitations in a one dimensional Bose-Einstein condensate*, [Eur. Phys. J. D](#) **40**, 387 (2006).
- [80] G. M. Falco, A. Pelster, and R. Graham, *Thermodynamics of a Bose-Einstein condensate with weak disorder*, [Phys. Rev. A](#) **75**, 063619 (2007).

- [81] V. I. Yukalov and R. Graham, *Bose-Einstein-condensed systems in random potentials*, [Phys. Rev. A](#) **75**, 023619 (2007).
- [82] V. I. Yukalov, E. P. Yukalova, K. V. Krutitsky, and R. Graham, *Bose-Einstein-condensed gases in arbitrarily strong random potentials*, [Phys. Rev. A](#) **76**, 053623 (2007).
- [83] L. Zhang, *Disordered boson systems: A perturbative study*, [Phys. Rev. B](#) **47**, 14364 (1993).
- [84] P. Nozières and D. Pines, *The Theory of Quantum Liquids*, Perseus Books (1999).
- [85] F. Dalfovo, S. Giorgini, L. P. Pitaevskii, and S. Stringari, *Theory of Bose-Einstein condensation in trapped gases*, [Rev. Mod. Phys](#) **71**, 463 (1999).
- [86] A. J. Leggett, *Bose-Einstein condensation in the alkali gases: Some fundamental concepts*, [Rev. Mod. Phys.](#) **73**, 307 (2001).
- [87] W. Ketterle and N. J. van Druten, *Bose-Einstein condensation of a finite number of particles trapped in one or three dimensions*, [Phys. Rev. A](#) **54**, 656 (1996).
- [88] S. Grossmann and M. Holthaus, *On Bose-Einstein condensation in harmonic traps*, [Physics Letters A](#) **208**, 188 (1995).
- [89] M. Lewenstein and L. You, *Quantum phase diffusion of a Bose-Einstein condensate*, [Phys. Rev. Lett.](#) **77**, 3489 (1996).
- [90] E. P. Gross, *Hydrodynamics of a superfluid condensate*, [Journal of Mathematical Physics](#) **4**, 195 (1963).
- [91] E. H. Lieb and R. Seiringer, *Proof of Bose-Einstein condensation for dilute trapped gases*, [Phys. Rev. Lett.](#) **88**, 170409 (2002).
- [92] L. Erdos, B. Schlein, and H.-T. Yau, *Rigorous derivation of the Gross-Pitaevskii equation*, [Phys. Rev. Lett.](#) **98**, 040404 (2007).
- [93] C. Mora and Y. Castin, *Extension of Bogoliubov theory to quasicondensates*, [Phys. Rev. A](#) **67**, 053615 (2003).
- [94] C. Mudry, *Bogoliubov theory of a dilute Bose gas*, Lecture notes, unpublished, PSI Villingen (2001), <http://people.web.psi.ch/mudry/FALL01/lecture02.pdf>.

- [95] T. D. Lee, K. Huang, and C. N. Yang, *Eigenvalues and eigenfunctions of a Bose system of hard spheres and its low-temperature properties*, [Phys. Rev.](#) **106**, 1135 (1957).
- [96] K. W. Madison, F. Chevy, W. Wohlleben, and J. Dalibard, *Vortex formation in a stirred Bose-Einstein condensate*, [Phys. Rev. Lett.](#) **84**, 806 (2000).
- [97] C. Raman, J. R. Abo-Shaeer, J. M. Vogels, K. Xu, and W. Ketterle, *Vortex nucleation in a stirred Bose-Einstein condensate*, [Phys. Rev. Lett.](#) **87**, 210402 (2001).
- [98] T. Wellens and B. Grémaud, *Coherent propagation of waves in dilute random media with weak nonlinearity*, [Phys. Rev. A](#) **80**, 063827 (2009).
- [99] L. Sanchez-Palencia, *Smoothing effect and delocalization of interacting Bose-Einstein condensates in random potentials*, [Phys. Rev. A](#) **74**, 053625 (2006).
- [100] C. Ryu, M. F. Andersen, P. Cladé, V. Natarajan, K. Helmerson, and W. D. Phillips, *Observation of persistent flow of a Bose-Einstein condensate in a toroidal trap*, [Phys. Rev. Lett.](#) **99**, 260401 (2007).
- [101] C. Gaul and C. A. Müller, *Anisotropic scattering of Bogoliubov excitations*, [Europhys. Lett.](#) **83**, 10006 (2008).
- [102] L. D. Landau and E. M. Lifschitz, *Fluid Mechanics*, chapter 8, § 78, Butterworth Heinemann (2004).
- [103] E. Merzbacher, *Quantum Mechanics*, chapter A, Wiley, New York (1998).
- [104] J. C. Butcher, *The numerical analysis of ordinary differential equations*, Wiley, New York (1987).
- [105] Y. Kagan, D. L. Kovrizhin, and L. A. Maksimov, *Anomalous tunneling of phonon excitations between two Bose-Einstein condensates*, [Phys. Rev. Lett.](#) **90**, 130402 (2003).
- [106] A. L. Fetter, *Nonuniform states of an imperfect Bose gas*, [Annals of Physics](#) **70**, 67 (1972).
- [107] V. Gurarie and J. T. Chalker, *Bosonic excitations in random media*, [Phys. Rev. B](#) **68**, 134207 (2003).

- [108] A. Mostafazadeh, *Pseudo-hermiticity versus PT-symmetry III: Equivalence of pseudo-Hermiticity and the presence of antilinear symmetries*, *J. Math. Phys.* **43**, 3944 (2002).
- [109] P. M. Morse and H. Feshbach, *Methods of Theoretical Physics*, chapter 7.5, p. 884, McGraw-Hill, New York (1953).
- [110] T. Paul, M. Hartung, K. Richter, and P. Schlagheck, *Nonlinear transport of Bose-Einstein condensates through mesoscopic waveguides*, *Phys. Rev. A* **76**, 063605 (2007).
- [111] P. C. Hohenberg, *Existence of long-range order in one and two dimensions*, *Phys. Rev.* **158**, 383 (1967).
- [112] Y. Castin and R. Dum, *Low-temperature Bose-Einstein condensates in time-dependent traps: Beyond the $U(1)$ symmetry-breaking approach*, *Phys. Rev. A* **57**, 3008 (1998).
- [113] T. Schulte, S. Denkelforth, J. Kruse, W. Ertmer, J. Arlt, K. Sacha, J. Zakrzewski, and M. Lewenstein, *Routes towards Anderson-like localization of Bose-Einstein condensates in disordered optical lattices*, *Phys. Rev. Lett.* **95**, 170411 (2005).
- [114] Y. P. Chen, J. Hitchcock, D. Dries, M. Junker, C. Welford, and R. G. Hulet, *Phase coherence and superfluid-insulator transition in a disordered Bose-Einstein condensate*, *Phys. Rev. A* **77**, 033632 (2008).
- [115] C. Gaul, N. Renner, and C. A. Müller, *Speed of sound in disordered Bose-Einstein condensates*, *Phys. Rev. A* **80**, 053620 (2009).
- [116] J. W. Goodman, *Introduction to Fourier optics*, McGraw-Hill, San Francisco (1968).
- [117] M. White, M. Pasienski, D. McKay, S. Q. Zhou, D. Ceperley, and B. DeMarco, *Strongly interacting bosons in a disordered optical lattice*, *Phys. Rev. Lett.* **102**, 055301 (2009).
- [118] S. Pilati, S. Giorgini, and N. Prokof'ev, *Superfluid transition in a Bose gas with correlated disorder*, *Phys. Rev. Lett.* **102**, 150402 (2009).
- [119] Y. Nambu and G. Jona-Lasinio, *Dynamical model of elementary particles based on an analogy with superconductivity. I*, *Phys. Rev.* **122**, 345 (1961).

- [120] E. Akkermans and G. Montambaux, *Mesoscopic physics of electrons and photons*, Cambridge Univ. Press (2007).
- [121] L. Isserlis, *On a formula for the product-moment coefficient of any order of a normal frequency distribution in any number of variables*, *Biometrika* **12**, 134 (1918), <http://www.jstor.org/stable/2331932>.
- [122] M. Hartung, T. Wellens, C. A. Müller, K. Richter, and P. Schlagheck, *Coherent backscattering of Bose-Einstein condensates in two-dimensional disorder potentials*, *Phys. Rev. Lett.* **101**, 020603 (2008).
- [123] D. Vollhardt and P. Wölfle, *Diagrammatic, self-consistent treatment of the Anderson localization problem in $d \leq 2$ dimensions*, *Phys. Rev. B* **22**, 4666 (1980).
- [124] D. J. Thouless, *Localization distance and mean free path in one-dimensional disordered systems*, *Journal of Physics C: Solid State Physics* **6**, L49 (1973).
- [125] V. Milman and G. Schechtman, *Asymptotic theory of finite-dimensional normed spaces*, Lecture Notes in Mathematics 1200, Springer-Verlag, Berlin (1986).
- [126] N. Renner, *Schallgeschwindigkeit von Bogoliubov-Anregungen in ungeordneten Bose-Einstein-Kondensaten*, Diplomarbeit, Universität Bayreuth (2009).
- [127] V. Gurarie and A. Altland, *Phonons in random elastic media and the Boson peak*, *Phys. Rev. Lett.* **94**, 245502 (2005).
- [128] P. Lugan, A. Aspect, L. Sanchez-Palencia, D. Delande, B. Grémaud, C. A. Müller, and C. Miniatura, *One-dimensional Anderson localization in certain correlated random potentials*, *Phys. Rev. A* **80**, 023605 (2009).
- [129] C. Gaul, R. P. A. Lima, E. Díaz, C. A. Müller, and F. Domínguez-Adame, *Stable Bloch oscillations of cold atoms with time dependent interaction*, *Phys. Rev. Lett.* **102**, 255303 (2009).
- [130] E. Díaz, C. Gaul, R. P. A. Lima, F. Domínguez-Adame, and C. A. Müller, *Dynamics and stability of Bose-Einstein solitons in tilted optical lattices*, [arXiv:0911.5633](https://arxiv.org/abs/0911.5633) (2009).

- [131] F. Bloch, *Über die Quantenmechanik der Elektronen in Kristallgittern*, [Zeitschrift für Physik](#) **52**, 555 (1929).
- [132] C. Zener, *Non-adiabatic crossing of energy levels*, [Proceedings of the Royal Society of London. Series A](#) **137**, 696 (1932).
- [133] —, *A theory of the electrical breakdown of solid dielectrics*, [Proceedings of the Royal Society of London. Series A](#) **145**, 523 (1934).
- [134] J. Feldmann, K. Leo, J. Shah, D. A. B. Miller, J. E. Cunningham, T. Meier, G. von Plessen, A. Schulze, P. Thomas, and S. Schmitt-Rink, *Optical investigation of Bloch oscillations in a semiconductor superlattice*, [Phys. Rev. B](#) **46**, 7252 (1992).
- [135] K. Leo, P. H. Bolivar, F. Brüggemann, R. Schwedler, and K. Köhler, *Observation of Bloch oscillations in a semiconductor superlattice*, [Solid State Communications](#) **84**, 943 (1992).
- [136] O. Morsch and M. Oberthaler, *Dynamics of Bose-Einstein condensates in optical lattices*, [Rev. Mod. Phys.](#) **78**, 179 (2006).
- [137] R. Morandotti, U. Peschel, J. S. Aitchison, H. S. Eisenberg, and Y. Silberberg, *Experimental observation of linear and nonlinear optical Bloch oscillations*, [Phys. Rev. Lett.](#) **83**, 4756 (1999).
- [138] T. Pertsch, P. Dannberg, W. Elflein, A. Bräuer, and F. Lederer, *Optical Bloch oscillations in temperature tuned waveguide arrays*, [Phys. Rev. Lett.](#) **83**, 4752 (1999).
- [139] A. Trombettoni and A. Smerzi, *Discrete solitons and breathers with dilute Bose-Einstein condensates*, [Phys. Rev. Lett.](#) **86**, 2353 (2001).
- [140] A. Smerzi and A. Trombettoni, *Nonlinear tight-binding approximation for Bose-Einstein condensates in a lattice*, [Phys. Rev. A](#) **68**, 023613 (2003).
- [141] M. Salerno, V. V. Konotop, and Y. V. Bludov, *Long-living Bloch oscillations of matter waves in periodic potentials*, [Phys. Rev. Lett.](#) **101**, 030405 (2008).
- [142] Y. V. Bludov, V. V. Konotop, and M. Salerno, *Long-lived matter wave Bloch oscillations and dynamical localization by time-dependent nonlinearity management*, [J. Phys. B: At. Mol. Opt. Phys.](#) **42**, 105302 (2009).

- [143] G. Teschl, *Ordinary differential equations and dynamical systems*, Lecture Notes, unpublished, University of Vienna (2008), <http://www.mat.univie.ac.at/~gerald/ftp/book-ode/>.

Acknowledgments

I thank everybody who contributed to the success of this work!

I thank my supervisor Cord Axel Müller for good advice, helpful and interesting discussions, simply for a great time! Thanks for a very active time with lots of conferences, summer schools and research stays in France and Spain.

Besonderer Dank gilt Frau Glas, die stets dafür sorgt, dass der Laden läuft, und die uns allen den Rücken freihält!

Ich danke allen meinen Freunden in Bayreuth, die meine Zeit hier erst lebenswert gemacht haben. Besonders genannt seien meine langjährigen Wegbegleiter Jana Schäferhans und Katharina Palmer.

Ich danke Martin Aicham, Christopher Groh und der ganzen Mountainbike-Hochschulgruppe für den sportlichen Ausgleich zum Alltag in der Physik.

Ich danke meinen Freunden aus meinen ersten Jahren in Bayreuth, die schon lange aus Bayreuth weggezogen sind für eine schöne Zeit. Besonders genannt seien Constantin Gaul, Christian Brunhuber, Jochen Endrejat ...

I thank Rodrigo Lima for providing me some C-code samples that helped me getting started with the numerical work.

Ich danke allen, die mich in den letzten Wochen ertragen und unterstützt haben. Allen, die mich extra nicht angerufen haben und trotzdem an mich gedacht haben. Allen, die mir in irgendeiner Weise den Rücken freigehalten haben.

Dank an Christopher Groh und Katharina Palmer fürs Korrekturlesen!

Dank geht an die Deutsche Forschungsgemeinschaft (DFG) für die Finanzierung meines Forschungsprojektes.

I thank everyone involved in the Bloch project: Elena Díaz Garcia, Rodrigo P. A. Lima, Francisco Domínguez-Adame and Cord A. Müller! It was great fun working and spending time with you!

Thanks to DAAD and Institut d'Optique, Palaiseau for the possibility to do part of my research in Palaiseau and Orsay.

I thank Christian Minatura and everyone involved in the Les Houches School of Physics in Singapore *Ultracold Atoms and Quantum Information*.

I thank the entire open-source community for providing us with wonderful software like Linux, LaTeX and gnuplot.